

AD-A095 073

MISSOURI UNIV-ROLLA DEPT OF ELECTRICAL ENGINEERING

F/6 17/9

ESTIMATION OF OCEANWAVE WAVENUMBER AND PROPAGATION DIRECTION FR--ETC(U)

JAN 81 @ E CARLSON, C L AGNE, C M MCENIRY

N00014-79-C-0343

CSR-81-1

NL

UNCLASSIFIED

1 of 2
AO
AO9F-073

A large grid of 100 small squares, arranged in 10 rows and 10 columns. The grid is mostly empty, with a few small black squares in the top-left corner. In the top-left corner, there is a small black square with the text "1 OF 2" and "2018-07-3" next to it. Below this, there is a small black square with the text "Page 1" and "1/1" below it.

LEVEL

12

AD A005173

**Estimation of Oceanwave
Wavenumber and Propagation
Direction From Limited Synthetic
Aperture Radar Data**

by

**Gordon E. Carlson
Craig L. Agne
Charles M. McEniry**

ONR Contract N00014-79-C-0343
Project NR 387-102
Technical Report CSR-81-1
January 1981

DISC
RECEIVED
JAN 20 1981
C

Department of

ELECTRICAL ENGINEERING

**COMMUNICATIONS AND SIGNAL
PROCESSING RESEARCH**



University of Missouri - Rolla

This document has been
approved for public release and
sale, its distribution is unlimited.

"Reproduction in whole or in part
is permitted for any purpose of
the United States Government".

81 2 17 078

UNCLASSIFIED

SECURITY CLASSIFICATION OF THIS PAGE (When Data Entered)

REPORT DOCUMENTATION PAGE		READ INSTRUCTIONS BEFORE COMPLETING FORM
1. REPORT NUMBER CSR-81-1	2. GOVT ACCESSION NO. AD-A095073	3. RECIPIENT'S CATALOG NUMBER
4. TITLE (and Subtitle) Estimation of Oceanwave Wavenumber and Propagation Direction from Limited Synthetic Aperture Radar Data		5. TYPE OF REPORT & PERIOD COVERED Technical and Final 3-1-79 to 1-31-81
		6. PERFORMING ORG. REPORT NUMBER
7. AUTHOR(s) Gordon E. Carlson, Craig L. Agne, Charles M. McEniry		8. CONTRACT OR GRANT NUMBER(s) N00014-79-C-0343
9. PERFORMING ORGANIZATION NAME AND ADDRESS University of Missouri-Rolla Rolla, Missouri 65401		10. PROGRAM ELEMENT, PROJECT, TASK AREA & WORK UNIT NUMBERS NR 387-102
11. CONTROLLING OFFICE NAME AND ADDRESS Coastal Sciences Program (Code 462) Office of Naval Research Arlington, Virginia 22217		12. REPORT DATE January 1981
		13. NUMBER OF PAGES 182
14. MONITORING AGENCY NAME & ADDRESS (if different from Controlling Office)		15. SECURITY CLASS. (of this report) Unclassified
		15a. DECLASSIFICATION/DOWNGRADING SCHEDULE
16. DISTRIBUTION STATEMENT (of this Report) This report has been approved for public release and sale; its distribution is unlimited		
17. DISTRIBUTION STATEMENT (of the abstract entered in Block 20, if different from Report)		
18. SUPPLEMENTARY NOTES		
19. KEY WORDS (Continue on reverse side if necessary and identify by block number) Wave Spectra Synthetic Aperture Radar		
20. ABSTRACT (Continue on reverse side if necessary and identify by block number) A system for determining wavenumber and propagation direction for the dominant ocean wave component from a few scans of synthetic aperture radar data is described and analyzed. The analysis uses actual synthetic aperture radar data and provides system parameter tradeoffs and statistical performance results. While reasonable estimates of wavenumber and propagation direction are achieved in some cases, the estimates are not sufficiently consistent to be satisfactory over a wide range of cases. The primary problem is one of low signal-to-noise ratio of the radar scan data.		

DD FORM 1 JAN 73 1473

EDITION OF 1 NOV 65 IS OBSOLETE
S/N 0102-LF-014-6601

UNCLASSIFIED

SECURITY CLASSIFICATION OF THIS PAGE (When Data Entered)

ESTIMATION OF OCEANWAVE WAVENUMBER
AND PROPAGATION DIRECTION FROM LIMITED
SYNTHETIC APERTURE RADAR DATA

by

Gordon E. Carlson
Craig L. Agne
Charles M. McEniry

Department of Electrical Engineering
University of Missouri-Rolla
Rolla, Missouri 65401

Technical Report CSR-81-1
January 1981

ONR Contract #N00014-79-C-0343
Project #NR 387-102

This document has been approved
for public release and sale;
its distribution is unlimited

"Reproduction in whole or in
part is permitted for any
purpose of the United States
Government"

ABSTRACT

A system for determining wavenumber and propagation direction for the dominant ocean wave component from a few scans of synthetic aperture radar data is described and analyzed. The analysis uses actual synthetic aperture radar data and provides system parameter tradeoffs and statistical performance results. While reasonable estimates of wavenumber and propagation direction are achieved in some cases, the estimates are not sufficiently consistent to be satisfactory over a wide range of cases. The primary problem is one of low signal-to-noise ratio of the radar scan data.

FORWARD

This technical report covers research performed for the Office of Naval Research under contract number N00014-79-C-0343, project number NR 387-102 and is the final report for that contract. The work was performed by Dr. Gordon E. Carlson, Principal Investigator, and Craig L. Agne and Charles M. McEniry, students in Electrical Engineering at the University of Missouri-Rolla, Rolla, Missouri under the supervision of Dr. James S. Bailey, Director of the Coastal Sciences Program, Arctic and Earth Sciences Division, Office of Naval Research.

Accession For	
NTIS CLASS	<input checked="" type="checkbox"/>
NTIC TAB	<input type="checkbox"/>
Unannounced	<input type="checkbox"/>
Justification	
By	
Distribution	
Availability Codes	
Avail and/or	
Dist	Special
A	

ACKNOWLEDGEMENT

The synthetic aperture radar image data used in performing the research described in this report was generously supplied by the Environmental Research Institute of Michigan (ERIM) in the form of digital data tapes and supporting documentation. Special thanks go to Mr. Robert A. Schuchman of ERIM for his assistance in making this data available in an extremely timely fashion and his willingness to provide counsel on its characteristics. The help of Dr. Omar Shemdin of the Jet Propulsion Laboratories in obtaining initial SEASAT synthetic aperture radar data is also appreciated.

TABLE OF CONTENTS

	Page
ABSTRACT	ii
FORWARD	iii
ACKNOWLEDGEMENT	iv
LIST OF ILLUSTRATIONS	vii
LIST OF TABLES	xiii
I. INTRODUCTION	1
II. INITIAL SYSTEM CONCEPT AND PARAMETERS	5
A. INITIAL SYSTEM CONCEPT	5
1. GENERATION OF A FEW RADAR SCANS	5
2. ALONG-SCAN WAVENUMBER ESTIMATION	12
3. INDICATED WAVE PROPAGATION ANGLE ESTIMATION	19
4. WAVE PROPAGATION ANGLE AND WAVENUMBER COMPUTATION	21
5. SUMMARY OF INITIAL SYSTEM CONCEPT	24
B. SYSTEM PERFORMANCE PARAMETERS	25
III. DATA USED AND ANALYSIS METHODS	27
A. DATA USED	27
B. SYSTEM ANALYSIS METHODS	35
IV. ANALYSIS OF ALONG-SCAN WAVENUMBER ESTIMATION PERFORMANCE	47
A. PRELIMINARY ANALYSES AND PARAMETER SELECTION	47
B. INITIAL STATISTICAL ANALYSIS	65
C. DEVELOPMENT OF A MODIFIED SYSTEM CONCEPT	69
1. THE MODIFIED SYSTEM	69
2. VARIATIONS OF THE MODIFIED SYSTEM	75

	Page
D. PARAMETER TRADEOFFS AND SELECTION	78
E. SYSTEM PERFORMANCE ANALYSIS USING VARIOUS ANALYSIS AREAS	85
F. OVERALL WAVENUMBER ESTIMATION CONCLUSIONS	107
V. ANALYSIS OF INDICATED PROPAGATION ANGLE ESTIMATION PERFORMANCE	113
A. PERFORMANCE OF INITIAL SYSTEM CONCEPT	113
B. SECOND SYSTEM CONCEPT	119
C. PERFORMANCE OF SECOND SYSTEM CONCEPT	121
D. THIRD SYSTEM CONCEPT	128
E. PERFORMANCE OF THIRD SYSTEM CONCEPT	131
VI. SUMMARY AND CONCLUSIONS	157
REFERENCES	161
APPENDIX A. PHOTOGRAPHS FOR ADDITIONAL ANALYSIS AREAS . .	163
APPENDIX B. SMOOTHED PERIODOGRAMS FOR BARTLETT AND TUKEY WINDOWS	167
APPENDIX C. INDIVIDUAL CASE WAVENUMBER ESTIMATES	173
DISTRIBUTION	181

LIST OF ILLUSTRATIONS

	Page
1. Geometry Showing Focused Radar Scan Locations Used by System	6
2. Block Diagram for Synthetic Aperture Radar which Processes Three Range Scans in Parallel	8
3. Relationship Between Slant-Range and Ground-Range Coordinate Systems	10
4. Example of Radar Data Scan Reconstruction Process for Several Interpolation Terms	11
5. Typical Ground-Range Scan and Associated Power Spectrum . .	13
6. Parabolic Interpolation to Find Wavenumber Corresponding to Spectrum Peak	18
7. Typical Ground-Range Scans and Associated Cross Correlation	20
8. Geometry Relating Wave Propagation Angle, θ_w , and Indicated Propagation Angle, θ_i	22
9. Examples of SAR Ocean Wave Images. Images are Shown in Slant-Range Format	29
10. (a) Slant-Range Data for Scan Number 274 of Image A (see Fig. 9) (b) Corresponding Ground-Range Data for Enclosed Slant-Range Data in (a)	34
11. Expanded View of the First 2140 Meters of the Ground-Range Scan Shown in Fig. 10(b)	36
12. Expanded View of the Second 2140 Meters of the Ground-Range Scan Shown in Fig. 10(b)	37
13. Ground-Range Scan of Fig. 10(b) with 25 Point (5x5) Averaging	38
14. Expanded View of the First 2140 Meters of the Ground-Range Scan Shown in Fig. 13	39
15. Expanded View of the Second 2140 Meters of the Ground-Range Scan Shown in Fig. 13	40
16. Locations of Image Scans for 20 Cases when $N_S = 3$ and $\Delta s = 5 \times$ Image Scan Spacing	43

	Page
17. Rotation of Image Area to Produce a Different Along-Scan Wavenumber and Indicated Propagation Angle for the Dominant Wave Component	45
18. Radar Scan Segment and Corresponding Non-Smoothed Periodogram for Scan 214 from Analysis Area A-1	48
19. Radar Scan Segment and Corresponding Non-Smoothed Periodogram for Scan 234 from Analysis Area A-1	49
20. Radar Scan Segment and Corresponding Non-Smoothed Periodogram for Scan 254 from Analysis Area A-1	50
21. Radar Scan Segment and Corresponding Non-Smoothed Periodogram for Scan 274 from Analysis Area A-1	51
22. Radar Scan Segment and Corresponding Non-Smoothed Periodogram for Scan 294 from Analysis Area A-1	52
23. Radar Scan Segment and Corresponding Non-Smoothed Periodogram for Scan 314 from Analysis Area A-1	53
24. Radar Scan Segment and Corresponding Non-Smoothed Periodogram for Scan 334 from Analysis Area A-1	54
25. Effect of Averaging Different Numbers of Non-Smoothed Periodograms	56
26. Periodograms Smoothing Effect for 3 Lag Windows with $M = N$	58
27. Periodograms Smoothing Effect for 3 Lag Windows with $M = 3N/4$	59
28. Periodograms Smoothing Effect for 3 Lag Windows with $M = N/2$	60
29. Periodograms Smoothing Effect for 3 Lag Windows with $M = 3N/8$	61
30. Average of 7 Smoothed Periodograms for Scan Lengths of 96m and 192m	63
31. Average of 7 Smoothed Periodograms for Scan Lengths of 384m and 768m	64
32. Along-Scan Wavenumber Estimate Performance Statistics for Two Analysis Areas Using the Initial System Concept	66
33. Along-Scan Wavenumber Estimate Performance Statistics for Two Analysis Areas Using the Scan Selection System Modification	70

	Page
34. Statistics for Number of Scans Used as a Function of Number of Scans Available for Analysis Area A-1	72
35. Along-Scan Wavenumber Estimate Statistics for Two Analysis Areas Using the Modified System	77
36. Along-Scan Wavenumber Estimate Statistics for Modified System Using a Rectangular Lag Window	79
37. Along-Scan Wavenumber Estimate Statistics for Modified System Using a Hamming Lag Window	80
38. Along-Scan Wavenumber Estimate Statistics for Modified System Using a Parzen Lag Window	81
39. Along-Scan Wavenumber Estimate Statistics as a Function of Number of Scans Used for Scan Lengths of 480, 600, and 720 Meters	82
40. Along-Scan Wavenumber Estimate Statistics as a Function of Number of Scans Used for Scan Lengths of 120, 240 and 360 Meters	83
41. Along-Scan Wavenumber Estimate Statistics as a Function of Scan Length	84
42. Along-Scan Wavenumber Estimate Statistics as a Function of Scan Spacing for Three Scan Lengths	86
43. Area A-3 Along-Scan Wavenumber Estimate Statistics for $\theta_r = 0^\circ$	88
44. Area A-3 Along-Scan Wavenumber Estimate Statistics for $\theta_r = 23^\circ$	89
45. Area A-3 Along-Scan Wavenumber Estimate Statistics for $\theta_r = 35^\circ$	90
46. Area A-4 Along-Scan Wavenumber Estimate Statistics for $\theta_r = 0^\circ$	92
47. Area A-4 Along-Scan Wavenumber Estimate Statistics for $\theta_r = 23^\circ$	93
48. Area A-4 Along-Scan Wavenumber Estimate Statistics for $\theta_r = 35^\circ$	94
49. Area A-5 Along-Scan Wavenumber Estimate Statistics for $\theta_r = 0^\circ$	98

	Page
50. Area A-5 Along-Scan Wavenumber Estimate Statistics for $\theta_r = 23^\circ$	99
51. Area A-5 Along-Scan Wavenumber Estimate Statistics for $\theta_r = 35^\circ$	100
52. Area B-1 Along-Scan Wavenumber Estimate Statistics for $\theta_r = 0^\circ$	103
53. Area B-1 Along-Scan Wavenumber Estimate Statistics for $\theta_r = 13^\circ$	104
54. Area B-1 Along-Scan Wavenumber Estimate Statistics for $\theta_r = 45^\circ$	105
55. Along-Scan Wavenumber Estimate Statistics for Analysis Areas C-1 and C-5	108
56. Along-Scan Wavenumber Estimate Statistics for Analysis Areas C-8 and C-4	109
57. Along-Scan Wavenumber Estimate Statistics for Analysis Areas C-3 and C-7	110
58. Along-Scan Wavenumber Estimate Statistics for Analysis Areas C-6 and C-2	111
59. Average of 10 Cross Correlation Functions for SL = 384m and $\Delta s = 7.5$ m and 15 m (Area A-1)	114
60. Average of 10 Cross Correlation Functions for SL = 384m and $\Delta s = 30$ m and 60m (Area A-1)	115
61. Average of 10 Cross Correlation Functions for SL = 768m and $\Delta s = 7.5$ m and 15m (Area A-1)	116
62. Average of 10 Cross Correlation Functions for SL = 768m and $\Delta s = 30$ m and 60m (Area A-1)	117
63. Data Peaks (Wave Crests) and Straight Line Fits to Them . .	120
64. First Results for Indicated Propagation Angle Estimate Using Second System Concept	122
65. Indicated Propagation Angle Estimate for Second System Concept and Two Different Number of Estimates Averaged . .	124
66. Indicated Propagation Angle Estimate for Second System Concept and Longer Scans	126

	Page
67. Indicated Propagation Angle Estimate for Second System Concept and Smaller Scan Spacing	127
68. Two-Dimensional Square Wave for Correlation with Radar Scan Data	130
69. Peak Cross Correlation Versus Propagation Angle for Third System Concept and First Case	132
70. Peak Cross Correlation Versus Propagation Angle for Third System Concept and First Case with 5x5 Smoothed Data . . .	133
71. Indicated Propagation Angle Estimates from All Variations of the Third System Concept for the First Case	134
72. Peak Cross Correlation Versus Propagation Angle for Third System Concept and Second Case	136
73. Peak Cross Correlation Versus Propagation Angle for Third System Concept and Second Case with 5x5 Smoothed Data . . .	137
74. Indicated Propagation Angle Estimates from All Variations of the Third System Concept for the Second Case	138
75. Peak Cross Correlation Versus Propagation Angle for Third System Concept and Third Case	140
76. Peak Cross Correlation Versus Propagation Angle for Third System Concept and Third Case with 5x5 Smoothed Data . . .	141
77. Indicated Propagation Angle Estimates from All Variations of the Third System Concept for the Third Case	142
78. Individual Case Indicated Propagation Angle Estimates for Third System Concept with No Smoothing as a Function of Number of Scans Used	144
79. Individual Case Indicated Propagation Angle Estimates for Third System Concept with 3-Point Smoothing as a Function of Number of Scans Used	145
80. Individual Case Indicated Propagation Angle Estimates for Third System Concept with 5-Point Smoothing as a Function of Number of Scans Used	146
81. Individual Case Indicated Propagation Angle Estimates Comparing Use of Estimated and Ground-Truth Wavelengths . .	148
82. Individual Case Indicated Propagation Angle Estimates Comparing Use of Different Scan Lengths	150

	Page
83. Individual Case Indicated Propagation Angle Estimates Comparing Use of Non-Smoothed and Smoothed Radar Data . . .	151
84. Individual Case Indicated Propagation Angle Estimates Comparing Use of Different Scan Spacings	152
85. Individual Case Indicated Propagation Angle Estimates for Three Different Wave Angles for Analysis Area A-3	154
86. Individual Case Indicated Propagation Angle Estimates for Two Different Wave Angles for Analysis Area A-4	155

LIST OF TABLES

	Page
I. Procedure for Computation of Smoothed Periodograms . .	17
II. Flight Information for Images Selected for System Evaluation	30
III. Ocean Wave Parameters for Selected Images	31
IV. Specifications for Actual Digitized Images Used	33
V. Identification of Analysis Areas Used from Selected Images	36
VI. Window Functions Used for Periodogram Smoothing	56
VII. Comparison of Along-Scan Wavenumber Estimates in rad/m for Various Combinations of Lag Window Functions and Lag Window Widths	62
VIII. Along-Scan Wavenumber Estimation Performance for Various System Modifications	68
IX. Example of Wavenumber Convergence Using Scan Selection Modification	73
X. Example of Spurious Wavenumber Estimates Using Scan Selection Modification	74
XI. Example of Non-Estimable Case Using Scan Selection Modification	76
XII. Summary of Along-Scan Wavenumber Estimate Performance for Analysis Area A-3	91
XIII. Summary of Along-Scan Wavenumber Estimate Performance for Analysis Area A-4	96
XIV. Summary of Along-Scan Wavenumber Estimate Performance for Analysis Area A-5	101
XV. Summary of Along-Scan Wavenumber Estimate Performance for Analysis Area B-1	106
XVI. Estimates of Wave Offset Between Scans and Indicated Propagation Angle from Average of 10 Cross Correlation Functions (Area A-1)	118

	Page
XVII. Indicated Propagation Angle Estimates for 9 Additional Cases Using the Second System Concept	123
XVIII. Second System Concept Estimates of Indicated Propagation Angle for 6 Cases With and Without Modification of Wave Displacement Estimate Locations .	128
XIX. Percent of Indicated Propagation Angle Estimates Within $\pm 5^\circ$ and $\pm 10^\circ$ for Third System Concept as a Function of Number of Scans Used	147

ESTIMATION OF OCEANWAVE WAVENUMBER
AND PROPAGATION DIRECTION FROM
LIMITED SYNTHETIC APERTURE
RADAR DATA

I. INTRODUCTION

Sensing of ocean wave fields to determine their directional wave spectra is important as an aid to understanding ocean wave phenomena and for generation of data for wave climate prediction at locations of interest. Such locations of interest include shipping lanes, coastal installations, and amphibious landing sites.

In order to obtain ocean wave spectra, ocean wave field measurements must be obtained. Ocean wave field measurements have been obtained by several different methods with each method having certain limitations. The most primitive method is measurements reported from ocean going ships. This method suffers due to the irregularity and inaccuracy of the reports. Also, reports from ships tend to be restricted to well travelled routes such as shipping lanes.

Wave riding buoys provide good measurements of the ocean surface. Multiple sensors on a single buoy or on an array of buoys may be used to make measurements which can be used to determine the wave field spectra at the buoy location. Unfortunately, as in the case of ship reporting, the application of wave riding buoys is limited by the amount of area that can be covered.

Another method for obtaining ocean wave measurements is to use images generated by aircraft-borne surface-imaging sensors on aircraft flights over the ocean surface. This method provides much wider coverage than is obtainable with the two previously indicated methods. Typically, the ocean wave directional spectra is obtained from such images by performing two-dimensional Fourier transforms of the portion of the image for which the spectrum is desired¹. This can be done optically or, if the image is digitized, by digital computations. Since the images are two-dimensional patterns which are fixed in time, a 180° ambiguity for the wave propagation direction exists. Therefore, only the wave propagation angle can be determined directly from the image data. Fortunately, other sensors of ocean surface properties and wind conditions can be used with geographical location information to resolve the 180° ambiguity in many cases.

While aircraft-borne imaging sensors are capable of providing wider coverage, it is not practical to conceive of their use for ocean wave measurements on a global scale. The advent of remote sensors transported by satellites has provided a potential method for obtaining ocean wave measurements on a global scale.

A possible sensor for obtaining the desired ocean wave field images from an airborne platform is a camera. However, a pulsed radar system operating at microwave frequencies can produce radar images of ocean waves and provide capability for image generation during either day or night and in the presence of clouds and nominal rainfall². Thus, it is the preferred sensor if sufficient resolution can be obtained to resolve wave fields of interest. With proper design, a synthetic aperture radar (SAR) provides focusing of the received backscatter energy from the earth's surface to give radar images from satellite altitudes with sufficient azimuth resolution to be useful in observation of land and sea. Sufficient range resolution is obtained by using narrow transmitted pulses or pulse compression. It is not within the scope of this report to discuss the theory of synthetic aperture radars or problems of imaging ocean waves with them since these are discussed elsewhere^{3,4}.

Synthetic aperture radars have been developed for and utilized with aircraft for a large number of years to obtain excellent radar images. The first application of an SAR in an earth observational satellite was as part of the sensor package in the SEASAT-A satellite. Data from the particular SAR on the SEASAT-A satellite was processed on the ground to provide the focusing necessary to obtain radar images with 25m resolution over a 100km swath width.

A problem with using an SAR on a satellite is the high rate at which data are acquired and must be recorded and the large amount of data storage required on board the satellite if images from many locations are to be stored for later transmission to ground receiver stations. Since the SEASAT-A satellite was a research and demonstration system, it circumvented this problem by only taking data when within line-of-sight of a ground receiver station and then transmitting the unprocessed radar data to the ground receiver station in real time as the radar generated it.

It would be desirable to have a technique for determining ocean wave directional spectra from less than full SAR images since this would permit global determination of such spectra with reasonable satellite on-board recording rate and storage. The limited SAR data could be in the form of a few digitized focused radar scans at a location where a wave spectrum is desired. An SAR with simplified focusing processor could be designed to produce the few digitized focused scans per image area in a parallel fashion on-board the satellite. This report presents the results of an initial feasibility study of such a system. The study encompasses the investigation of the feasibility of determining the wavenumber and propagation angle of the dominant wave component in an area from a few focused radar scans. Even though a number of parameter variations and system modifications were considered, it was not possible to obtain a system which provides consistently good results with a few focused scans. Thus, the extension of the feasibility study to include system configurations which could determine the characteristics of components of multiple wave components in an area could not be considered.

The primary problem which generated the inconsistent performance obtained and which could not be overcome appears to be one of poor signal-to-noise characteristics of the radar scans. The low signal-to-noise characteristics did not come as a surprise since it has been known to adversely affect efforts to obtain ocean wave directional spectra from images by two-dimensional Fourier transform techniques. However, it was initially hoped that the signal-to-noise was sufficient to permit determination of spectral information from a few radar scans in a large variety of situations.

This report consists of four parts. The first describes the initial system concept and indicates system parameters of interest and parameters to be used for system performance evaluation. The second part describes the data used in evaluating the system and the method used to analyze system performance. The third part presents performance results obtained for wavenumber estimation, indicates problems encountered and describes system modifications made to improve performance. The fourth part describes several approaches used to attempt to estimate wave propagation angle, indicates problems encountered, and presents performance results. The final section presents a summary of the study and conclusions.

II. INITIAL SYSTEM CONCEPT AND PARAMETERS

This section describes the initial system concept defined for determination of the wavenumber and propagation angle of the dominant ocean wave component in an area from a few digitized focused radar scans. Also, included is an indication of system parameters for which performance trade-off information must be generated and a definition of performance parameters which will be used for system performance evaluation.

A. INITIAL SYSTEM CONCEPT

An initial system concept is defined to begin analysis of the system capability. Modifications to this initial concept will be discussed later in conjunction with the presentation of performance results.

1. GENERATION OF A FEW RADAR SCANS

The radar data to be used by the system in determining wavenumber and propagation angle of the dominant wave component in an area are sequences of radar backscatter values along a few focused scans across the ocean wave field of interest. Since the area over which the scans are obtained is small, it is reasonable to assume that the data is from a stationary stochastic process so a spectrum can be defined and computed. The geometry of the flight path, wave field, and radar scans is illustrated in Fig. 1. The scans locations indicated are not necessarily adjacent scans of a radar image. The only requirement is that the scans be close enough together so they all illuminate the same wave field. Note that the wavefield dominant component wavelength, λ_w , and the dominant component wavelength along the scan, λ_y , are defined in Fig. 1. In addition, the wave propagation angle, θ_w , is defined as being measured counter clockwise with respect to the scan direction. The wavenumber of the dominant wave component is given by $k_w = 2\pi/\lambda_w$ and the wavenumber of the dominant component along the scan is given by $k_y = 2\pi/\lambda_y$.

Each radar scan is a time sequence of backscatter data generated on-board a vehicle carrying an SAR which includes a real-time focusing processor. The processor coherently adds phase weighted versions of individual pulse radar return scans obtained by the radar while the particular earth location desired is within the radar antenna beamwidth. This coherent addition causes the energy received from a particular scatterer on the earth's surface to be focused in a narrow doppler frequency range. Scatterers which are adjacent in azimuth are focused in adjacent frequency ranges. Selection of the doppler frequency ranges by filtering separates the adjacent scatterer returns so azimuth resolution is obtained like that which would result from an antenna of length equal to the distance travelled in gathering the data used.

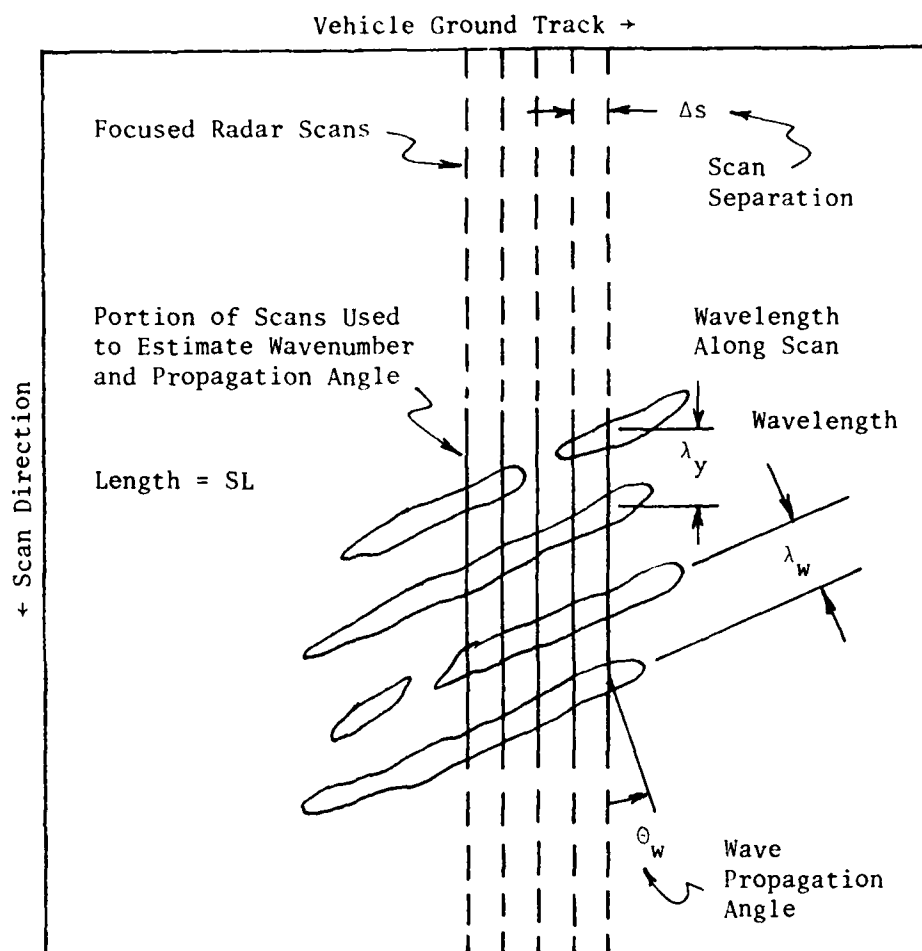


Fig. 1. Geometry Showing Focused Radar Scan Locations Used by System.

Since only a few focused radar scans nearly adjacent to each other are needed, they can be obtained from parallel coherent phase weighted additions of one set of radar range returns. Only a single focusing phase weighting as a function of range is required for each radar return along with a different doppler offset phase weighting for each focused radar scan of interest. Actually, less than 10% azimuth resolution degradation over the radar scan results for a reasonable swath width if the same focusing phase weighting is used for each radar return at all ranges. Use of a single phase weighting for each return and parallel coherent sums permits utilization of a simplified real-time processor on-board the satellite. A block diagram for such a radar and processor which might be used to obtain 3 scans is illustrated in Fig. 2.

The digitized focused radar scans obtained from the processor can be recorded at a slower rate than real-time after they have been obtained. Since only a few radar scans are recorded and at a slower rate than real-time, then recording rate and storage required are much reduced over that necessary to record and store a complete radar image of the area of interest.

The radar scans obtained at one location could be processed on-board the satellite to obtain the dominant wave component wavenumber and propagation angle. However, analyst interaction and, thus, greater processing flexibility is obtained if the radar scans are transmitted to ground receiving stations for subsequent processing to determine the wavenumber and propagation angle.

The backscatter data along the focused radar scan is a function of the slant range to the scatterer rather than the ground-range. Areas at ground-ranges close to nadir (the point directly under the vehicle) are compressed in slant-range extent when compared with areas of the same ground-range dimension that are further from nadir. The non-linear compression of radar scan data as nadir is approached causes a non-linear change in the apparent ocean wavelength in the scan direction. This results in the smearing of any wavenumber estimate obtained from scans in slant-range coordinates. Also, the apparent wave propagation angle will be changed. Therefore, radar scans in slant-range coordinates must be converted to ground-range coordinates before estimation of wavenumber and propagation angle can be performed. The steps needed in the system to perform this conversion are now described.

The radar scan data in digitized form will consist of backscatter data samples at equally spaced slant-range coordinate locations. From these, a sequence of data samples corresponding to equally spaced ground-range coordinate locations is desired for ease in processing. In order to generate such a sequence, the desired equally spaced ground-range locations must first be identified. Their equivalent locations in a slant-range coordinate are then computed by

$$y_s = \sqrt{y_g^2 + h^2} - h \quad (1)$$

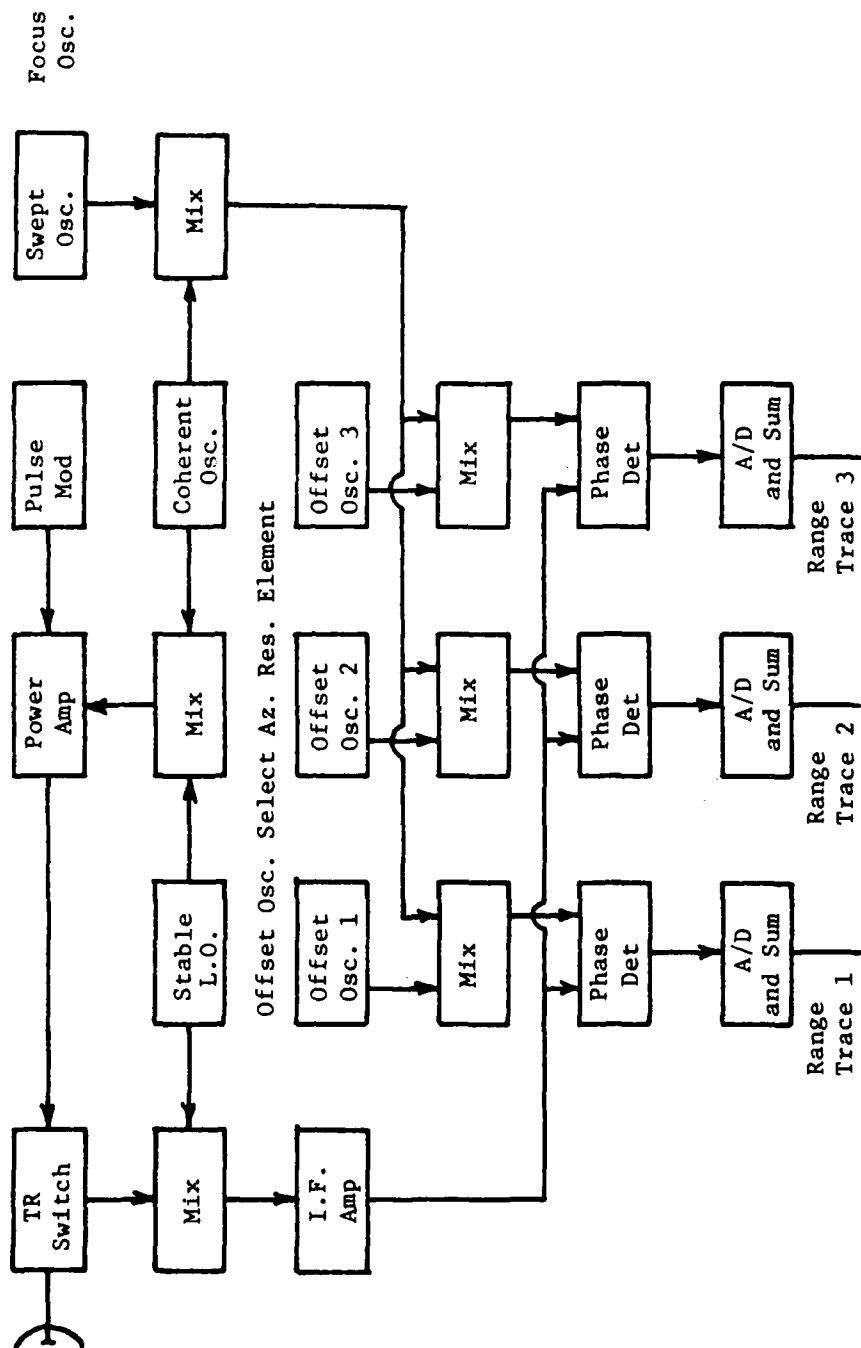


Fig. 2. Block Diagram for Synthetic Aperture Radar which Processes Three Range Scans in Parallel.

where y_s is the slant-range distance from the nadir return along the scan, y_g is the ground-range distance from nadir to the point being considered, and h is the vehicle altitude. The geometry defining the coordinate relationship leading to Eqn. 1 is shown in Fig. 3. The slant-range locations obtained will not necessarily correspond to existing data sample slant-range locations; therefore, the desired ground-range sample values must be reconstructed from existing slant-range samples. The slant-range to ground-range conversion algorithm can thus be completed by selecting an appropriate reconstruction algorithm.

Reconstruction of a stochastic process from its sampled version can be accomplished for a bandlimited process⁵. Such reconstruction requires that the stochastic process be sampled at a rate, f_s , that is at least twice the highest frequency, B , in the power spectrum of the process. Typically, data sequences such as ocean wave image scans are not bandlimited processes; however, minimal distortion is caused by picking f_s on the basis of a frequency B above which the power spectrum is very small.

Given the above constraint, consider a scan of radar data in slant-range coordinates given by $i(y_s)$ which is sampled every Δy_s meters resulting in the sampled signal $i(n\Delta y_s)$ $n=0, \pm 1, \pm 2, \pm 3, \dots$. It can be shown⁵ that data at any point along the scan can be reconstructed from the sampled scan data, $i(n\Delta y_s)$, by the so called sinc function (i.e. $\text{sinc}(x) = (\sin \pi x) / \pi x$) interpolation formula

$$i(y_s) = \sum_{n=-\infty}^{\infty} i(n\Delta y_s) \frac{\sin(\pi(y_s - n\Delta y_s)/\Delta y_s)}{\pi(y_s - n\Delta y_s)/\Delta y_s} \quad (2)$$

The reconstruction formula is graphically described by considering a few terms in the infinite sum as shown in Fig. 4. The reconstructed value $i(y_{s1})$ is found by summing the values of the weighted sinc functions at $y=y_{s1}$.

In order to implement Eqn. 2, samples which exist for infinite past and future locations are required. Obviously, ocean wave image data cannot be of infinite duration; however, if it is assumed that distant samples have roughly the same amplitude as the samples near the point to be reconstructed, then their contribution in the reconstruction process is small. This can be seen by observing Eqn. 2 for large magnitudes of n . With the above consideration the interpolation formula is re-defined as

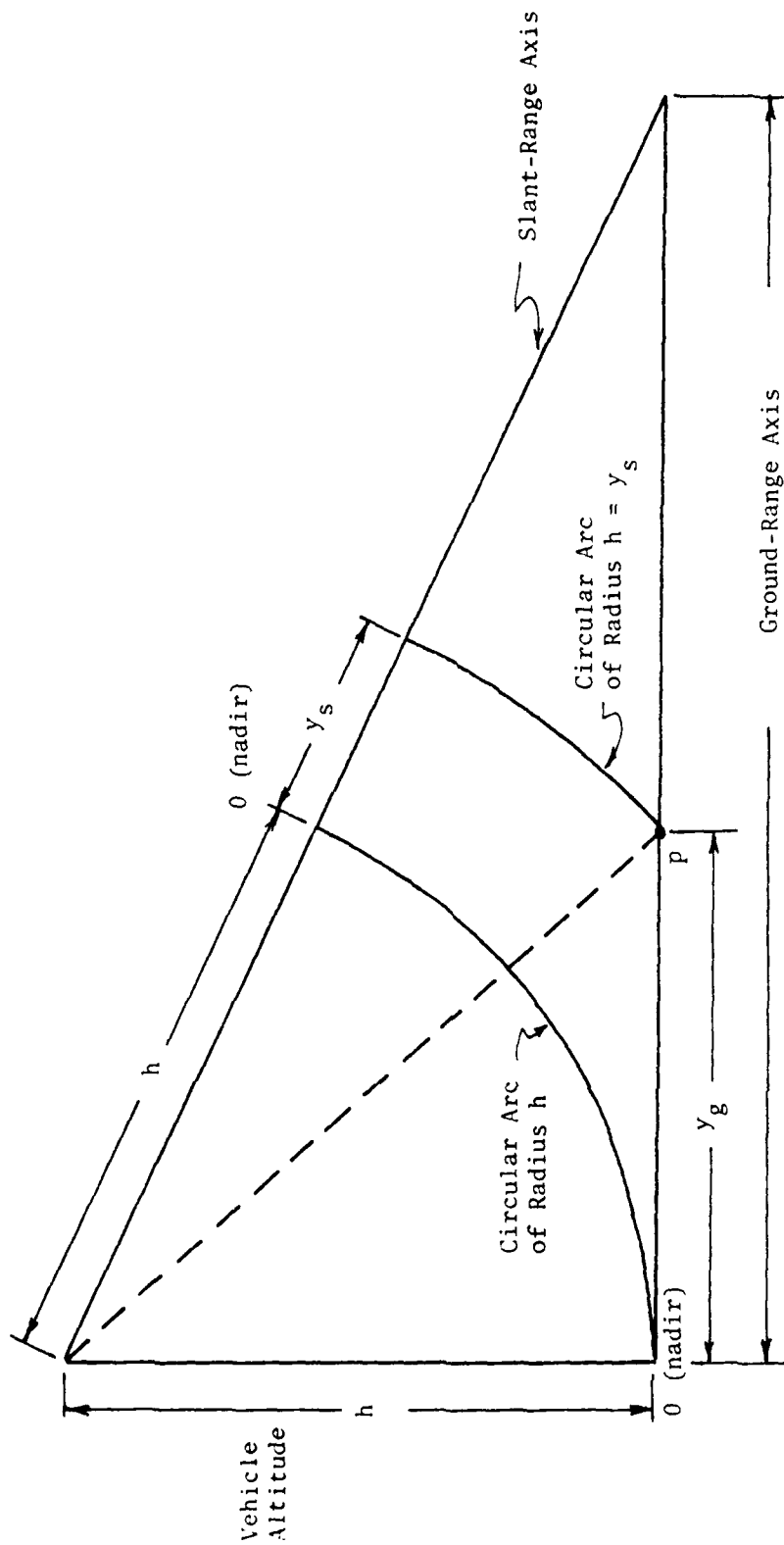


Fig. 3. Relationship Between Slant-Range and Ground-Range Coordinate Systems.

$$s(y_s) = \frac{\sin[\pi(y_s/\Delta y_s)]}{\pi(y_s/\Delta y_s)}$$

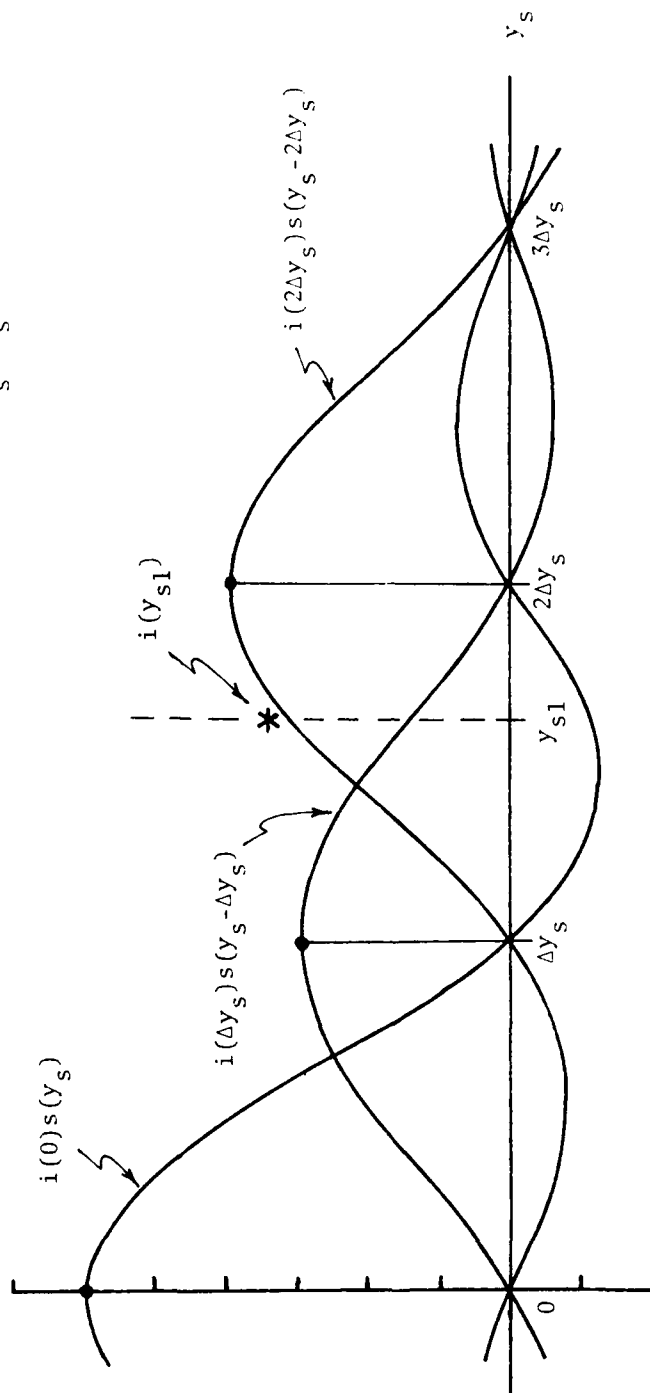


Fig. 4. Example of Radar Data Scan Reconstruction Process for Several Interpolation Terms.

$$i(y_s) \approx \sum_{n=n_1}^{n_2} i(n y_s) \frac{\sin[\pi(y_s - n\Delta y_s)/\Delta y_s]}{\pi(y_s - n\Delta y_s)/\Delta y_s} \quad (3)$$

where

$$n_1 = \lceil y_s / \Delta y_s \rceil - \frac{1}{2} N_r + 1 \quad (4)$$

and

$$n_2 = \lceil y_s / \Delta y_s \rceil + \frac{1}{2} N_r \quad (5)$$

In Eqns. 4 and 5, N_r is the total number of terms used in the reconstruction of a single point and the brackets ($\lceil \rceil$) symbolize the interger part of the enclosed argument. The total number of points N_r is assumed to be even, thus yielding an equal number of contributing values on either side of the value to be reconstructed. Eqn. 3 is the desired reconstruction algorithm to compute radar scan data for slant-range locations corresponding to desired ground-range locations.

In specifying the ground-range locations for samples to be obtained, it should be remembered that the resolution changes along the ground-range coordinate. In order to prevent excessive smearing of the ground-range data near nadir due to the changing resolution, the first ground-range value to be computed is usually chosen at a location that is a reasonable distance from nadir. If this first ground-range point is identified as y_{g1} then all of the ground-range points to be converted have locations given by

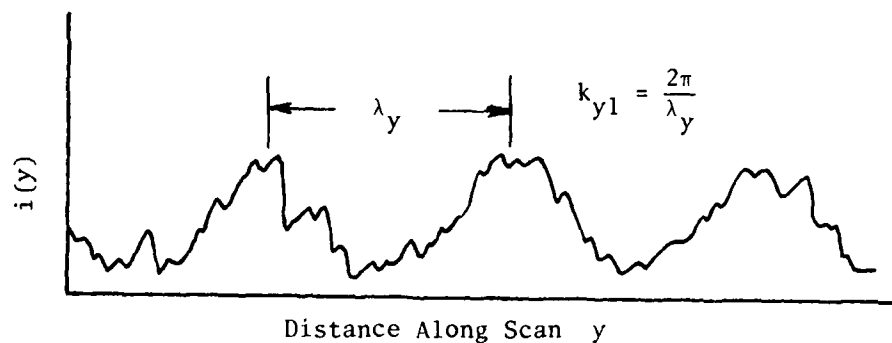
$$y_g = y_{g1} + j\Delta y_g \quad j = 0, 1, 2, \dots, J-1 \quad (6)$$

where J is the total number of points to be converted and Δy_g is the increment in meters between successive ground-range locations.

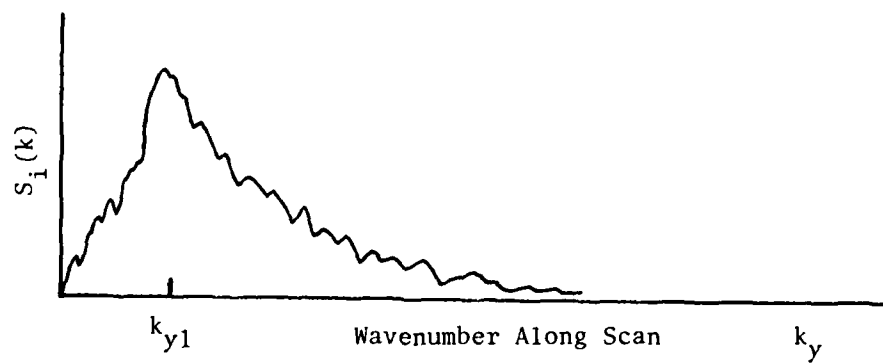
Before closing the discussion on slant-range to ground-range coordinate conversion it should be noted that the sinc function interpolation formula is one of several that could have been used. In fact, if the sampling rate is high enough, then a simple linear interpolation between the two values enclosing the point to be reconstructed will result in negligible error.

2. ALONG-SCAN WAVENUMBER ESTIMATION

A typical ground-range corrected radar scan across the wave field shown in Fig. 1 might look like the function shown in Fig. 5a. A non-digitized version is shown for convenience. If a one-dimensional power spectrum were computed and plotted as a function of wavenumber along the scan, k_y , for this scan data, it would look like that shown in



(a) Ground-Range Corrected Radar Scan



(b) Power Spectrum of Scan

Fig. 5. Typical Ground-Range Scan
and Associated Power Spectrum.

Fig. 5b. The location of the peak of the spectrum should correspond to the wavenumber, k_{y1} , of the dominant wave component along the scan seen in Fig. 5a and thus can be used as an estimate for the wavenumber of this dominant component.

Actually, the power spectrum computed for a single radar data scan is an estimate of the true one-dimensional power spectrum of the stochastic process along the scan and is noisy since the data scan is noisy. It can be smoothed by using appropriate windows on the data. Further smoothing can be achieved by obtaining smoothed spectrum estimates for each of several radar scans across the wave field and then averaging them. Thus, the initial concept for the portion of the system which estimates the wavenumber of the dominant wave component seen along a radar scan is: (1) compute the smoothed power spectrum estimate for several radar scans across the wave field, (2) average the smoothed spectrum estimates, (3) estimate the wavenumber along the scan as the location of the peak of the average spectrum estimate. Details of these steps are now presented.

The radar scan data is in digital form and is defined as the N point sequence $i(n\Delta y)$ where $n=0,1,2,\dots,N-1$ and Δy is the separation of the sample points in meters. The autocorrelation sequence estimate for this scan data sequence is

$$\hat{R}_i(u) = \frac{1}{N} \sum_{n=1}^{N-|u|-1} i_n i_{n+|u|} \quad (7)$$

where the sequence $i(n\Delta y)$ has been abbreviated to i_n for notational convenience. The parameter u is the correlation lag index for samples separated by the distance Δy and is contained in the range $-(N-1) < u < N-1$. The number of sample points to be used for a radar scan of length SL meters is

$$N = SL/\Delta y \quad (8)$$

Once the autocorrelation estimate has been obtained, the power spectrum estimate is computed as

$$\hat{S}_i(\omega) = FT[\hat{R}_i(u)] \quad (9)$$

where FT is the Fourier Transform operator. It can be shown⁶ that the power spectrum estimate computed in (9) can be equivalently computed as

$$\hat{S}_i(\omega) = \frac{1}{N} |I(\omega)|^2 \quad (10)$$

where $I(\omega)$ is the Fourier Transform of the sequence i_n , $n=0,1,2,\dots,N-1$. The power spectrum estimate defined by Eqn. 10 has often been referred to as the periodogram. This term will be used in the remainder of this report for simplicity. Eqn. 10 shows the method by which the periodogram can be generated without first computing $\hat{R}_i(u)$. With the advent of the

FFT, this has indeed become the preferred method. In fact, for large N it is more efficient to compute $\hat{R}_i(u)$ as the inverse Fourier Transform of Eqn. 10 rather than using the implementation of Eqn. 7.

The accuracy with which the periodogram approximates the true power spectrum can be statistically determined by considering the average or expected value of the periodogram as well as its variance at all points. For good accuracy it is desired that on the average the periodogram should be very close to the true power spectrum (i.e. small bias) with a very small variance (i.e. good consistency).

It can be shown that the periodogram is asymptotically unbiased⁶. That is, for a given sample spacing Δy , the expected value of the periodogram approaches the true power spectrum as the number of sample points, N , is increased. The evaluation of the variance of the periodogram is generally not easy to do; however, it has been shown that for linear Gaussian stochastic processes, the variance of the periodogram does not approach zero as N becomes large⁶. While it is not reasonable to assume that an ocean wave image may be exactly represented by a linear Gaussian stochastic process, the above result serves as a useful guideline.

Reduction of the periodogram variance may be accomplished, at the expense of additional bias and reduced resolution by the use of windowing operations during periodogram generation. The general form of such a window function (referred to as a lag window) is given by

$$\begin{aligned} w(u) &\neq 0 & , & & |u| \leq M \\ &= 0 & , & & \text{elsewhere} \end{aligned} \quad (11)$$

and is multiplied term by term with the autocorrelation estimate (Eqn. 7) resulting in

$$\bar{R}_i(u) = w(u) \cdot \hat{R}_i(u) \quad (12)$$

The resulting periodogram is given by

$$S_i(\omega) = \text{FT}[\bar{R}_i(u)] \quad (13)$$

and is referred to as the smoothed periodogram since it is a smoothed version of $\hat{S}_i(\omega)$ formed by the convolution of $\hat{S}_i(\omega)$ with the Fourier Transform of the window function. Selection of a given window $w(u)$, and window width $2M \cdot \Delta y$, involves a trade-off between the bias and variability of the resulting smoothed periodogram.

Another parameter that must generally be considered in the selection of smoothing windows is the spectral resolution resulting from window application. If more than one spectral component is to be identified, the spectral resolution determines how closely the components can be located to each other and still be individually identified. Since the

system is to identify a single fundamental component of the spectrum estimate, extremely fine resolution is not required. However, it must be adequate so the location of the peak is not displaced significantly by contributions on either side of it.

As discussed earlier, evaluation of Eqn. 10 using FFT techniques has made the computation of periodograms much more efficient. The use of such FFT techniques results in a sampled version, $\bar{S}_i(m)$, of the smoothed periodogram where m is an integer indicating the sample number. The specific method by which the FFT is used for smoothed periodogram computation is given in Table I. It should be noted that the mean value of the data sequence is removed prior to computation. This prevents the d.c. component of the data sequence from dominating the spectrum.

After smoothed periodograms have been obtained for several radar scans using the technique given in Table I, then these smoothed periodograms are averaged to obtain the averaged smoothed periodogram, $\bar{\bar{S}}_i(m)$, which exhibits further smoothing with no decrease in resolution. This is followed by determining the wavenumber estimate along the scan \hat{k}_y . One way in which this could be done is to identify the sample location $m = m_p$ at which the maximum value of the averaged periodogram is located. The wavenumber estimate along the scan is then roughly given by

$$\hat{k}_y = m_p \cdot \Delta k \quad (\text{radians/meter}) \quad (14)$$

where Δk is the spacing between samples expressed in wavenumber units and is given by

$$\Delta k = \frac{2\pi}{\Delta y \cdot L} \quad (\text{radians/meter/sample}) \quad (15)$$

In order to more closely approximate the true peak location, a parabolic interpolation using the peak sample $\bar{S}_i(m_p)$ and the two neighboring samples $\bar{S}_i(m_p-1)$ and $\bar{S}_i(m_p+1)$ is used. The resulting peak location is given by

$$\tilde{m}_p = m_p + \Delta m \quad (16)$$

where Δm is given by

$$\Delta m = \frac{[\bar{\bar{S}}_i(m_p - 1) - \bar{\bar{S}}_i(m_p + 1)]}{2[\bar{\bar{S}}_i(m_p - 1) - 2\bar{\bar{S}}_i(m_p) + \bar{\bar{S}}_i(m_p + 1)]} \quad (17)$$

This interpolation process is shown in Fig. 6. Once \tilde{m}_p is obtained, then the interpolated wavenumber estimate along the scan is given by

$$\tilde{k}_y = \tilde{m}_p \cdot \Delta k \quad (18)$$

TABLE I. Procedure for Computation of Smoothed Periodograms.

1. Obtain data sequence i_n , $n=0,1,2,\dots,N-1$. It is assumed that the mean value of the data has been removed.
2. Pad the sequence with zeros.
i.e., $i_n = 0$; $n=N, N+1, N+2, \dots, L-1$
where $L \geq 2N-1$
3. Obtain $I(m)$ as the L point FFT of $i(u)$
4. Compute the non-smoothed periodogram of $i(u)$ as
$$\hat{S}_i(m) = \frac{1}{N} |I(m)|^2; \quad m=0,1,2,\dots,L-1$$
5. Obtain the biased autocorrelation function estimate of $i(u)$ as
$$\hat{R}_i(u) = \text{FFT}^{-1}[\hat{S}_i(m)]$$
6. Multiply $\hat{R}_i(u)$ by a lag window of specified lag width $(2M \cdot \Delta y)$ corresponding to the desired spectral window to obtain $\bar{R}_i(u)$ i.e.,
$$\bar{R}_i(u) = w(u) \cdot \hat{R}_i(u)$$
7. Obtain smoothed periodogram of $i(u)$ as
$$\bar{S}_i(m) = \text{FFT}[\bar{R}_i(u)]$$

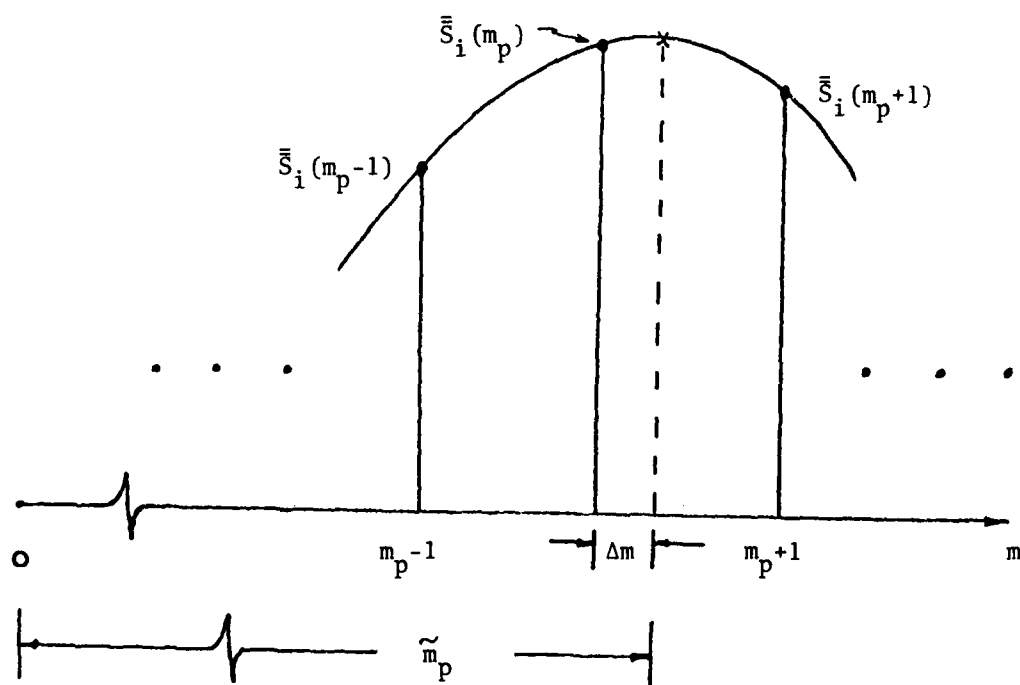
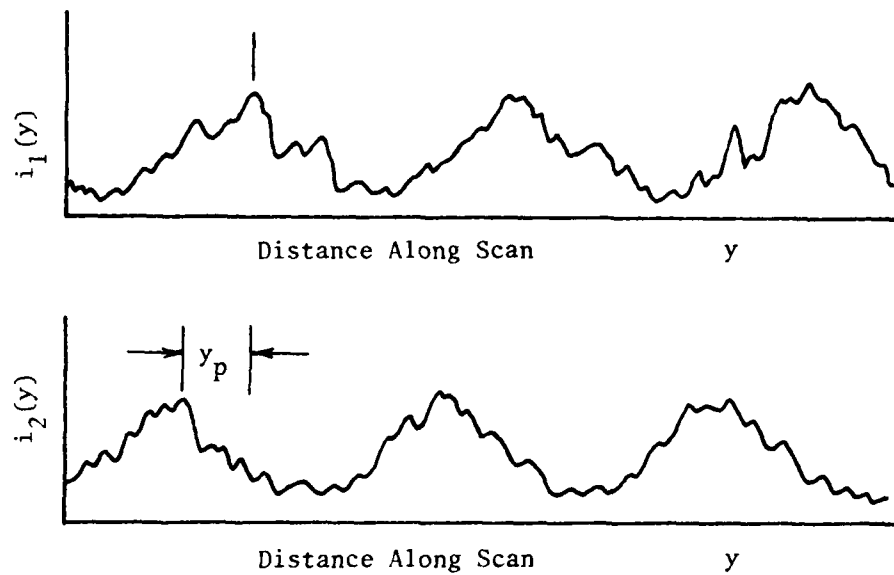
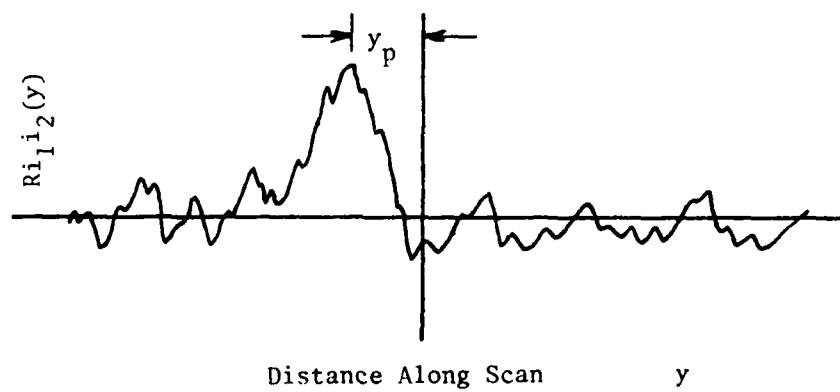


Fig. 6. Parabolic Interpolation to Find Wavenumber Corresponding to Spectrum Peak.



(a) Ground-Range Corrected Radar Scans



(b) Cross Correlation of Scans

Fig. 7. Typical Ground-Range Scans and Associated Cross Correlation.

3. INDICATED WAVE PROPAGATION ANGLE ESTIMATION

Two typical ground-range corrected radar scans across the wave field shown in Fig. 1 which are obtained sequentially at a separation of Δs in the along-track direction might look like the functions shown in Fig. 7a. Again, a non-digitized version is shown for convenience. If the one-dimensional cross correlation function was computed for the two scans, it would look like that shown in Fig. 7b. The location of the peak of the cross correlation function should correspond to the offset, y_p , of the location of the dominant wave component on the second scan with respect to the location of the dominant wave component on the first scan and thus can be used as an estimate for this offset.

Actually, the cross correlation function computed for a single pair of scans separated by the distance Δs is an estimate for the true cross correlation function between scans of the stochastic process separated by the distance Δs and is noisy since the data scan is noisy. A smoothed cross correlation function estimate can be obtained by averaging the cross correlation function estimates for several pair of radar scans taken with the same separation.

Using the above ideas, the initial concept for the portion of the system which estimates the indicated propagation angle of the dominant wave component is specified as follows. First the cross correlation sequence estimate, $\hat{R}_{i_1 i_2}(u)$, for two N point radar scan sequences, i_{1n} and i_{2n} , separated by the distance Δs is computed as

$$\begin{aligned} \hat{R}_{i_1 i_2}(u) &= \frac{1}{N} \sum_{n=0}^{N-1-u} i_{1n} i_{2(n+u)} \quad u=0,1,\dots,N-1 \\ &= \frac{1}{N} \sum_{n=|u|}^{N-1} i_{1n} i_{2(n+u)} \quad u=-1,-2,\dots,-(N-1) \end{aligned} \quad (19)$$

This cross correlation sequence estimate is asymptotically unbiased and consistent.

Additional cross correlation sequence estimates are computed for several other pair of radar scans with the same separation and the resulting cross correlation sequence estimates are averaged to obtain a smoothed cross correlation sequence estimate. The location of the peak, \hat{y}_p , of the smoothed cross correlation estimate is determined by using a parabolic interpolation scheme like that defined in the previous section. The indicated wave propagation angle estimate, $\hat{\gamma}_I$, is then computed as

$$\hat{\gamma}_I = -\tan^{-1} \frac{\hat{y}_p}{\Delta s} \quad (20)$$

The indicated wave propagation angle, θ_I , that is estimated is not the true wave propagation angle, θ_w , defined in Fig. 1 since the two scans are not taken at the same time and wave motion has occurred between the times that the two scans were obtained.

4. WAVE PROPAGATION ANGLE AND WAVENUMBER COMPUTATION

At this point, an estimate of the wavenumber of the dominant wave component along the radar scans, k_y , and an estimate of the indicated propagation angle, θ_I , of the dominant wave component have been determined by the system. The next step is to use these estimates to compute the estimate of wavenumber, k_w , and the estimate of propagation angle, θ_w , for the dominant wave component. To do so, relations between, k_w , θ_w , k_y , and θ_I must be available. These are developed below.

First the relationship which can be used to determine θ_w from k_y and θ_I is considered. To begin, consider the geometry of the wave crests and radar scans shown in Fig. 8. where the ocean wave velocity, V_w , is taken as positive when it is away from the vehicle ground track, the wave propagation angle, θ_w , and the indicated propagation angle, θ_I , are measured counterclockwise from the radar scan direction as shown (note that both θ_w and θ_I lie in the range $-90^\circ < \theta < 90^\circ$), and the vehicle velocity, V_A , is defined positive to the right. The indicated propagation angle, θ_I , is

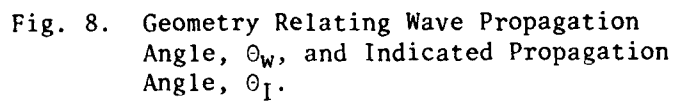
$$\begin{aligned}\theta_I &= \tan^{-1} \left[\frac{y_w - y_T}{V_A T} \right] \\ &= \tan^{-1} \left[\frac{V_A T \tan \theta_w - V_w T \sec \theta_w}{V_A T} \right] \\ &= \tan^{-1} \left[\tan \theta_w - \frac{V_w}{V_A} \sec \theta_w \right]\end{aligned}\quad (21)$$

Therefore

$$\frac{V_w}{V_A} \cos \theta_I = \sin \theta_w \cos \theta_I - \sin \theta_I \cos \theta_w \quad (22)$$

which yields

$$\theta_w = \theta_I + \sin^{-1} \left[\frac{V_w}{V_A} \cos \theta_I \right] \quad (23)$$



Equation 23 can be used to compute the wave propagation angle θ_w from the indicated propagation angle θ_I and the vehicle and wave velocities.

Equation 23 contains the wave propagation velocity, V_w , which would be unknown for a wavefield whose wavenumber and propagation angle are being estimated. However, the wave velocity is given in terms of the wavenumber by⁷

$$V_w = \pm \left(\frac{g}{k_w} \tanh k_w d \right)^{1/2} \quad (24)$$

where g is the acceleration due to gravity and d is the water depth. The wavenumber, k_w , can be expressed in terms of the wavenumber along the scan, k_y , and the wave propagation angle, θ_w , by

$$k_w = k_y / \cos \theta_w \quad (25)$$

Therefore, Eqn. 23 can be written as

$$\theta_w = \theta_I \pm \sin^{-1} \left\{ \frac{\cos \theta_I}{V_A} \left[\frac{g \cos \theta_w}{k_y} \tanh \left(\frac{k_y d}{\cos \theta_w} \right) \right]^{1/2} \right\} \quad (26)$$

Equation 26 is a transcendental equation relating the wave propagation angle, θ_w , to the indicated propagation angle, θ_I , the wavenumber along the scan, k_y , and the water depth, d . It cannot be easily solved for θ_w . However, the estimate for the wave propagation angle, $\hat{\theta}_w$, can be obtained from the estimate of the wavenumber along the scan, \hat{k}_y , and the estimate of the indicated propagation angle, $\hat{\theta}_I$, by iteratively solving the equation.

$$\hat{\theta}_w = \hat{\theta}_I \pm \sin^{-1} \left\{ \frac{\cos \hat{\theta}_I}{V_A} \left[\frac{g \cos \hat{\theta}_w}{\hat{k}_y} \tanh \left(\frac{\hat{k}_y d}{\cos \hat{\theta}_w} \right) \right]^{1/2} \right\} \quad (27)$$

with an initial guess of $\hat{\theta}_w = \hat{\theta}_I$. If the ocean area for which the estimates are being made is deep water ($d > \lambda_w/2$) then the hyperbolic tangent can be considered equal to unity and the water depth is not needed. For shallower water, the water depth would have to be obtained from other available bathymetry data for the area. Note that the second term on the right of Eqn. 27 is the required correction to the indicated propagation angle estimate to obtain the wave propagation angle estimate.

A problem exists with using Eqn. 27 to obtain the estimate for the wave propagation angle. This is that the sign associated with the correction term depends on whether the waves are approaching the vehicle flight path (negative sign) or receding from it (positive sign). This cannot be determined from the radar scan data due to the 180° ambiguity problem indicated in the introduction of this report. Thus, the sign can only be correctly assigned if the 180° ambiguity can be

resolved by using other sensor data.

It is not necessary to use Eqn. 27 to obtain the estimate for the wave propagation angle when radar scans obtained with a satellite-borne radar are used. This is true since satellite velocities are so much greater than wave velocities that negligible wave motion occurs between scans which means that $\theta_I \approx \theta_w$. Thus, the estimate for the indicated propagation angle, $\hat{\theta}_I$, can be used as the estimate for the wave propagation angle, $\hat{\theta}_w$, for estimates made from radar scan data obtained with a satellite. In this case, the water depth does not need to be known and the 180° ambiguity to be resolved to obtain a good estimate for the wave propagation angle.

For data obtained on an aircraft flight it is necessary to use Eqn. 27 to estimate the wave propagation angle. In this case, other sensor data would be required so the sign associated with the correction term can be correctly assigned and water depth would need to be known if the area was not a deep water area. Otherwise, the estimate of the wave propagation angle may be considerably in error.

After the wave propagation angle estimate has been computed for the dominant wave component, then it is a simple matter to compute the wavenumber estimate, \hat{k}_w , for this dominant wave component. The relation shown in Eqn. 25 is used to compute this estimate from the previously obtained estimates for wave propagation angle, $\hat{\theta}_w$, and the wavenumber along the scan, \hat{k}_y and gives

$$\hat{k}_w = \hat{k}_y / \cos \hat{\theta}_w \quad (28)$$

5. SUMMARY OF INITIAL SYSTEM CONCEPT

Since the development of the initial system concept for determination of the wavenumber and propagation angle of the dominant ocean wave component in an area from a few digitized focused radar scans has been spread over several sections it is deemed appropriate to briefly summarize the steps here. They are:

- (1) Obtain a few digitized focused radar scans with a simplified SAR processor on-board a satellite or an aircraft.
- (2) Transmit the radar scan data to a processing station.
- (3) Convert the radar scans from slant-range coordinates to ground-range coordinates.
- (4) Compute an estimate of the wavenumber along the scan, \hat{k}_y , by computing smoothed periodograms for each scan, averaging the smoothed periodograms and determining the location, \hat{k}_y , of the peak of the average periodogram using parabolic interpolation.

- (5) Compute an estimate of the indicated wave propagation angle, $\tilde{\theta}_I$, by computing the cross correlation sequence for several pairs of scans separated by the same distance, Δs , averaging the cross correlation sequences, determining the location, \tilde{y}_p , of the peak of the average cross correlation sequence using parabolic interpolation, and computing the estimate of the indicated propagation angle as $\tilde{\theta}_I = -\tan^{-1} (\tilde{y}_p / \Delta s)$.
- (6) Compute the estimate of the dominant wave component propagation angle, $\tilde{\theta}_w$, by iteratively solving

$$\tilde{\theta}_w = \tilde{\theta}_I \pm \sin^{-1} \left\{ \frac{\cos \tilde{\theta}_I}{V_A} \left[\frac{g \cos \tilde{\theta}_w}{\tilde{k}_y} \tanh\left(\frac{\tilde{k}_y d}{\cos \tilde{\theta}_w}\right) \right]^{1/2} \right\}$$

with an initial guess of $\tilde{\theta}_w = \tilde{\theta}_I$.

- (7) Compute the estimate of the dominant wave component wavenumber, \tilde{k} , by solving

$$\tilde{k}_w = \tilde{k}_y / \cos \tilde{\theta}_w$$

B. SYSTEM AND PERFORMANCE PARAMETERS

There are a number of system parameters which must be determined for an actual system implementation. These include: (1) number of scans to be generated and used in the estimation, N_s , (2) the length of the scans, SL , (3) the distance between scans, Δs , and (4) the type and width of lag window to be used in the power spectrum estimation. Reasonable values for these parameters will be determined in subsequent sections by performing performance tradeoffs.

System performance indications are necessary in order to be able to evaluate system feasibility, performance, and parameter tradeoffs. The system is analyzed using the Monte Carlo technique to obtain performance statistics. Statistical performance parameters identified as performance indicators are: (1) mean, μ_k , and standard deviation σ_k of wavenumber estimates, and (2) mean, μ_θ , and standard deviation σ_θ , of propagation angle estimates. Additional performance parameters include the percentage of cases for which a valid (convergent) estimate can be obtained and the percentage of cases for which propagation angle estimates are within certain angular constraints.

III. DATA USED AND ANALYSIS METHODS

This section first describes the SAR data used in the evaluation of system performance. The discussion of data used is followed by a description of the analysis methods used.

A. DATA USED

In order to evaluate the system, individual digitized focused radar scans were selected from existing SAR images. Digitized SAR images were obtained which had been generated on both aircraft and SEASAT-A satellite flights. The data used was that generated on aircraft flights since it was better and thus was more appropriate for initial feasibility studies. The plan was to perform evaluations using the SEASAT-A data after the feasibility had been shown using the aircraft generated data. The SEASAT-A data was not used since consistently good results were not achieved with the aircraft generated data.

Digital data used for system evaluation was generously supplied by the Environmental Research Institute of Michigan (ERIM). The SAR images, originally obtained as part of a feasibility study for the SEASAT-A program, were taken of ocean waves off the coast of Marineland, Florida, on December 14, 1975. Several images using different flight paths were generated by both X-band and L-band radars. A total of 22 images were supplied, most of which were taken over the same local wave field. Of these, 10 X-band images, 9 of which view the same local wave field from several different aspect angles, were used.

The images were classified as follows. Two of the images supplied were in slant-range format and are labelled images A and B. The remaining 8 images used were supplied in geometrically (i.e. converted to ground-range) and radiometrically corrected form. These images are identified by the codes C-1 through C-8. The radiometric correction used is simply a process of subtracting from each digital range scan the average of all scans on a given image. The purpose of the radiometric correction is to remove noise effects that were common to the digitization process as well as to compensate for attenuation effects in the main lobe of the antenna pattern.

During the experiment when the images were being taken, ocean wave measurements were also being collected by a pitch-and-roll buoy. Therefore, ground truth data is available at one location for comparison. The dominant wave component wavenumber along the direction of propagation of the wave field imaged was obtained from the pitch-and-roll buoy measurements and was found to be $k_w = 0.076$ rad/m. This corresponds to a wavelength of $\lambda_w = 82.6735$ m. The propagation direction of the wave field was found to be 270° measured clockwise from due north (i.e. the waves are propagating to the west toward the coast). Finally, the time period between successive wave crests was measured to be approximately

8 seconds yielding a wave propagation velocity of $V_w = 10.33\text{m/sec.}$

As an example of the SAR ocean wave images used, consider the images shown in Figs. 9a and 9b. Figure 9a is a non-digital version of the image identified by the letter A. The aircraft ground track is to the right along the upper edge of the image and waves seen are propagating down across the image. The resolution of this image as well as image B is 3m in range and 4.5m in azimuth (along-track). Image A was used extensively in the analysis of the proposed system because the pitch-and-roll buoy is contained in this image. The pitch-and-roll buoy can be identified as the first from the left of four bright spots located near the center of the image shown in Fig. 9a. The buoy location is indicated by arrows in Figs. 9a and 9b for clarity. An expanded view, in digitized format, of the buoy area (area subsequently labelled A-1) is shown in Fig. 9b. In this view, the extremely noisy nature of the data is evident.

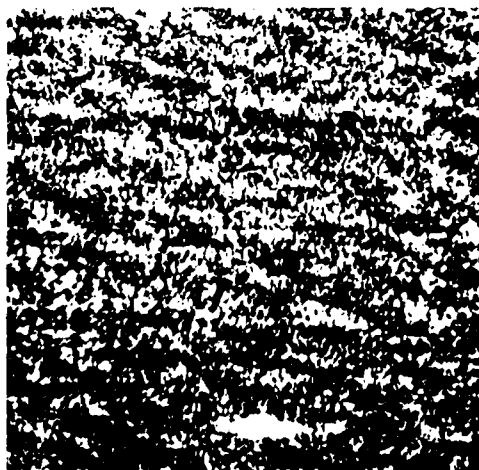
The aircraft used in the generation of image A was flying at a velocity of 81.09 m/sec. The flight ground track is taken left to right along the top of the image shown in Fig. 9a and is heading in a direction measuring 160° clockwise from north. Since the wave field is travelling in a direction due west (270° clockwise from north) at a velocity $V_w = 10.33\text{ m/sec.}$, the wave propagation angle is $\theta_w = -20^\circ$ and the indicated wave propagation angle given by Eqn. 21 is $\theta_I = -26.54^\circ$. Since the image shown in Fig. 9 is in slant-range format, the apparent angle of -26.54° is not seen on the image. This is because of the non-linear distortion of ground-range distances along the slant-range coordinate. Coincidentally, the slant-range distortion of the image shown nearly compensates the indicated wave propagation angle due to the imaging process. Thus, the waves appear to be travelling due west as indeed they are.

Flight information for all of the images used is given in Table II. The information in Table II, coupled with the knowledge of the ocean wave field given by the pitch-and-roll buoy data, can be used to compute the indicated wave propagation angle, θ_I . This data is summarized in Table III for the selected images. The dominant wave component wavenumber along a given scan in ground-range coordinates, $k_y = k_w \cos \theta_w$, and the direction of wave travel are also given in Table III.

In reference to Tables II and III, it is seen that the ocean wave parameters for image A are identical with those of image C-4. Indeed the geometrically and radiometrically corrected image C-4 was obtained from a selected area of the much larger slant-range image A. Also, note that the flight information (Table II) for images B and C-2 is identical. In this case, images B and C-2 were obtained during the same flight pass; however, image B was obtained during the later part of the pass. Specific information about image B was not provided and the ocean wave parameters for image B (Table III) are approximations inferred from measurements on photographs of the digitized image as well as the assumption that the wave field observed was a deep water wave with a fundamental time period of 8 seconds between crests.



(a) X-band Non-digital Version of Image A.



(b) Digitized Version of Buoy Area.

Fig. 9. Examples of SAR Ocean Wave Images.
Images are Shown in Slant-Range Format.

Table II. Flight Information for Images Selected for System Evaluation.

Image	Aircraft Altitude (m)	Aircraft Velocity (m/sec)	Aircraft Heading [†] (deg)
A	4023	81.09	160
B	4023	77.01	70
C-1	4023	81.09	25
C-2	4023	77.01	70
C-3	4023	75.48	115
C-4	4023	81.09	160
C-5	4023	82.62	205
C-6	4023	85.17	250
C-7	4023	88.74	295
C-8	4023	85.68	340

[†] Flight headings are measured clockwise from north.

Table III. Ocean Wave Parameters for Selected Images.

Image	k_w (rad/m)	θ_w (deg)	θ_i (deg)	k_y (rad/m)	Sign of v_w
A	0.076	-20	-26.54	0.071	+
B	0.063	38	44.50	0.050	-
C-1	0.076	25	31.25	0.069	-
C-2	0.076	70	72.33	0.026	-
C-3	0.076	-65	-67.95	0.032	+
C-4	0.076	-20	-26.54	0.071	+
C-5	0.076	25	18.18	0.069	+
C-6	0.076	70	67.32	0.026	+
C-7	0.076	-65	-61.85	0.032	-
C-8	0.076	-20	-13.26	0.071	-

Table IV gives the digitization parameters for each of the images used. It should be noted that the pixel dimensions for images A and B are smaller than the resolution parameters for the images. Each range resolution cell contains 2 pixels and each azimuth resolution element contains 3 pixels. Images classified by code C all have equal resolution and pixel dimensions (6m x 6m). The larger resolution cells were created by ERIM when processing the original radar data to provide some image smoothing.

Before analysis could begin, images A and B had to be converted from slant-range coordinates to ground-range coordinates. The spacing for the points in ground-range coordinates was chosen to be equal to that for the points in slant-range coordinates (i.e. 1.5m). The number of points, N_r , in the sinc reconstruction equation (Eqn. 3) was chosen to be 40 in a compromise between accuracy and required computation time.

Selection of parameters y_{g1} and J (see Eqn. 6) required some consideration of the given slant-range data. As discussed earlier, y_{g1} must be selected in order to reduce resolution smearing at ground-range locations close to nadir. The value of $y_{g1} = 1406m$ was selected and the remaining scan data was converted from slant-range to ground-range coordinates. From Table IV it is seen that the total number of slant-range samples per scan is 1982. If ground-range sample values are to be reconstructed from these 1982 points using an $N_r = 40$ point reconstruction algorithm, then the last ground-range location that can be reconstructed must translate to a slant-range location that is less than or equal to 1962 (i.e. $1982 - N_r/2$) sample points. Slant-range pixel location 1962 can be translated to a ground-range location in meters by using the geometry shown in Fig. 3 and is given by

$$\begin{aligned} y_{gmax} &= \sqrt{(4023 + 1962 \cdot 1.5)^2 - 4023^2} \\ &= 5686m \end{aligned} \quad (29)$$

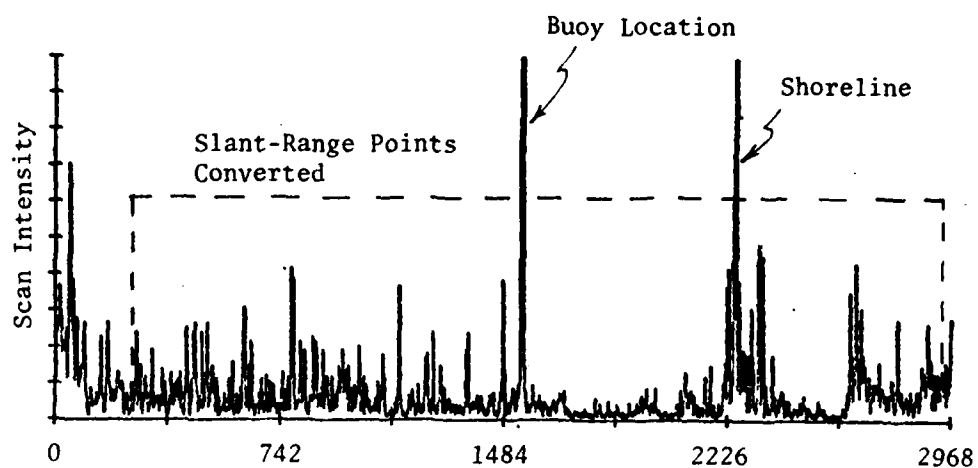
Therefore, the total number of ground-range points to be reconstructed is given by

$$\begin{aligned} J &= [(y_{gmax} - y_{g1})/\Delta y_g] \\ &= [(5686 - 1406)/1.5] \\ &= 2853 \text{ samples} \end{aligned} \quad (30)$$

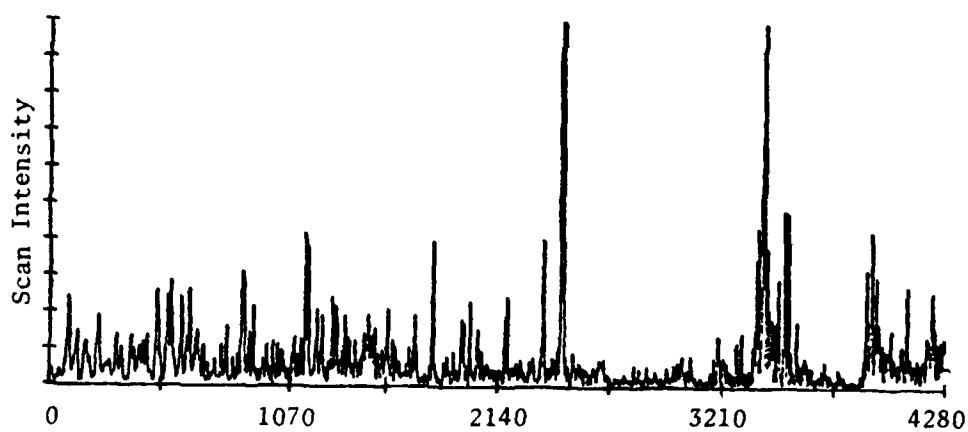
As an example of the conversion process, consider the slant-range and ground-range versions of scan number 274 of image A shown in Figs. 10a and 10b respectively. Several distinctive features are easily recognized in Fig. 10a when compared to the image shown in Fig. 9a. The buoy location and approximate shoreline location are identified for reference. Also shown in Fig. 10a are the slant-range locations that are actually converted. These locations are enclosed by a rectangular window (shown in dash marks). When comparing Figs. 10a and 10b it should

Table IV. Specifications for Actual Digitized Images Used.

Image	Data Format	Pixel Dimension (m)	Number of Lines	Pixels Per Line
A	slant-range	1.5 x 1.5	1362	1982
B	slant-range	1.5 x 1.5	1362	1982
C-1	ground-range	6 x 6	256	256
C-2	ground-range	6 x 6	256	256
C-3	ground-range	6 x 6	256	256
C-4	ground-range	6 x 6	256	256
C-5	ground-range	6 x 6	256	256
C-6	ground-range	6 x 6	256	256
C-7	ground-range	6 x 6	256	256
C-8	ground-range	6 x 6	256	256



(a) Distance Along Scan (m)



(b) Distance Along Scan (m)

Fig. 10. (a) Slant-Range Data for Scan Number 274 of Image A (see Fig. 9).

(b) Corresponding Ground-Range Data for Enclosed Slant-Range Data in (a).

be noted that the origin in Fig. 10a represents the radar return intensity from nadir while the origin in Fig. 10b corresponds to the radar return intensity at a ground-range distance of 1406m from nadir. Even though an initial ground-range location of 1406m was chosen to prevent resolution smearing, some resolution degradation can be seen for ground-range locations near the origin in Fig. 10b. Figures 11 and 12 shown an expanded version of the scan in ground-range coordinates illustrated in Fig. 10b. Note the noisy nature of the data which obscures the expected dominant wave component.

Some system analyses were performed using radar scan data which was smoothed by averaging image data from 25 points in a square area surrounding each data point. This was done in an attempt to improve performance by reducing the data noisiness with smoothing. In an actual system, this type of smoothing would require generation of more scans than actually required so averaging could be done prior to storing the data. This would be possible if the individual pulse returns were closer together than the final resolution required. Figure 13 shows the 25 point averaged version of the same scan previously shown in Fig. 10b. Figures 14 and 15 show the expanded version of this averaged scan and can be compared with the non-averaged scan shown in Figs. 11 and 12. The smoothing of the noise is apparent.

Table V identifies the specific locations of the areas within the selected images (in ground-range coordinates) that were used for analysis. Analysis areas within the selected images are identified by their center locations for convenience. As an example, analysis area A-1 is centered about line 320 (out of 1362) and ground-range pixel number 1336 (out of 2853) on the ground-range corrected version of digital image A. Figure 9b displays the image area described by area A-1 and a portion of image areas A-2 and A-3. Additional image photographs for analysis areas A-4, A-5 and B-1 are given in Appendix A. No photographs were generated for images C-1 through C-8. The approximate position of the pitch-and-roll buoy in digital image A is given by scan line 274 and ground-range pixel number 1622; therefore, it is anticipated that ground truth information obtained from pitch-and-roll buoy data will be especially accurate for image analysis areas A-1, A-2 and A-3 (see Table V).

B. SYSTEM ANALYSIS METHODS

Analyses of estimates of along-scan wavenumber and indicated propagation angle for the dominant wave component were made using the Monte Carlo technique to obtain values for the statistical performance parameters previously indicated. These estimates proved not to be consistently reasonable and could not be expected to lead to consistently reasonable results for estimates of the wavenumber and propagation angle of the dominant wave component. Therefore, the final system step of computing estimates of the wavenumber and propagation angle of the dominant wave components from the estimates of the along-scan wavenumber and the indicated propagation angle was not considered.

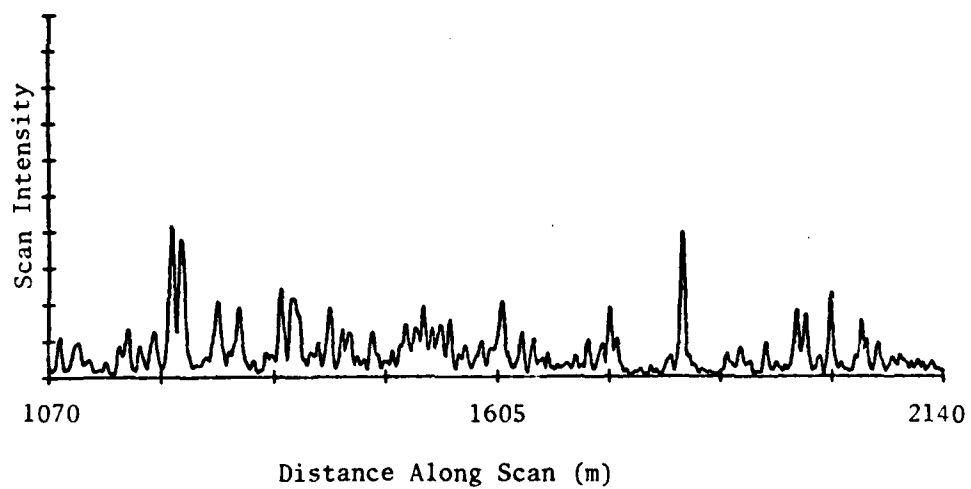
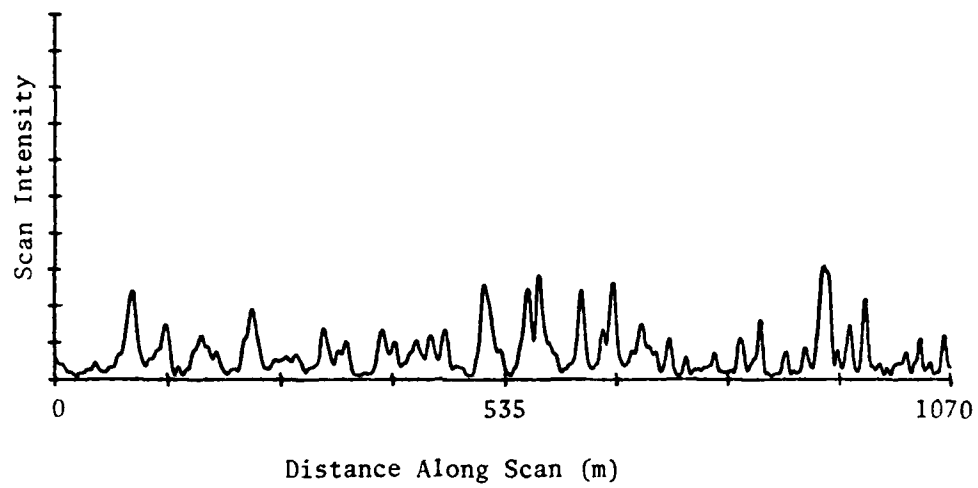


Fig. 11. Expanded View of the First 2140 Meters of the Ground-Range Scan Shown in Fig. 10b.

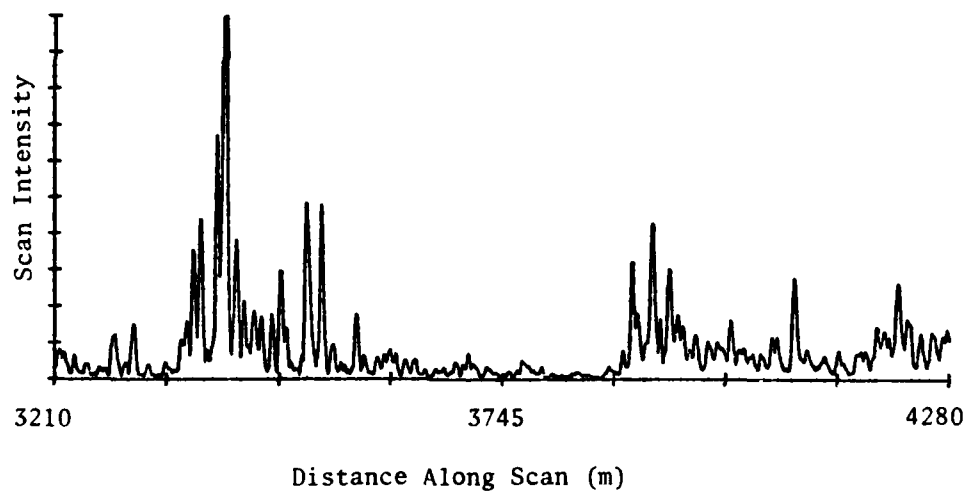
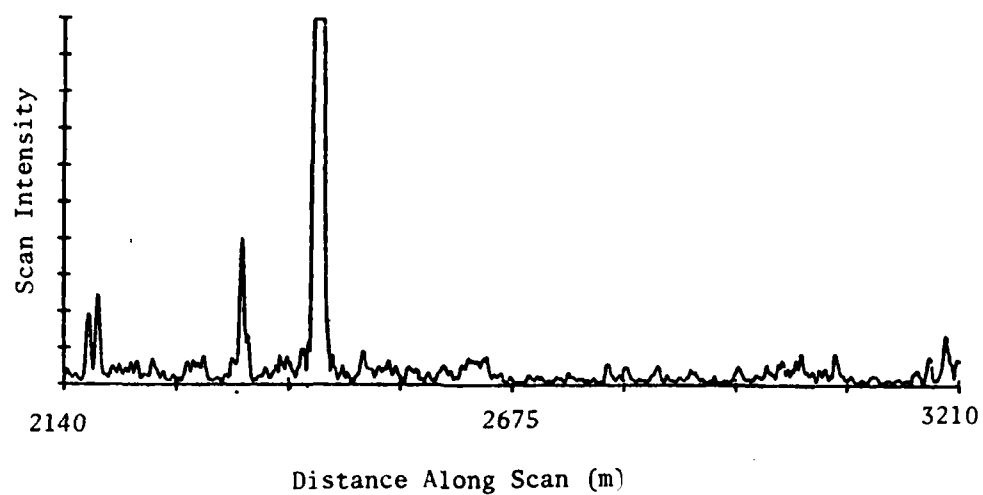


Fig. 12. Expanded View of the Second 2140 Meters of the Ground-Range Scan Shown in Fig. 10b.

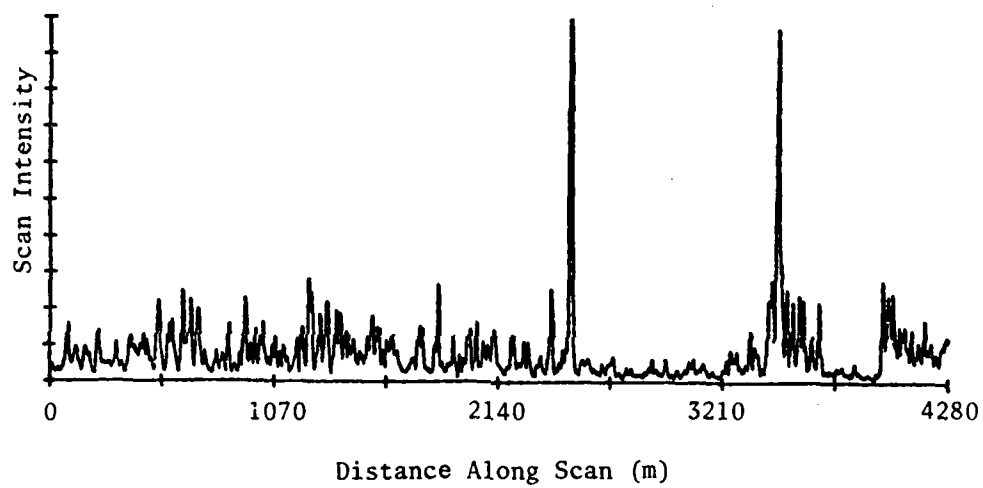


Fig. 13. Ground-Range Scan of Fig. 10b with
25 point (5x5) Averaging.

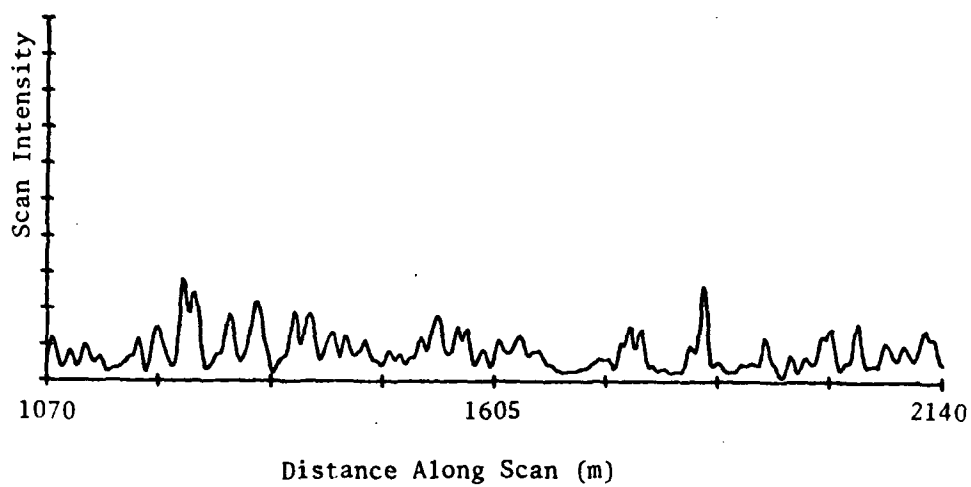
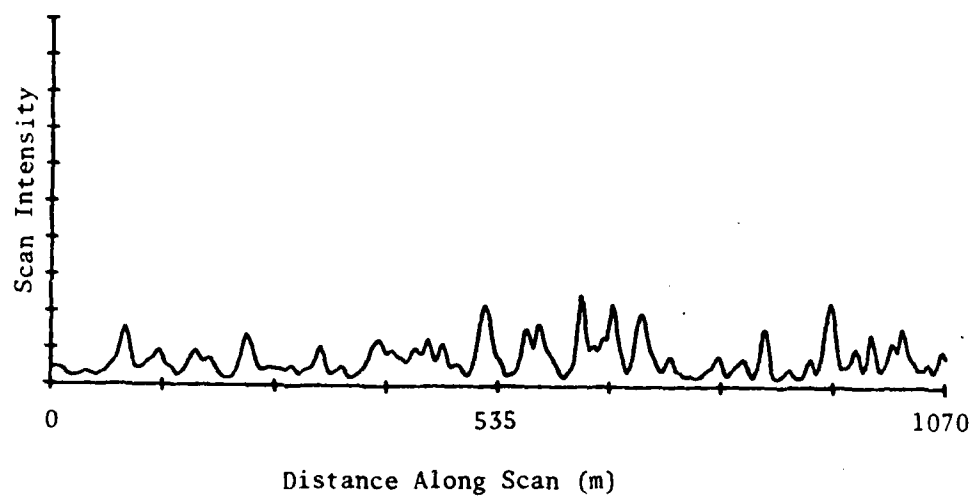


Fig. 14. Expanded View of the First 2140 Meters of the Ground-Range Scan Shown in Fig. 13.

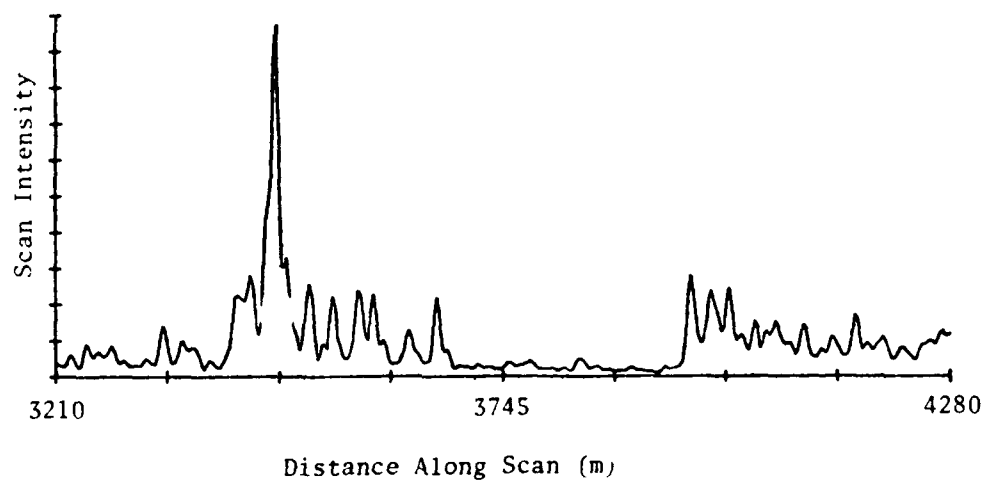
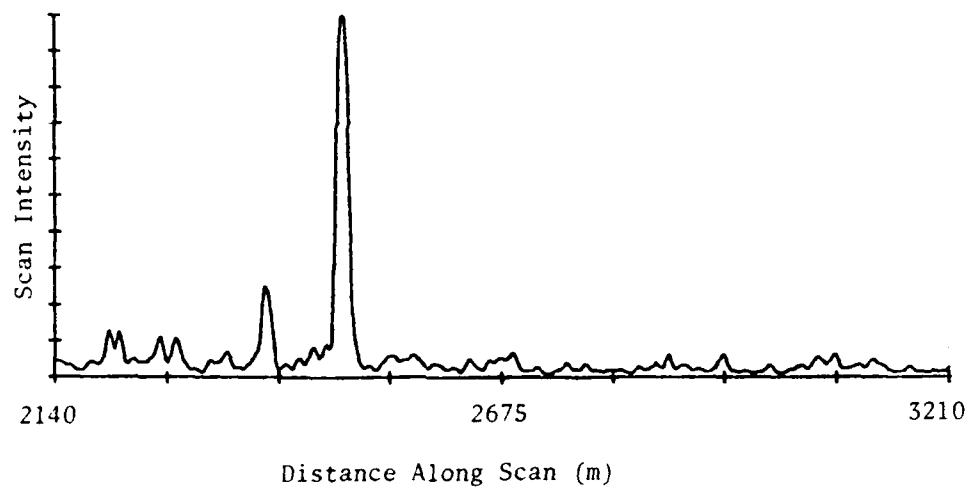


Fig. 15. Expanded View of the Second 2140 Meters of the Ground-Range Scan Shown in Fig. 13.

Table V. Identification of Analysis Areas
Used from Selected Images

Image-Area	Center Coordinates	
	Line	Pixel Number
A-1	320	1336
A-2	320	1000
A-3	330	1190
A-4	681	1066
A-5	1032	1190
B-1	681	667
C-1	126	128
C-2	126	128
C-3	126	128
C-4	126	128
C-5	126	128
C-6	126	128
C-7	126	128
C-8	126	128

In order to use the Monte Carlo technique, estimates of along-scan wavenumber and indicated propagation angle must be computed with a given set of system parameters for a number of individual cases within a particular analysis area. Sample means and standard deviations can then be computed for these estimates. These sample statistics are good approximations of the true statistics for the estimates of along-scan wavenumber and indicated propagation angle if a large enough set of statistically independent cases can be evaluated in each analysis area.

For most system parameter combinations used, it was possible to compute estimates for 20 cases and still stay within a reasonably small area where wave parameters could sensibly be assumed to be constant. The bulk of the analysis was done with the images whose scans were separated by 1.5m (images A and B). Since this separation is much closer than would be reasonable to use in an actual system, individual cases used non-adjacent scans and were interleaved to make use of all data in an analysis area and thus keep the area as small as possible. This interleaving of cases to obtain 20 analysis cases is illustrated in Fig. 16 for a system with scan separation, Δs , equal to 5 image scan spacings and number of scans, N_s , equal to 3.

Adjacent image scans are definitely not statistically independent. Thus the sample means and standard deviations computed are not as good estimates of the true statistics as could be obtained if each case were statistically independent of the others. This is particularly true when the smoothed data obtained by averaging 25 data points surrounding each data point is used. However, the resulting individual case estimates of along-scan wavenumber and indicated propagation angle exhibit enough independence when the complete set of cases in each analysis area is considered to indicate that the sample statistics computed are probably a reasonable indicator of performance.

The basic analysis procedure specified for determining performance in a given analysis area for a particular set of system parameters is as follows:

- (1) Select the scans to be used for the individual cases in an analysis area based on the number of scans to be used by the system and the desired scan spacing.
- (2) Compute smoothed periodograms for all scans using the portion of the scans corresponding to the desired scan length.
- (3) Average the smoothed periodograms for all the system scans corresponding to each case.
- (4) Compute the estimate of the along-scan wavenumber for each case by locating the peak of the averaged periodogram using parabolic interpolation.

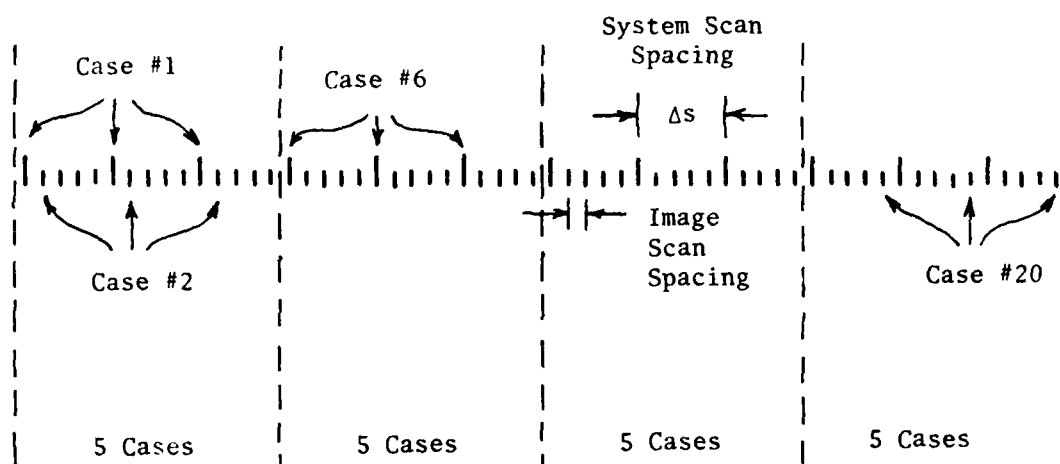


Fig. 16. Locations of Image Scans for 20 Cases
when $N_S = 3$ and $\Delta s = 5 \times \text{Image Scan Spacing}$.

(5) Compute the sample mean and standard deviation of the estimate of along-scan wavenumber from the individual case estimates computed in step (4).

(6) Compute cross-correlation functions for all pairs of scans with the desired separation for each case.

(7) Average the individual cross correlation functions computed for each case to obtain a smoothed cross-correlation function for that case.

(8) Compute the estimate of the indicated propagation angle for each case by locating the peak of the average cross-correlation functions using parabolic interpolation.

(9) Compute the sample mean and standard deviation of the estimate of indicated propagation angle from the individual case estimates computed in step (8).

Trade-offs for system parameter selection require that all but one system parameter be held constant while the given parameter is varied and performance computed. Therefore, some of the parameters must be initially set by intuitive observations rather than statistical evaluation. In fact, initial single case observations of system performance for a range of parameter values were made to establish rough choice of all system parameters. Once these rough choices had been made, then they were refined with the more rigorous statistical evaluation.

Initial observations of the performance of a few single cases was found to indicate the necessity of modifying the system concept for estimation of indicated propagation angle before it was reasonable to proceed with a statistical performance evaluation. The necessity of modifying the concept for estimation of along-scan wavenumber was also indicated after initial statistical results were obtained. These system modifications are discussed in the sections describing performance results when the need for them is indicated.

It is desirable to analyze system performance for waves of different along-scan wavenumbers and different indicated propagation angles with respect to the radar scan directions. In order to do this with images A and B, for which most of the analysis was done, the image analysis areas were resampled along rotated scan lines within the image. The rotated image analysis area is defined in Fig. 17. The rotation angle, θ_r , is measured counter-clockwise with respect to the initial scan direction as shown. A computer program was written to first compute the location of new image sample points such as the top right hand point (x'_i, y'_i) of the rotated image area shown in Fig. 17. After the new sample point locations were determined, then the sample values at these locations were computed. This was done with a simple two-dimensional linear interpolation from the initial sample values of the images obtained from ERIM. The indicated wave propagation angle with respect to the rotated scans is

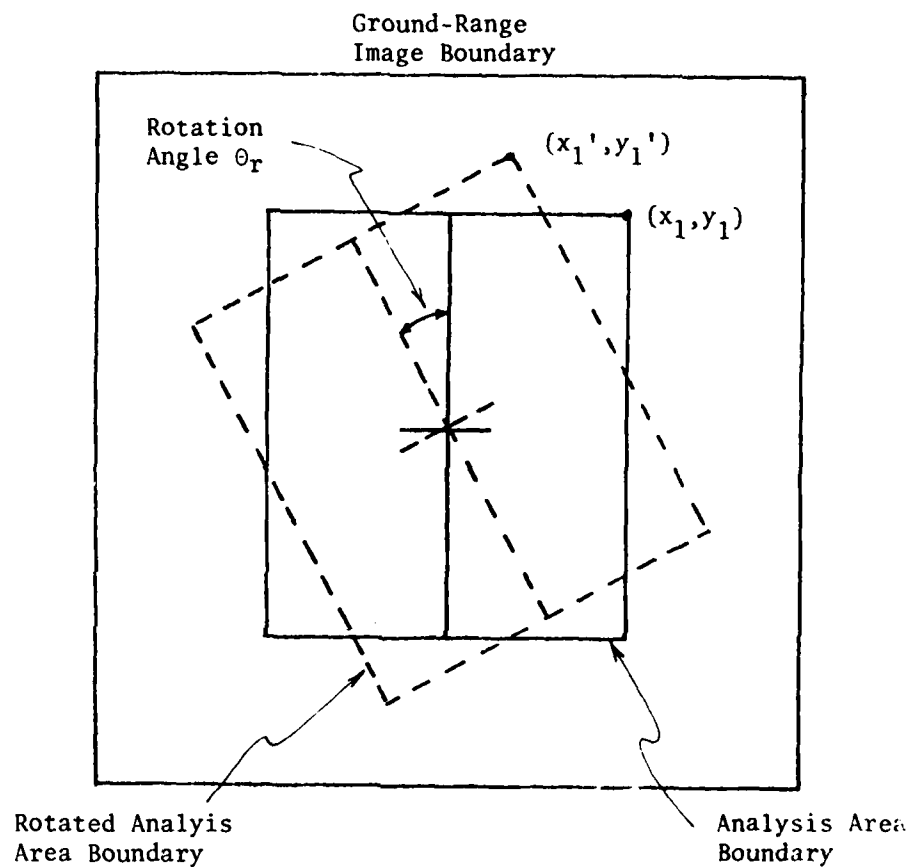


Fig. 17. Rotation of Image Area to Produce a Different Along-Scan Wavenumber and Indicated Propagation Angle for the Dominant Wave Component.

$$\theta_{Ir} = \theta_r - \theta_I \quad (31)$$

and the wavenumber along the rotate scans is

$$k_{yr} = k_y \cos \theta_{Ir} / \cos \theta_I \quad (32)$$

It should be noted that resampling the image along rotated scans is not quite equivalent to generating these scans with a different radar scan direction resulting from a different vehicle flight direction. This is true since radar backscatter characteristics are different for radar energy coming from different directions with respect to the wave propagation direction. It was for this reason that the 8 images designated as the C series were obtained from ERIM and considered. These are all images of the same area and a look at Table II reveal that they are obtained for flight path directions which proceed around the image area in 45° increments.

Results obtained using the above analysis methods are presented in the following two major sections of this report. The first section considers the system performance in estimating the along-scan wavenumber and the second section considers the system performance in estimating the indicated propagation angle.

IV. ANALYSIS OF ALONG-SCAN WAVENUMBER ESTIMATION PERFORMANCE

The performance of the portion of the system which estimates the dominant wave component wavenumber along the scan is analyzed in this section and results presented. The along-scan wavenumber estimate will be referred to as simply a wavenumber estimate in most cases in this analysis for text simplicity. However, in reading the text it should be remembered that the estimate being considered is the dominant wave component wavenumber along the scan.

The analysis includes system parameter trade-offs and leads to some system concept modifications to improve performance. The system parameter trade-offs are performed with data from an image area closest to the ground-truth buoy (area A-1). This is followed by consideration of performance when data from other areas is used.

A. PRELIMINARY ANALYSES AND PARAMETER SELECTION

One-dimensional power spectrum estimates (periodograms) were initially computed for sinusoidal test sequences in order to debug and verify computer programs required for the smoothed periodogram generation algorithm shown in Table I. Once the computer program was checked out, periodograms were generated for several radar scans to obtain preliminary observations. For these preliminary trials, image analysis area A-1 was used. Seven examples of radar scan segments and their corresponding non-smoothed periodogram are shown in Figs. 18 through 24. The scans shown are scans number 214, 234, 254, 274, 294, 314 and 334 of image A and contain every other sample of the original segment on the supplied digital image. The resulting sample spacing is 3 meters which is the same as the slant-range resolution for the image. This 3 meter sample spacing was used throughout the analysis to reduce computation time requirements except where a change is specifically noted. Since the image is oversampled, use of every other data point does not affect results significantly.

Using Eqn. 18, the along-scan wavenumber estimates found from the peak locations of the periodograms are $k_y = 0.068, 0.211, 0.074, 0.179, 0.071, 0.089$ and 0.324 (rad/m) for scans 214 through 334, respectively. The majority of these values compare favorably with the along-scan wavenumber of 0.071 rad/m given in Table III for image A. However, a number of the estimates are considerably in error and thus indicate the need for periodogram smoothing and averaging. Note that Figs. 18 through 24 indicate that periodogram averaging can be expected to lead to improved wavenumber estimates since secondary peaks in the correct location usually occur even when the preliminary peak is in the wrong location. The above wavenumber estimate results for a few individual scans were sufficiently encouraging to permit continuing with the evaluation of preliminary selections for the system parameters.

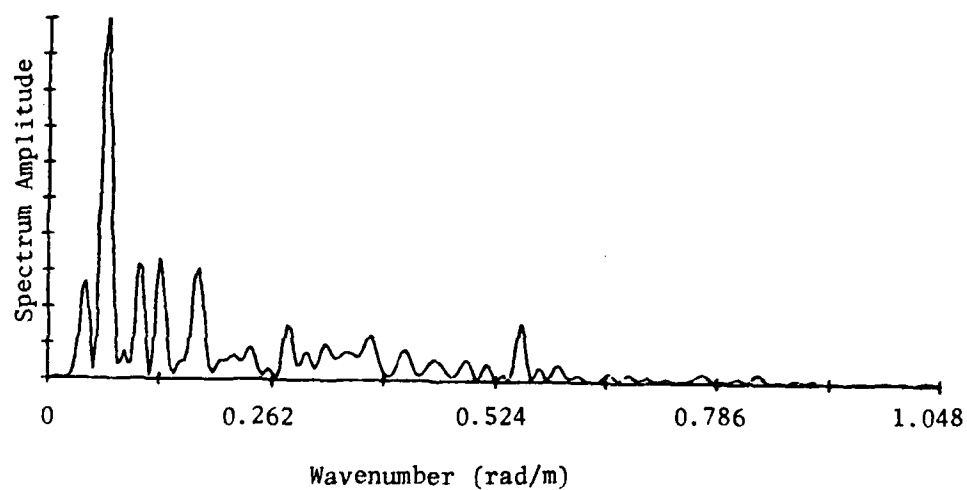
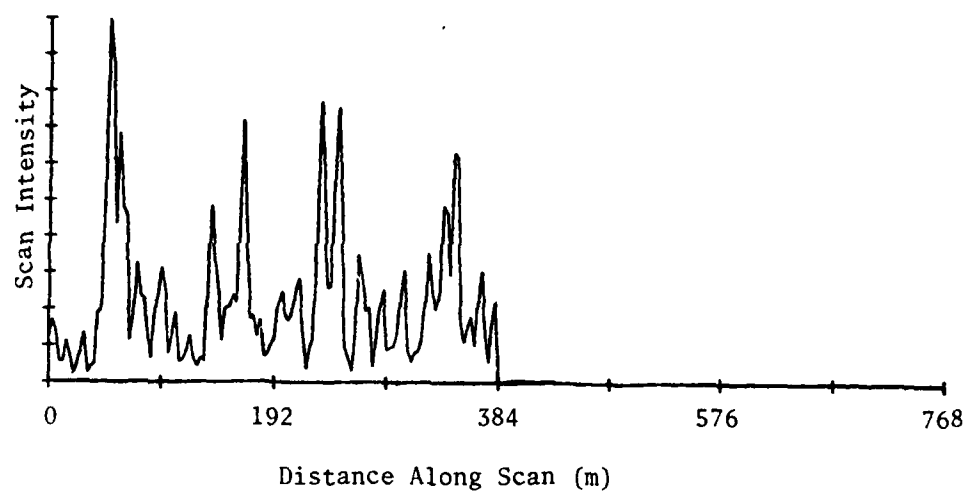


Fig. 18. Radar Scan Segment and Corresponding Non-Smoothed Periodogram for Scan 214 from Analysis Area A-1.

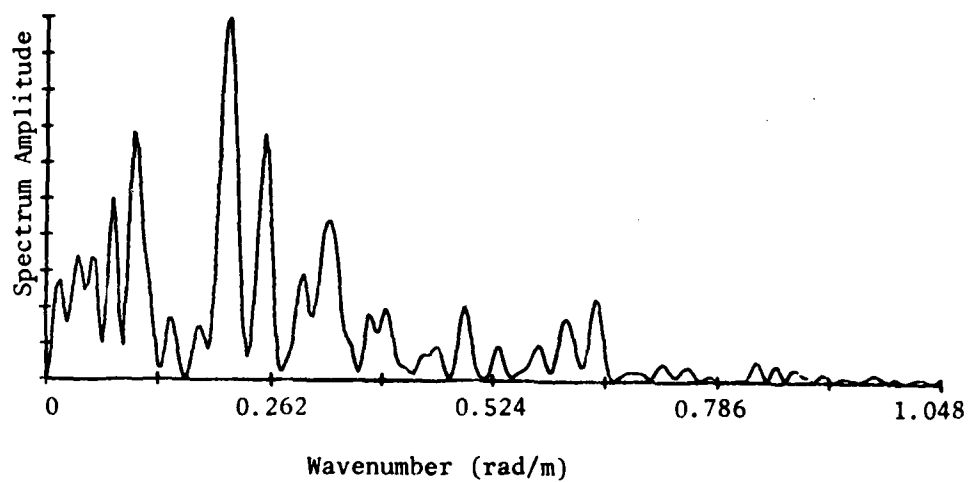
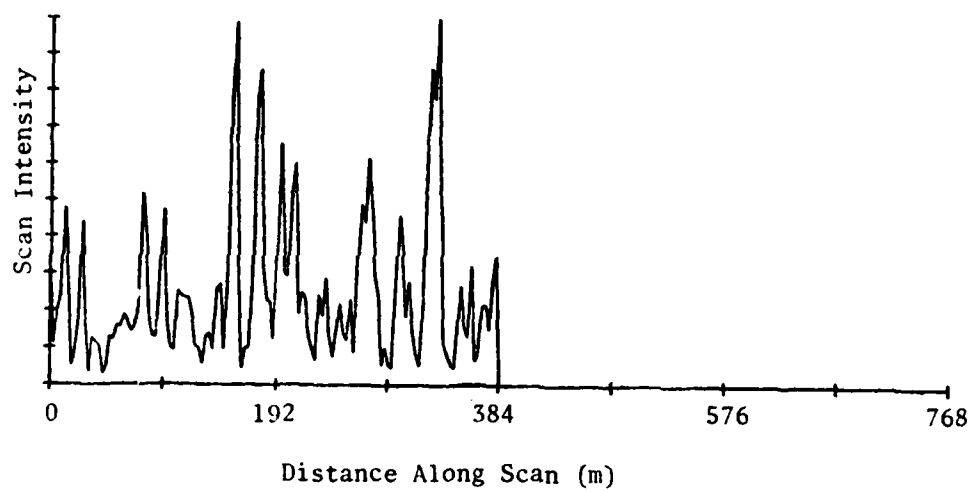


Fig. 19. Radar Scan Segment and Corresponding Non-Smoothed Periodogram for Scan 234 from Analysis Area A-1.

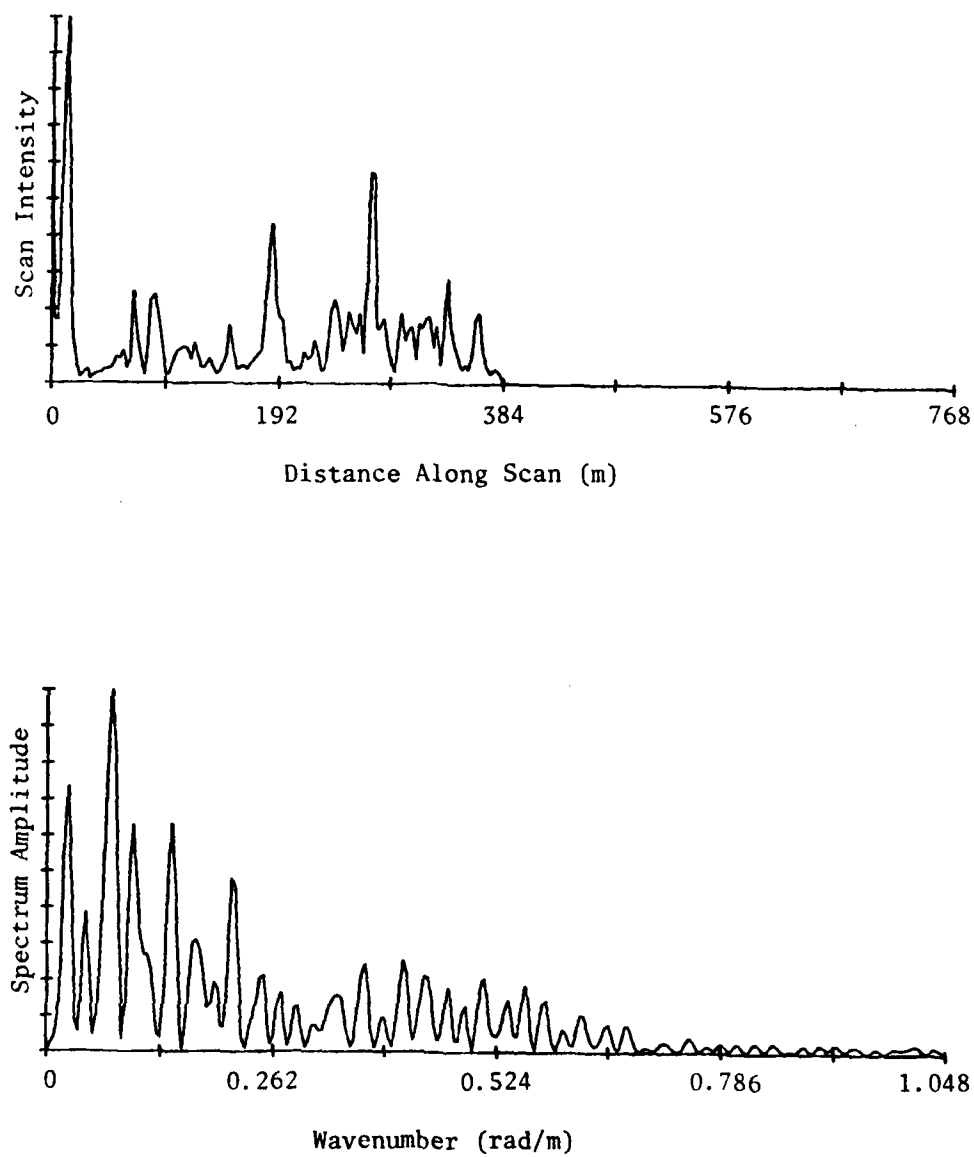


Fig. 20. Radar Scan Segment and Corresponding Non-Smoothed Periodogram for Scan 254 from Analysis Area A-1.

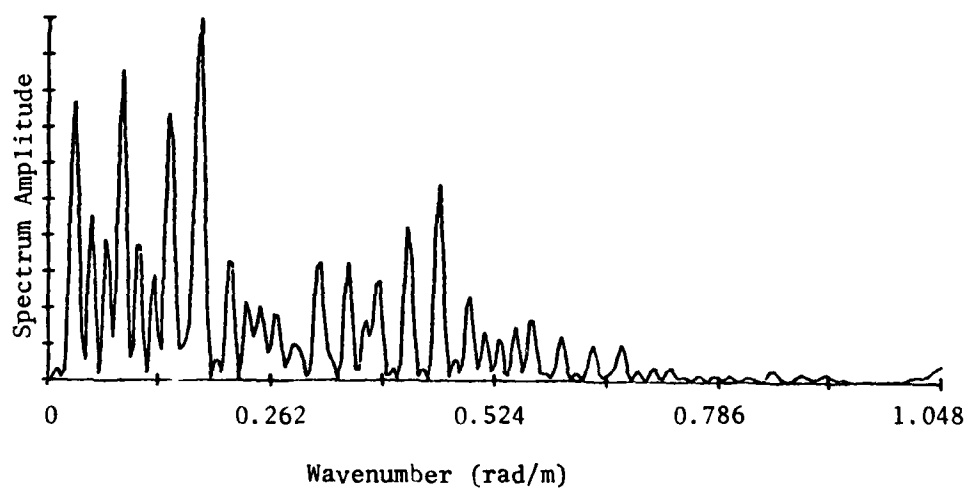
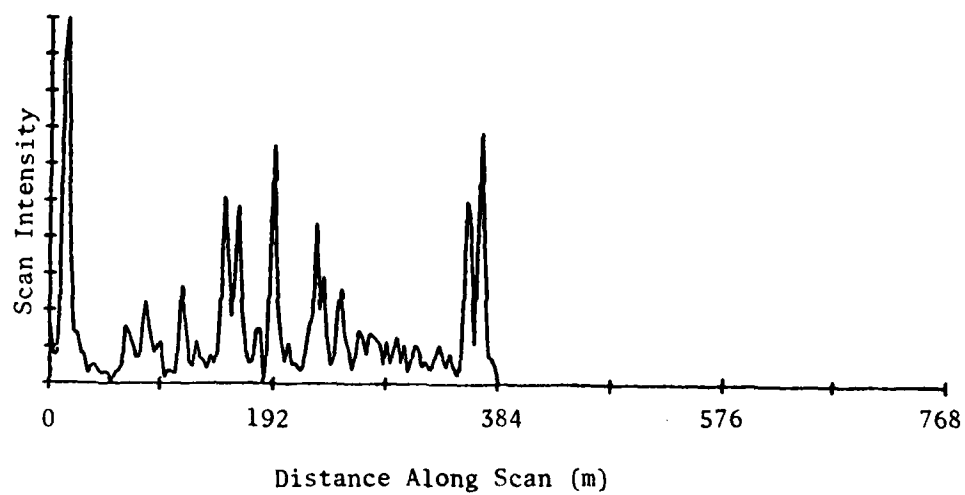


Fig. 21. Radar Scan Segment and Corresponding Non-Smoothed Periodogram for Scan 274 from Analysis Area A-1.

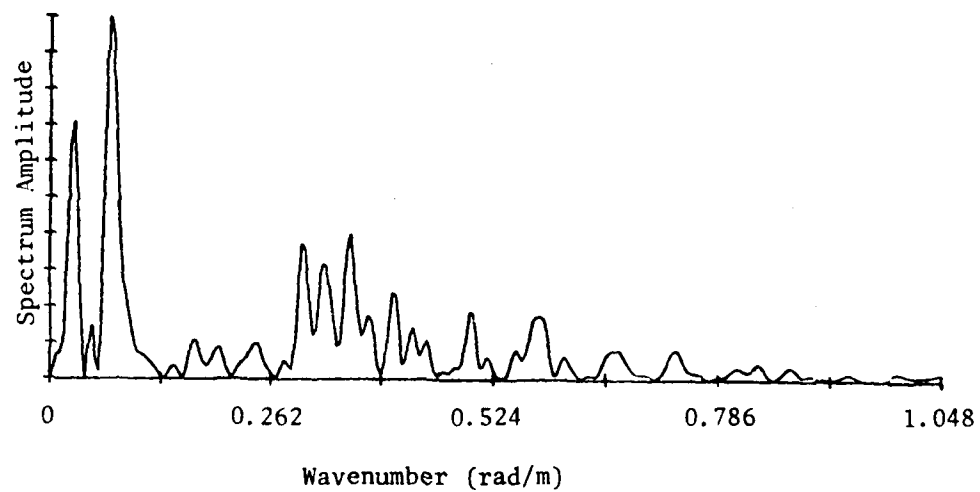
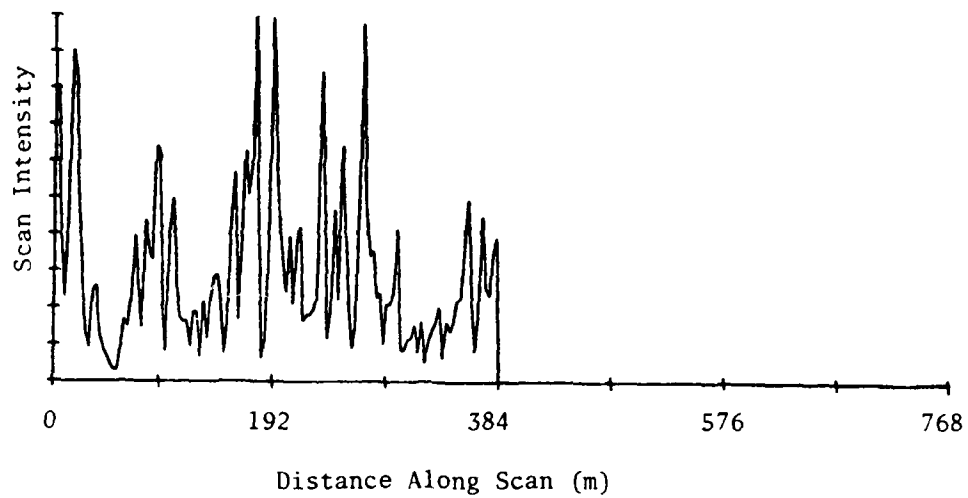


Fig. 22. Radar Scan Segment and Corresponding Non-Smoothed Periodogram for Scan 294 from Analysis Area A-1.

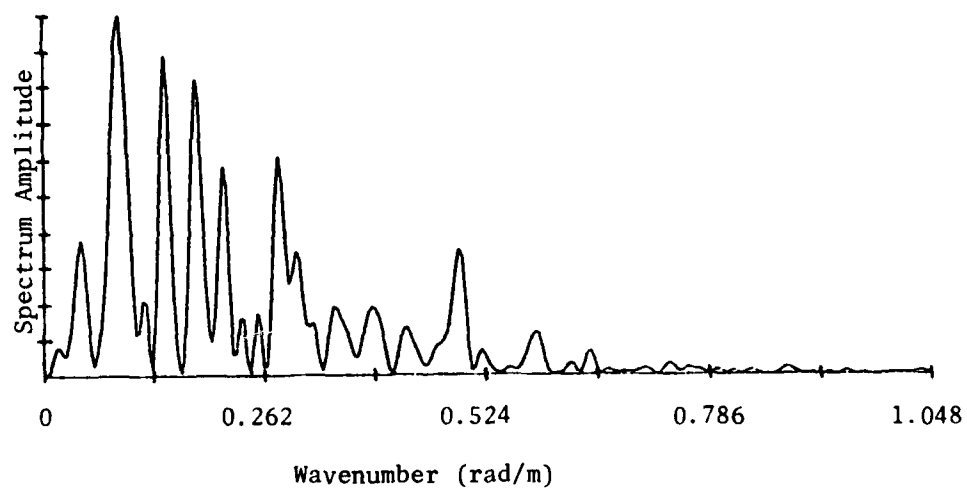
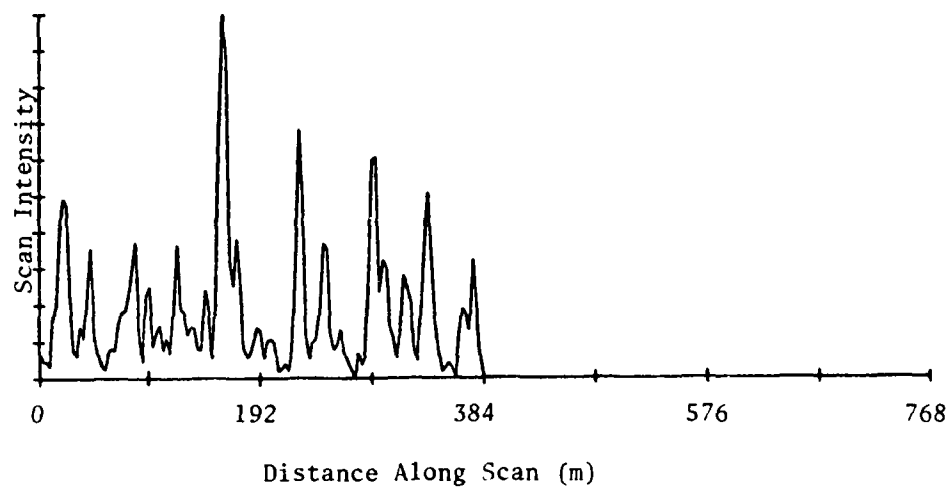


Fig. 23. Radar Scan Segment and Corresponding Non-Smoothed Periodogram for Scan 314 from Analysis Area A-1.

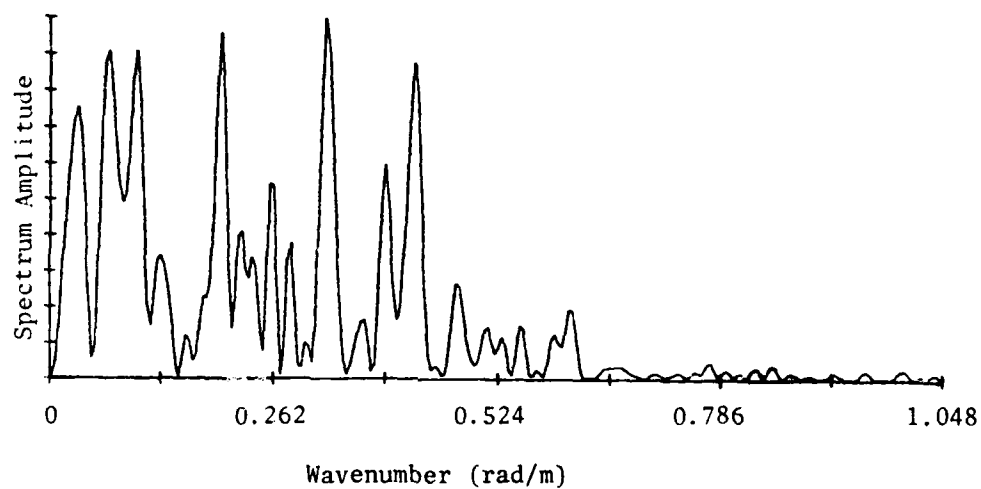
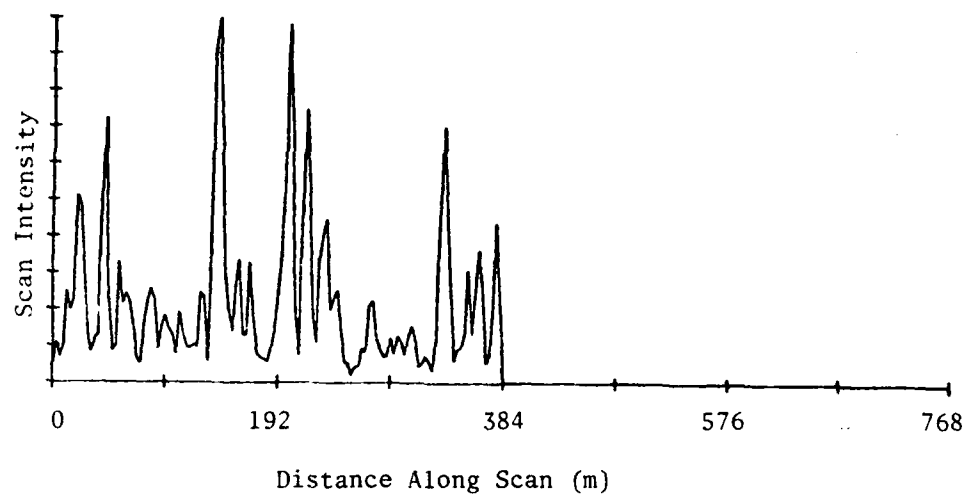


Fig. 24. Radar Scan Segment and Corresponding Non-Smoothed Periodogram for Scan 334 from Analysis Area A-1.

The first system parameter considered for preliminary selection was the number of scans to be averaged. For this selection, a scan length of 384m (i.e. 128 points) and a scan spacing of 30m (i.e. 20 image scans) were chosen based on observations of periodograms generated. Averages are shown in Fig. 25 for 2, 4, and 7 of the periodograms illustrated in Figs. 18 through 24. Observations of the averaged periodograms indicated that a well defined peak in the proper location could be obtained with a few as 3 or 4 periodograms averaged. However, the number of individual scan periodograms in the set which have peaks in the wrong location indicated that reliable wavenumber estimates would probably require the average of a larger number of periodograms. Therefore, the average of all 7 periodograms was chosen as a preliminary standard for further preliminary parameter selections.

Evaluation and comparison of window functions and window function widths was considered next. The specific window functions and corresponding equations used in the analysis are listed in Table VI. The windows are listed in order of increasing main lobe width of their corresponding spectra if the Tukey window parameter is $\alpha = 0.5$.

As discussed earlier, a window function having sample length $2M + 1$ is applied to the autocorrelation function estimate of sample length $2N - 1$, where N is the total number of samples of the data from which the autocorrelation estimate is obtained. If the sample length of the window is specified as a certain fraction of the autocorrelation estimate sample length, then the variance reduction of the resulting smoothed periodograms is approximately the same regardless of the length of scan⁶. For analysis purposes, the window function width is defined by specifying M to be a given percentage of N .

Examples of periodogram smoothing for various lag window widths are shown in Figs. 26 through 29 for the Rectangular, Hamming and Parzen windows. Additional results for the Bartlett and Tukey windows are given in Appendix B.

In order to select a specific window and window width, a comparison of the bias and consistency of the resulting smoothed periodogram and the accuracy of wavenumber estimates made with them should be made. Although it is not feasible to quantitatively analyze either the bias or the variability of the smoothed periodograms, it is reasonable to qualitatively assess the variability of the smoothed periodograms and to observe the effect of the smoothing operations on the wavenumber estimate obtained for various window and window width combinations. Table VII shows the along-scan wavenumber estimates obtained from several combinations of window functions and window function lengths. While the wavenumber estimate results are not greatly different for the various windows, a Hamming window with width equal to three-fourths of the autocorrelation function width was preliminarily selected as a good compromise in terms of periodogram variability smoothing and wavenumber estimate accuracy. More rigorous evaluation of this choice is deferred for later statistical analysis.

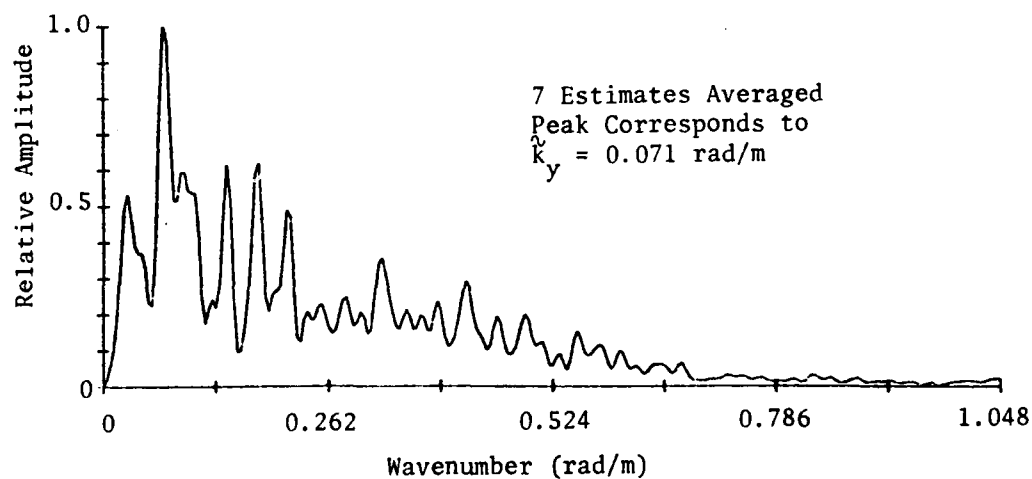
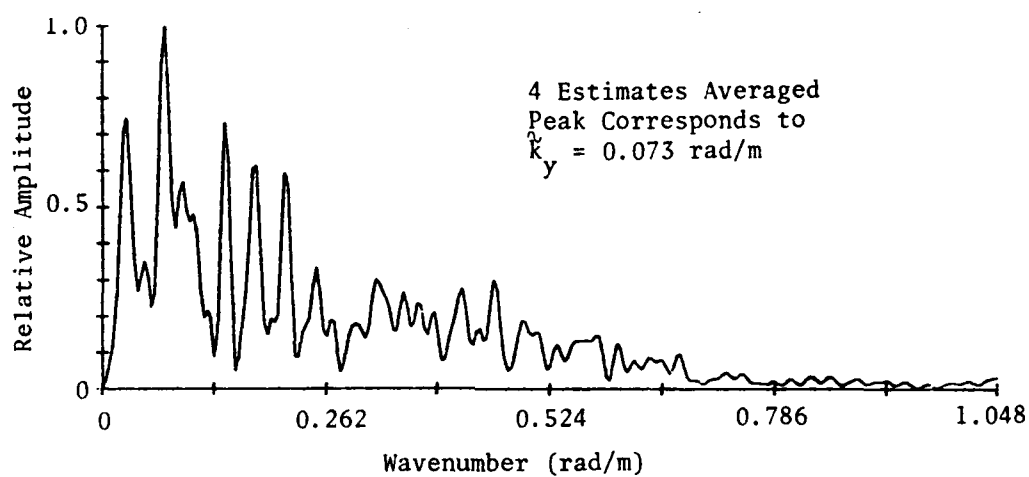
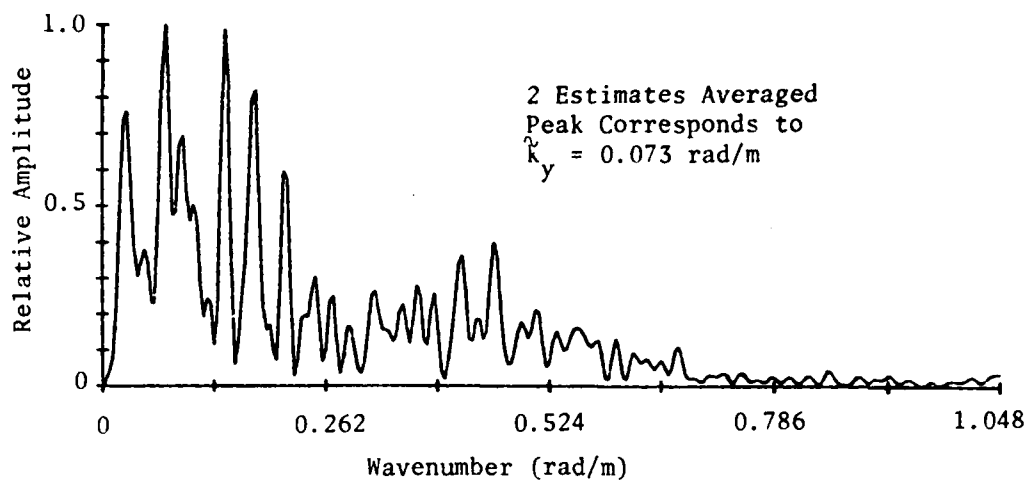


Fig. 25. Effect of Averaging Different Numbers of Non-Smoothed Periodograms.

Table VI. Window Functions Used for Periodogram Smoothing.

Description	Lag Window	
Rectangular	$w_R(u) = \begin{cases} 1 & , u \leq M \\ 0 & , \text{elsewhere} \end{cases}$	
Tukey	$w_T(u) = \begin{cases} 1 & , u \leq M \\ \frac{1}{2} \left[1 + \cos \left(\frac{\pi(u-\alpha M)}{(1-\alpha)M} \right) \right] & , \alpha M < u \leq M \\ 0 & , \text{elsewhere} \end{cases}$	
Bartlett	$w_B(u) = \begin{cases} 1 - \frac{ u }{M} & , u \leq M \\ 0 & , \text{elsewhere} \end{cases}$	
Hamming	$w_H(u) = \begin{cases} 0.54 + 0.46 \cos(\pi u/M) & , u \leq M \\ 0 & , \text{elsewhere} \end{cases}$	
Parzen	$w_P(u) = \begin{cases} 1 - 6(u /M)^2 + 6(u /M)^3 & , u \leq M/2 \\ 2(1 - u /M)^3 & , M/2 < u \leq M \\ 0 & , \text{elsewhere} \end{cases}$	

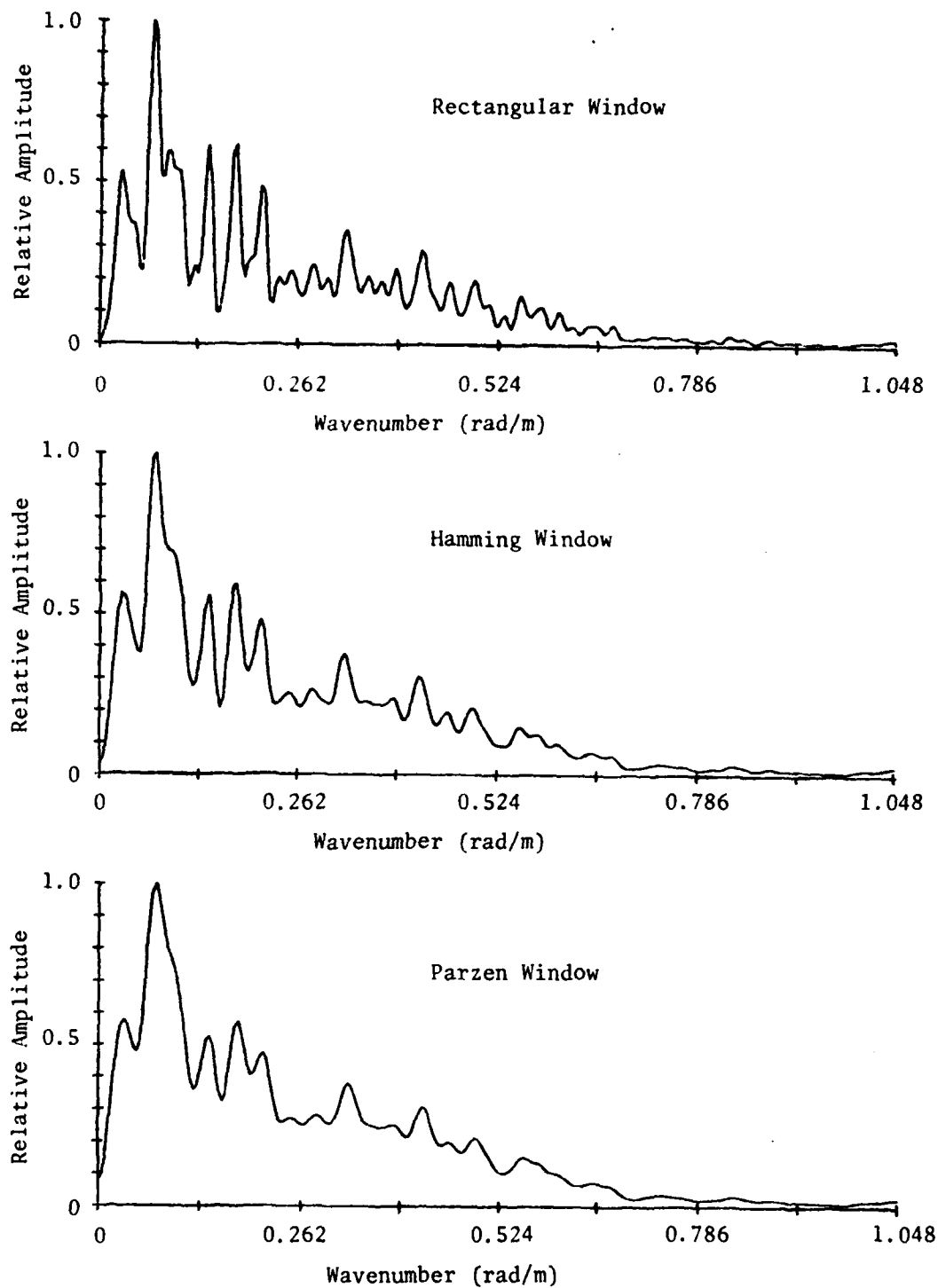


Fig. 26. Periodogram Smoothing Effect for 3 Lag Windows with $M = N$.

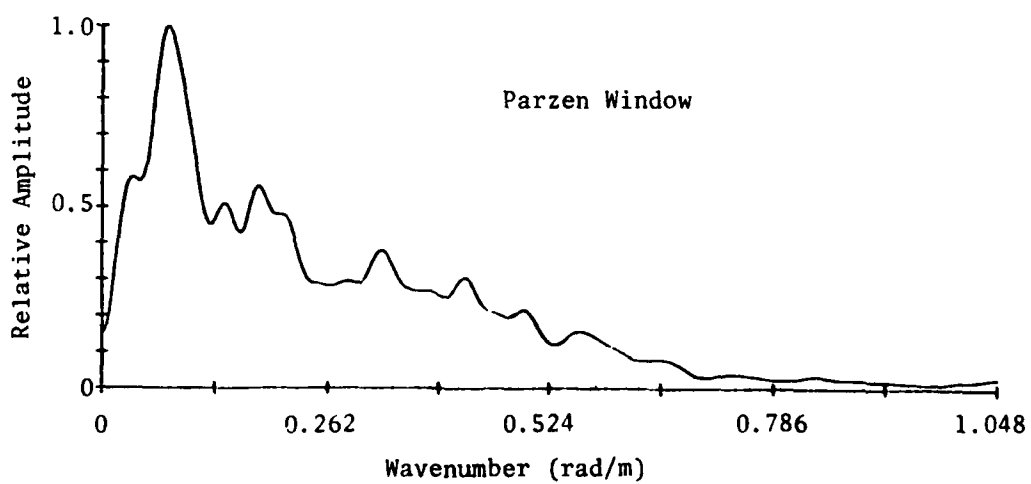
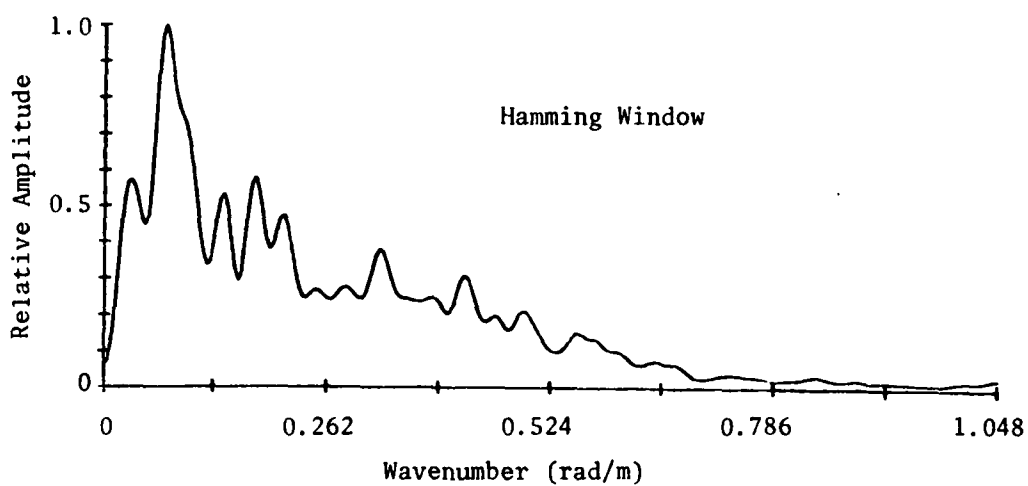
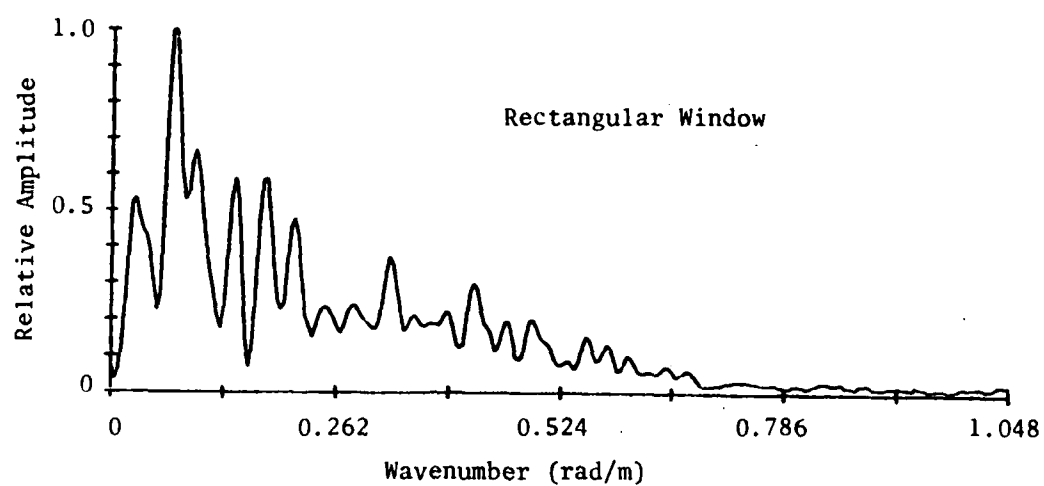


Fig. 27. Periodogram Smoothing Effect for
3 Lag Windows with $M = 3N/4$.

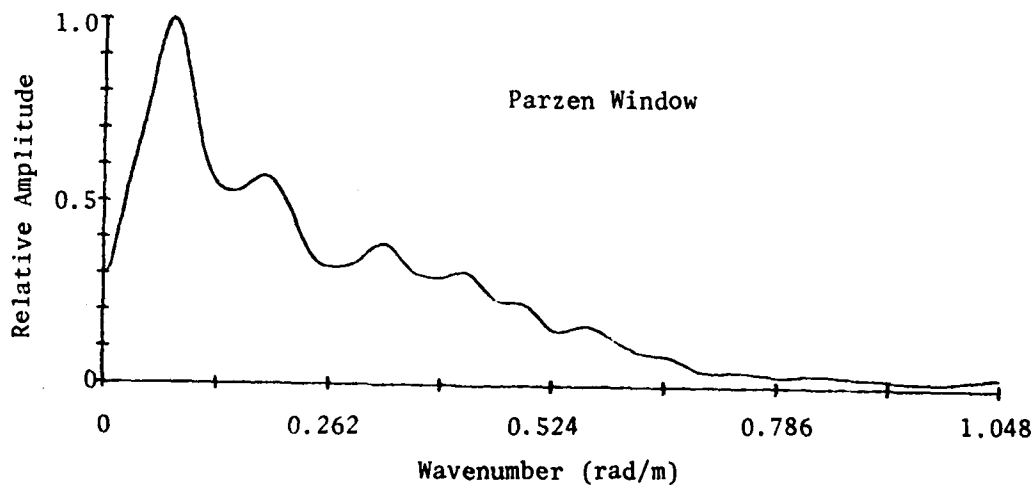
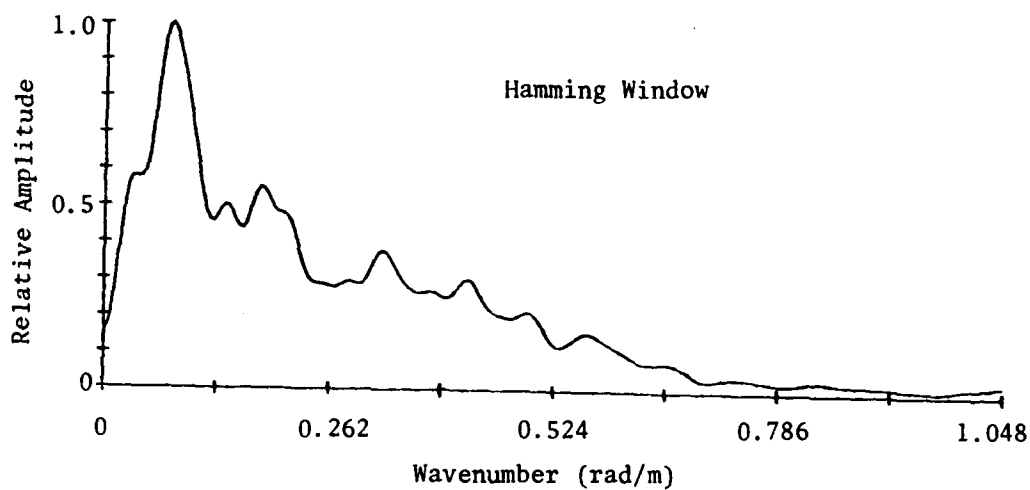
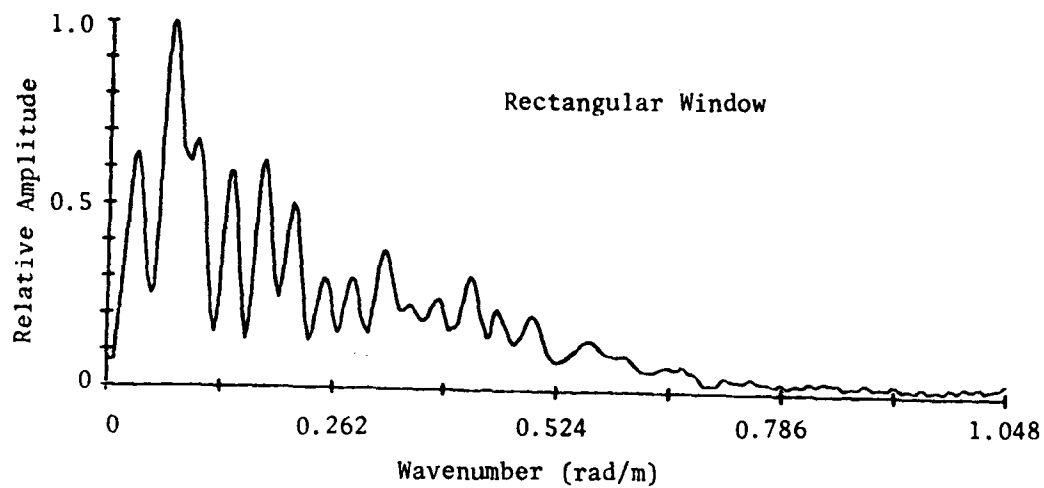


Fig. 28. Periodogram Smoothing Effect for 3 Lag Windows with $M = N/2$.

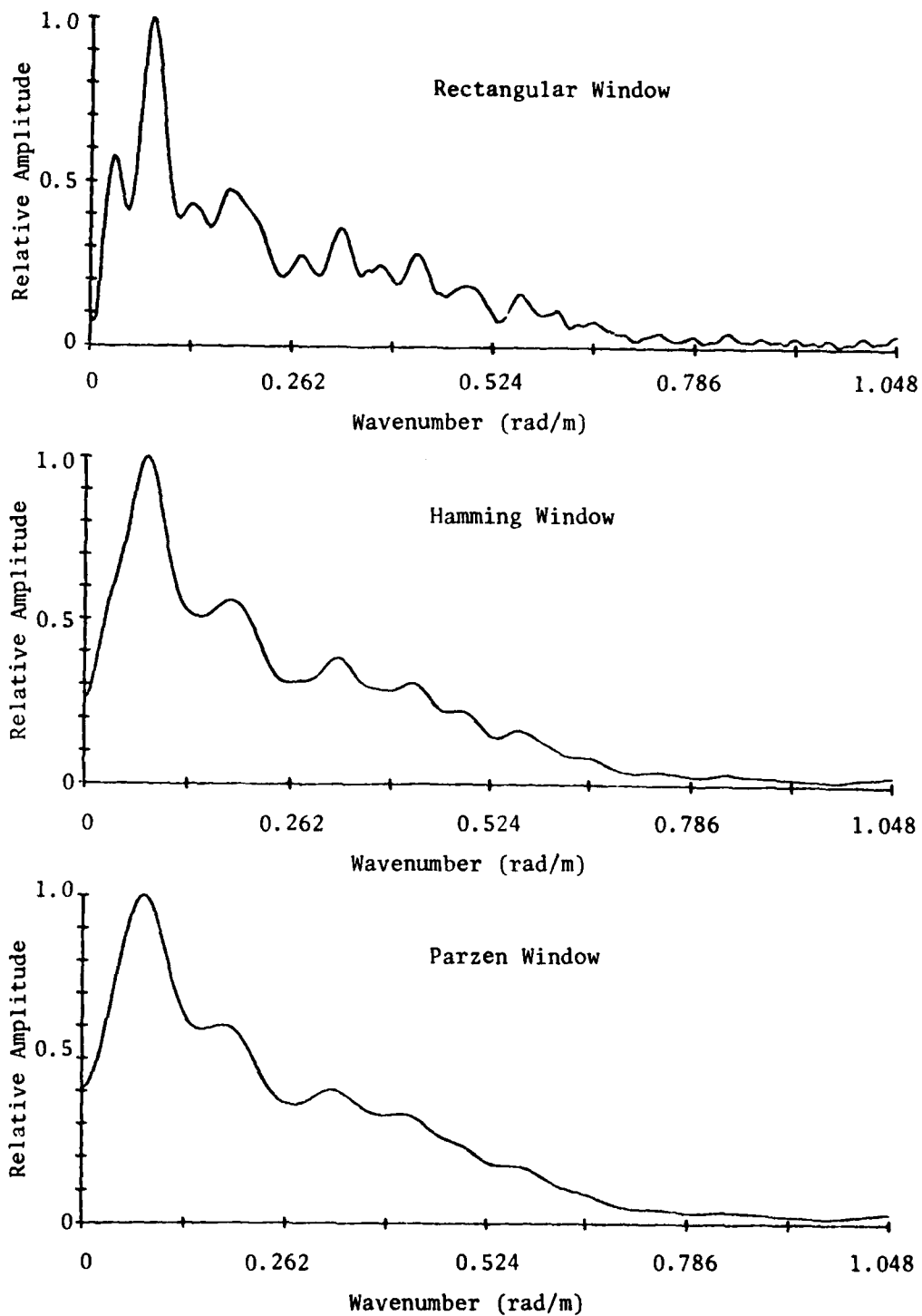


Fig. 29. Periodogram Smoothing Effect for 3 Lag Windows with $M = 3N/8$.

Table VII. Comparison of Along-Scan Wavenumber Estimates in rad/m for Various Combinations of Lag Window Functions and Lag Window Widths.

Lag Window	Lag Window Width as a Fraction of Autocorrelation Width				
	1	3/4	5/8	1/2	3/8
Rectangular	0.071	0.072	0.072	0.072	0.079
Tukey ($\alpha = 0.5$)	0.071	0.072	0.074	0.078	0.080
Bartlett	0.071	0.073	0.074	0.077	0.080
Hamming	0.072	0.073	0.075	0.077	0.079
Parzen	0.076	0.076	0.078	0.079	0.078

Ground truth wavenumber along the scan = 0.071 rad/m.

Data scan lengths of 96m, 192m, 384m and 768m were initially investigated to determine length of radar scan required. Spectral estimates for an average of 7 smoothed periodograms (using the previously selected three-fourths Hamming window) are shown in Figs. 30 and 31. The results indicate that for the particular wave field present, it is necessary to have a scan length of at least 384m to obtain a smoothed periodogram with reasonable spectral peak definition. Using the ground truth along-scan wavenumber of 0.071 rad/m ($\lambda_y=88m$) it is seen that the selection of a 384m scan length corresponds to approximately 4.4 wavelengths along the scan. It is expected that the length of scan should be proportional to the ocean wavelength present. Therefore, longer scan lengths will be required for longer ocean wavelengths. This will be evaluated later by resampling the data along rotated scan lines.

With the exception of scan spacing, preliminary choices of system parameters have been made by non-statistical analysis. Summarizing, the preliminary selections are: (1) a total of 7 scans required for

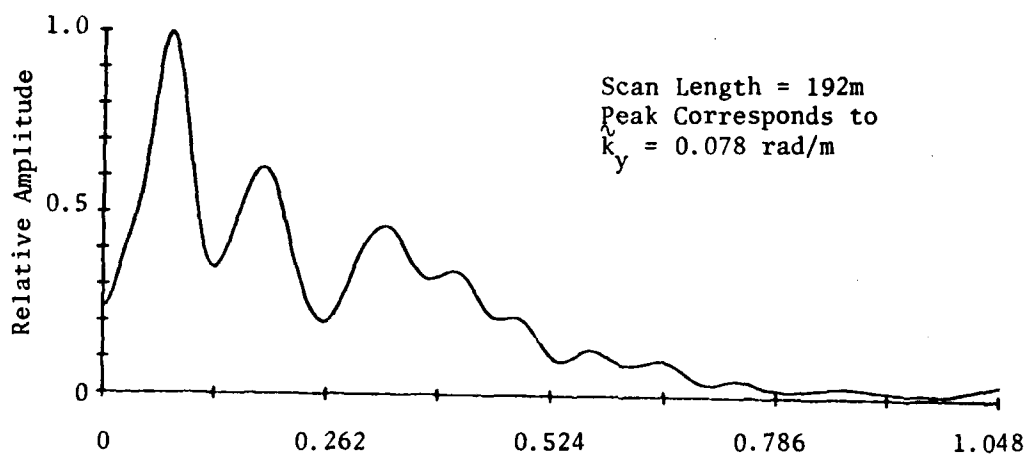
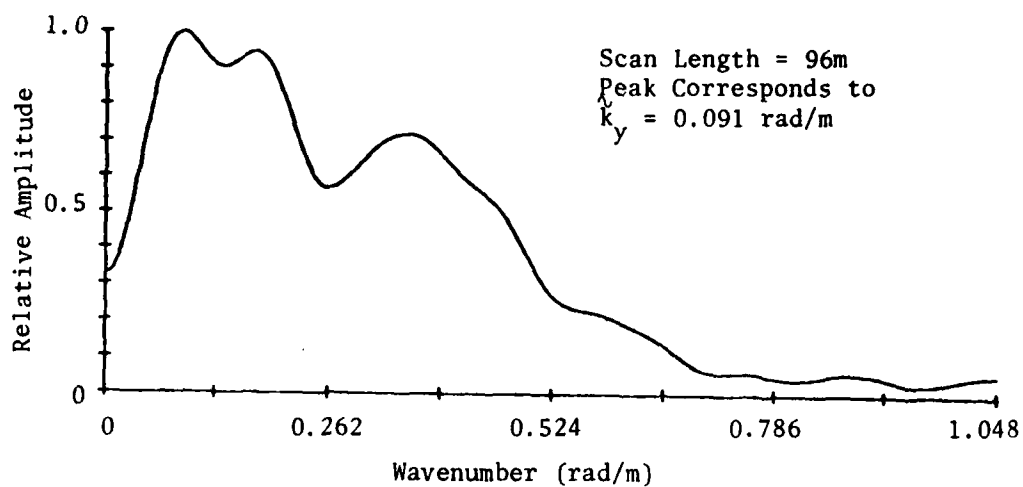


Fig. 30. Average of 7 Smoothed Periodograms for Scan Lengths of 96m and 192m.

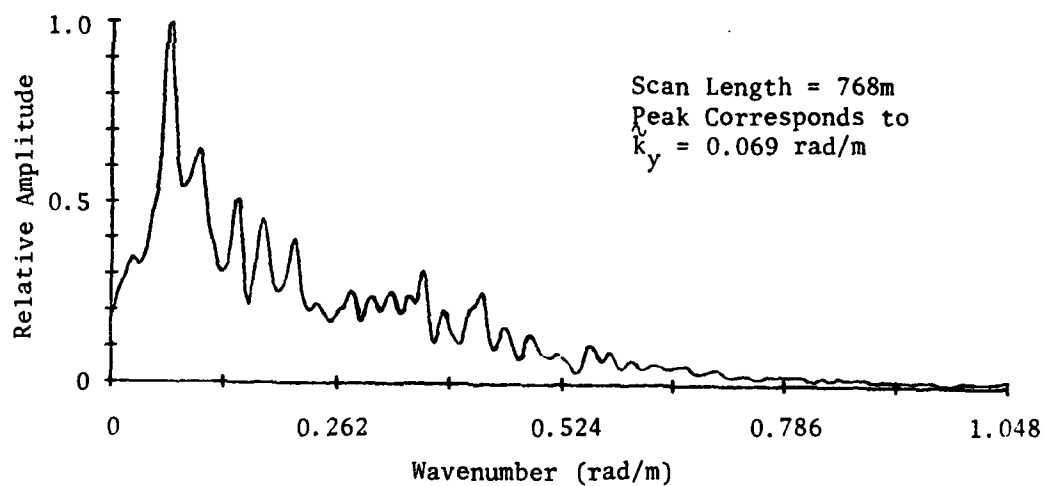
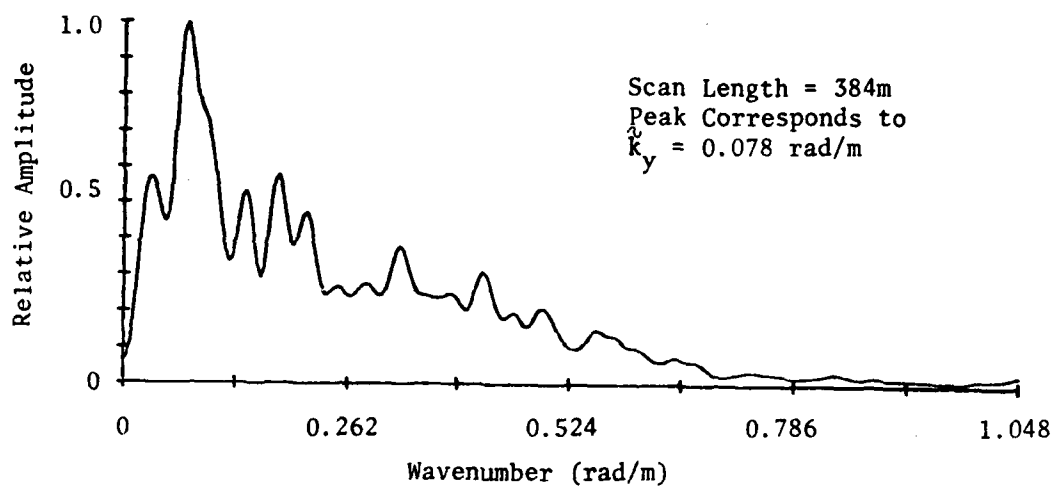


Fig. 31. Average of 7 Smoothed Periodograms for Scanlengths of 384m and 768m.

averaging smoothed periodograms, (2) a Hamming window with width equal to three-fourths the autocorrelation estimate width for smoothing the periodograms, and (3) a scan length with at least 4.4 along-scan wavelengths present. A more detailed evaluation of all system parameters (including scan spacing) is deferred for statistical analysis.

B. INITIAL STATISTICAL ANALYSIS

The initial statistical evaluation of the system performance of the portion of the system which estimates along-scan wavenumber is based on analysis areas A-1 and A-2. In each area 20 sets of 18 scans were identified so performance statistics (i.e. samples means and standard deviations of wavenumber estimates) could be computed for dominant component along-scan wavenumber estimates from the averages of up to 18 smoothed periodograms. The initial statistical performance results are plotted as a function of number of scans used in Fig. 32. System parameters for the performance statistics shown are: (1) scan length = 768m or 256 samples, (2) scan spacing = 15m or 10 image scans, and (3) a Parzen window with width equal to 3/4 of the autocorrelation function width (Note: The utilization of a Parzen window instead of a Hamming window was accidental; however, this error did not prove to significantly affect results). The results shown in Fig. 32 indicate that the wavenumber estimation performance is not nearly as good as had been implied by preliminary observations.

As a simple indicator of the performance, consider the relative average bias and relative average standard deviation of the wavenumber estimates obtained with 10 through 18 scans. The relative average bias, in percent, is defined by

$$\bar{b} = \frac{\sum_{j=ja}^{jb} [E(\tilde{k}_{yj}) - k_y]}{(jb - ja + 1)k_y} \times 100 \quad (33)$$

where $(jb - ja + 1)$ is the total number of bias values averaged (9 in this case), $E(\tilde{k}_{yj})$ is the sample mean of the wavenumber estimate for a given parameter j (number of scans in this case), and k_y is the ground truth dominant wave component along-scan wavenumber. The relative average standard deviation, in percent, is defined by

$$\bar{\sigma} = \frac{\sum_{j=ja}^{jb} \sqrt{\text{Var}(k_{yj})}}{(jb - ja + 1)k_y} \times 100 \quad (34)$$

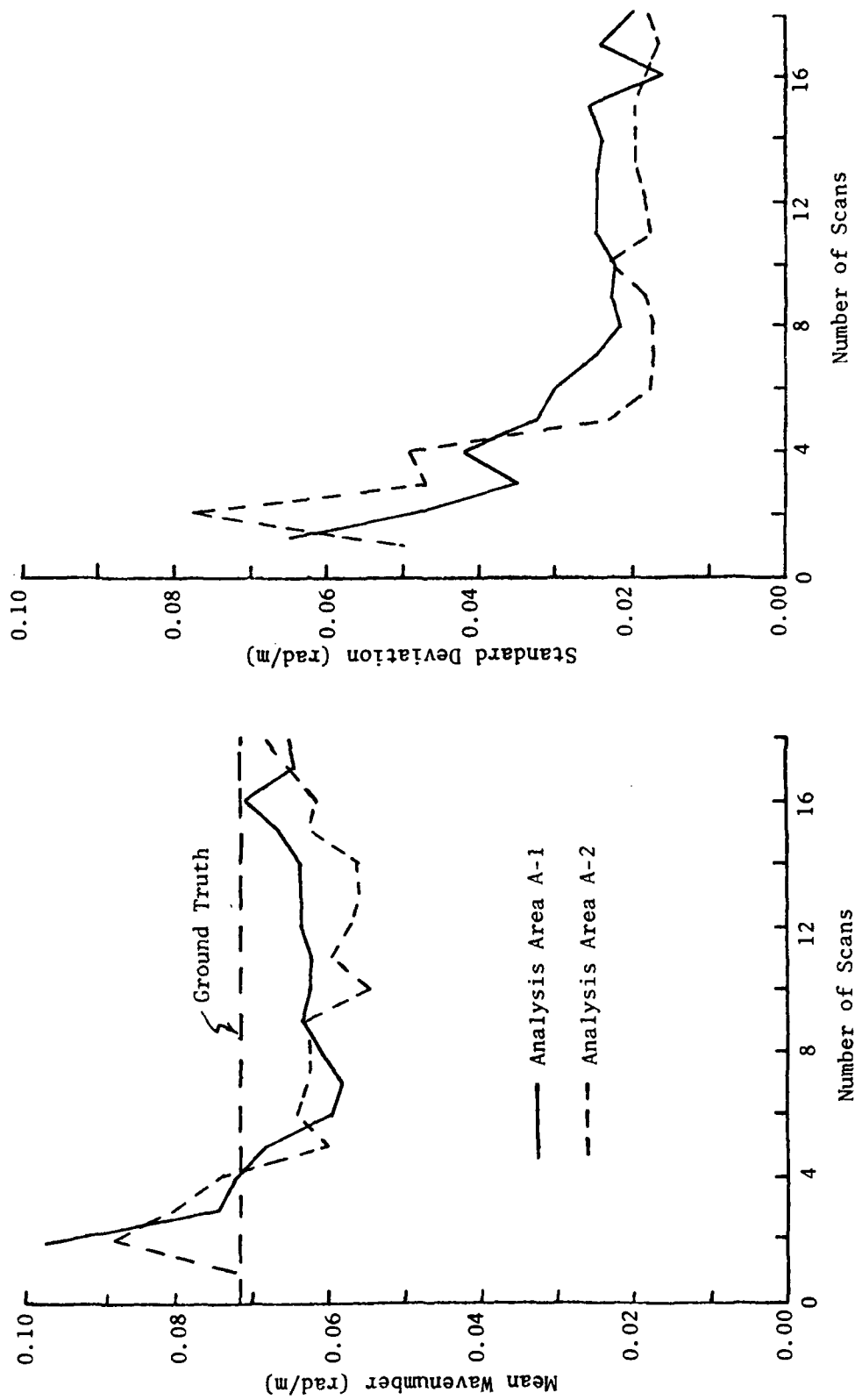


Fig. 32. Along-Scan Wavenumber Estimate Statistics for Two Analysis Areas Using the Initial System Concept.

where $\text{Var}(\hat{k}_{y,j})$ is the sample variance of the wavenumber estimate for a given parameter j . Using these definitions, the relative average bias for analysis area A-1, when 10 through 18 scans are used, is found to be approximately $\bar{\beta} = -8.3\%$ and the corresponding relative average standard deviation is $\bar{\sigma} = 32.4\%$. For analysis area A-2, the relative average bias is $\bar{\beta} = 14.9\%$ and the relative average standard deviation is $\bar{\sigma} = 26.9\%$. The quantities indicate that, on the average, the wavenumber estimation system produces a large relative error. Although the average bias is not good, it is the extremely large average standard deviation that is particularly unacceptable.

Inspection of several smoothed and averaged periodograms and their resulting wavenumber estimates indicated that many of the estimates are in fact quite good with respect to ground truth but that a few individual scan periodograms occur for some cases which, because of their magnitude and large error tend to heavily influence the final estimate for that case. This results in a large estimation error which has a large effect on the estimate performance statistics. Due to the extremely noisy nature of the data it was felt that changing the available system parameters within reasonable limits would not solve the estimation accuracy problem (some variations of parameters were evaluated and the results support this conjecture). Therefore, various system concept modifications were proposed and tested as possible solutions to the accuracy problem. These modified concepts are briefly described below. Comparative performance results are presented after the description of the concepts.

The first modification considered was to construct a median periodogram rather than an average periodogram. This was analyzed to determine if a more robust estimation leading to better wavenumber estimation performance could be achieved.

The second modification consisted of squaring the values of the scan data prior to computing smoothed periodograms and averaging. The rationale behind this modification was that it would enhance the larger returns from the wave crests and thus make estimations of wavenumber easier and more accurate.

The third modification considered consisted of: (1) dividing the wavenumber range of interest into several intervals, (2) picking the three largest peaks of each individual periodogram and associating their values with the interval in which they were found, (3) adding peak values from all individual periodograms found in each interval, (4) selecting the interval with the largest peak sum, (5) averaging the individual periodograms only over the selected wavenumber interval, and (6) using parabolic interpolation to find the location of the peak of this portion of the averaged periodogram to use as the wavenumber estimate. This modification is essentially a two-step estimation process. It was developed in an attempt to discriminate against isolated narrow and high peaks in the noisy smoothed periodograms generated for each individual scan and give more weight to groups of high peaks.

The fourth and fifth modifications considered were concepts that eliminated the averaging of the periodograms. Instead, the mean value or median value of the peak locations of the individual scan periodograms were computed as an estimate of the wavenumber. This was analyzed to determine if more robust estimations of wavenumbers were achieved.

Each of the above system modifications was tested by computing along-scan wavenumber estimate statistics using the previously indicated 20 cases of 18 scans for analysis area A-1. The relative average bias and relative average standard deviation was computed for 10 to 18 scans for estimates obtained with each system modification. The results are shown in Table VIII. These results indicate that no significant performance improvement is obtained using any of these system modifications.

Table VIII. Along-Scan Wavenumber Estimation Performance for Various System Modifications.

System Concept	Relative Average Bias %	Relative Average Standard Deviation %
Initial Concept	-8.3	32.4
Median Periodogram	-6.6	36.6
Squared Data	0.5	30.1
Two-Step Concept	-3.6	40.8
Peak Mean Location	32.4	27.3
Peak Median Location	19.3	28.9

A sixth system modification considered consisted of clipping the data prior to computing periodograms. A histogram of all data in analysis area A-1 was computed to determine clipping levels which would save 95% or 98% of the data. The rationale for this modification is that it would eliminate spurious large noise peaks. No statistical

results were obtained for this system modification. Consideration of results obtained for several good and bad individual cases indicated that no significant performance improvement resulted. The following section develops another system modification in more detail which does provide some wavenumber estimation performance improvements.

C. DEVELOPMENT OF A MODIFIED SYSTEM CONCEPT

As previously indicated, several smoothed periodograms that resulted in extremely poor wavenumber estimates in a few individual cases significantly degraded performance statistics. The modified system approach developed in this section attempts to reject smoothed periodograms whose wavenumber estimates indicate they are significantly different from the other smoothed periodograms that are used in the average for a specific case. In addition, a mechanism is defined whereby the modified system rejects those cases for which it cannot obtain a convergent estimate. Variations of this modified system are also defined so they may be investigated in parallel with the original modification.

1. THE MODIFIED SYSTEM

Of the several techniques considered in an effort to either reduce noise effects or to develop a system which is less sensitive to the noise, the modification to be presented here produces the best improvement in performance. The method selected requires that the wavenumber estimate from the smoothed periodogram of an individual scan used in the averaging process be contained within the range of wavenumbers that is given by the mean plus and minus one standard deviation of the wavenumber estimates for all smoothed periodograms available for averaging in a given case. If a wavenumber estimate does not meet this requirement, it is not used in the average. The sequence of steps required in this modification are: (1) wavenumber estimates for each smoothed periodogram to be averaged are computed, (2) the mean and standard deviation of this set of wavenumber estimates are computed, (3) all smoothed periodograms whose wavenumber estimates lie within the wavenumber range specified by the mean plus and minus one standard deviation computed in step (2) are averaged, thus rejecting smoothed periodograms whose wavenumber estimates indicate they are significantly different, and (4) the final wavenumber estimate is computed from the average of the selected periodograms.

Statistical performance curves resulting from implementation of the system with the above modification are shown in Fig. 33 for analysis areas A-1 and A-2. The results shown were obtained using the same system parameters that were used in the generation of performance curves shown in Fig. 32. Thus, the two figures serve as a useful comparison of the two systems. For analysis area A-1, the relative average bias for wavenumber estimates using a total number of 10 through 18 scans is found to be $\bar{\beta} = 4.0\%$ and the corresponding

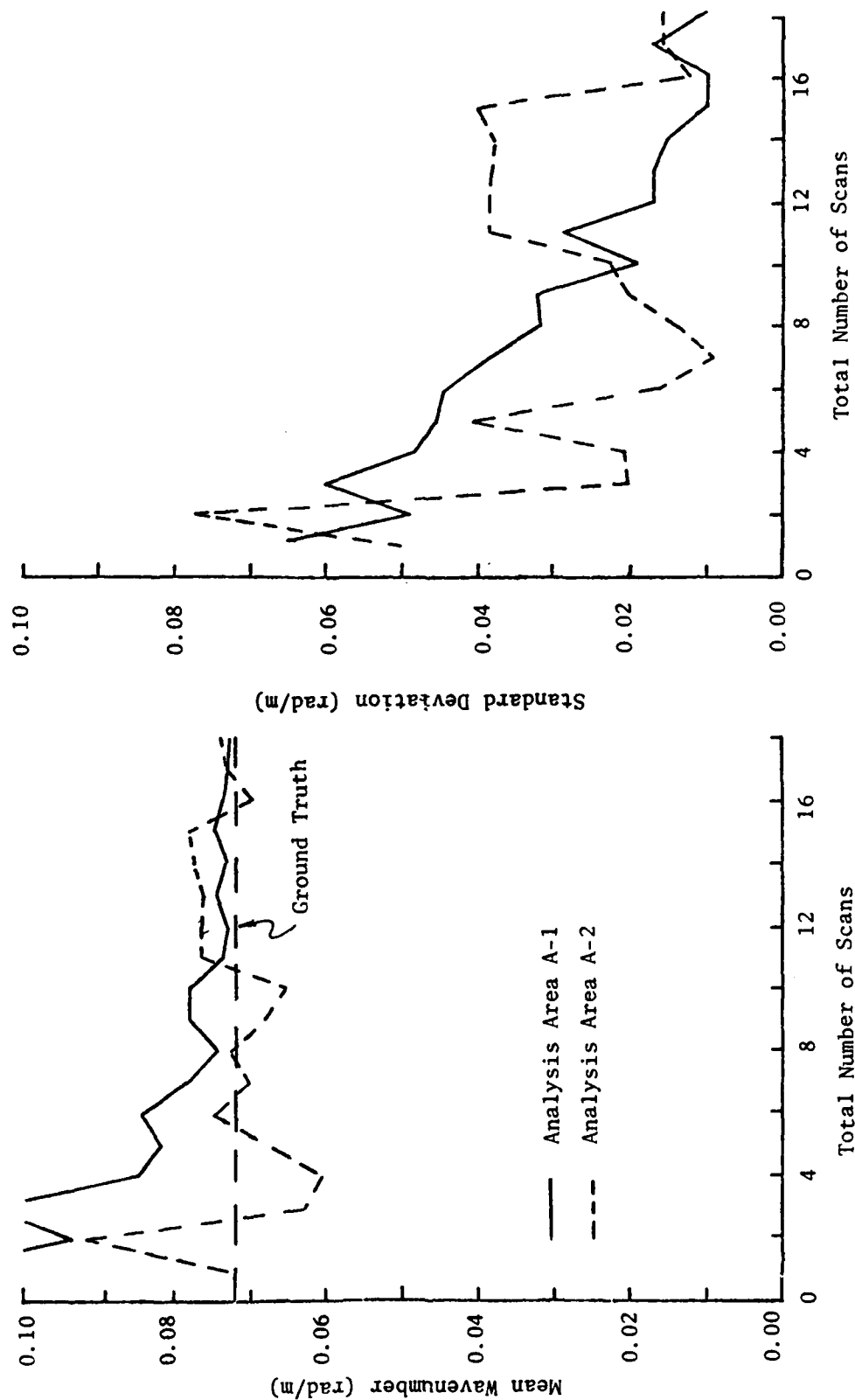


Fig. 33. Along-Scan Wavenumber Estimate Statistics for Two Analysis Areas Using the Scan Selection System Modification.

relative average standard deviation is $\bar{\sigma} = 22.3\%$ for the scan selection modified system. The same performance numbers for analysis area A-2 are $\bar{\beta} = 4.0\%$ and $\bar{\sigma} = 40.4\%$. Recall that the relative average bias and relative average standard deviation for the original system are $\bar{\beta} = 8.3\%$ and $\bar{\sigma} = 32.4\%$ for analysis area A-1 and $\bar{\beta} = 14.9\%$ and $\bar{\sigma} = 26.9\%$ for analysis area A-2. It is seen that the scan selection system modification does indeed provide some improvement of the system performance for area A-1. The relative bias is significantly improved for area A-2 but the relative standard deviation is degraded significantly. Investigation of the number of smoothed periodograms used in obtaining the estimates indicates that approximately 70% of the total number of available scans are typically kept. This assertion is supported by considering the statistics for number of scans used as a function of number of scans available for analysis area A-1 as shown in Fig. 34. Very similar results are obtained for analysis area A-2.

While some performance improvement has been obtained through the use of the scan selection modification, the standard deviation of the wave number estimates shown in Fig. 33 indicate that problems still exist. This is particularly true for analysis area A-2. These problems are again attributable to the noisy nature of the data and the ability of this noise to mask out important fundamental wavenumber information in the data. Although the scan selection modification reduces the effect of the extremely noisy data within a selected set of scans, it does not eliminate it.

Ideally, if wavenumber estimates from the modified system are observed for increasingly larger numbers of scans, then the wavenumber estimates will start to converge after a certain number of scans are used. As an example consider the individual case shown in Table IX. It appears that the wavenumber estimates begin to converge after approximately 5 scans are used. Unfortunately, the noisiness of the data may sometimes cause spurious wavenumber estimates that do not follow the general wavenumber convergence pattern. Table X shows a case where spurious results occur. In this case, the wavenumber estimates begin to converge after four scans are used. However, spurious results are identified when 8 or 9 scans are used. Another result is identified as spurious when 18 scans are used. In order to eliminate the effect of these spurious results on system performance, the system is further modified so spurious estimates are replaced by the average of the two wavenumber estimates on either side of them. If a spurious estimate results for the largest number of scans used, such as shown in Table X when 18 scans are used, then the wavenumber estimates is replaced with the estimate directly before it (i.e. the result when 17 scans are used).

In the worst case, no convergence of the wavenumber estimates occurs as periodograms from more scans are averaged. If the estimates do not converge the particular case is identified as non-estimable since the system cannot obtain a valid estimate of wavenumber. Therefore, such cases will not be used in the computation of performance statistics but will be counted as another measure of system performance

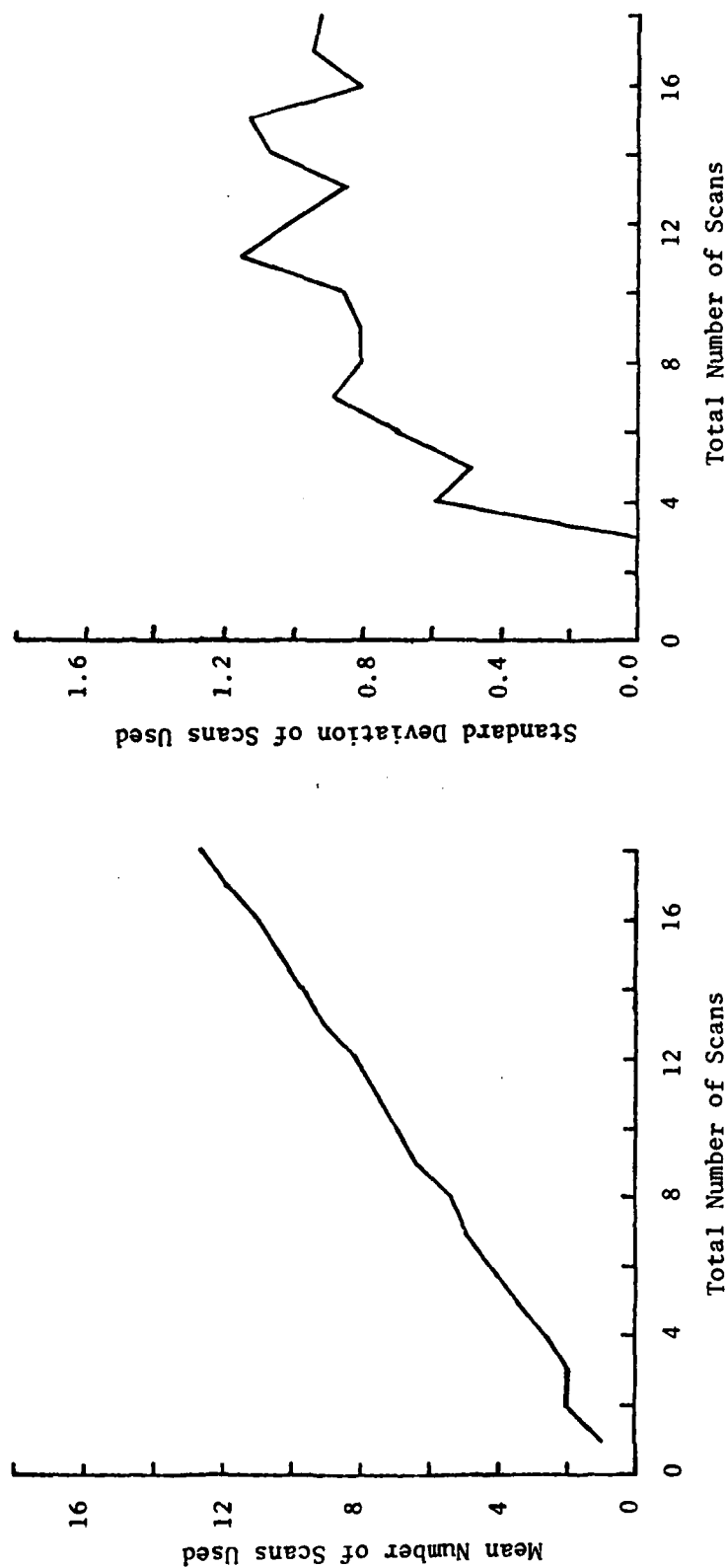


Fig. 34. Statistics for Number of Scans Used as a Function of Number of Scans Available for Analysis Area A-1.

Table IX. Example of Wavenumber Convergence
Using Scan Selection Modification.

Number of Scans Used	Number of Scans Selected	Wavenumber Estimate
1	1	0.130
2	2	0.138
3	2	0.138
4	2	0.137
5	3	0.072
6	4	0.072
7	5	0.070
8	5	0.069
9	6	0.069
10	7	0.069
11	8	0.069
12	9	0.069
13	9	0.069
14	10	0.069
15	11	0.070
16	11	0.069
17	12	0.071
18	12	0.071

Table X. Example of Spurious Wavenumber Estimates Using Scan Selection Modification.

Number of Scans Used	Number of Scans Selected	Wavenumber Estimate
1	1	0.191
2	2	0.192
3	2	0.192
4	3	0.064
5	3	0.066
6	3	0.066
7	5	0.067
8	6	<u>0.190</u>
9	6	<u>0.102</u>
10	7	0.064
11	8	0.065
12	9	0.065
13	9	0.066
14	9	0.065
15	10	0.066
16	12	0.068
17	13	0.068
18	14	<u>0.101</u>

since they indicate how often the system will not give useful results. Such a non-estimable case is shown in Table XI.

After the above system modifications have been made, one final feature is incorporated in the system to further smooth the estimate. This feature replaced the wavenumber estimate obtained for the number of scans being used by the system, N_S , with the average of itself and the estimates obtained with N_S-1 and N_S-2 scans. This eliminates the possibility of using an estimate which, while not spurious, is somewhat different from the basic estimate value to which the system has converged. As an example, the wavenumber estimate obtained with 18 scans in Table IX would be replaced by the average of wavenumber estimates obtained with from 16 through 18 scans (i.e. 0.070 rad/m). Application of the three additional system modifications just indicated results in a system which will be simply referred to in future discussion as the modified system. Modified system performance for the same cases as previously used to obtain the performance shown in Figs. 32 and 33 are shown in Fig. 35. For analysis area A-1, $\bar{\beta} = 7.0\%$ and $\bar{\sigma} = 15.2\%$ when a total of 10 through 18 scans are used. For analysis area A-2, $\bar{\beta} = -2.7\%$ and $\bar{\sigma} = 15.1\%$ when a total of 10 through 18 scans is used. Although the average bias error is slightly larger for analysis area A-1 than for the original scan selection modification (Fig. 33), excellent convergence properties for both the mean and standard deviation of the wavenumber estimates are apparent. More importantly, the average standard deviation error has been reduced significantly by the additional system modifications.

2. VARIATIONS OF THE MODIFIED SYSTEM

Even though the modified system does improve performance for the above analysis areas, it became evident from results obtained from other analysis areas that certain types of additional system variations may be required. These variations are logical suggestions that result from observations of the data and knowledge of the system requirements.

The first variation considered involves using the smoothed data (average of 25 data points surrounding the data point of interest) previously defined. In the second variation, wavenumber estimates corresponding to wavelengths longer than 400m are ignored. This is done as an attempt to improve performance by eliminating the portion of the spectrum for which it is known that results are not good due to the fact that the scan length encompasses too few wavelengths to obtain a reliable estimate of wavenumber. This particular system will be referred to as the 400m low wavenumber cut off system (abbreviated 400m LWC).

The system configurations may now be grouped into four different variations of the modified system previously discussed. These are: (1) the modified system, (2) the modified system using smoothed (5x5 Ave) data, (3) the modified system using 400m low wavenumber cut off, and (4) the modified system using smoothed (5x5 Ave) data

Table XI. Example of Non-estimable Case Using
Scan Selection Modification.

Number of Scans Used	Number of Scans Selected	Wavenumber Estimate
1	1	0.189
2	2	0.191
3	2	0.191
4	2	0.191
5	3	0.190
6	4	0.071
7	5	0.190
8	6	0.058
9	7	0.056
10	7	0.056
11	10	0.016
12	9	0.017
13	10	0.017
14	10	0.021
15	11	0.060
16	11	0.061
17	13	0.017
18	13	0.061

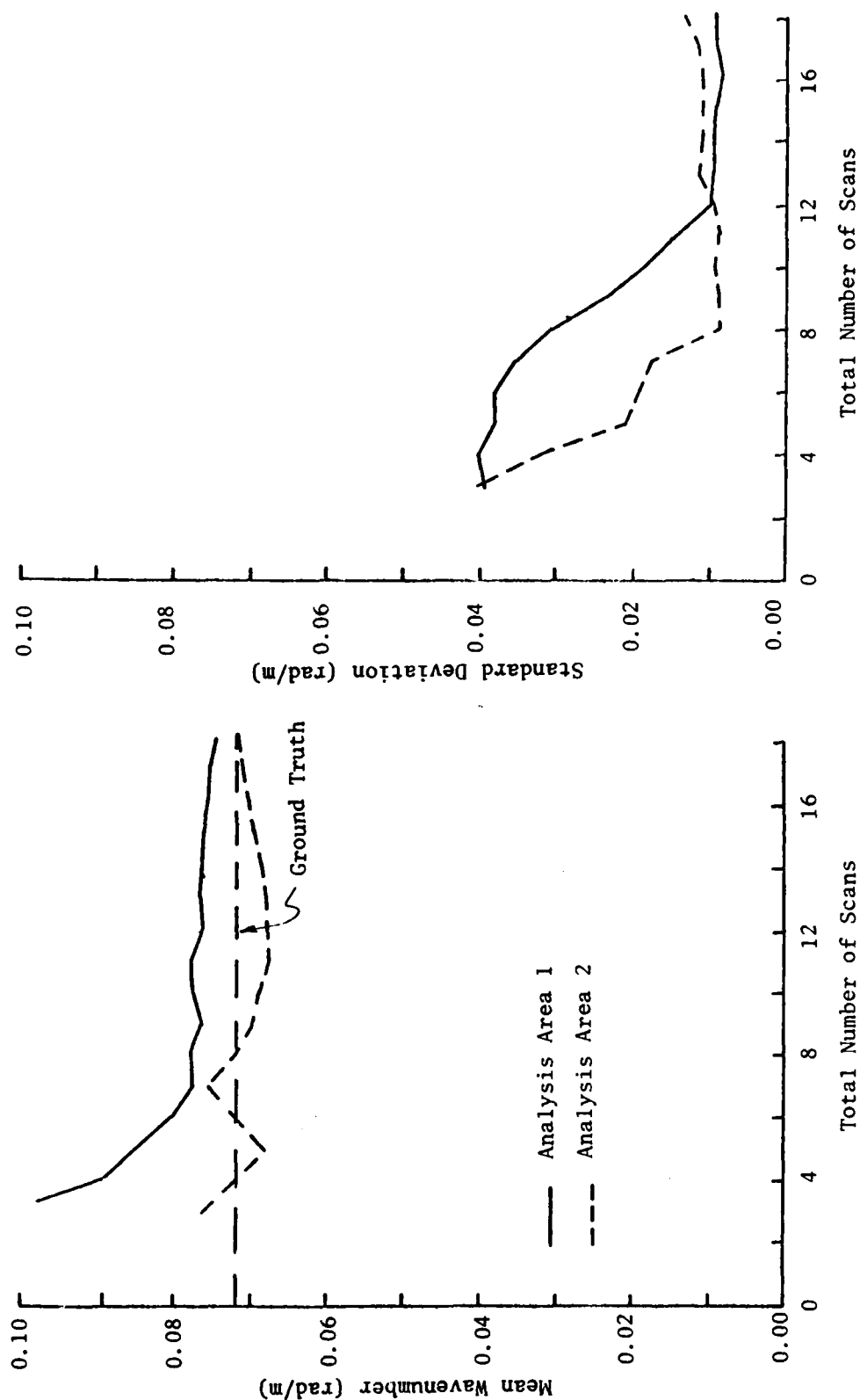


Fig. 35. Along-Scan Wavenumber Estimate Statistics for Two Analysis Areas Using the Modified System.

and 400m low wavenumber cut off. These four types of system configurations will be referred to in future analysis as: (1) No Ave, (2) 5x5 Ave, (3) 400m LWC, and (4) Ave & LWC.

D. PARAMETER TRADEOFF AND SELECTION

Parameter tradeoff and selection were next done on a more rigorous statistical basis since the final system modifications and its variations had been identified. In the system parameter selection discussed here, only the modified system (No Ave) configuration was used. It is reasonable to conclude that parameter selection based on the modified system configuration will be satisfactory for the other three system configurations defined as well since they are minor variations of the modified system configurations. It should be noted once again that image analysis area A-1 is the only area used in the following analysis and tradeoffs because of its close proximity to ground truth measurements. Unless otherwise indicated, 20 cases are used to perform all of the statistical computations to follow.

The first system parameters selected were the lag window and lag window width. The scan length and spacing were held constant at 786m (N=256) and 15m respectively and performance statistics were obtained for three different windows with three different widths. The results for these different windows are shown in Figs. 36, 37, and 38. Based on these performance curves, selection of a specific window and window width is not a clear cut decision. Recall that even though the Hamming 3/4 window width was originally selected, the Parzen 3/4 width window was accidentally used in subsequent preliminary statistical analysis. For consistency, it was used for all further analysis since the performance statistics indicate that the Parzen 3/4 width window is as good as any other combination and previously shown periodograms using this window exhibit good variability characteristics.

The next parameters to be considered were the scan length and number of scans used. Scan lengths from 120m (1.36 wavelengths) to 720m (8.18 wavelengths) were considered. Performance statistics obtained for these various scan lengths are shown in Figs. 39 and 40 as a function of number of scans used. An additional scan length of 768m (8.73 wavelengths) has already been considered (see Fig. 35 for analysis area A-1). In total, 140 cases were considered, 5 or approximately 3.6% were declared nonestimable and are not included in the statistics. It is apparent from the figures that a minimum of 12 to 14 scans are required to obtain the best performance possible. The number of scans required was selected to be 14 since this also gives a better determination of whether wavenumber estimate convergence has occurred and determination of estimate convergence is required to make the estimable/non-estimable decision. Performance statistics obtained for a system using 14 scans are shown in Fig. 41 as a function of scan length. It is apparent that approximately 480m (i.e. 5.46 wavelengths) is the scan length required in order to minimize

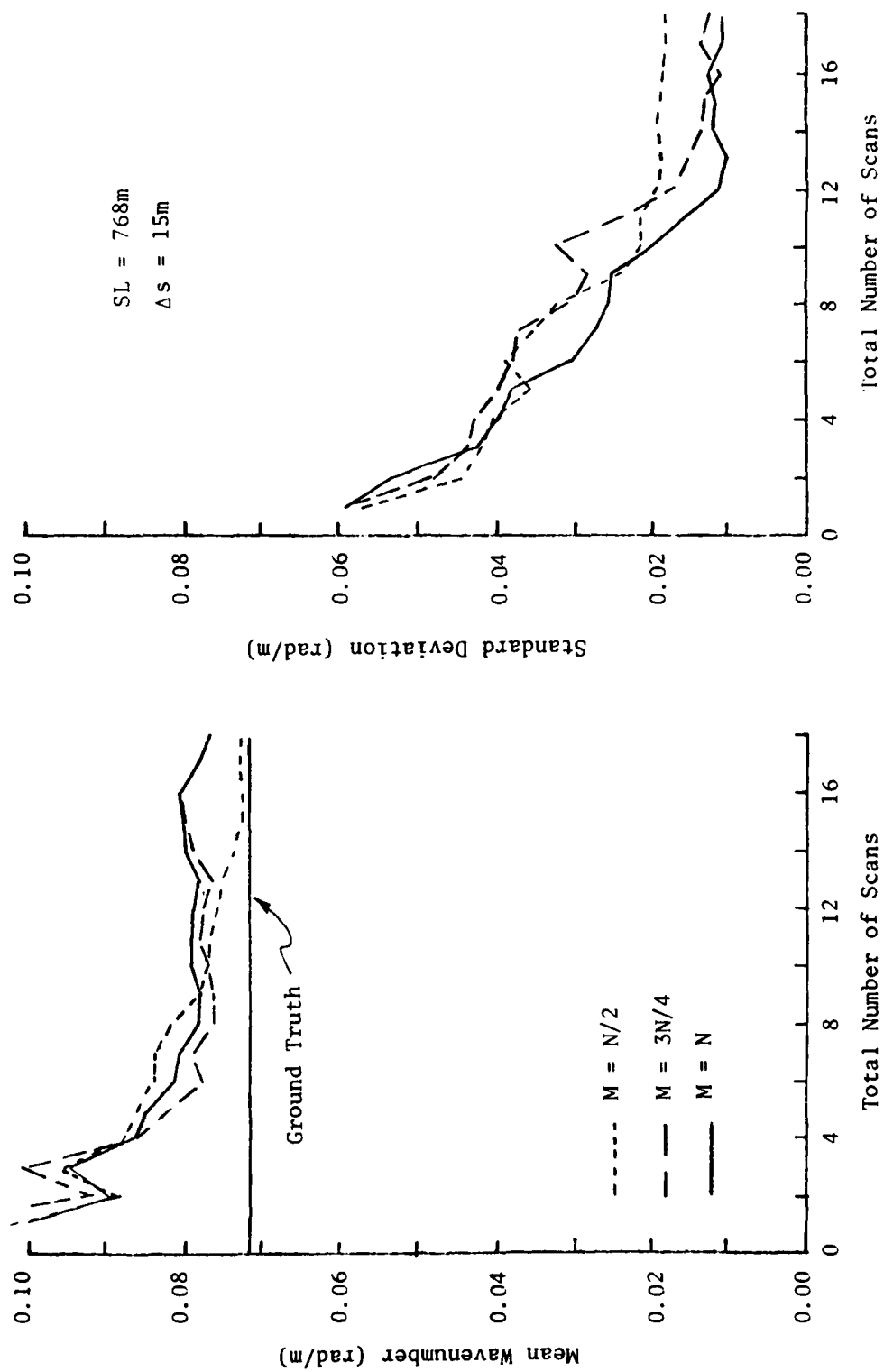


Fig. 36. Along-Scan Wavenumber Estimate Statistics for Modified System Using a Rectangular Lag Window.

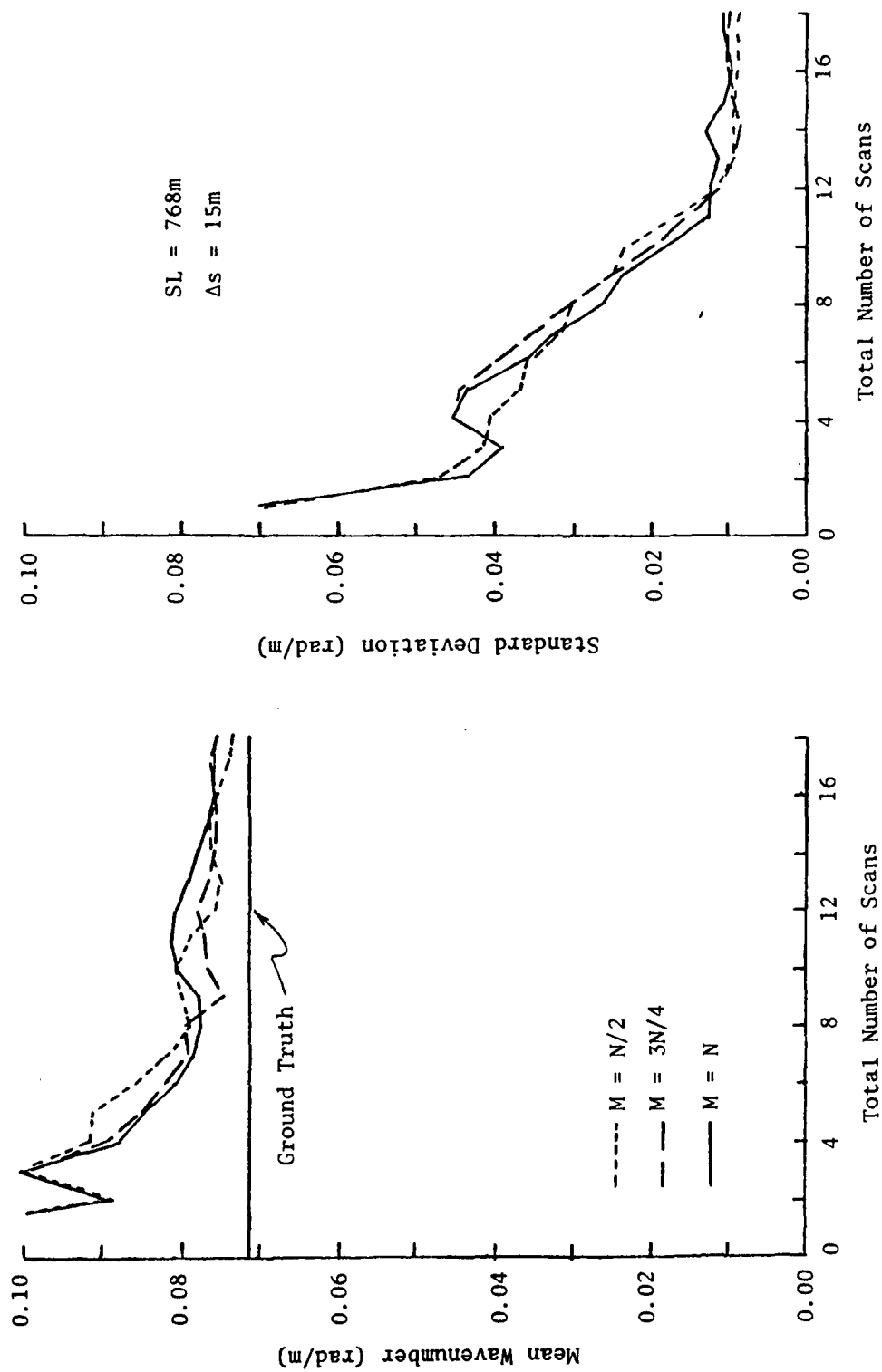


Fig. 37. Along-Scan Wavenumber Estimate Statistics for Modified System Using a Hamming Lag Window.

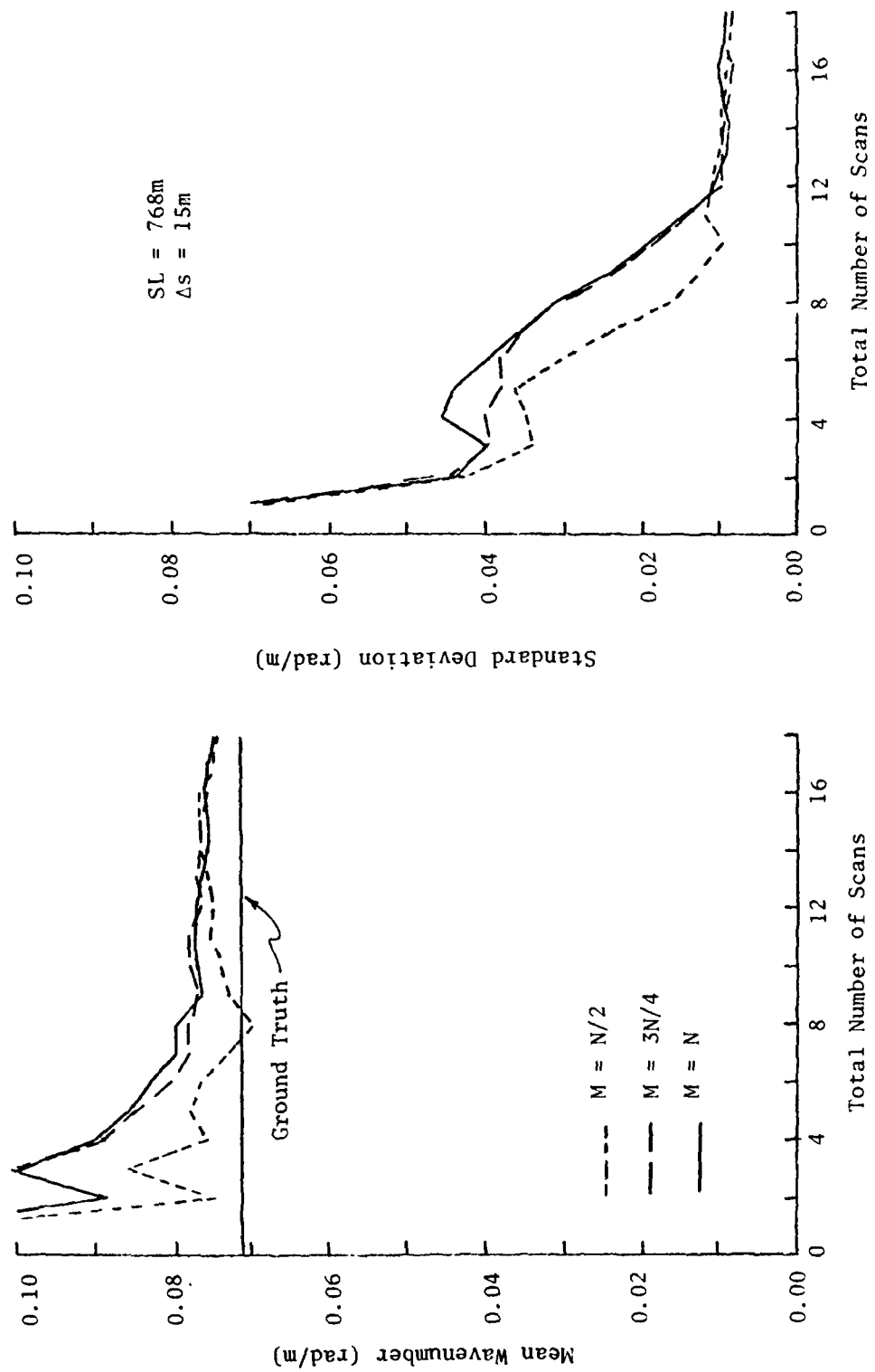


Fig. 38. Along-Scan Wavenumber Estimate Statistics for Modified System Using a Parzen Lag Window.

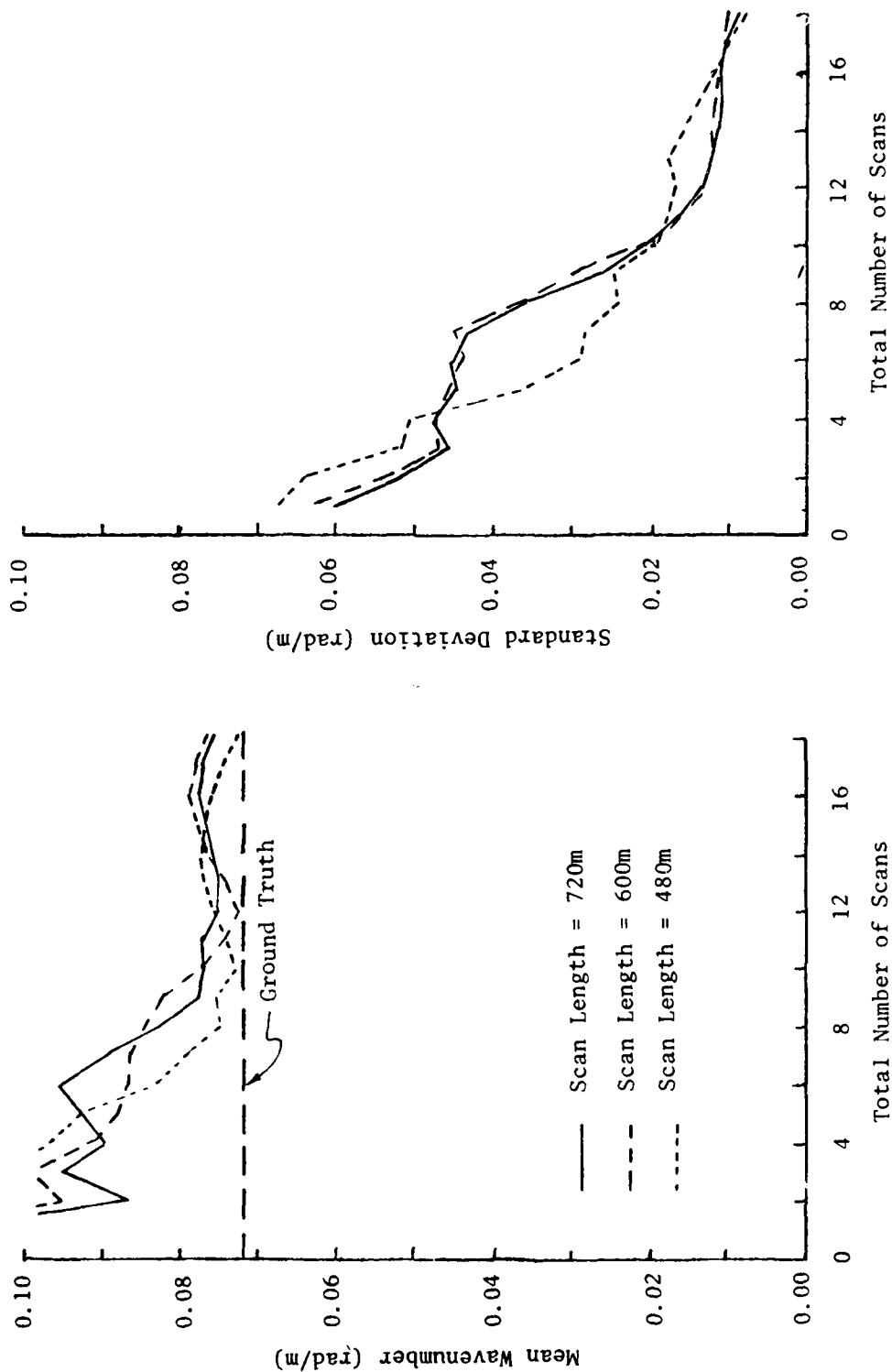


Fig. 39. Along-Scan Wavenumber Estimate Statistics as a Function of Number of Scans Used for Scan Lengths of 480, 600, and 720 Meters.

AD-A095 073

MISSOURI UNIV-ROLLA DEPT OF ELECTRICAL ENGINEERING

F/8 17/9

ESTIMATION OF OCEANWAVE WAVENUMBER AND PROPAGATION DIRECTION FR--ETC(U)

JAN 81 G E CARLSON, C L AGNE, C M MCENIRY

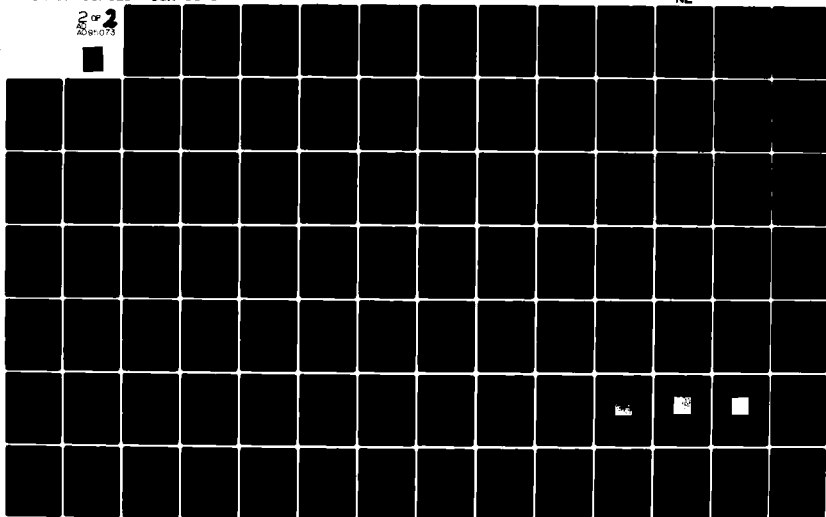
N00014-79-C-0343

UNCLASSIFIED

CSR-81-1

NL

2 of 2
AD-A095 073



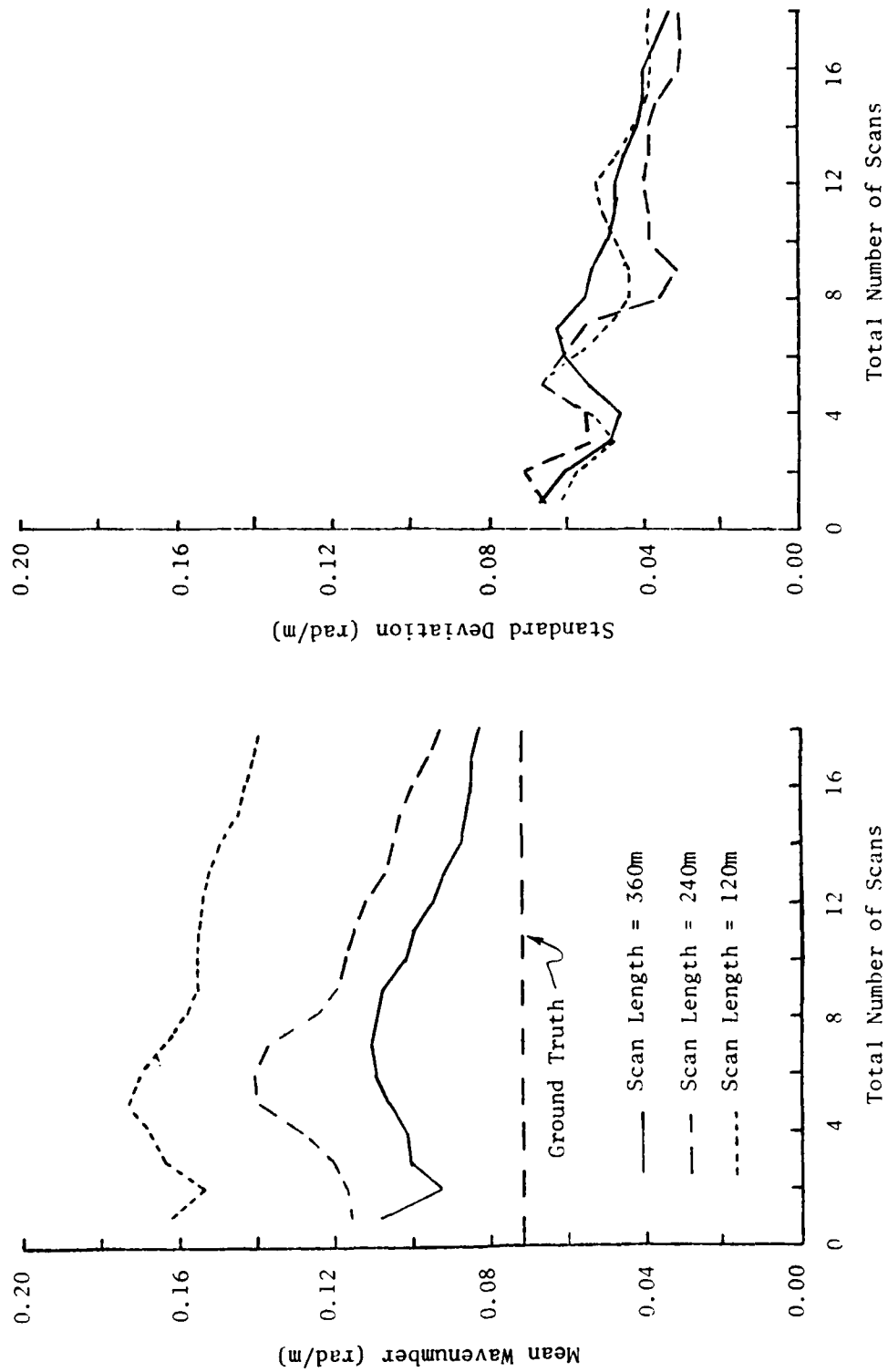


Fig. 40. Along-Scan Wavenumber Estimate Statistics as a Function of Number of Scans Used for Scan Lengths of 120, 240, and 360 Meters.

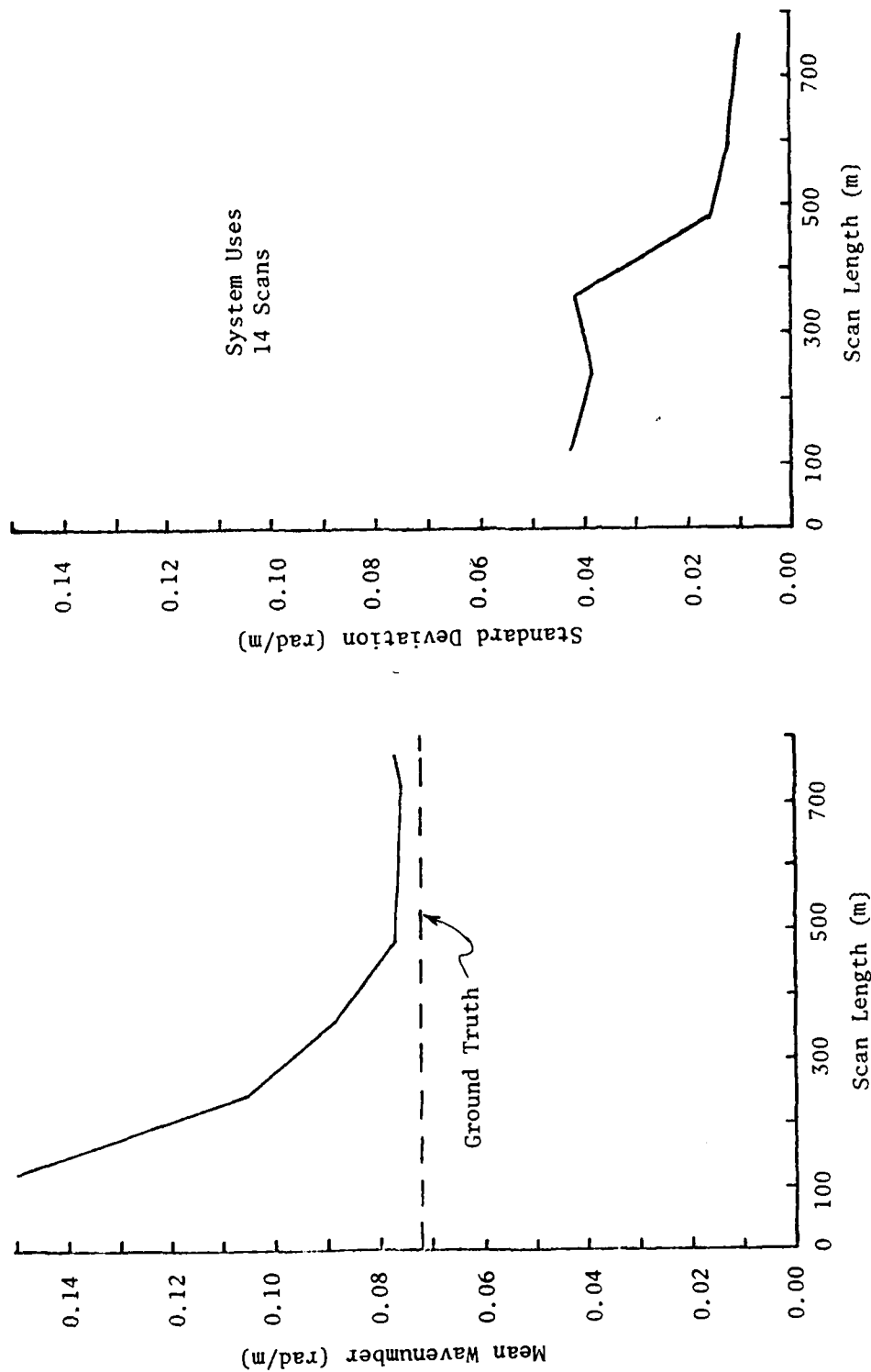


Fig. 41. Along-Scan Wavenumber Estimate Statistics as a Function of Scan Length.

the bias and variability of the estimate. The performance for scans of length greater than or equal to that required for convergence is characterized by 5% non-estimable cases, a relative average bias of 7.3% and a relative average standard deviation of 17.1%. Note that the relative average statistics are larger than desirable.

The effect of scan spacing was evaluated by repeating the above analysis using the selected 14 scan system and scan spacings ranging from 7.5m to 45m. Statistical performance results are shown in Fig. 42 for three different scan lengths. In the analysis of the scan spacing requirement, the number of cases used for statistics was reduced for the 22.5m scan spacing so that the data would be in a localized area. In other cases, the number of cases was increased to accommodate unused data within the analysis area. Exceptions to the 20 case statistics standard for results presented in Fig. 42 are as follows: (1) 15 cases for 22.5 scan spacing, (2) 25 cases for 37.5m scan spacing, and (3) 30 cases for 45m scan spacing. Except for a spurious point at a scan spacing of 22.5m, it can be said that scan spacing does not have much effect on system performance when the scan length is greater than 480m; however, when very large scan spacings are used, the wave field spanned by the scans may change somewhat and the resulting wavenumber estimates may not converge. Using the above considerations a scan spacing of 15m was chosen for all further analysis unless indicated otherwise.

In the above analysis, a total of 520 cases for scan lengths greater than or equal to 480m were considered. Of these, 10 or 1.9% were declared non-estimable.

After the system parameters had been established on a statistical performance basis, evaluation of system performance for different wavenumbers along the scan as well as extension of the analysis to other image analysis areas could proceed. The selected parameters are summarized as follows:

- (1) A Parzen window having width equal to $3/4$ of the autocorrelation function width is used for periodogram smoothing.
- (2) A total of 14 scans is used.
- (3) Scans of length greater than approximately 5.5 wavelengths are required.
- (4) The scan spacing is selected to be 15m.

E. SYSTEM PERFORMANCE ANALYSIS USING VARIOUS ANALYSIS AREAS

The performance of the modified system for estimating along-scan wavenumbers was analyzed by using a number of different analysis areas. The system parameters used were those selected in the previous section

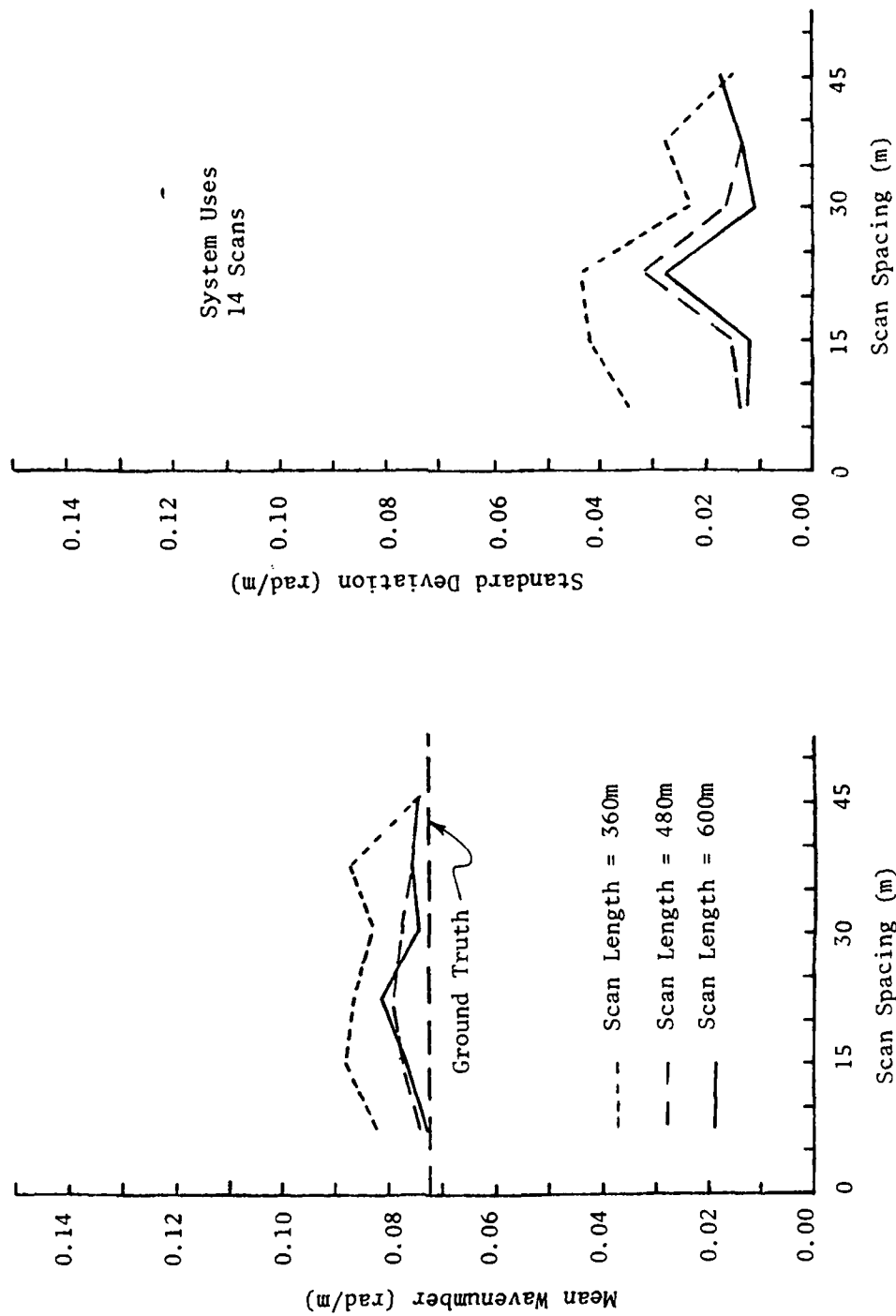


Fig. 42. Along-Scan Wavenumber Estimate Statistics as a Function of Scan Spacing for Three Scan Lengths.

except that evaluation was done for a range of scan lengths so the wavenumber estimate convergence could be observed. Neither analysis area A-1 or A-2 were used since they were too close to the left image edge to permit much evaluation of performance when rotated scans were considered.

The first analysis area considered was area A-3 which still is quite close to the pitch-and-roll buoy so it can be expected that this buoy gives good ground truth. Wavenumber estimate statistics for this analysis area are shown as a function of scan length in Figs. 43, 44, and 45 for scans rotated from the original data scans by $\theta_r = 0^\circ$, 230° , and 350° respectively. For each rotation angle, statistics are shown for both the modified system (No Ave) and the modified system using smoothed data (5x5 Ave). Individual case wavenumber estimates are shown in Fig. C1 in Appendix C for both system configurations and all rotation angles for a system using 14 scans of length approximately equal to 6.5 wavelengths.

For the statistical results shown, the wavenumber estimates converge on the average to values near the ground truth values as longer scans are used. Unfortunately, the image edge limited the length of scan which could be investigated for the rotated data scans and thus convergence is not as clearly defined. Nevertheless, all results shown appear to have wavenumber estimates that converge. Since good wavenumber estimate convergence was achieved on the average, performance of the additional variations of the modified system were not analyzed. The wavenumber estimate performance of the system for analysis area A-3 is summarized in Table XII. In this table, the relative average bias, relative average standard deviation, and percent of non-estimable cases were obtained by considering cases and results for scan lengths greater than or equal to that required for convergence.

Several conclusions about wavenumber estimation performance for analysis area A-3 are readily apparent from Table XII. The first is that performance with $\theta_r = 0^\circ$ is similar to that achieved with analysis area A-1 except that the relative average bias is considerably smaller. The second conclusion is that the standard deviation of the wavenumber estimate is larger than is desirable and increases for smaller along-scan wavenumbers (larger along-scan wavelengths). The third conclusion is that the percent of non-estimable cases is larger with the modified system than would be desired. The fourth conclusion is that the major effect of using smoothed data is to reduce the number of cases which are non-estimable.

The second analysis area considered was area A-4 which was taken near the center of image A. Wavenumber estimate statistics for this analysis area are shown as a function of scan length in Figs. 46, 47, and 48 for scans rotated from the original data scans by $\theta_r = 0^\circ$, 230° , and 350° respectively. For each rotation angle, statistics are shown for the modified system (No Ave) and all its variations. Individual case wavenumber estimates are shown in Figs. C2, C3, and C4 in Appendix

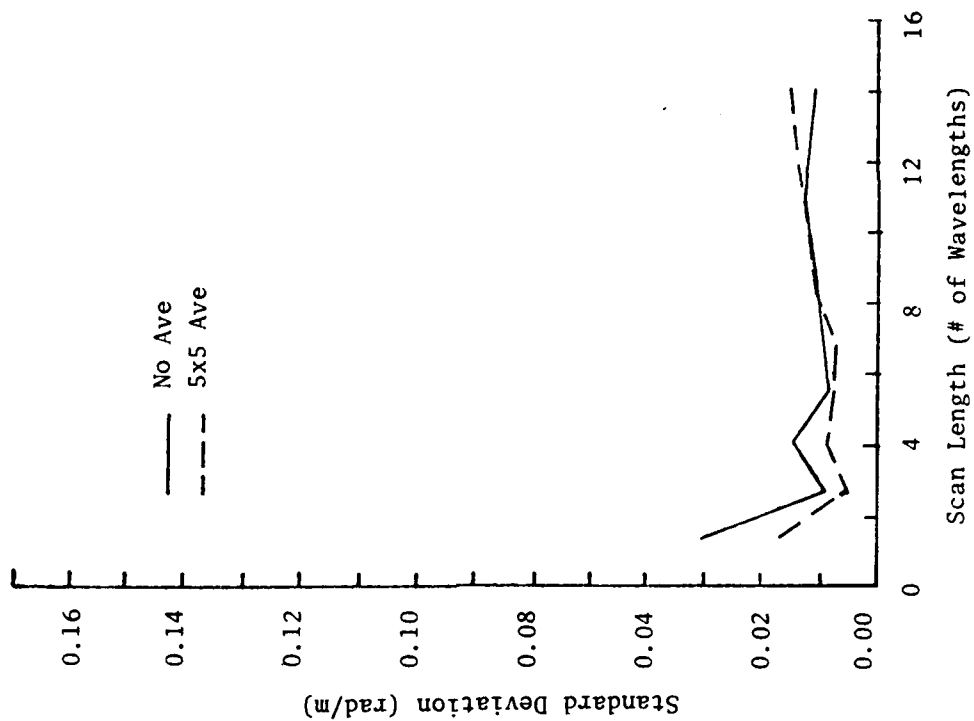
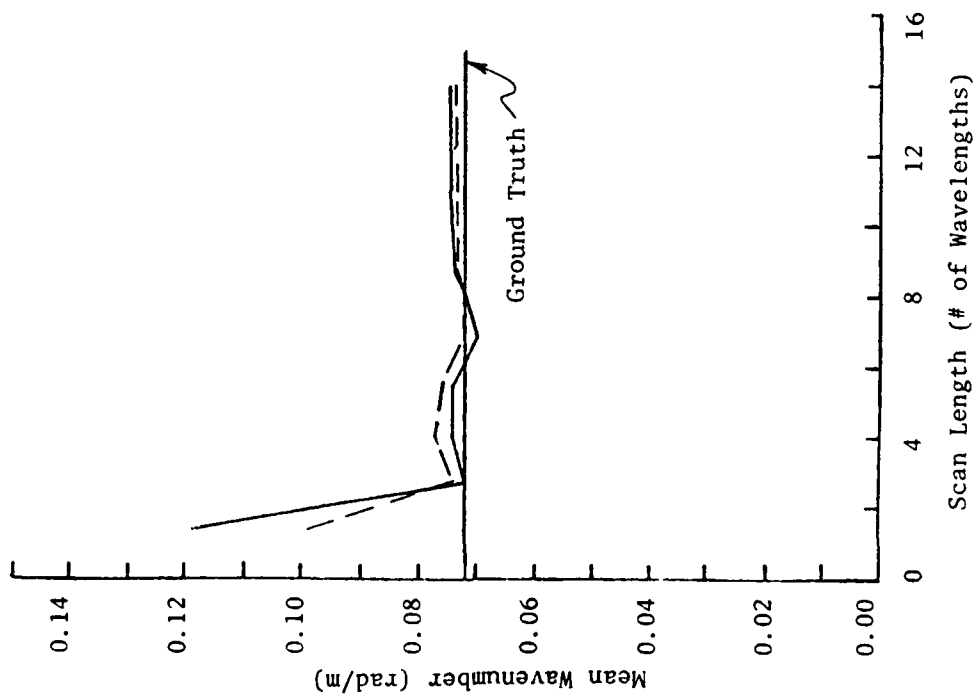


Fig. 43. Area A-3 Along-Scan Wavenumber Estimate Statistics for $\theta_r = 0^\circ$.

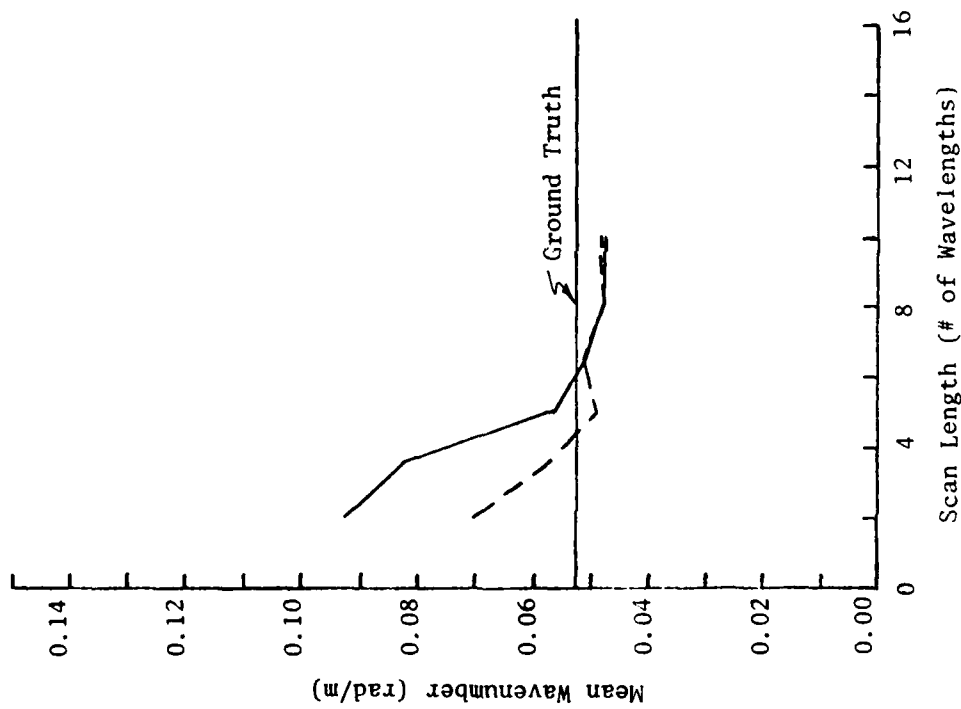
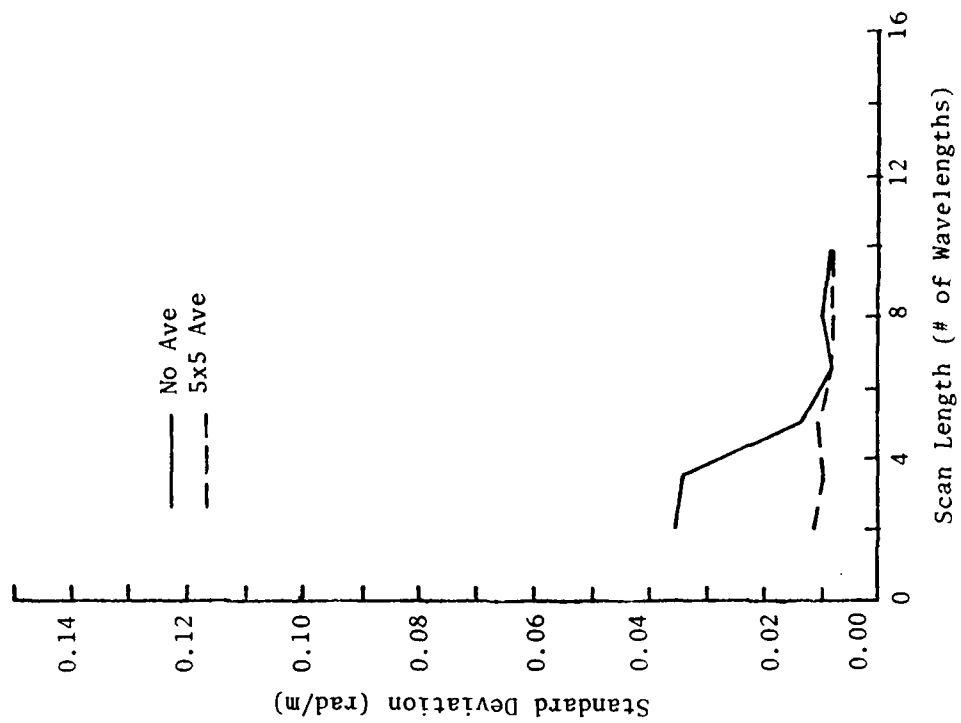


Fig. 44. Area A-3 Along-Scan Wavenumber Estimates for $\theta_r = 23^\circ$.

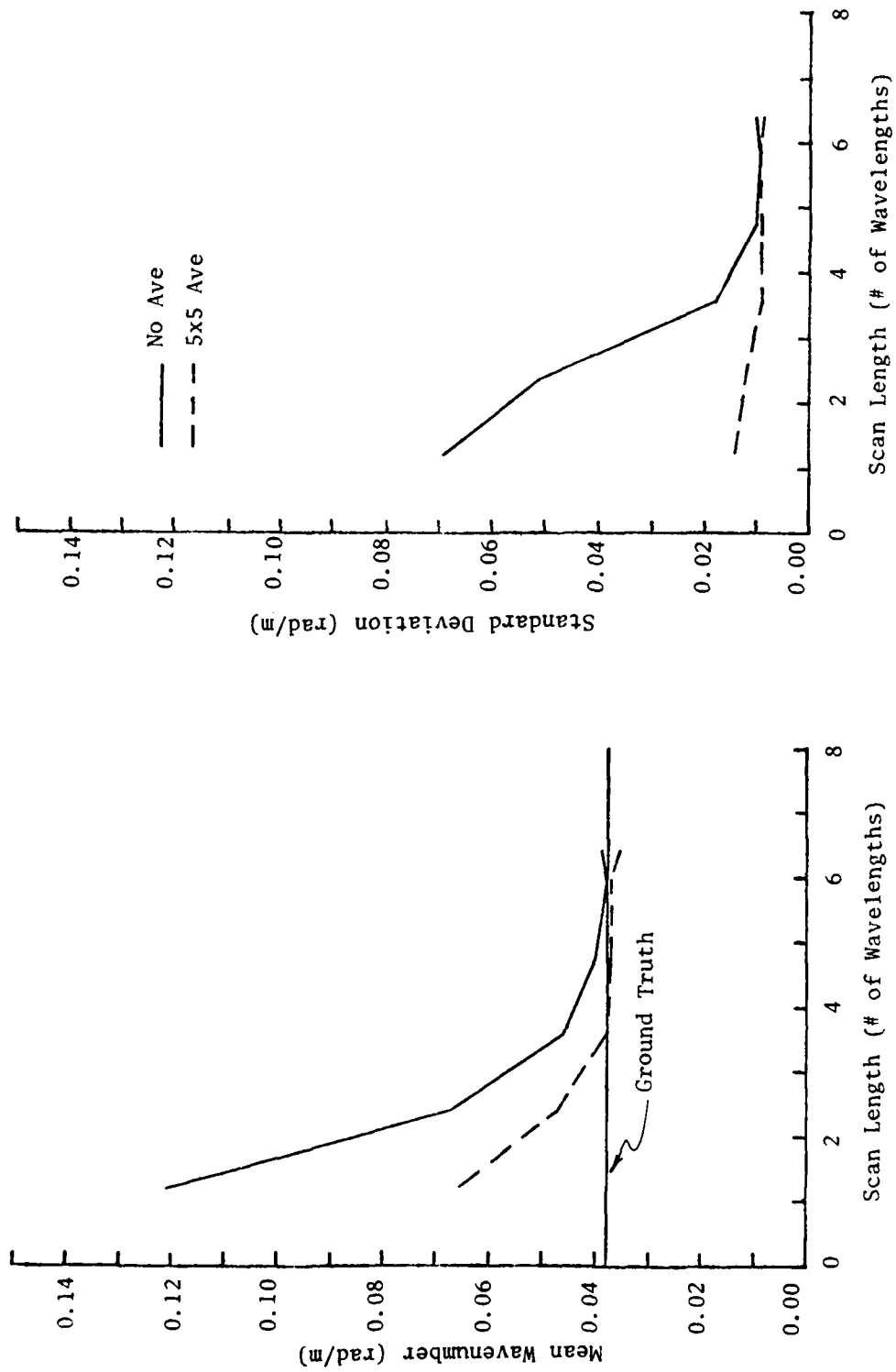


Fig. 45. Area A-3 Along-Scan Wavenumber Estimate Statistics for $\theta_r = 35^\circ$.

Table XII. Summary of Along-Scan Wavenumber
Estimate Performance for Analysis
Area A-3.

Scan Rotation Angle θ_r	Ground Truth Wavenumber k_y	Convergence Scan Length in Wavelengths	Non Estimable Cases	Relative Average Bias	Relative Average Std. Dev.
Modified System (No Ave)					
0°	0.071	3	7.5%	1.8%	15.1%
23°	0.052	5	17.5%	-2.7%	19.3%
35°	0.038	5	5.0%	1.8%	26.7%
Modified System with Smoothed Data (5x5 Ave)					
0°	0.071	3	3.8%	3.0%	13.9%
23°	0.052	5	7.5%	-6.0%	16.7%
35°	0.038	5	0%	-4.2%	24.2%

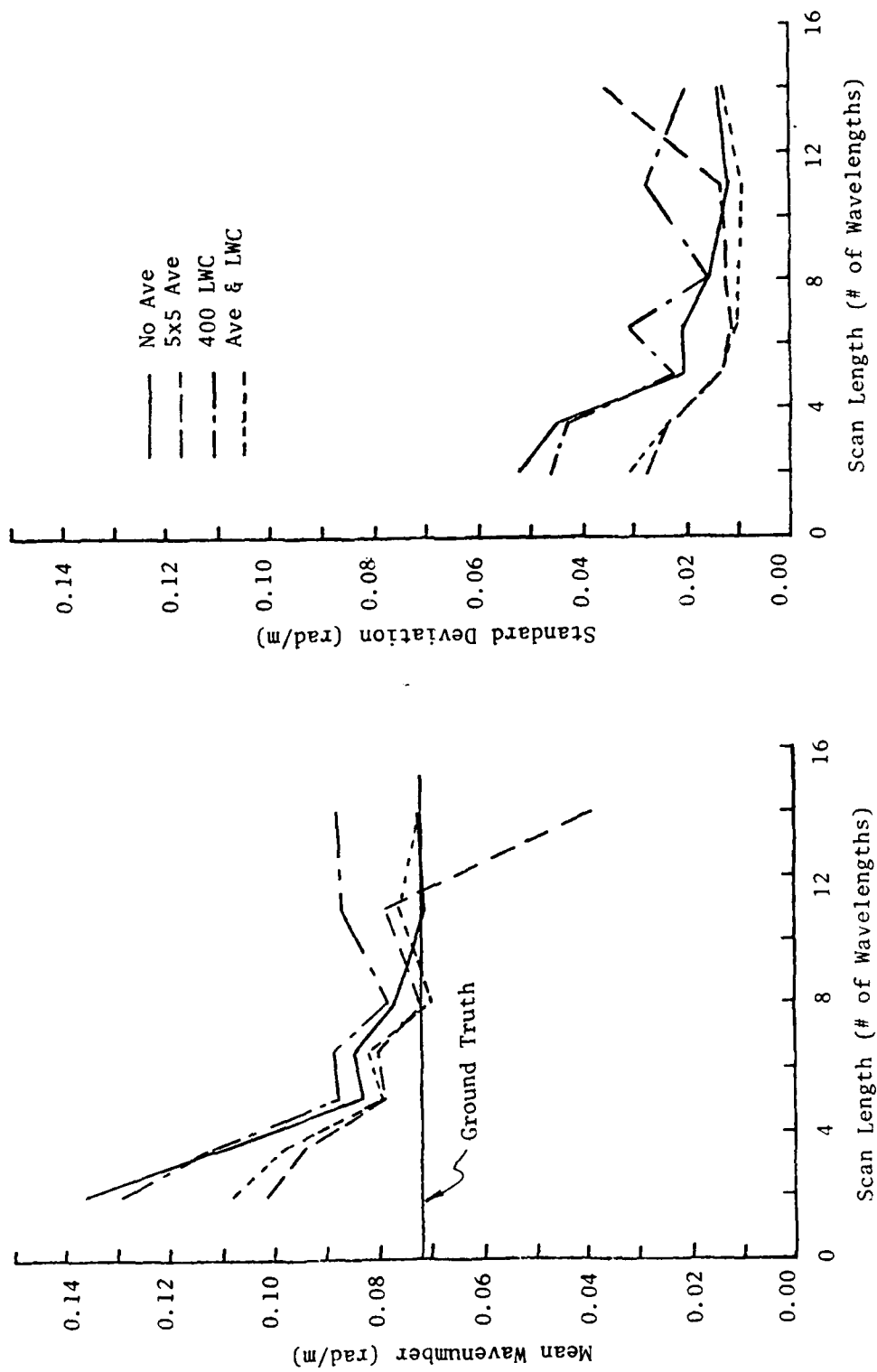


Fig. 46. Area A-4 Along-Scan Wavenumber Estimates for $\theta_r = 0^\circ$.

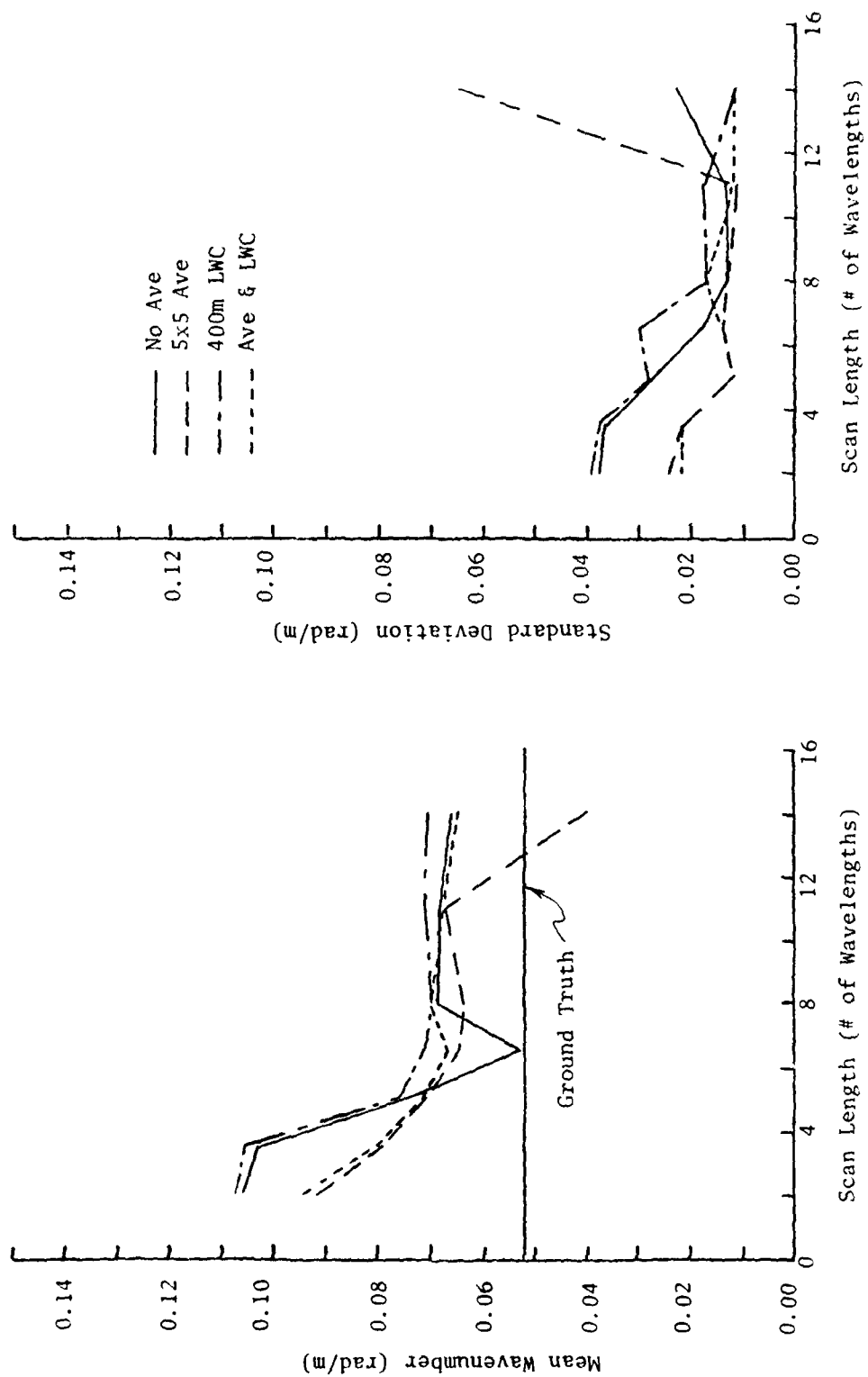


Fig. 47. Area A-4 Along-Scan Wavenumber Estimate Statistics for $\theta_r = 23^\circ$.

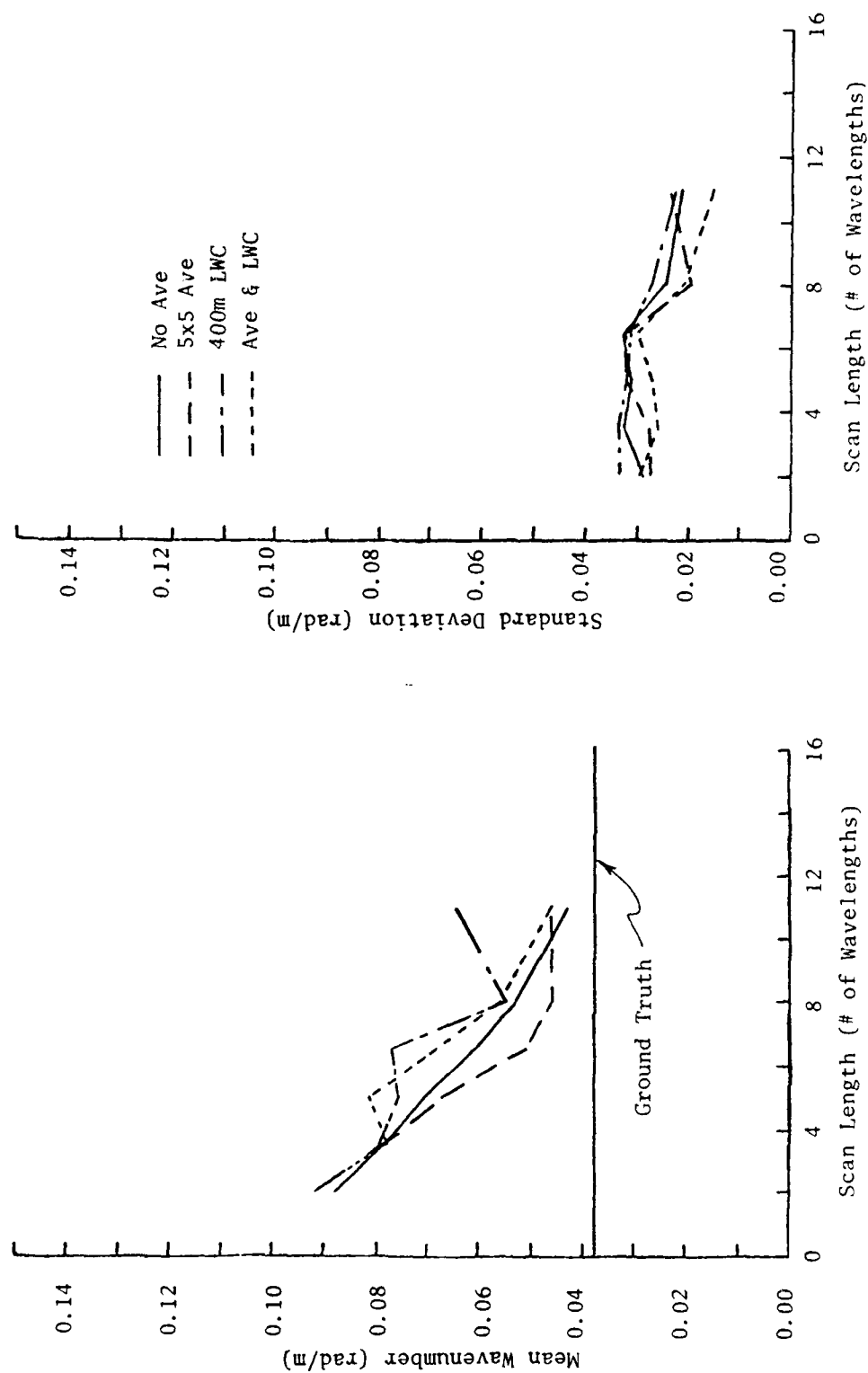


Fig. 48. Area A-4 Along-Scan Wavenumber Estimate Statistics for $\theta_r = 35^\circ$.

C for all system configurations and all rotation angles for a system using 14 scans of length approximately equal to 11 wavelengths.

The wavenumber estimate performance for analysis area A-4 is summarized in Table XIII for the modified system (No Ave) and the modified system using smoothed data and low wavenumber cutoff (Ave & LWC). In this table, the relative average bias, relative average standard deviation, and percent of non-estimable cases were obtained by considering cases and results for scan lengths greater than or equal to that required for convergence except for $\theta_r = 35^\circ$ when no convergence was apparent. Results shown are for scan lengths equal to approximately 8 and 11 wavelengths when $\theta_r = 35^\circ$.

It can be seen that the system performance for analysis area A-4 is considerably poorer than for analysis area A-3 except for results obtained with the Ave & LWC variation of the systems when $\theta_r = 0^\circ$. The performance curves show no good reason for choosing any of the system variations over the basic modified system (No Ave). The number of non-estimable cases is reduced when smoothed data is used, however.

Upon closer inspection of photographs for image A and the analysis areas within it, it is evident that several well defined wave crests are located within analysis areas A-3 (see Fig. 9b). Similar wave structure is not nearly as well defined in analysis area A-4 (see Appendix A). It is most likely that the lack of well defined wave structure on the image (poor signal-to-noise characteristic) is the major cause of the observed performance degradation in area A-4 with respect to area A-3.

It is interesting to note the extreme changes in wavenumber estimate mean and standard deviation for the 5x5 Ave system configuration at rotation angles of 0° and 23° when the maximum scanlength of approximately 14 wavelengths is considered. Observation of the image photograph for analysis area A-4 (see Appendix A) shows an apparent overall illumination change from a brighter level at nadir to a darker level at maximum range. This is reasonable due to the increase in range. This effect is not nearly as pronounced in area A-3 for some reason. Because the illumination level changes very slowly, a long scan length must be considered in order for the illumination level change to be significant. It is felt that this may be an explanation for the poor performance when the scan length is long. Although it is not exactly clear why the problem did not occur for non-averaged data, it is possible that since the changing illumination is a low frequency effect, the 5x5 averaging of the data, which acts as a low pass filter, enhances the illumination effect. Also note that the 400m Low Wavenumber Cut off system variation ignores extremely low wavenumber components and thus does not produce the extreme results observed for the 5x5 Ave system.

One method which could be used to reduce the illumination level change along the scans would be to divide the value of the data at each scan location by the average of the data values at that location

Table XIII. Summary of Along-Scan Wavenumber
Estimate Performance for Analysis
Area A-4.

Scan Rotation Angle θ_r	Ground Truth Wavenumber k_y	Convergence Scan Length in Wavelengths	Non Estimable Cases	Relative Average Bias	Relative Average Std. Dev.
Modified System (No Ave)					
0°	0.071	8	15.0%	2.7%	18.9%
23°	0.052	8	15.0%	29.6%	31.4%
35°	0.038	?	35.0%	24.9%	60.3%
Modified System Variation (Ave & LWC)					
0°	0.071	8	1.7%	1.3%	14.4%
23°	0.052	6.5	7.5%	28.9%	25.6%
35°	0.038	?	20.0%	33.0%	47.4%

on all scans used. This was tried for the (5x5 Ave) system variation with $\theta_r = 0^\circ$ and scan lengths of approximately 11 wavelengths and did indeed remove the spurious result. The wavenumber estimate mean and standard deviation obtained were comparable with those obtained for the modified system (No Ave). The only problem with using this type of scan data correction is that a wave travelling along the radar scan would be effectively suppressed.

The third analysis area considered was area A-5 which was taken the same distance from the right side of image A as analysis area A-3 was taken from the left side of image A. Wavenumber estimate statistics for this analysis area are shown as a function of scan length in Figs. 49, 50, and 51 for scans rotated from the original data scans by $\theta_r = 0^\circ$, 23° , and 35° respectively. As for analysis area A-3, the image edge limited the length of scan which could be investigated for the rotated data scans. Individual case wavenumber estimates are shown in Figs. C5, C6, and C7 in Appendix C for all system configurations and all rotation angles for a system using 14 scans of length approximately equal to 6.5 wavelengths.

The wavenumber estimate performance for analysis area A-5 is summarized in Table XIV for the modified system (No Ave) and the modified system using smoothed data and low wavenumber cutoff (Ave & LWC). Since well defined convergence did not occur in most cases, the relative average bias, relative average standard deviation, and percent of non-estimable cases were obtained by considering results for scan-lengths greater than or equal to approximately 11, 6.5, and 5 wavelengths for $\theta_r = 0^\circ$, 23° , and 35° respectively.

It can be seen that performance for analysis area A-5 is similar to that for analysis area A-4 except for a much larger bias when estimates are made along the original scan direction (i.e. $\theta_r = 0^\circ$). One might question whether this was due to changed wave characteristics in this area so the buoy ground truth would not apply. This does not seem likely when the image photograph and the bathymetry for the two areas is considered.

The performance curves once again show no good reason for choosing any of the system variations over the basic modified system (No Ave). The number of non-estimable cases is reduced when smoothed data is used as has previously been noted for the other analysis areas. The similarity of the performance to that from analysis area A-4 does not come as a surprise when the photographs of image data for these two analysis areas are considered (see Appendix A). This is true since the definition of the wave structure is similar on these two images.

Note that an extreme change in wavenumber estimate mean and standard deviation occurs for the 5x5 Ave system configuration at $\theta_r = 23^\circ$ when the maximum scan length of 11 wavelengths is considered. The same illumination level change reason for this occurrence as discussed previously is assumed to cause this spurious result. Once again, this

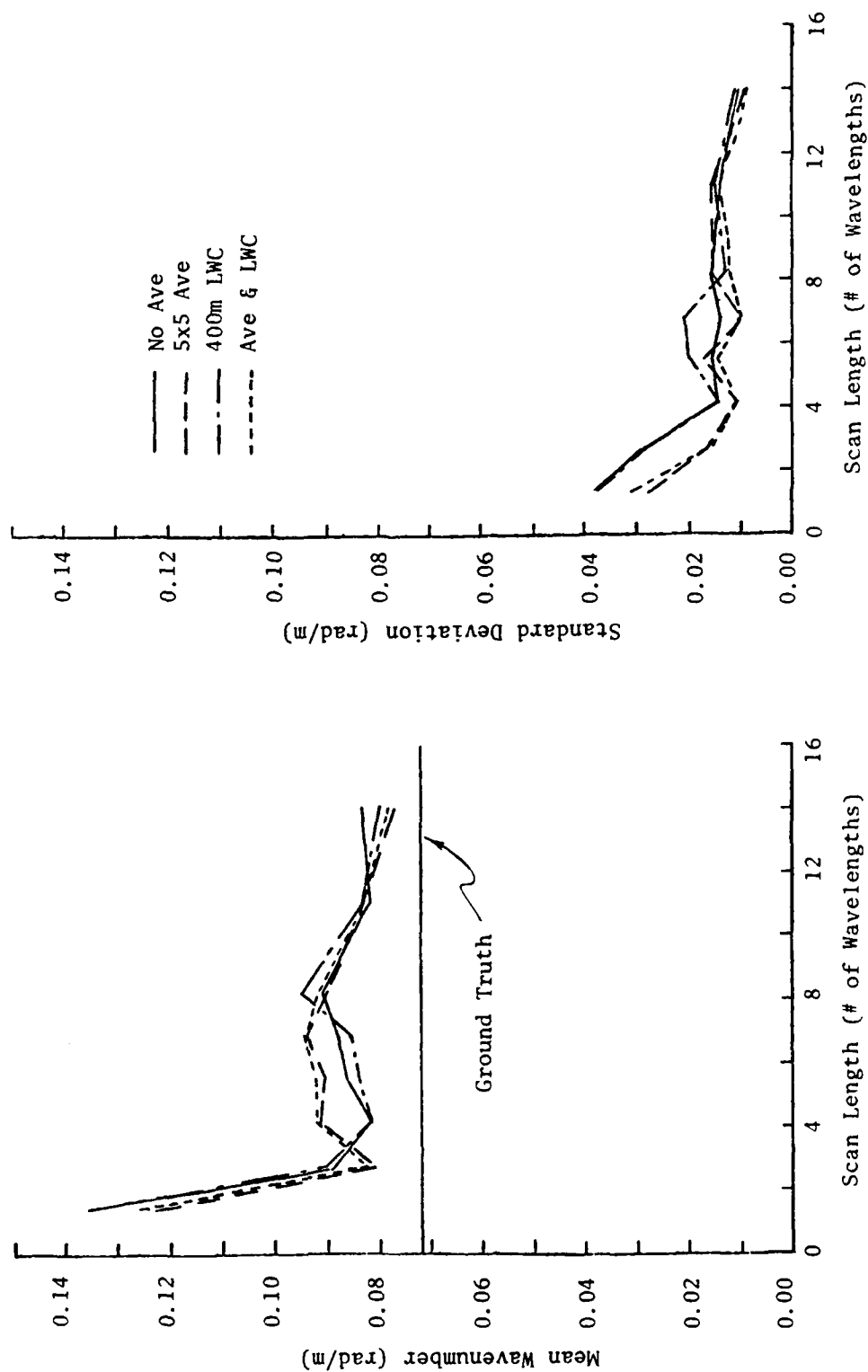


Fig. 49. Area A-5 Along-Scan Wavenumber Estimate Statistics for $\theta_r = 0^\circ$.

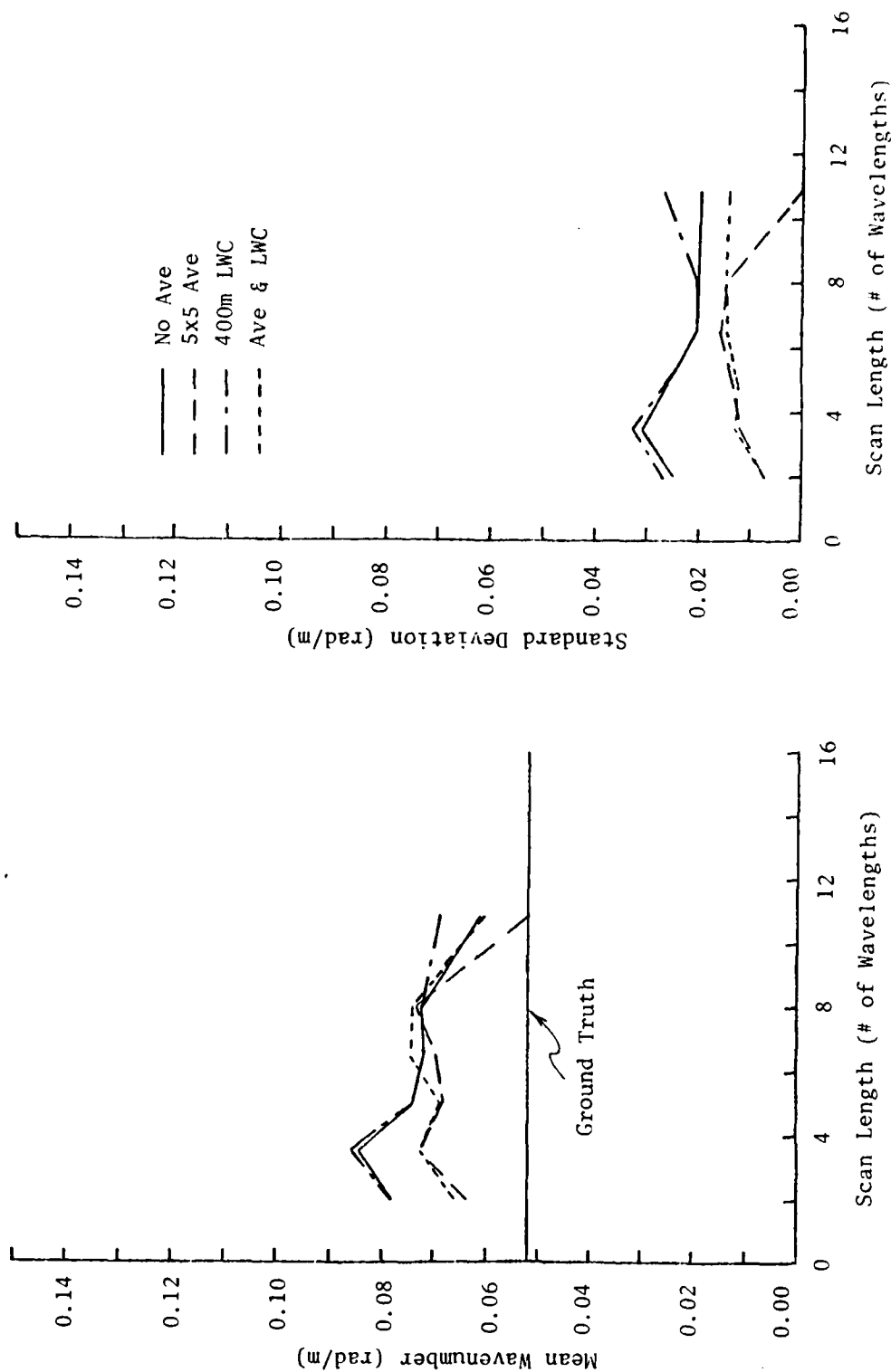


Fig. 50. Area A-5 Along-Scan Wavenumber Estimate Statistics for $\theta_r = 23^\circ$.

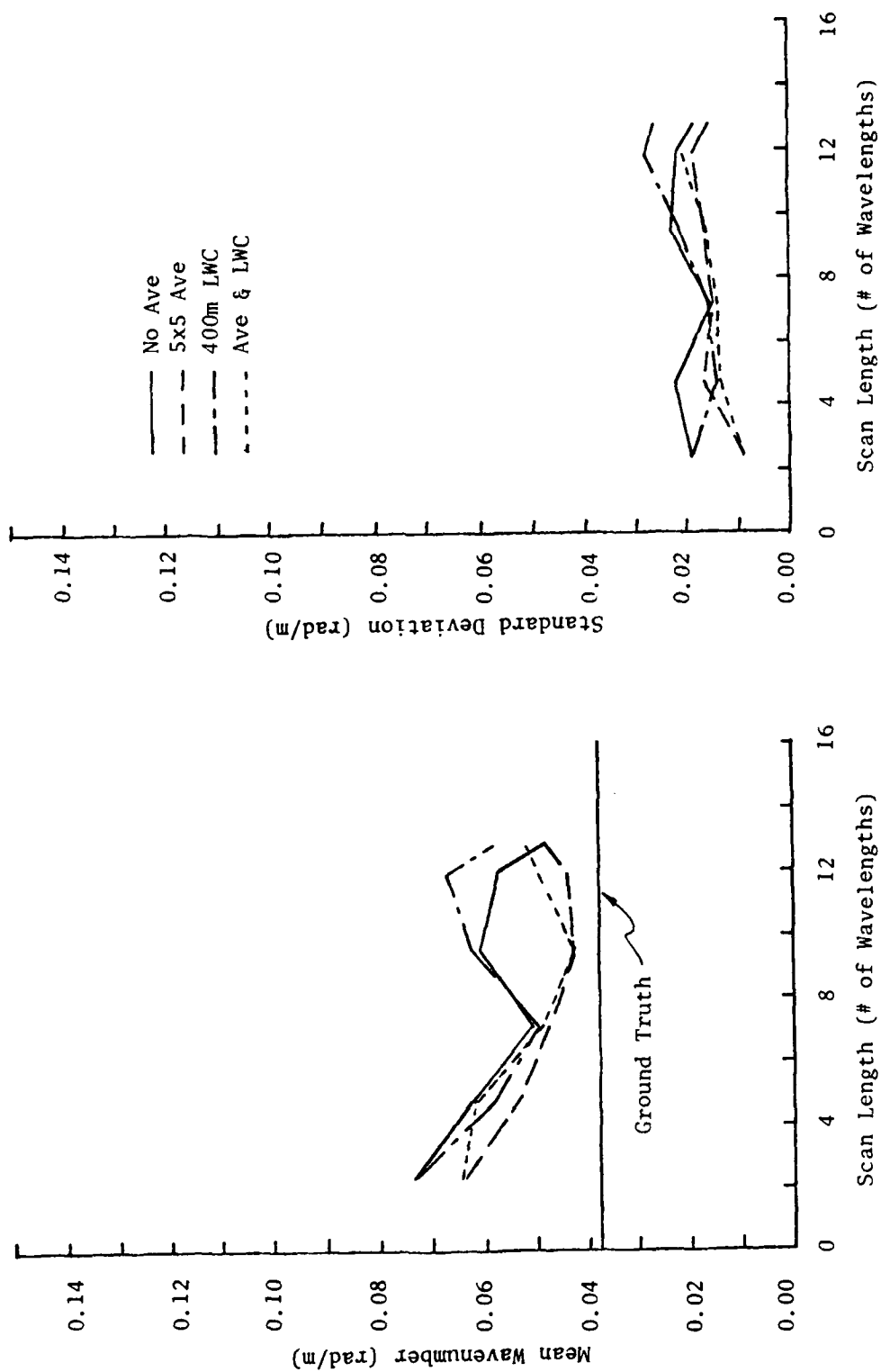


Fig. 51. Area A-5 Along-Scan Wavenumber Estimate Statistics for $\theta_r = 35^\circ$.

Table XIV. Summary of Along-Scan Wavenumber
Estimate Performance for Analysis
Area A-5.

Scan Rotation Angle θ_r	Ground Truth Wavenumber k_y	Convergence Scan Length in Wavelengths	Non Estimable Cases	Relative Average Bias	Relative Average Std. Dev.
Modified System (No Ave)					
0°	0.071	11	15.0%	15.0%	16.7%
23°	0.052	?	10.0%	32.4%	38.8%
35°	0.038	?	21.7%	46.5%	55.6%
Modified System Variation (Ave & LWC)					
0°	0.071	?	0%	12.4%	15.5%
23°	0.052	?	5.0%	34.1%	27.8%
35°	0.038	?	20.0%	26.8%	48.5%

particular analysis was repeated using the average scan division correction to the data. Again, the spurious result was eliminated. The wavenumber estimate mean and standard deviation obtained were comparable with those obtained for the rest of the system variations.

The fourth analysis area considered was taken near the center of the second image used and is designated B-1. Recall that ground truth was not available for this image. The wave period was inferred from the wave period present on image A since the two images were taken near the same time in relatively close ocean areas. The indicated propagation angle was estimated by making measurements on the image. The computed along-scan wavenumber from these considerations is used for comparison and referred to as the reference wavenumber. Wavenumber estimate statistics for this analysis area are shown as a function of scan length in Figs. 52, 53, and 54 for scans rotated by $\theta_r = 0^\circ$, 130° , and 45° respectively. Note that $\theta_r = 45^\circ$ should give scans that are approximately along the wave propagation direction.

Results for the basic modified system are not included for the second two rotation angles since results were quite poor when $\theta_r = 0^\circ$. The low wavenumber cutoff system variations were not considered since they did not provide significantly different performance for previous analysis areas. However, a new system variation was used which incorporates the average scan division previously defined. This is referred to as the ASD variation if original data is used and the Ave & ASD variation if 5x5 smoothed data is used.

The wavenumber estimate performance for analysis area B-1 is summarized in Table XV for the two system variations using average scan division (ASD and Ave & ASD). Results for only these two variations are summarized since it is apparent that average scan division is necessary to obtain estimates with the data from analysis area B-1. The relative average bias, relative average standard deviation, and percent of non-estimable cases were obtained by considering results for scan lengths greater than or equal to approximately 8 wavelengths since all configurations considered had converged as well as they were going to when the scan lengths had become this long.

When comparing system performance for analysis area B-1 with that for other analysis areas, two things are immediately evident. The first is that the number of non-estimable cases is considerably larger and the second is that the standard deviation of the estimate is considerably larger for estimates made along the scan direction. In general, the performance is quite poor which did not come as a surprise after seeing the performance available in other analysis areas since the photograph of the image data in analysis area B-1 does not show much wave crest definition at all.

When analyzing system performance with scan data from images A and B, scans were rotated to observe the performance for varying wavenumber along the scan. As previously indicated, rotation of the scans does not produce the same data as actual SAR processing would if the

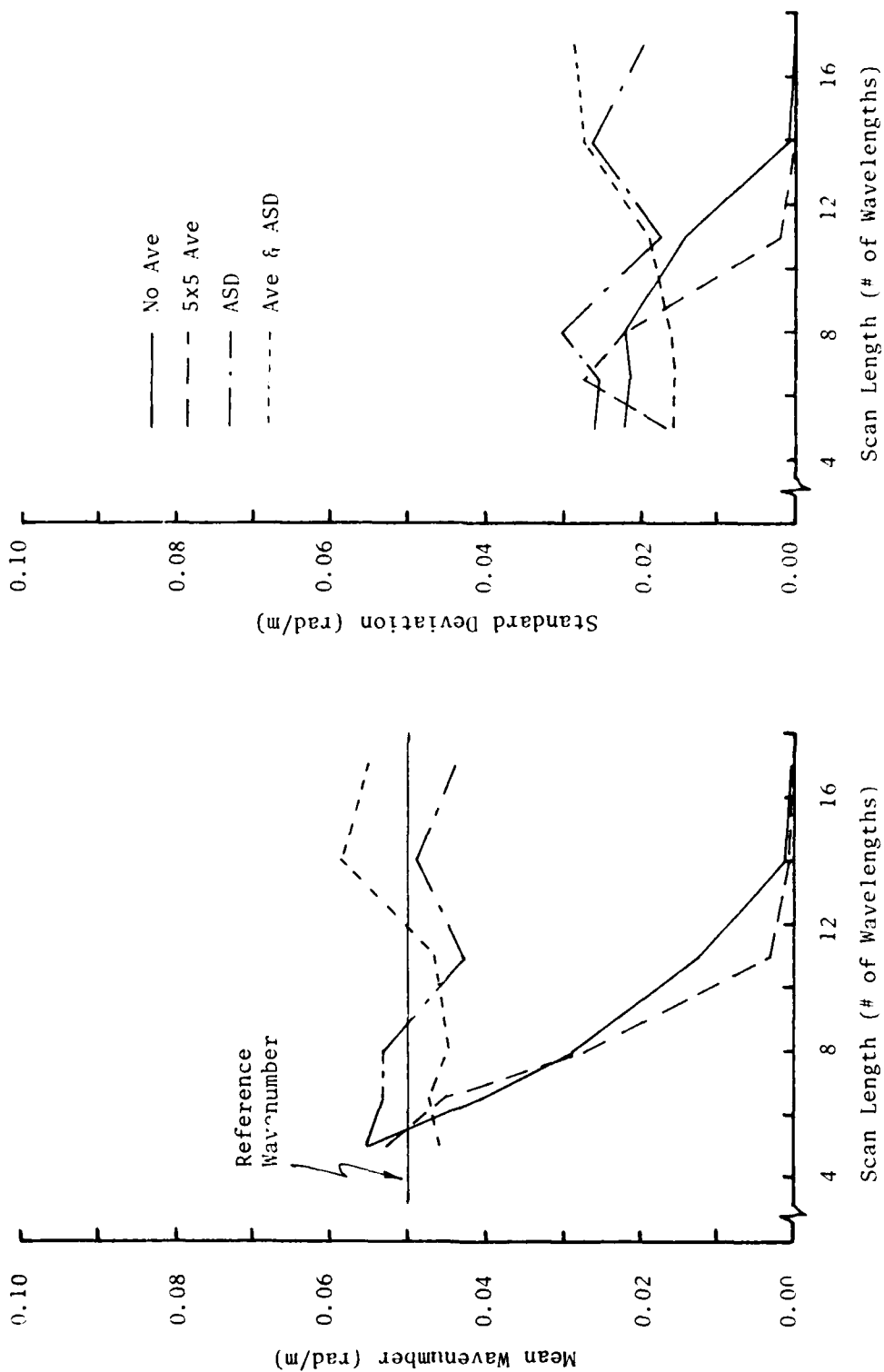


Fig. 52. Area B-1 Along-Scan Wavenumber Estimate Statistics for $\theta_r = 0^\circ$.

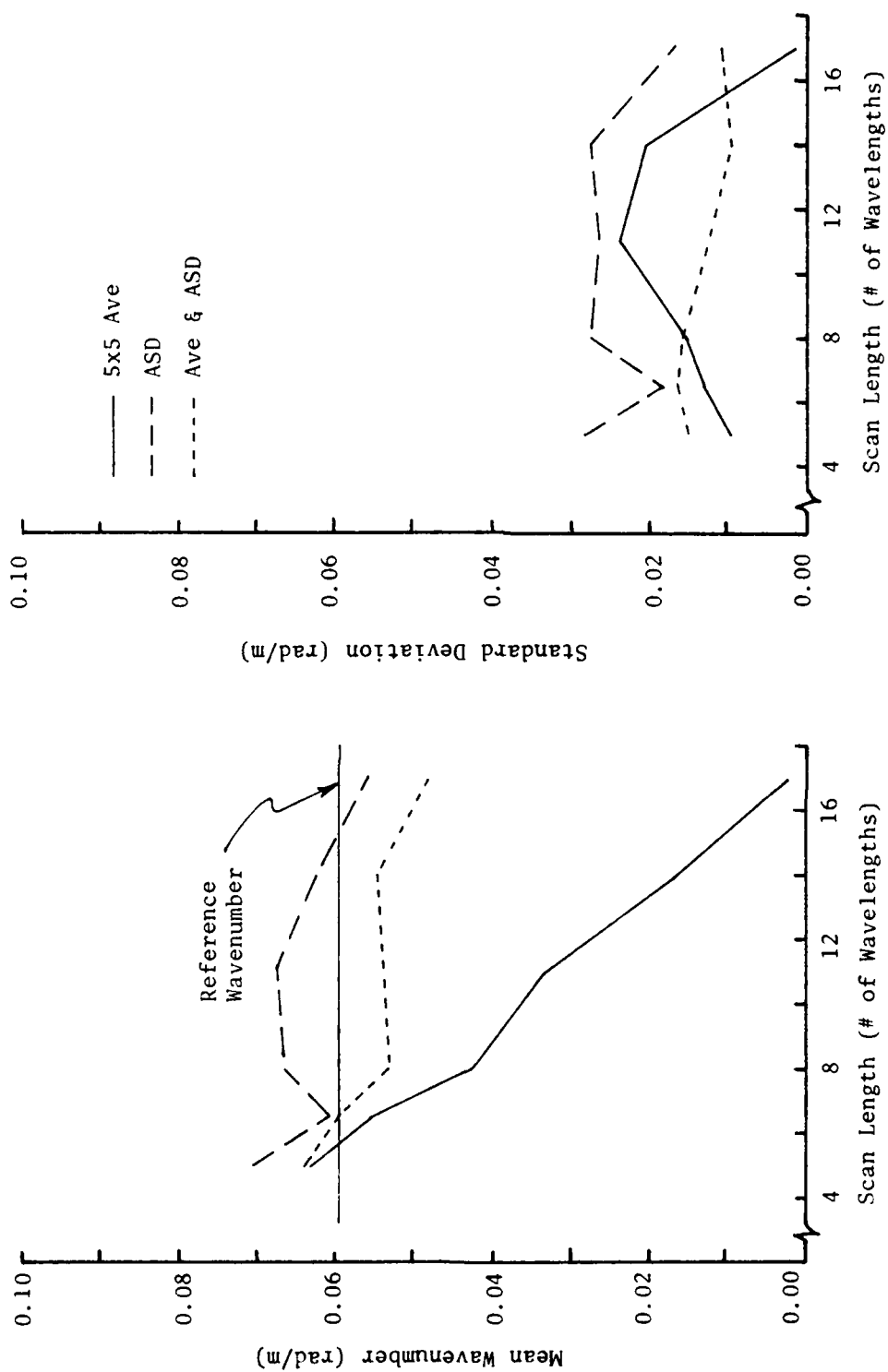


Fig. 53. Area B-1 Along-Scan Wavenumber Estimate Statistics for $\theta_r = 13^\circ$.

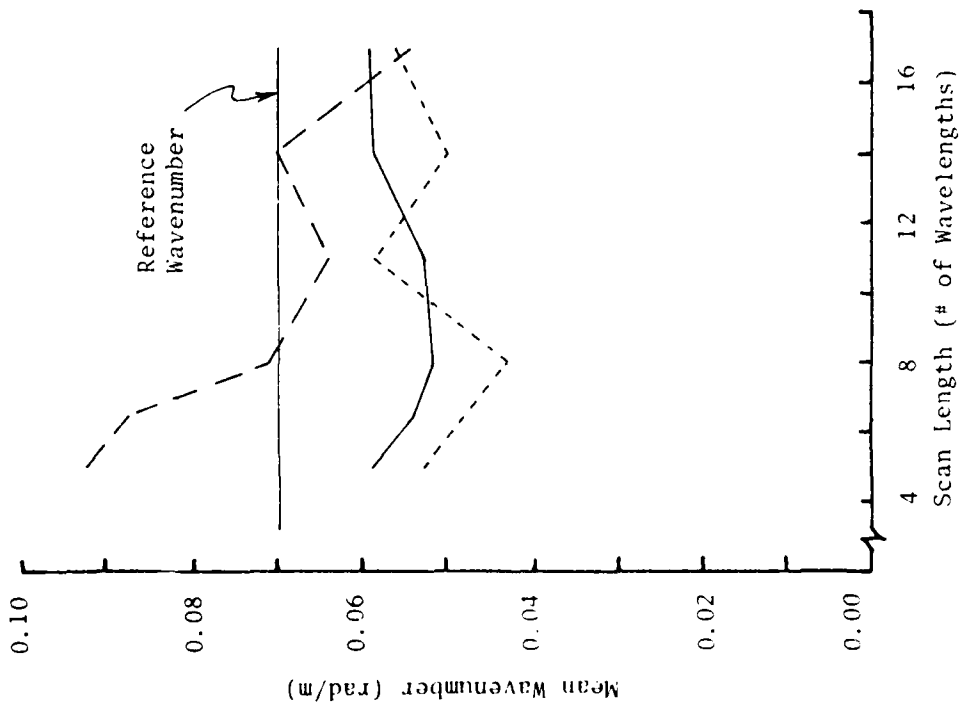
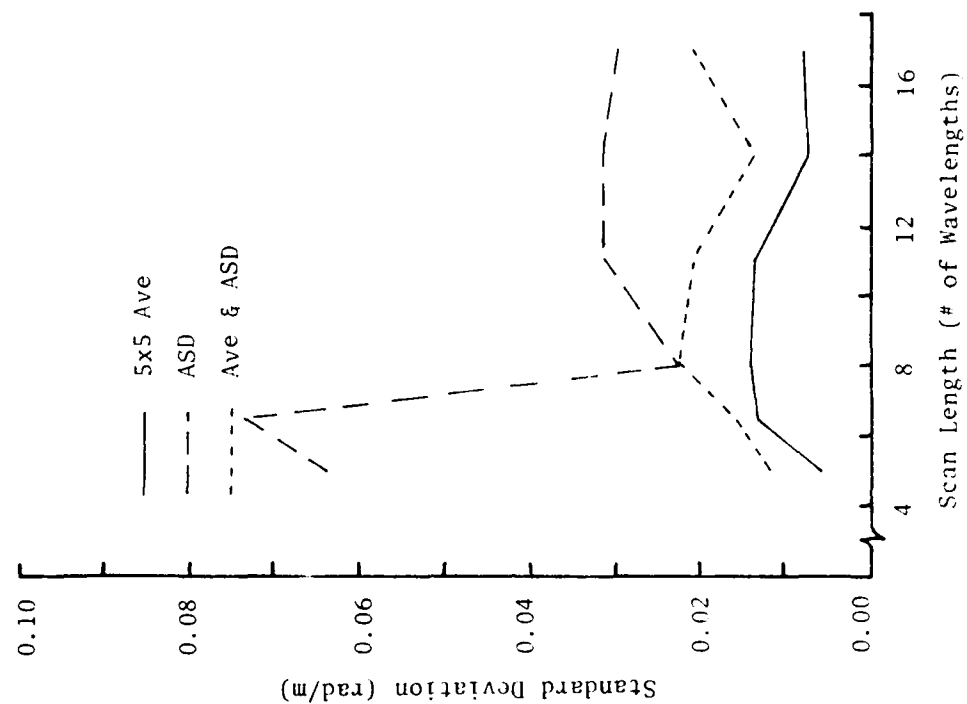


Fig. 54. Area B-1 Along-Scan Wavenumber Estimate Statistics for $\theta_r = 45^\circ$.

Table XV. Summary of Along-Scan Wavenumber
Estimate Performance for Analysis
Area B-1.

Scan Rotation Angle θ_r	Ground Truth Wavenumber k_y	Convergence Scan Length in Wavelengths	Non Estimable Cases	Relative Average Bias	Relative Average Std. Dev.
Modified System with ASD					
0°	0.050	?	27.5%	-5.1%	47.5%
13°	0.059	?	17.5%	5.9%	41.4%
45°	0.070	?	32.5%	-7.2%	41.4%
Modified System with Ave Data & ASD					
0°	0.050	?	16.3%	2.9%	45.9%
13°	0.059	?	11.3%	-12.0%	20.3%
45°	0.070	?	20.0%	-25.6%	28.4%

SAR look direction is parallel to the rotated scan lines due to the dependence of wave backscatter on illumination angle. In order to actually observe system performance for radar scans generated by a synthetic aperture radar for different look directions, eight images obtained by ERIM for eight different look directions were used and are identified as C-1 through C-8 in Tables II through V. Recall that these eight images were taken over the same area as image A and thus, ground truth information is available. Also recall that the data was geometrically and radiometrically converted by ERIM.

Referring to Table III, notice that each analysis area pair (C-1, C-5), (C-2, C-6), (C-3, C-7), and (C-4, C-8) has the same along-scan wavenumber, k_y , and wave propagation angle, θ_w . However, the indicated propagation angle, θ_i , is different for the two members of each pair since the wave is travelling toward the aircraft on one of them and away from the aircraft on the other one.

Performance statistics for the various like pairs are shown in Figs. 55 through 58 for the basic modified system configuration system (No Ave). The No Ave system was the only configuration considered in this analysis since previous analysis with other analysis areas showed that the system variations did not produce significant performance improvement. The scan spacing system parameter was necessarily changed because the resolution provided by the image data is 6m x 6m for each pixel in the two-dimensional image (see Table IV). In order to keep the scan spacing system parameter as close to 15m as possible, a scan spacing of 2 scans or 12m was chosen. Also note that the total number of cases (each requiring 14 scans) was reduced to 18 since the amount of data available is limited (i.e. 256 x 256 pixels/image). A total of 720 cases were considered for scan lengths ranging from 2 to 18 wavelengths. Of these, 181 or approximately 25% were declared non-estimable. This is obviously an unacceptably high percentage.

Observation of the results is not encouraging. For all but one analysis area (i.e. C-7), an extremely large bias occurs. Also note that a very good wavenumber estimate convergence is seen for all cases; however, the final estimates are never the same for image pairs (e.g. (C-1, C-5)). No real reason for the extremely poor performance and inconsistencies has been established.

F. OVERALL WAVENUMBER ESTIMATION PERFORMANCE CONCLUSIONS

The primary conclusion which can be reached from the analysis of along-scan wavenumber estimation performance for the system using a few scans of SAR data is that the performance is in general not very consistent or satisfactory. In the first analysis area considered (A-3), the relative estimate bias is somewhat reasonable since it is in the neighborhood of 5% or less on the average. However, the estimate variability as indicated by the estimate relative standard deviation is larger than desired since the relative standard deviation is greater

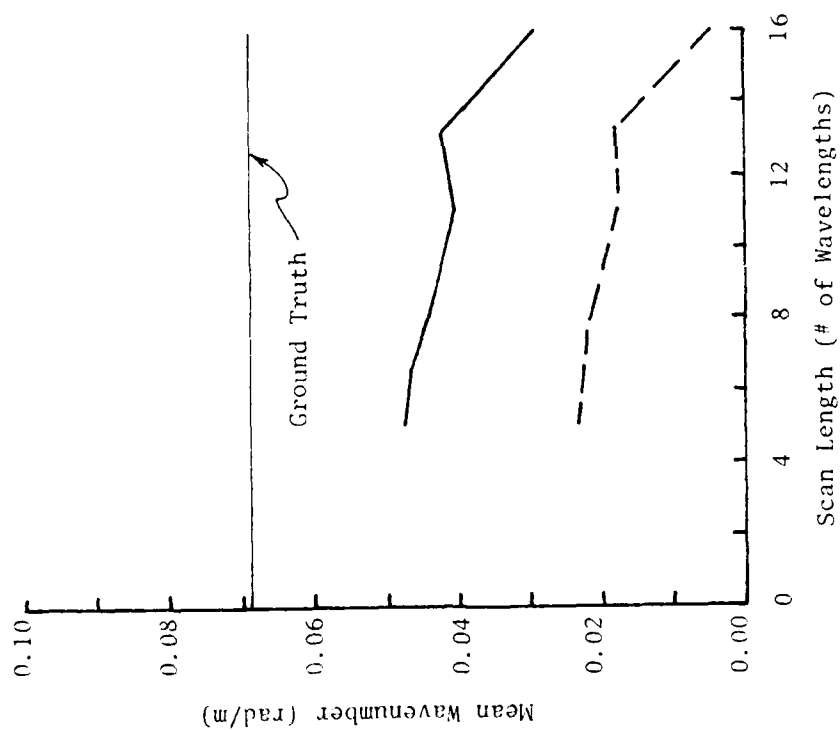
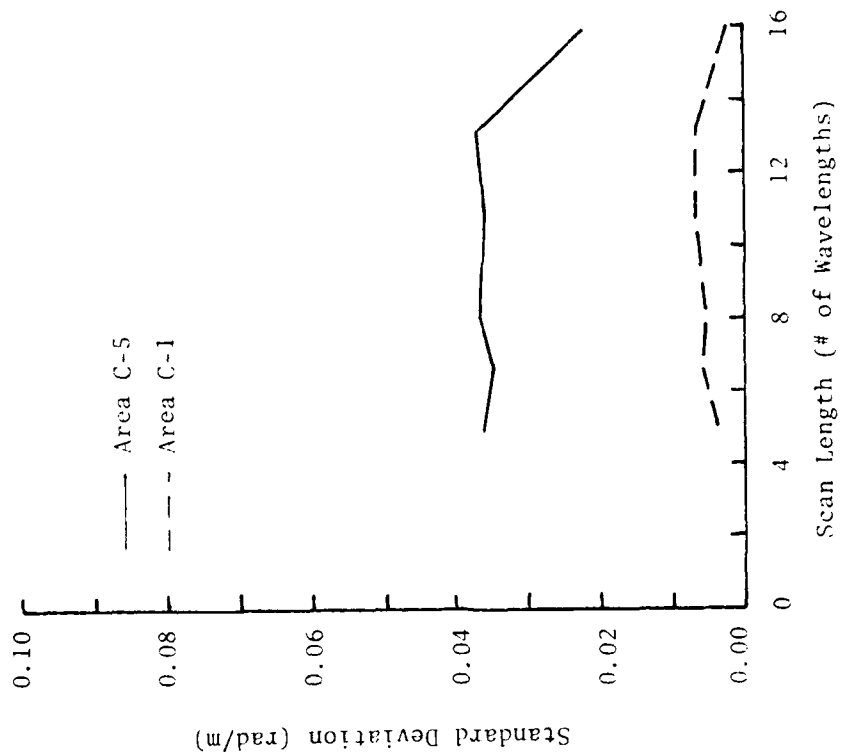


Fig. 55. Along-Scan Wavenumber Estimate Statistics for Analysis Areas C-1 and C-5.

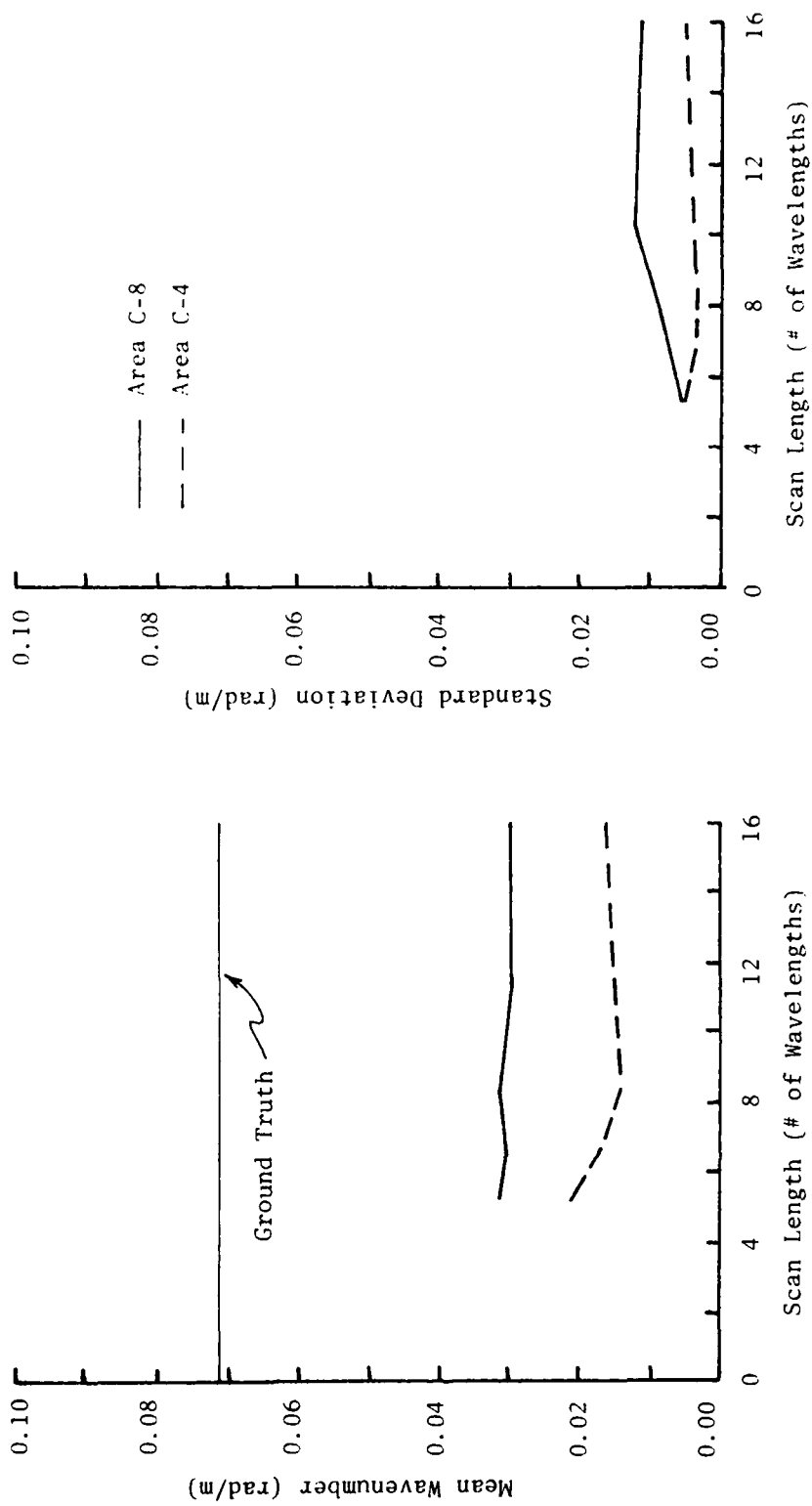


Fig. 56. Along-Scan Wavenumber Estimate Statistics for Analysis Areas C-8 and C-4.

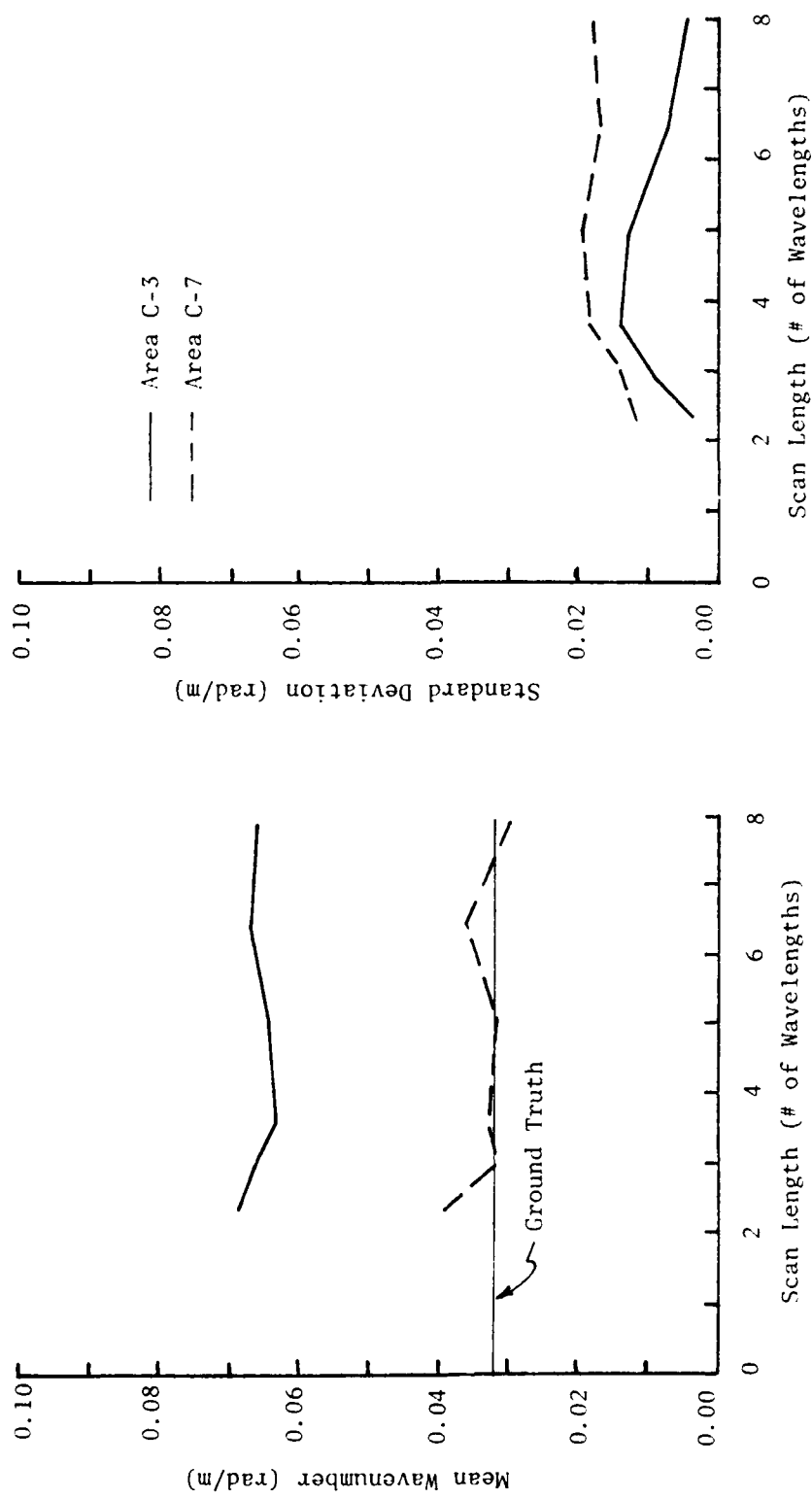


Fig. 57. Along-Scan Wavenumber Estimate Statistics for Analysis Areas C-3 and C-7.

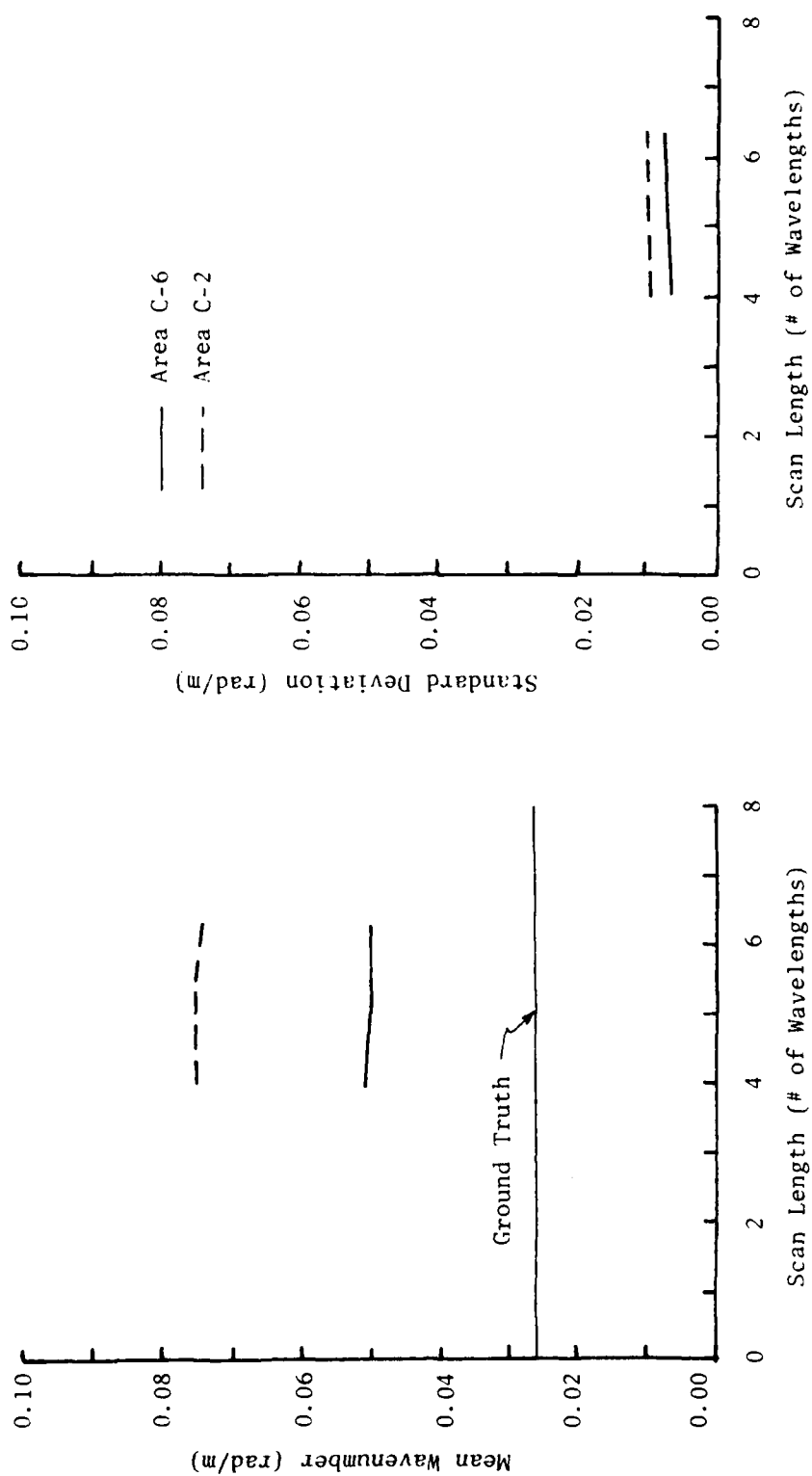


Fig. 58. Along-Scan Wavenumber Estimate Statistics for Analysis Areas C-6 and C-2.

than approximately 14% for all analyses considered. The relative variability of the estimates increases as the wavenumber being estimated decreases. The number of cases in the first analysis area for which estimates cannot be achieved with the basic modified system because of non-convergence is also somewhat larger than would be desired. However, a decrease in non-estimable cases can be achieved by using smoothed scan data.

Wavenumber estimation performance in analysis areas other than the first is in general poorer. It is apparent that this poorer performance is a result of a lower signal-to-noise ratio in the data scans since the image photographs of these areas show far less well defined wave crest return. This indicates that very good signal-to-noise ratios (well defined wave structure) is required for the system to give acceptable wavenumber estimation performance.

V. ANALYSIS OF INDICATED PROPAGATION ANGLE ESTIMATION PERFORMANCE

The performance of the portion of the system which estimates the indicated propagation angle of the dominant wave component is analyzed in this section and performance results presented. The indicated propagation angle estimate will be referred to as simply a wave angle estimate in most cases in this analysis for text simplicity. However, in reading the text, it should be remembered that the estimate being considered is the indicated propagation angle of the dominant wave component.

The relatively poor performance obtained for along-scan wavenumber estimation indicates that it is unlikely that the wave angle estimate can be obtained with any degree of accuracy. However, much of the wave angle estimate analysis was performed in parallel with the wavenumber estimation analysis and the results are indicated here for completeness.

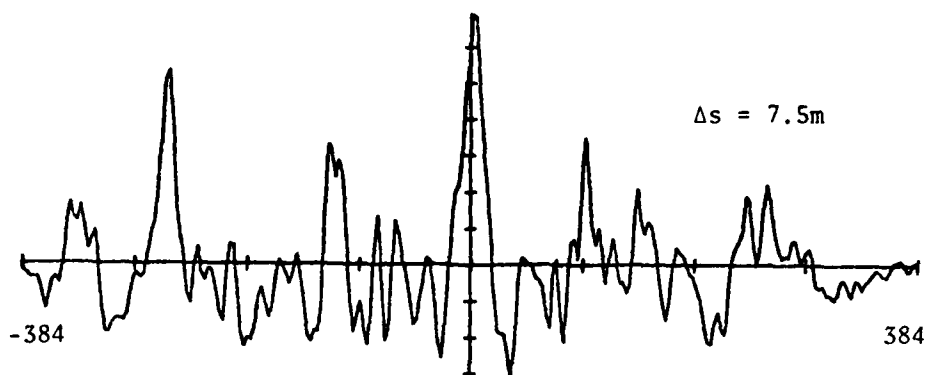
The analysis performed first considered the initial system concept defined earlier. Performance results indicated that modifications of the system concept were required. Thus, two additional system concepts were defined and results of the analysis of these system concepts are presented.

A. PERFORMANCE OF INITIAL SYSTEM CONCEPT

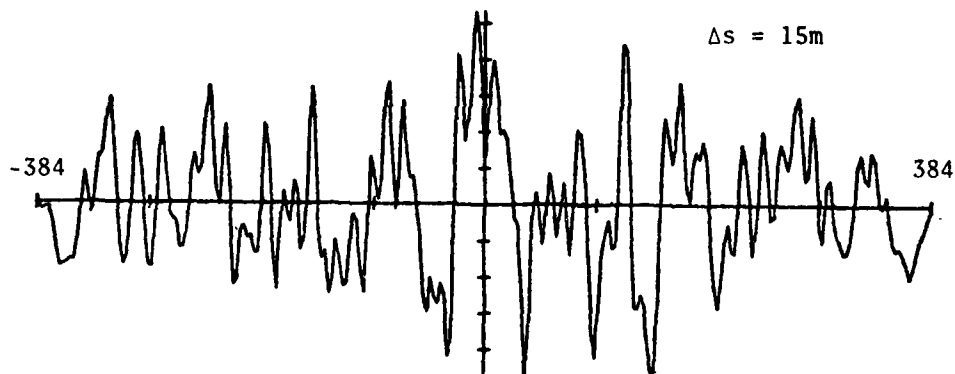
The initial system concept uses averages of cross correlation functions for a set of scan pairs to determine an estimate for wave offset between the scans. This estimate in turn is used to compute an estimate for the indicated propagation angle. To begin analysis of this system concept, a group of non-rotated scans were selected from analysis area A-1. Several different spacings, Δs , between scans being cross correlated and several different numbers of scan pairs, N_c , were considered for several different scan lengths, SL .

Figures 59 through 62 show examples of the average cross correlation functions obtained. Figures 59 and 60 show the average cross correlation functions obtained when cross correlations from 10 pairs of scans were averaged. The length of scans used was 384m and the scan spacings considered were $\Delta s = 7.5m, 15m, 30m, \text{ and } 60m$. Figures 61 and 62 show the average cross correlation functions for the same cases with the only change being that longer scans (768m) were used. (Note that only the center one-half of the cross correlation functions are plotted in Fig. 62.)

The wave offset estimate, \hat{y}_p , and resulting wave angle estimate, $\hat{\theta}_I = -\tan^{-1} (\hat{y}_p / \Delta s)$, are shown in Table XVI for the eight cases considered. It can be seen that no valid wave angle estimates were obtained for these example cases since the ground truth indicated



Lag Distance Along Scan (m)



Lag Distance Along Scan (m)

Fig. 59. Average of 10 Cross Correlation Functions for $SL = 384m$ and $\Delta s = 7.5m$ and $15m$ (Area A-1).

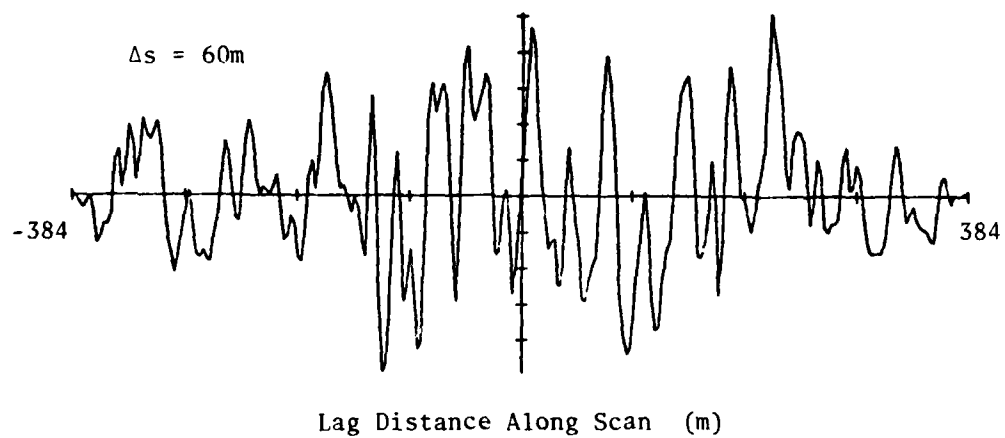
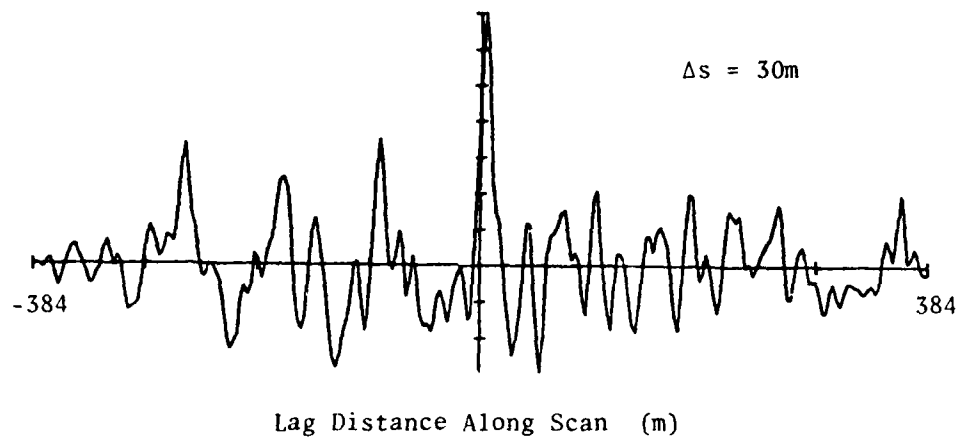


Fig. 60. Average of 10 Cross Correlation Functions for $SL = 384\text{m}$ and $\Delta s = 30\text{m}$ and 60m (Area A-1).

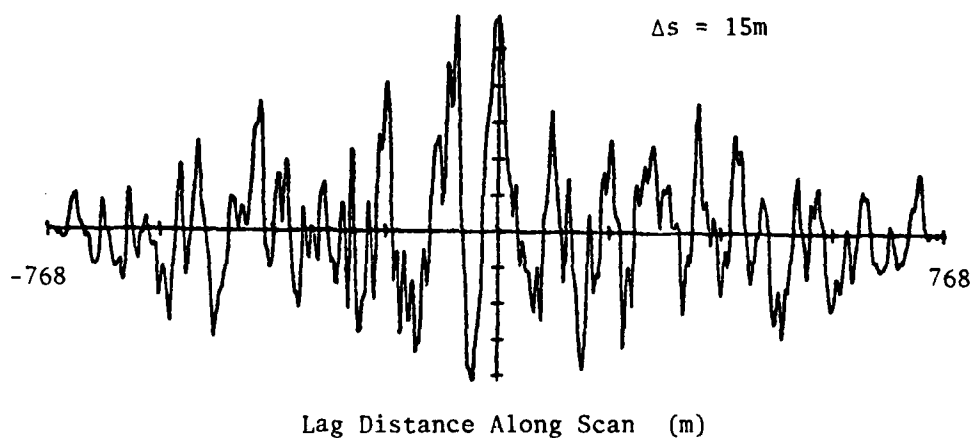
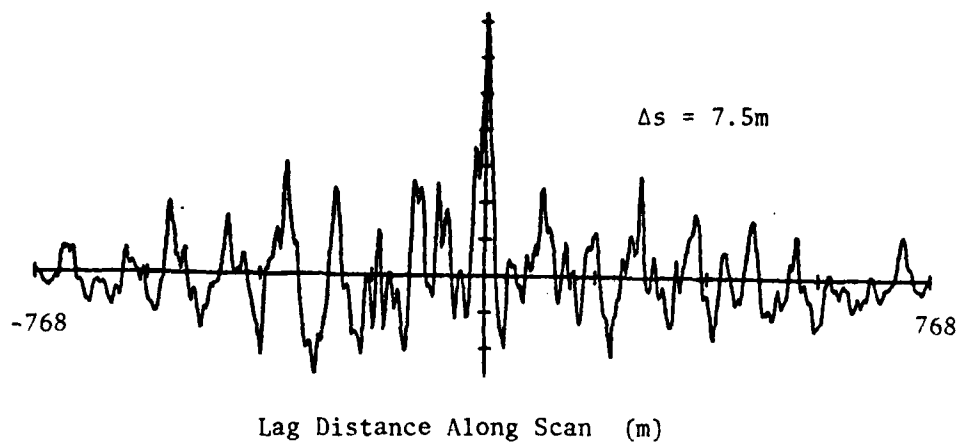


Fig. 61. Average of 10 Cross Correlation Functions for $SL = 768\text{m}$ and $\Delta s = 7.5\text{m}$ and 15m (Area A-1).

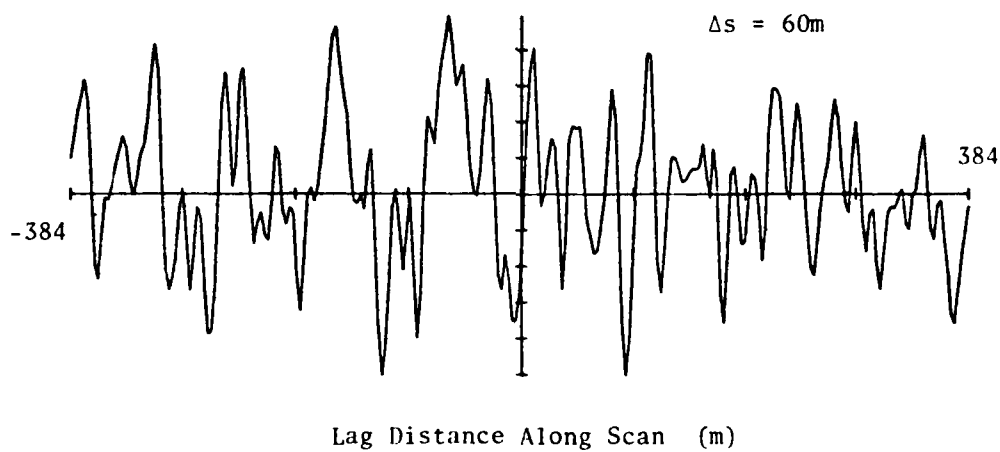
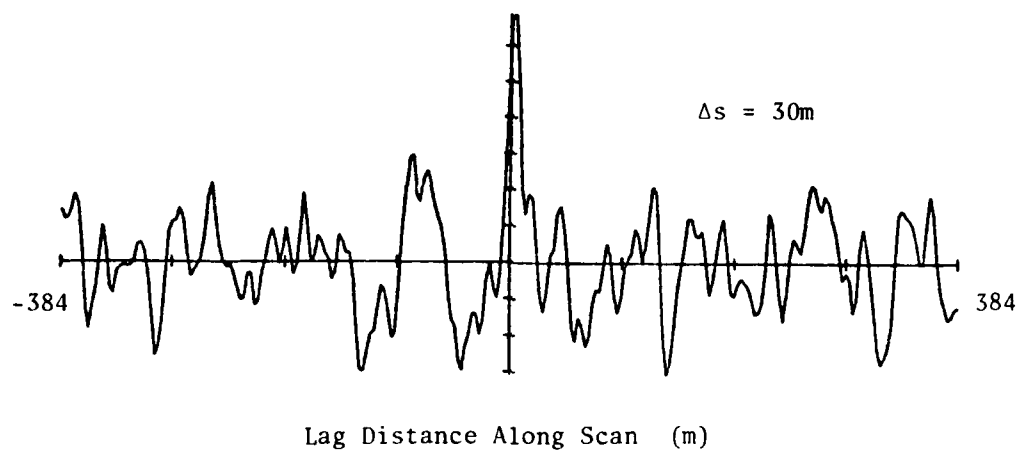


Fig. 62. Average of 10 Cross Correlation Functions for $SL = 768\text{m}$ and $\Delta s = 30\text{m}$ and 60m (Area A-1).

Table XVI. Estimates of Wave Offset Between Scans and Indicated Propagation Angle from Average of 10 Cross Correlation Functions (Area A-1).

Scan Length SL	Scan Separation Δs	Wave Offset Estimate \hat{y}_p	Wave Angle Estimate $\hat{\theta}_1$
384m	7.5m	1.32m	-9.97°
	15m	-8.54m	29.66°
	30m	2.29m	-4.36°
	60m	213.85m	-74.33°
768m	7.5m	0.41m	-3.13°
	15m	-72.82m	78.36°
	30m	1.64m	-3.13°
	60m	-81.16m	53.52°

propagation angle is -26.54° . This was true for all cases considered using the average cross correlation function system concept. Consequently, no statistical performance analysis was performed for this system concept. Obviously, noise on the scan data causes wave crest data to be insufficiently unique to permit computation of a wave angle estimate from averages of cross correlation functions obtained with a single scan spacing.

B. SECOND SYSTEM CONCEPT

The failure of the average cross correlation function system concept to provide good wave angle estimates led to the question as to whether wave crest data was observable in the radar scan data. To check this, data from eleven scans with a scan spacing of 30m (scans 174 - 374) were considered for analysis area A-1. The first two successive peaks along the scans were identified and their locations are identified in Fig. 63. Straight lines were fit in a least squares error sense to the two sets of peak locations to identify the average wave crest location. These are also shown in Fig. 63 along with the wave angle indicated by them. It can be seen that the two wave angles obtained (i.e. -19.8° and -19.2°) are relatively close to the ground truth wave angle of -26.54° .

The above observation of data peak locations led to the second system concept considered for estimating the indicated propagation angle. This system concept uses cross correlation function peak locations obtained with scans separated by several different scan spacings to estimate the wave crest displacement as a function of distance perpendicular to the scans. These wave crest displacement estimates are smoothed by averaging for several sets of scans and then fit with a straight line to estimate the wave angle. Specifically, the steps used by this system concept to estimate the wave angle from $N_L + N_A - 1$ scans with scan spacing of Δs are:

- (1) Compute $N_L - 1$ cross correlation functions using the first scan paired with each of the next $N_L - 1$ scans and determine their peak locations. This gives estimates of wave displacement as a function of distance perpendicular to the scans for N_L points with locations $n\Delta s$ ($n = 0, 1, \dots, N_L - 1$) with respect to the first scan.
- (2) Repeat step (1) $N_A - 1$ additional times starting with the 2nd scan, 3rd scan, ..., (N_A) th scan to give N_A locations along the direction perpendicular to the scans.
- (3) Average the N_A wave displacement estimates obtained in steps (1) and (2) for each of the N_L locations along the direction perpendicular to the scans.

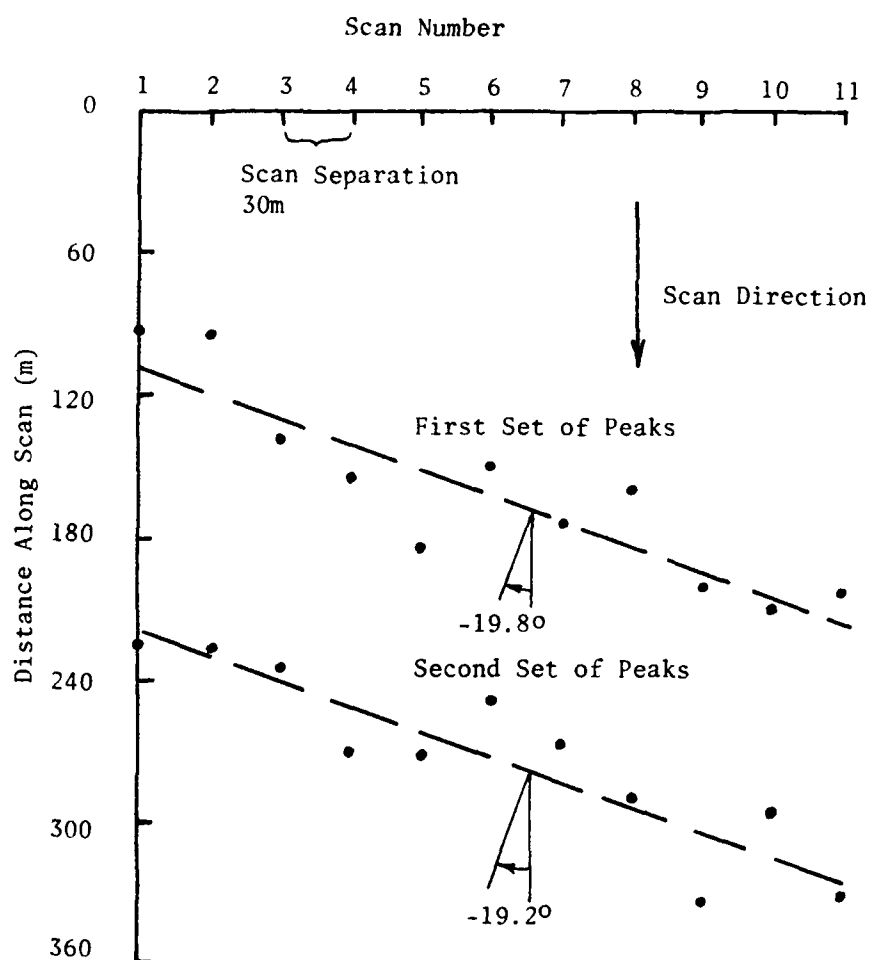


Fig. 63. Data Peaks (Wave Crests) and Straight Line Fits to Them.

- (4) Fit the averaged wave displacement estimates with a straight line in the least squares error sense and use the angle of the straight line with respect to a line perpendicular to the scans as an estimate for the wave angle.

In the analysis of this system concept to follow, the particular configuration used will be referred to as a system using N_A sets of N_L scans. Since the sets overlap, only $N_A + N_L - 1$ scans are actually required by the system.

C. PERFORMANCE OF SECOND SYSTEM CONCEPT

To begin analysis of the second system concept, a group of non-rotated scans (154 through 394) with length of 384m and separated by 30m were selected from analysis area A-1. Figure 64 shows the average wave displacement estimates and the straight line fit, in a least squares error sense, to these estimates for three different combinations of number of sets of scans, N_A , and number of scans per set, N_L . Note that the negative of the wave displacement estimates is plotted since $\hat{\theta}_I = -\tan^{-1}(\hat{y}_p/\Delta s) = \tan^{-1}(-\hat{y}_p/\Delta s)$. The resulting wave angle estimates for the three cases shown are -30.53° for $N_A = N_L = 6$, -27.22° for $N_A = 8$ and $N_L = 6$, and -17.80° for $N_A = 6$ and $N_L = 8$. These results were sufficiently close to the ground truth wave angle of -26.54° to encourage further analysis of the second system concept.

Wave angle estimates obtained for 9 additional cases are shown in Table XVII. The wave angle estimate results shown in Table XVII are not encouraging. Only two of the cases produced estimates which are close to the ground truth indicated propagation angle of -26.54° . Note that estimates obtained from scan sets which are in very close proximity produce markedly different estimates. This indicates that scan data noise is quite effective in causing estimation problems.

A number of additional cases were considered with varying system parameters in an attempt to identify the specific causes of wave angle estimation problems when the second system concept is used. Plots of the average wave displacement estimates and the straight line fit in a least squares error sense, to these estimates for some of these additional cases are shown as examples in the next several figures.

The first parameter varied was the number of individual wave displacement values averaged (i.e. number of sets, N_A). Figure 65 shows results obtained by increasing the number of sets of scans used in the first case shown in Table XVII to 10 sets and 17 sets. The number of scans per set was also increased from 8 to 9 to simplify the computation of the straight line parameters. Up to 32 sets were considered in analyzing the effect of changing the number of individual displacement values averaged. The wave angle estimate was not consistently improved by averaging more individual wave displacement estimates.

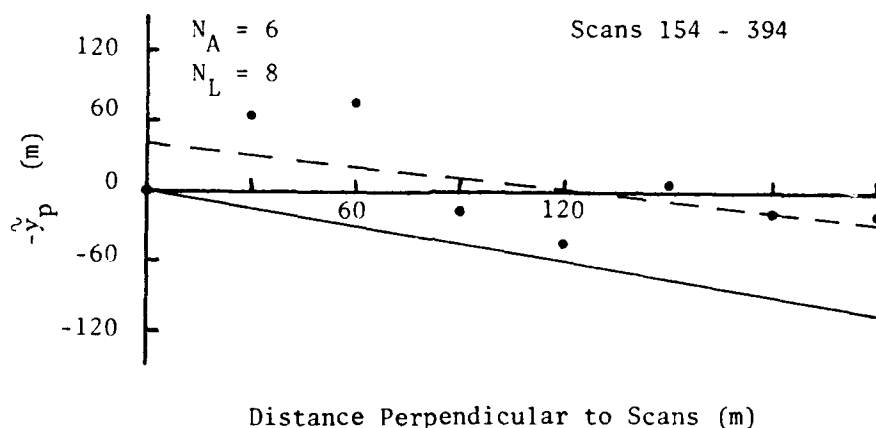
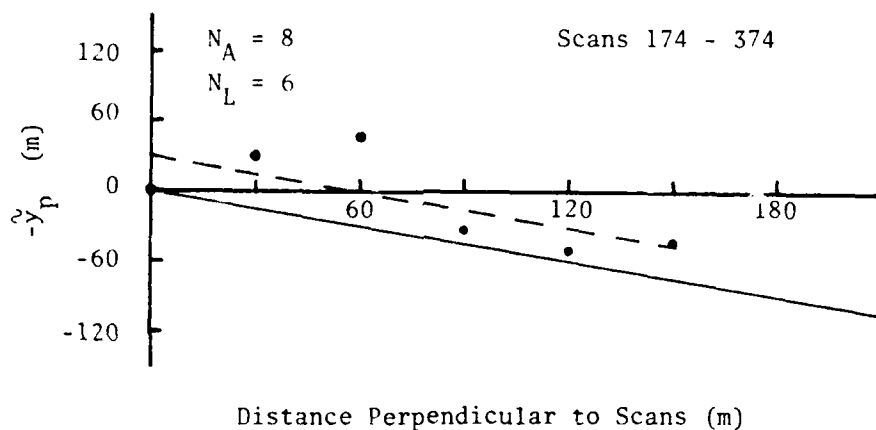
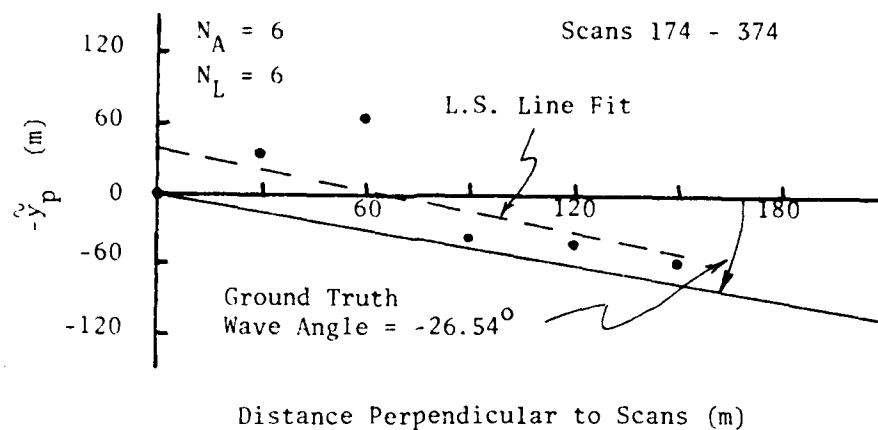
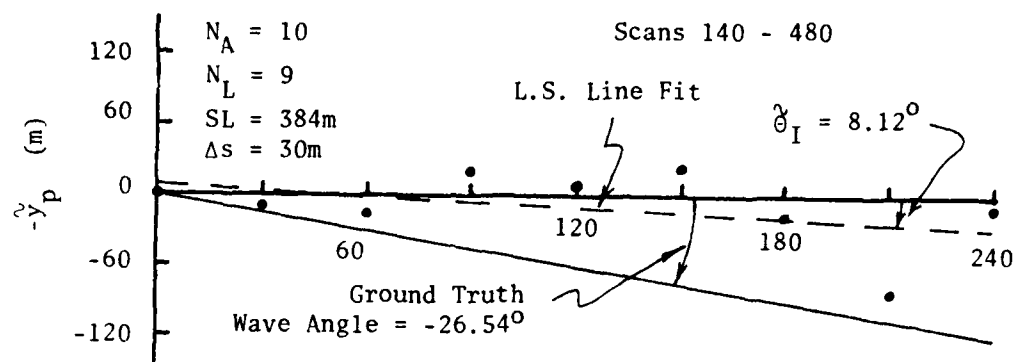


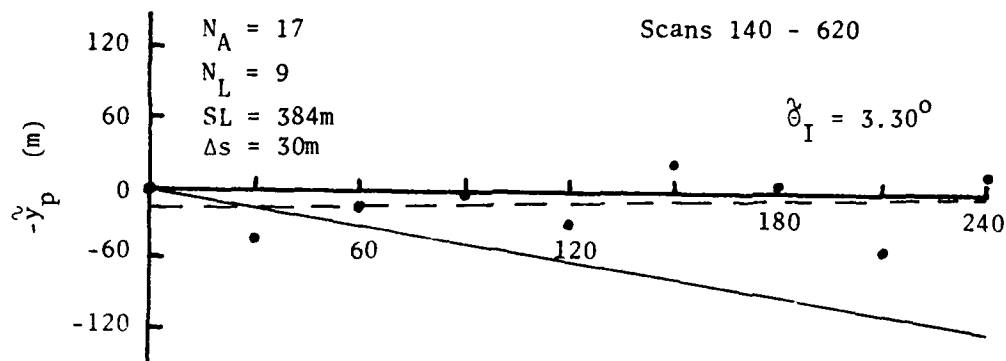
Fig. 64. First Results for Indicated Propagation Angle Estimate Using Second System Concept.

Table XVII. Indicated Propagation Angle Estimates
for 9 Additional Cases Using the
Second System Concept.

Scans Used	Number of Sets N_A	Scans Per Set N_L	Scan Length SL	Scan Spacing Δs	Wave Angle Estimate θ_I
140-380	6	8	384m	30m	6.10°
140-260	6	8	384m	15m	-19.92°
145-265	6	8	384m	15m	32.81°
150-270	6	8	384m	15m	-8.09°
155-275	6	8	384m	15m	10.93°
165-285	6	8	384m	15m	-5.27°
190-310	6	8	384m	15m	6.09°
210-330	6	8	384m	15m	-33.48°
214-334	6	8	384m	15m	0.34°



(a) Distance Perpendicular to Scans (m)



(b) Distance Perpendicular to Scans (m)

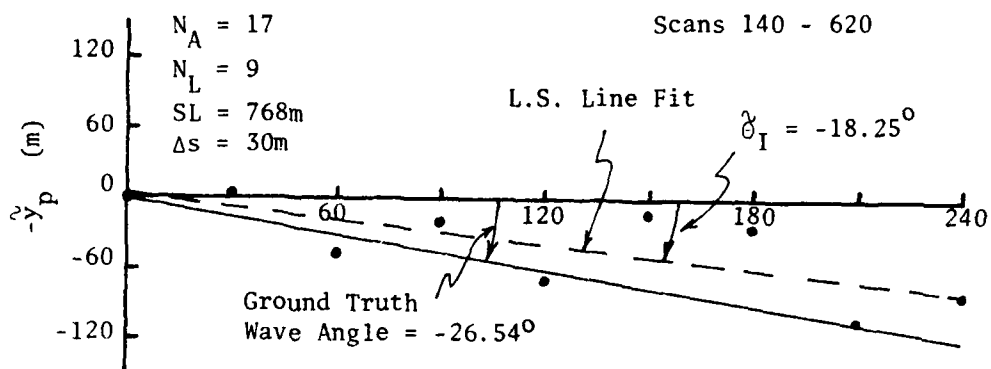
Fig. 65. Indicated Propagation Angle Estimate for Second System Concept and Two Different Number of Estimates Averaged.

Figure 66 shows results obtained for two cases using longer scans ($SL = 768m$). The first of these cases (Fig. 66a) is the same as the case shown in Fig. 65b except that the scan length is twice as long. The results for this case show improvement when the longer scan length is used. However, the second case with the longer scan length once again gave poor results. Analysis of the second system concept with scan lengths up to 2400m were considered. In general, no consistent performance improvement was achieved by using longer scans.

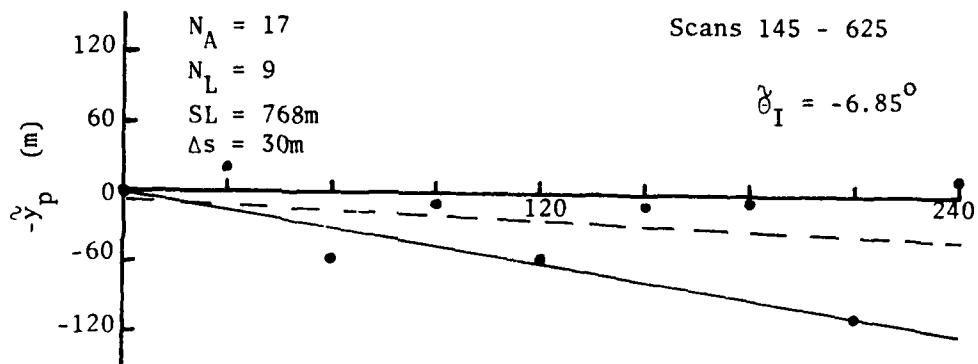
Figure 67 shows results obtained for two cases using the scan length used to obtain the results shown in Fig. 66 (i.e. $SL = 768m$) and a decreased scan spacing ($\Delta s = 15m$). The first scan in each case is the same scan that was used in the two cases in Fig. 66 so they are for comparable areas. Note that no consistent performance change is observed as a function of a change in scan spacing. System performance with scan spacings as close as 7.5m were analyzed. In general, no consistent performance effects of scan spacing were seen for all cases analyzed with different scan spacings.

As indicated above, the analysis of the performance of the second system concept for estimating the indicated propagation angle did not produce any consistent results. One of the reasons appears to be that the wave crest signatures are not sufficiently unique. Thus, the greatest cross correlation value may be achieved for a wave crest on one scan with a wave crest on another scan which is adjacent to the wave crest of interest. This possible error source was indicated by average wave displacement estimates in some cases which appeared to be greater or less than expected by approximately one along-scan wavelength. For the example results shown in Figs. 65, 66, and 67 it appears that the following wave displacement values should be changed by one wavelength (87.98m): (1) Fig. 65a - shift points 4, 5, 6, 7, and 9 one wavelength negative, (2) Fig. 65b - shift points 6, 7, 8, and 9 by one wavelength negative, (3) Fig. 66a - shift points 6 and 7 by one wavelength negative, (4) Fig. 66b - shift points 6, 7, and 9 by one wavelength negative, (5) Fig. 67a - shift point 2 by one wavelength positive, and (6) Fig. 67b - shift points 4, 5, 7, 8, and 9 by one wavelength negative. The wave angle estimates obtained with the individual average wave displacement values changed as above are compared with the original wave angle estimates in Table XVIII. In all cases except those with smaller scan spacing, shifting those wave displacement estimates which appear to be out of line by approximately one wavelength significantly improves the wave angle estimate. This provides strong support for the conjecture that the non-uniqueness of wave crest signature results in the greatest cross correlation between adjacent wave crests in some cases.

Unfortunately, the system cannot be modified to identify those wave displacement estimates which need to be shifted. This is true since knowledge of the true propagation angle was used to decide which estimates to shift and the system does not know what the true propagation angle is since it is what is being estimated. For example, in Fig. 66b, average displacement estimate points 3, 5, and 8 could be

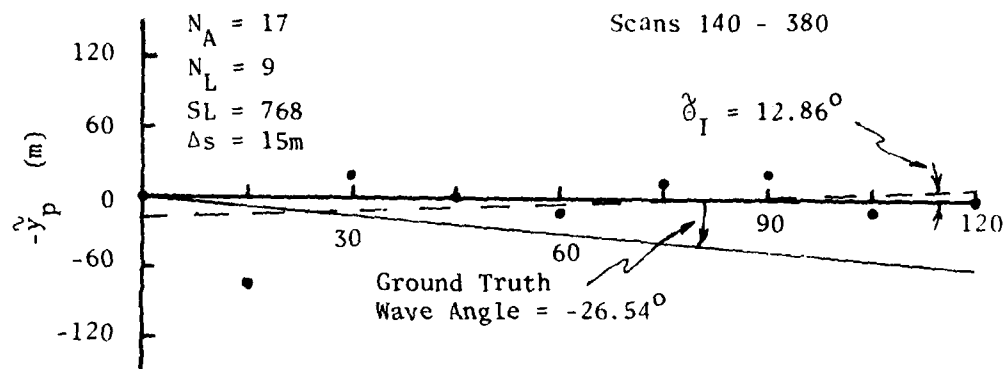


(a) Distance Perpendicular to Scans (m)

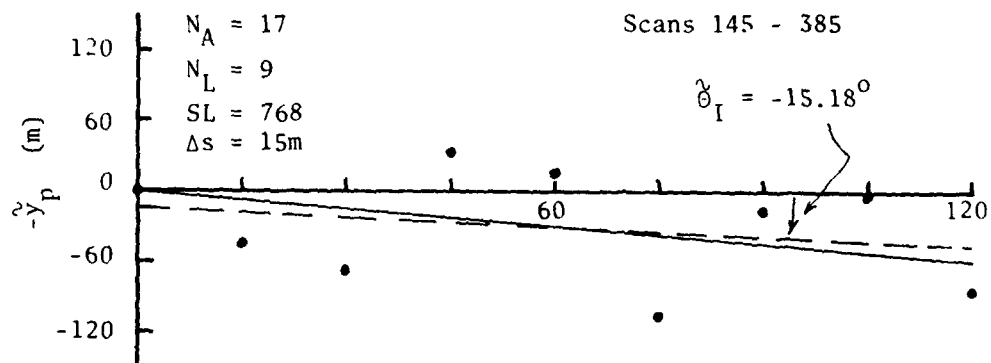


(b) Distance Perpendicular to Scans (m)

Fig. 66. Indicated Propagation Angle Estimate for Second System Concept and Longer Scans.



(a) Distance Perpendicular to Scan (m)



(b) Distance Perpendicular to Scan (m)

Fig. 67. Indicated Propagation Angle Estimate for Second System Concept and Smaller Scan Spacing.

Table XVIII. Second System Concept Estimates of Indicated Propagation Angle for 6 Cases with and Without Modification of Wave Displacement Estimate Values.

Case Identification (Fig. No.)	Original Wave Angle Estimate	Wave Angle Estimate with Shifted Displacement Estimates
65a	-8.12 ⁰	-23.55 ⁰
65b	3.30 ⁰	-23.32 ⁰
66a	-18.25 ⁰	-25.47 ⁰
66b	-6.85 ⁰	-24.81 ⁰
67a	12.86 ⁰	-3.72 ⁰
67b	-15.18 ⁰	-46.49 ⁰

shifted by one wavelength in the positive direction and achieve as good a fit to a straight line with angle close to 0⁰ as was achieved for a straight line with angle of -24.81⁰ by shifting displacement estimate points 6, 7, and 9. Thus, the non-uniqueness of wave crest signatures effectively precludes using the second system concept for estimating the indicated propagation angle. No statistical analysis was performed for the second system concept since consistent performance results were not obtained for the individual cases investigated.

D. THIRD SYSTEM CONCEPT

The non-uniqueness of wave crest signatures from scan to scan has been identified as a primary reason for the failure of the initial system concept and the second system concept to obtain consistent indicated propagation angle estimates. This suggests that some form of two dimensional processing of the data available along a few radar scans is necessary to estimate the indicated propagation angle.

Thus, a third system concept for estimating the indicated propagation angle was defined and analyzed.

The third system concept defined consists of:

- (1) Compute the along-scan wavelength estimate, $\hat{\lambda}_y$, from the previously obtained along-scan wavenumber estimate, \hat{k}_y , by $\hat{\lambda}_y = 2\pi/\hat{k}_y$.
- (2) Select the largest radar scan segments containing an integer number of estimated wavelengths from the portion of each radar scan used for wavenumber estimation and remove the mean value from each scan segment.
- (3) Construct a two dimensional square wave function with propagation angle ϕ spanning the area encompassed by the radar scan segments selected as shown in Fig. 68. The wavelength of the square wave function along the radar scans is set equal to the along-scan wavelength estimate, $\hat{\lambda}_y$.
- (4) Compute a two dimensional cross correlation value for the radar scan data and the square wave function with propagation angle $\phi = 0^\circ$ and offset $\Delta B = 0$ by adding all radar scan data values located where the square wave function has a value of 1.
- (5) Shift the two dimensional square wave along the scan direction (i.e. increase the offset ΔB) in steps of one data point and repeat step (4). The total shift required is one along-scan wavelength since the cross correlation values obtained will then start repeating. The values obtained in this step give a cross correlation function for along-scan shifts of the two dimensional data and the square wave function with propagation angle equal to 0° . The peak value of this cross correlation function is computed.
- (6) Steps (4) and (5) are repeated for other values of square wave propagation angle, ϕ , to give samples with respect to propagation angle of a function referred to as the peak cross correlation function. The propagation angle giving the largest cross correlation function value is the estimate for the indicated wave propagation angle. Actually, since the propagation angle of the square wave must be varied in steps, parabolic interpolation is used to find a more accurate indicated propagation angle estimate from the largest peak value and its two neighbors.

It should be noted that the number of radar scan values added along each scan will vary slightly from scan to scan at some square wave propagation angles unless the along-scan wavelength is an integer multiple of scan point spacings. To avoid this problem and make the peak

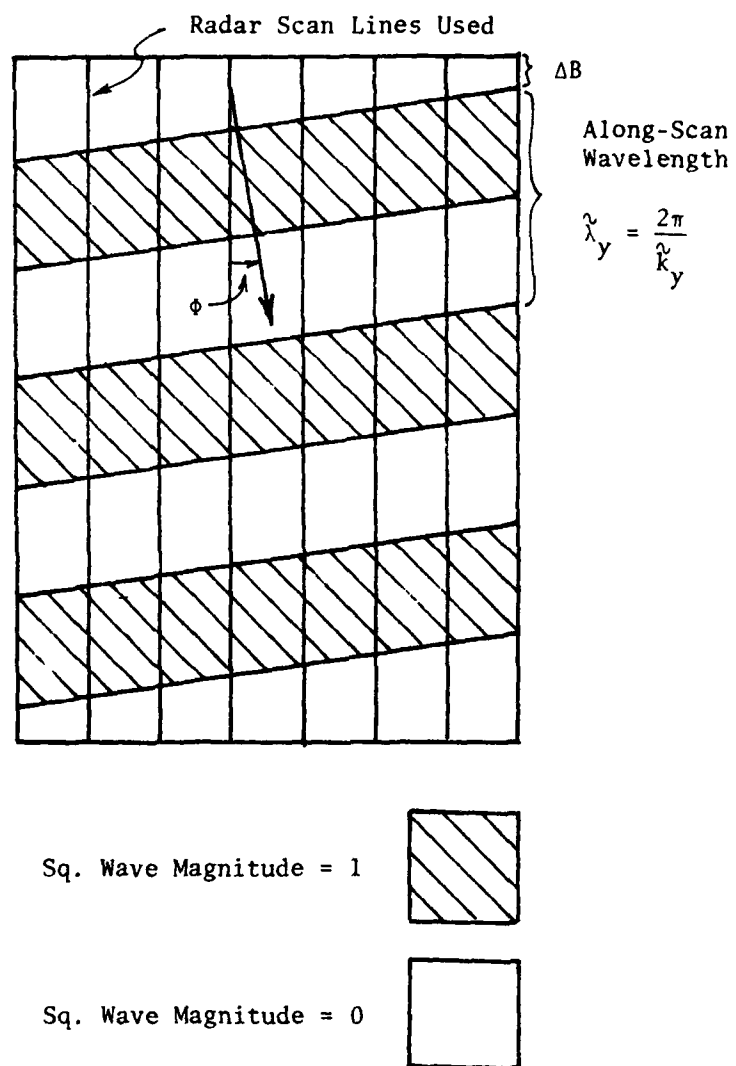


Fig. 68. Two-Dimensional Square Wave for Correlation with Radar Scan Data.

values obtained more directly comparable, the sum of radar scan values along each scan was scaled by the number of values added.

E. PERFORMANCE OF THIRD SYSTEM CONCEPT

To begin analysis of the third system concept for estimating the indicated propagation angle, several individual cases were considered prior to statistical performance evaluation so wave angle estimation characteristics of the system could be observed. All of these cases were analyzed for a range of number of scans used. To simplify the initial analysis, a single along-scan wavelength estimate was used for each case to define the two dimensional square wave regardless of the number of scans being considered. The along-scan wavelength estimates used were obtained from along-scan wavenumber estimates obtained with a system using 14 scans. In general, these estimates were reasonably close to those which were obtained with other numbers of scans as long as the number of scans was greater than that required for along-scan wavenumber estimate convergence. Results from three of the individual cases considered are shown here to illustrate the wave angle estimation characteristics of the third system concept.

The first case considered used up to 18 scans (320 - 490) of length equal to 768m and spacing equal to 15m from analysis area A-1. The estimate of along-scan wavenumber obtained for the first 14 of these scans was $k_y = 0.0684$ which gives an along-scan wavelength estimate of $\lambda_y = 91.9\text{m}$ to be used to generate the two dimensional square wave. There are 8.36 of these wavelengths along the 768m scans. Thus, segments of the scans encompassing 8 wavelengths or 735.2m were used by the system.

Figure 69a shows the plot of peak cross correlation function value with respect to the two dimensional square wave propagation angle (in 50 steps) for the first case with 14 scans used. In order to smooth this function, 3 point and 5 point moving averages were used. The resulting smoothed peak cross correlation functions are shown in Figs. 69b and 69c. Note that the peaks of the peak cross correlation function and its smoothed versions are well defined and near the ground truth indicated propagation angle of -26.54° .

Figure 70 shows the peak cross correlation function and its smoothed versions for the same case as Fig. 69 with the only difference being that smoothed radar scan data (5x5 averaging) is used. The wavelength estimate used to construct the two dimensional square wave was not changed since a wavenumber estimate had not been performed with 5x5 averaged radar data in analysis area A-1. Once again, the peaks of the peak cross correlation function and its smoothed versions are well defined and near the ground truth indicated propagation angle.

Figure 71 shows the wave angle estimate obtained from the peak locations of the peak cross correlation functions as a function of

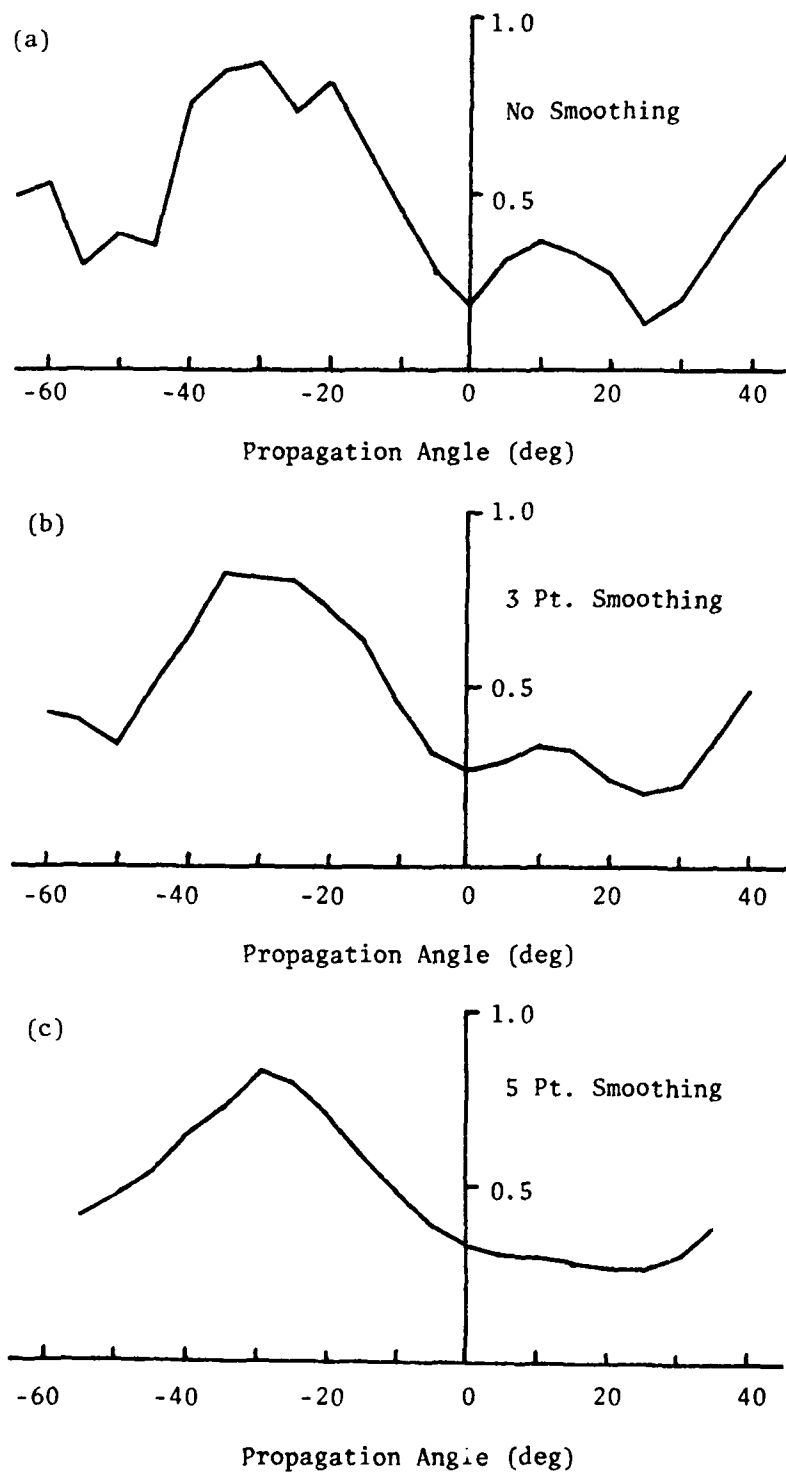


Fig. 69. Peak Cross Correlation Versus Propagation Angle for Third System Concept and First Case.

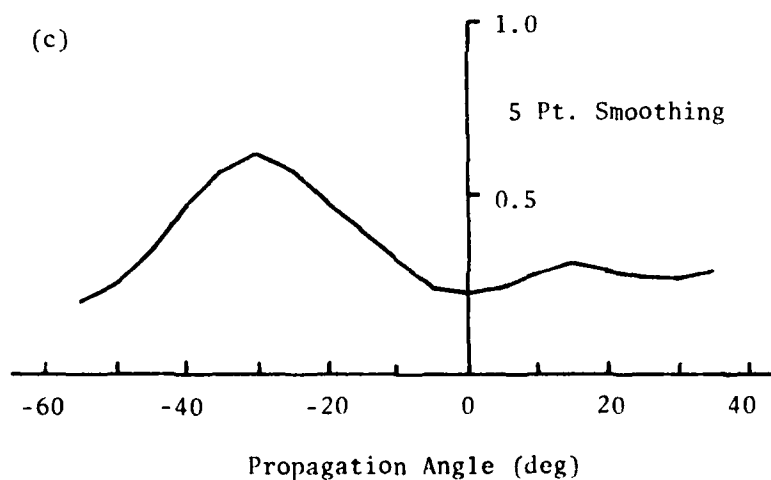
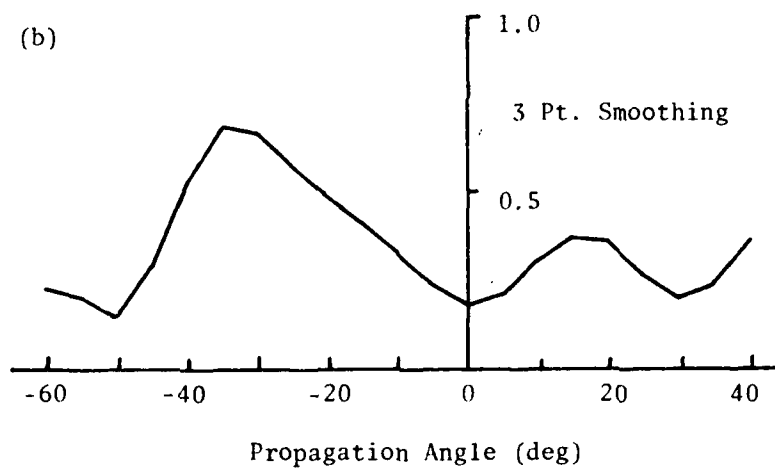
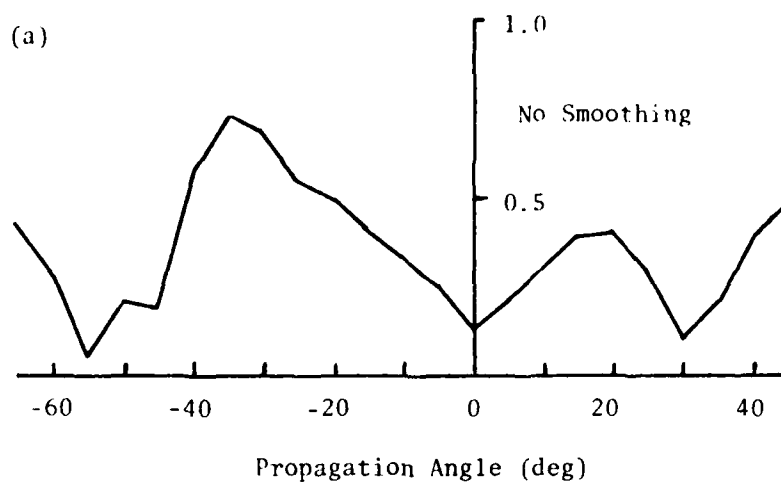


Fig. 70. Peak Cross Correlation Versus Propagation Angle for Third System Concept and First Case with 5x5 Smoothed Data.

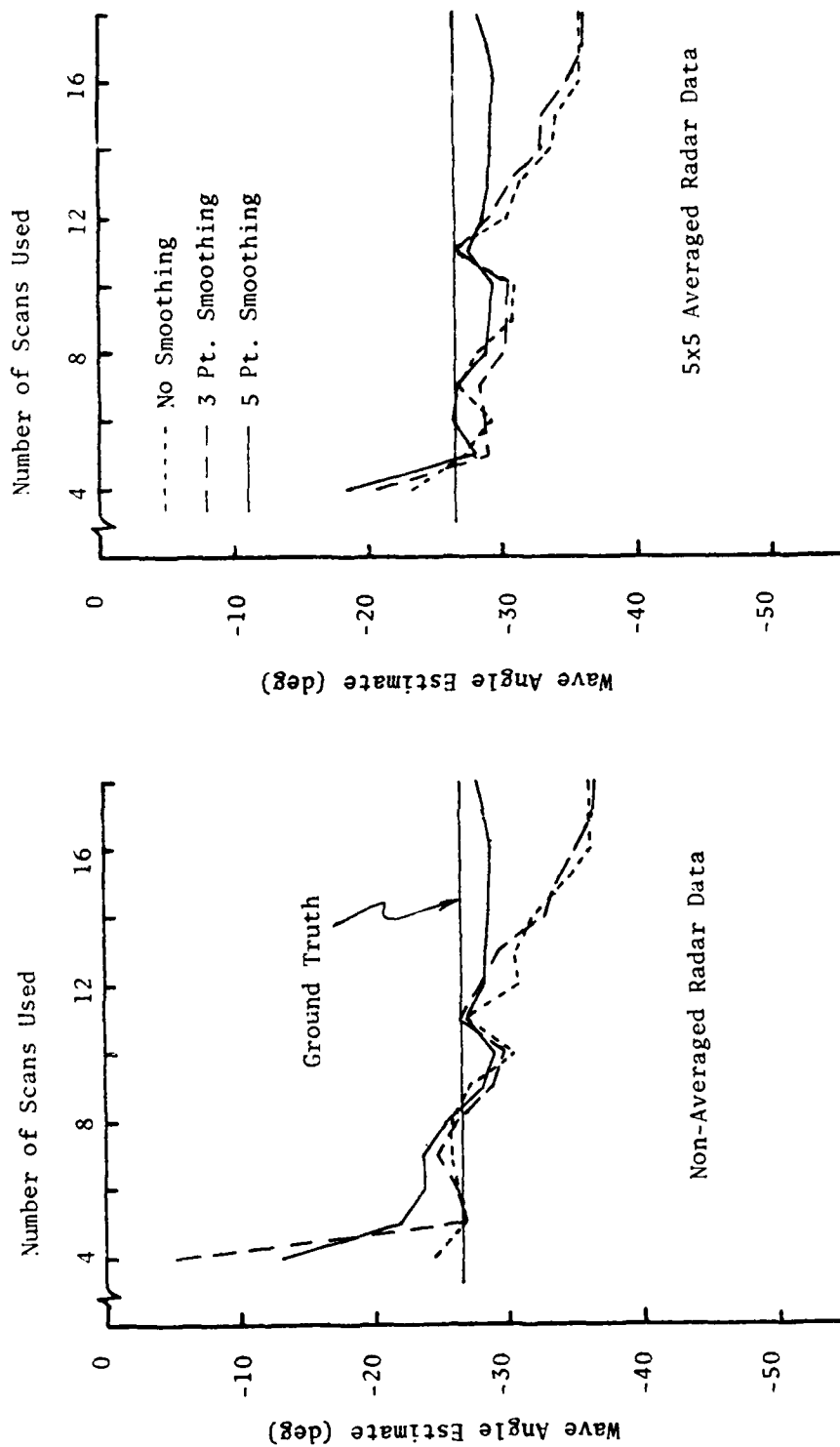


Fig. 71. Indicated Propagation Angle Estimates from All Variations of the Third System Concept for the First Case.

number of scans used for all variations considered for the first case. Good estimates are obtained when 5 point smoothing and greater than 8 scans are used with non-averaged radar scan data and when 5 point smoothing and greater than 5 scans are used with 5x5 averaged radar scan data. Non-smoothed and 3 point smoothed peak cross correlation functions do not give as good estimates for larger numbers of scans used. Note that wave angle estimate performance is quite similar for non-averaged and 5x5 averaged radar scan data.

The second case considered used up to 18 scans (330 - 500) of length equal to 1200m and spacing equal to 15m from analysis area A-3. The estimates of along-scan wavenumber obtained for the first 14 of these scans were $\hat{k}_y = 0.0743$ for non-averaged radar data and $\hat{k}_y = 0.0638$ for 5x5 averaged radar data. These give along-scan wavelength estimates of $\hat{\lambda}_y = 84.6\text{m}$ and 98.5m respectively to be used to generate the necessary two dimensional square waves. The scan length used to obtain the wavenumber estimates was erroneously chosen to be 768m rather than 1200m. However, the resulting wavenumber estimates are undoubtedly close to those which would be achieved with the longer scan lengths. There are 14.18 and 12.18 wavelengths along the 1200 scans for the two wavelengths respectively. Thus, segments of the scans encompassing 14 and 12 wavelengths were used by the system for non-averaged and 5x5 averaged radar scan data respectively.

Figures 72 and 73 show the peak cross correlation functions with respect to the two dimensional square wave propagation angle (in 5° steps) for the second case with 14 scans used for non-averaged and 5x5 averaged radar data respectively. In this second case, the peak of the peak cross correlation function does not occur near the ground truth angle for non-average radar data even when 5 point smoothing is used. However, the peak cross correlation function does appear to have a much broader peak structure (which unfortunately has a large dip in the center) surrounding the correct angle. The use of 5x5 averaged radar data corrects this problem as can be seen in Fig. 73.

Figure 74 shows the wave angle estimates obtained from the peak locations of the peak cross correlation functions as a function of number of scans used for all variations considered for the second case. No good estimates are obtained when non-averaged radar data is used. Fairly reasonable estimates are obtained when more than 10 scans are used with 5x5 average radar data. No estimates are shown for less than 10 scans used with 5x5 average radar data since the estimated wave angle was positive.

The third case considered used up to 18 scans (290 - 460) from analysis area A-3 with length equal to 1071m, spacing equal to 15m, and rotated by 35° from the radar scan lines. This case was considered to observe the characteristics of the third system concept in estimating larger indicated propagation angles. The estimates of along-scan wavenumber obtained for the first 14 of the scans used were $\hat{k}_y = 0.0300$ for the non-averaged radar data and $\hat{k}_y = 0.0296$ for the 5x5 averaged radar data. These give along-scan wavelength estimates of $\hat{\lambda}_y = 209.6\text{m}$

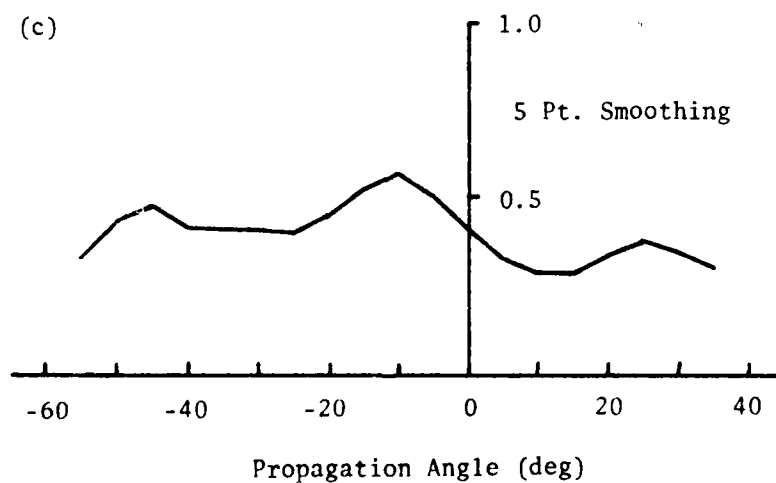
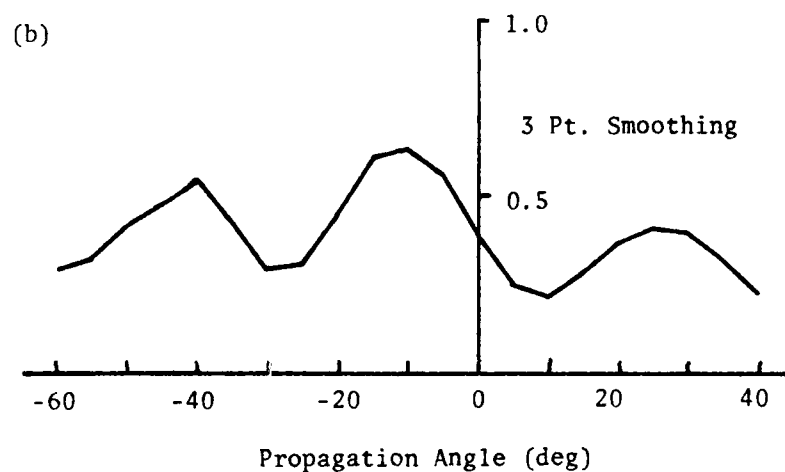
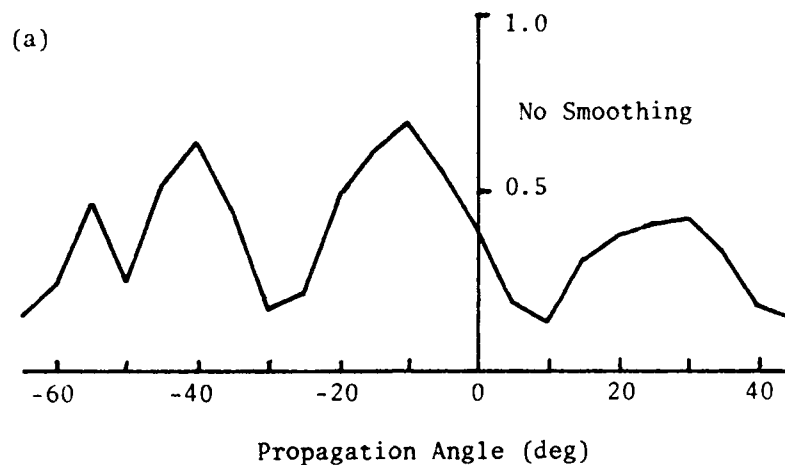


Fig. 72. Peak Cross Correlation Versus Propagation Angle for Third System Concept and Second Case.

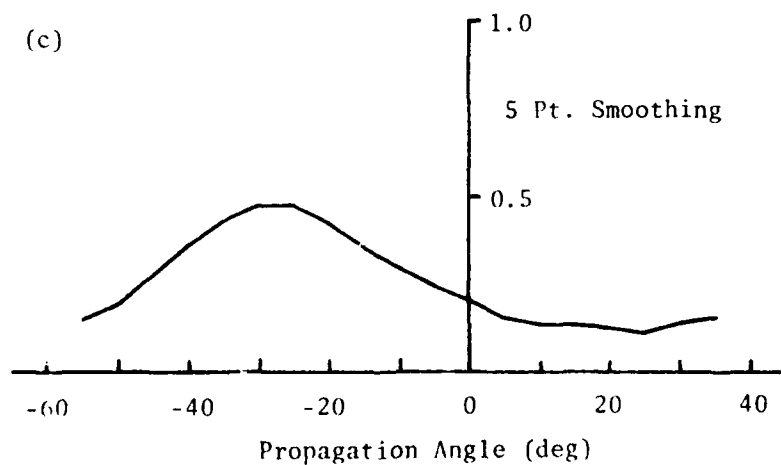
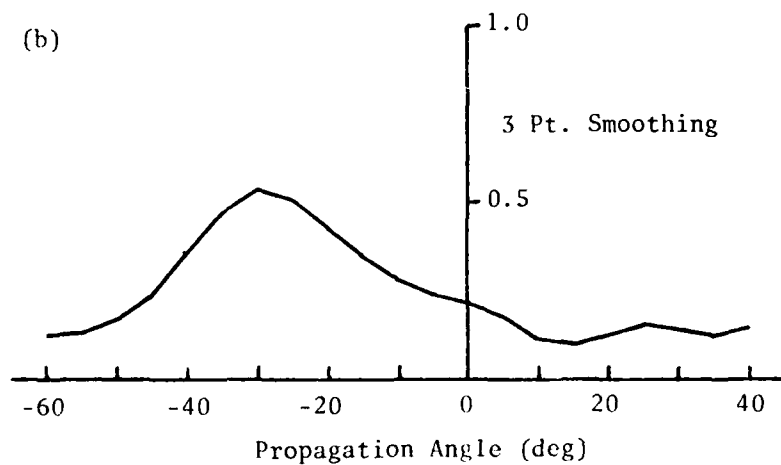
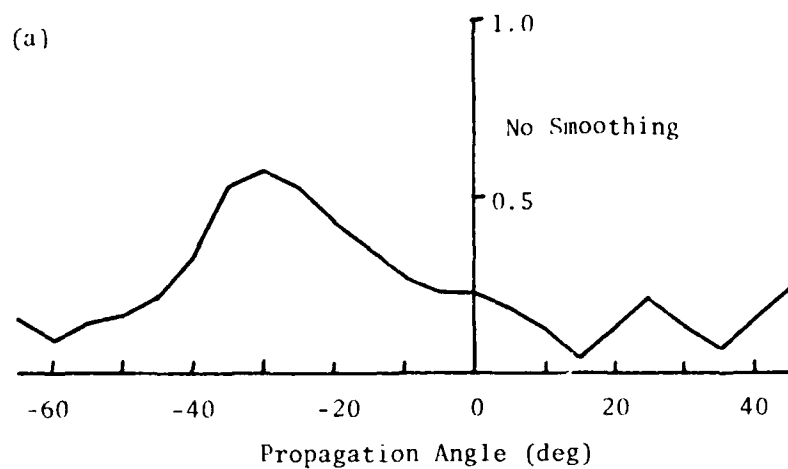


Fig. 73. Peak Cross Correlation Versus Propagation Angle for Third System Concept and Second Case with 5x5 Smoothed Data.

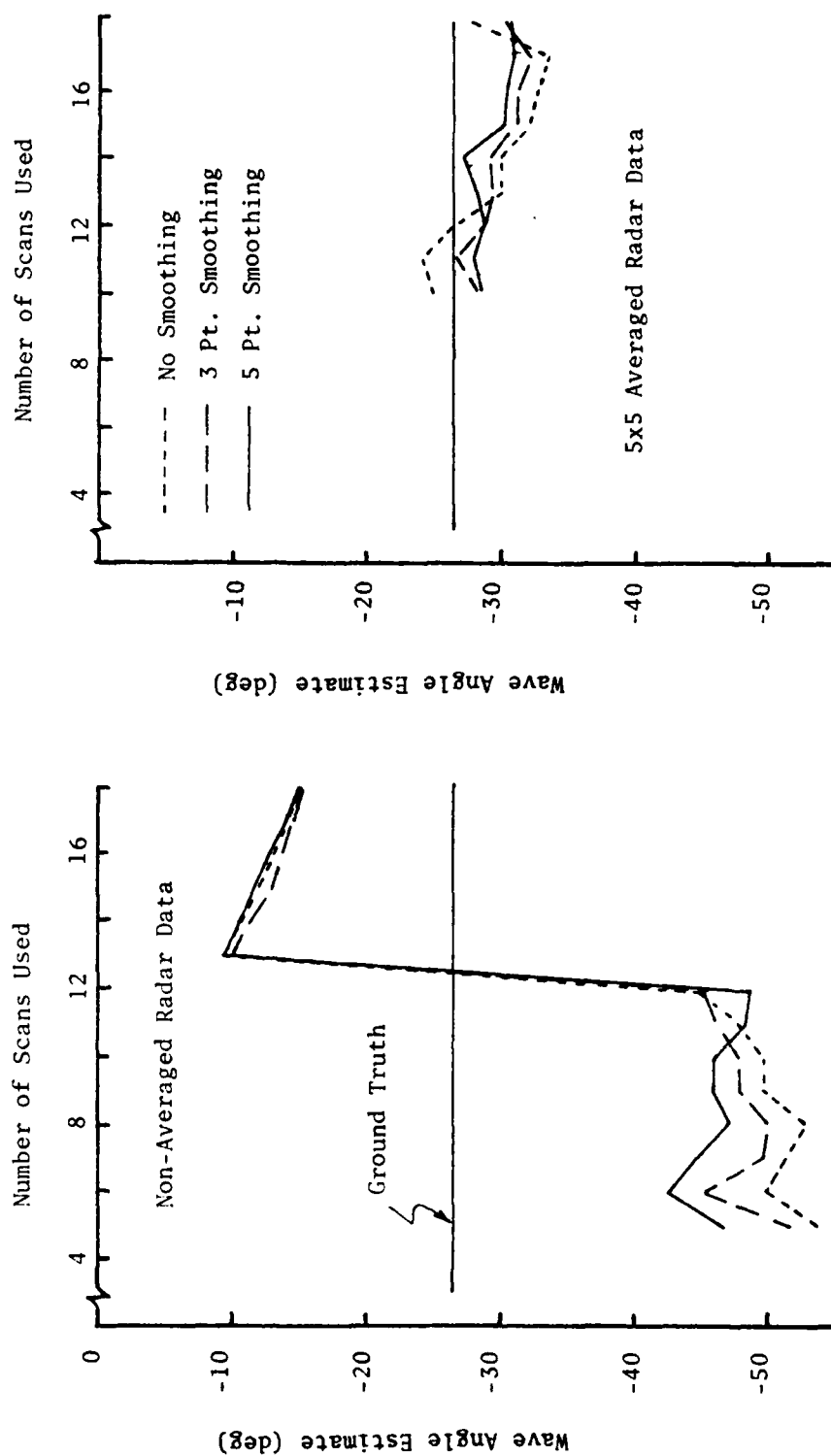


Fig. 74. Indicated Propagation Angle Estimates from All Variations of the Third System Concept for the Second Case.

and 212.3m respectively to be used to generate the necessary two dimensional square wave. There are 5.11 and 5.04 of these wavelengths along the 1071m scans for the two wavelengths respectively. Thus, segments of the scans encompassing 5 wavelengths were used by the system.

Figures 75 and 76 show the peak cross correlation functions with respect to the two dimensional square wave propagation angle (in 5° steps) for the third case with 14 scans used for the non-averaged and 5x5 averaged radar data respectively. Well defined peaks of the peak cross correlation function occur near the ground truth indicated propagation angle value of -61.54° for both non-averaged and 5x5 averaged radar data when non-smoothed or 3 point smoothed peak cross correlation functions are considered. When 5 point smoothing of the peak cross correlation function is considered, no peak occurs when non-averaged radar data is used and a rather poorly defined peak occurs when 5x5 averaged radar data is used.

Figure 77 shows the wave angle estimates obtained from the peak locations of the peak cross correlation functions as a function of number of scans used for all variations considered for the third case (note that a maximum of 14 scans was used with the non-averaged radar data). Good estimates are obtained when 5 point smoothing and greater than 5 scans are used with 5x5 averaged radar data. This is also true for non-averaged radar data as long as the number of scans used does not exceed 9. No estimates were obtained for greater than 9 scans used with non-averaged radar data and 5 point smoothing of the peak cross correlation function since no peak occurred in this function. Non-smoothed and 3 point smoothed peak cross correlation functions do not give as good estimates as obtained with 5 point smoothing.

The three examples cases shown above of the initial analysis of the third system concept for estimating the indicated propagation angle show that good estimates are obtainable in some cases. The use of smoothed radar data (5x5 averaging) and peak cross correlation function smoothing does affect the estimate performance. Closer spacing of peak cross correlation function values (i.e. 2.5°) was considered also but did not have much affect. The same is true for a reduced duty cycle for the square wave (i.e. on 1/4 of the time and off 3/4 of the time). Therefore, all further analysis was done with peak cross correlation function values spaced by 5° and a 50% duty cycle for the square wave.

Further analysis of the third system concept for estimating the indicated propagation angle was performed using Monte Carlo statistical methods to obtain statistical indications of the performance of this system concept in estimating the indicated wave propagation angle. System parameters were varied to determine their effect on system performance. Analysis area A-3 was used to perform the statistical performance analysis with varying system parameters. The same scan location format as used for the along-scan wavenumber estimate analysis was used for obtaining wave angle estimates for 20 cases. The along-scan wavelengths for the two dimensional square waves were

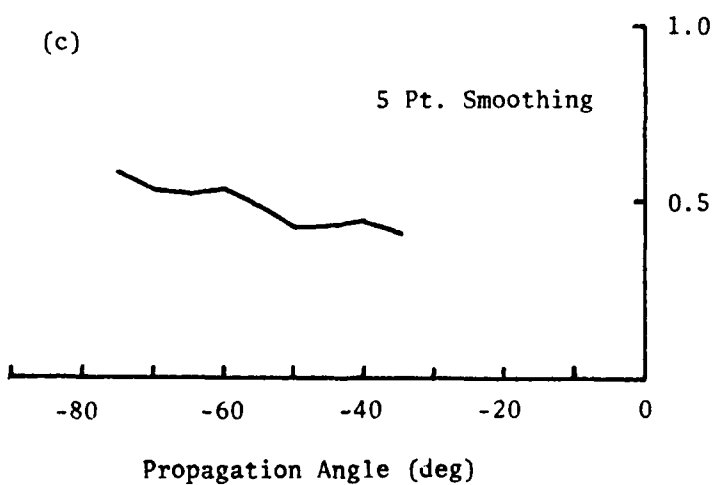
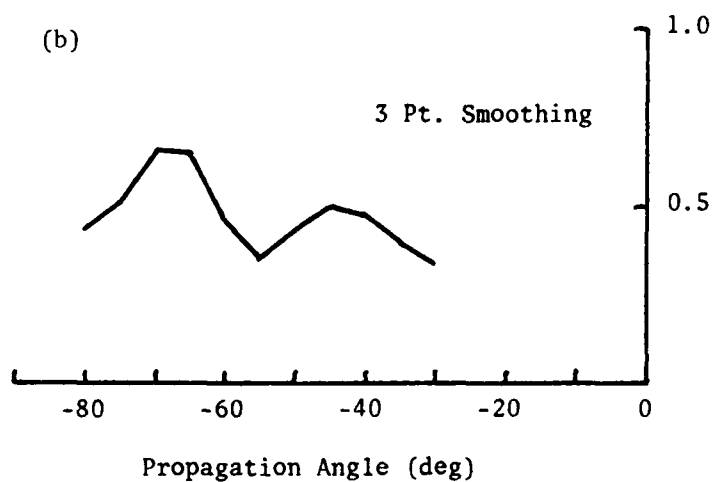
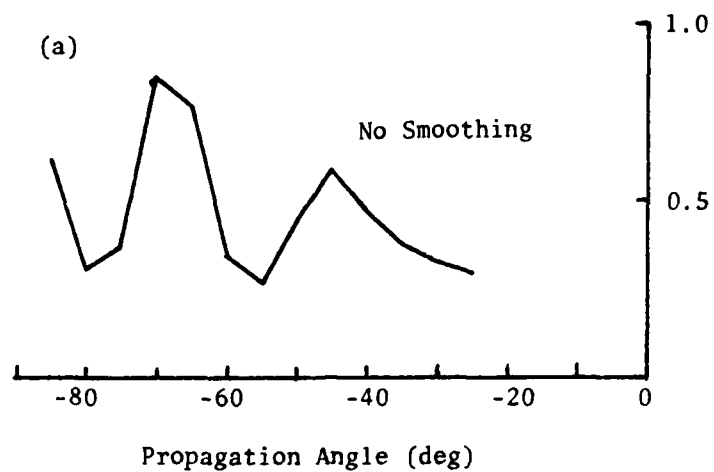


Fig. 75. Peak Cross Correlation Versus Propagation Angle for Third System Concept and Third Case.

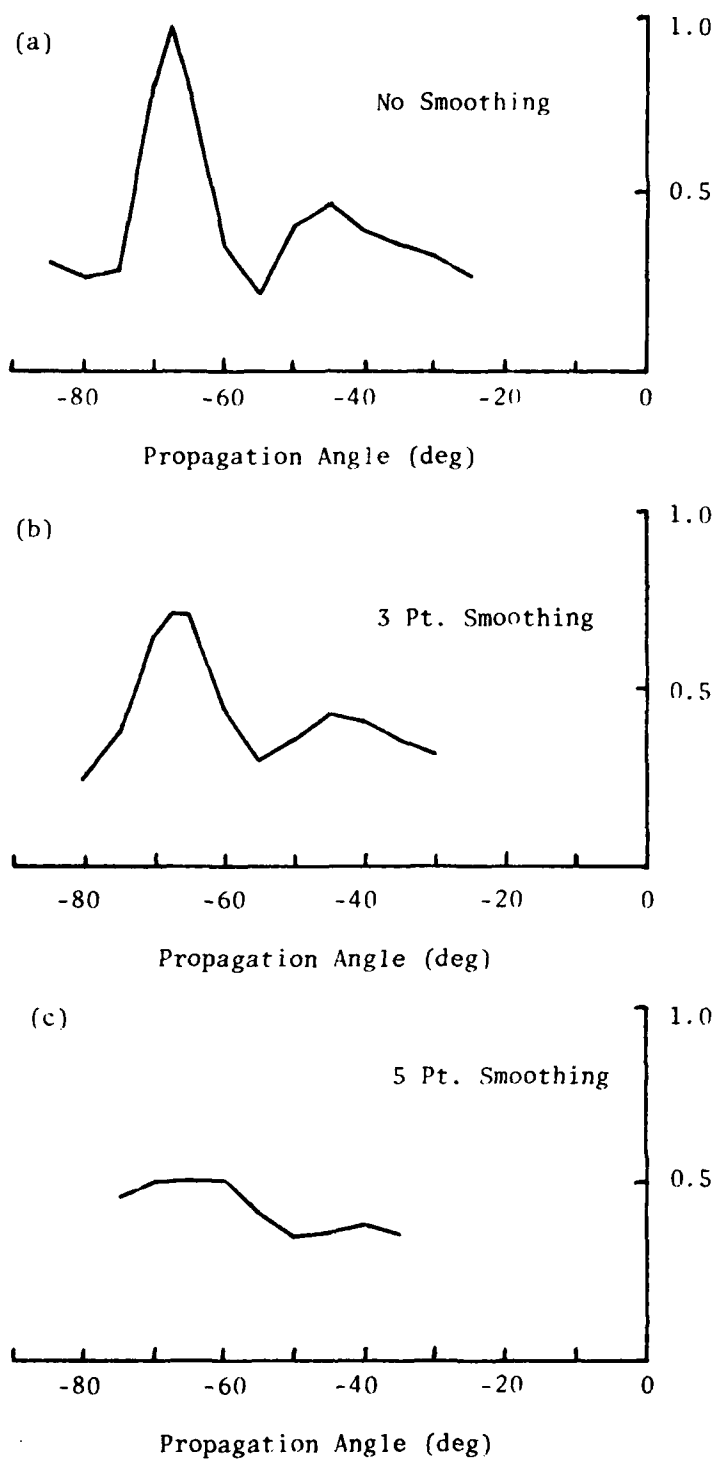


Fig. 76. Peak Cross Correlation Versus Propagation Angle for Third System Concept and Third Case with 5x5 Smoothed Data.

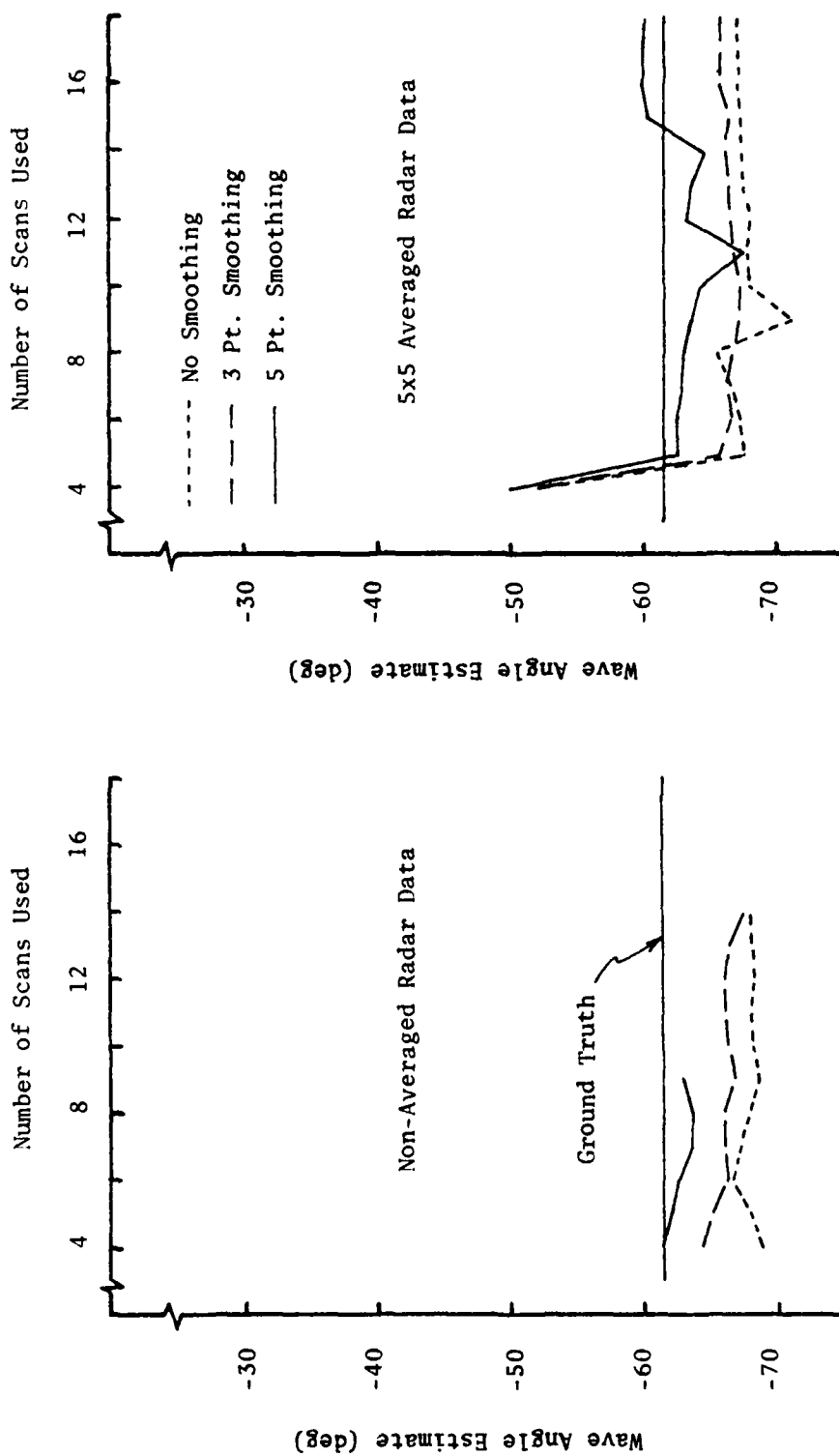


Fig. 77. Indicated Propagation Angle Estimates from All Variations of the Third System Concept for the Third Case.

obtained from the previously determined along-scan wavenumber estimates.

The statistical analysis was first performed with analysis area A-3 scans of length, SL , equal to 720m along the radar scan direction ($\theta_r = 0^\circ$) and spacing, Δs , equal to 15m. The 720m scan length corresponds to 8.18 ground truth along-scan wavelengths. Thus, approximately 8 wavelengths are used by the third system concept in estimating wave angle. The exact number for a particular case depends on the along-scan wavelength estimated for that case.

Individual case wave angle estimates for 9 through 14 scans used are shown in Figs. 78, 79, and 80 for non-smoothed, 3 point smoothed, and 5 point smoothed peak cross correlation functions respectively. While there is some concentration of the estimates near the ground truth indicated propagation angle of -26.54° , the estimates in general are quite widely spread indicating that the third system concept is not too satisfactory.

Since the wave angle estimates are quite widely spread from case to case, the standard deviation of the wave angle estimate is quite large. Therefore, it was felt that it is more appropriate to express the wave angle estimate performance in terms of the percent of estimates which are within $\pm 5^\circ$ and $\pm 10^\circ$ of the ground truth value. This performance indication is shown in Table XIX. Table XIX indicates that wave angle estimates within $\pm 10^\circ$ and $\pm 5^\circ$ of the known wave angle are achieved in about only 50% and 30% of the cases respectively when peak cross correlation function smoothing is used. Still fewer cases with estimates within the $\pm 10^\circ$ and $\pm 5^\circ$ bounds are noted when no smoothing of the peak cross correlation function is used.

The plots of individual case wave angle estimates do not show much difference in performance for scans used by the system numbering more than 10. Thus, 14 scans were used for further analysis since this corresponds with the number selected for along-scan wavenumber estimation. Also, further analysis results will only be shown for 3 point smoothing of the peak cross correlation function. This is done since little difference is noted here between the performance of the system with 3 point or 5 point smoothing and the previous individual case analysis gave poorly defined peaks of the peak cross correlation function when larger wave angles were being estimated with 5 point smoothing.

Since the along-scan wavenumber estimate is used in obtaining the wave angle estimate with the third system concept, it is natural to question whether the rather poor performance obtained is due to poor wavenumber estimates for the individual cases. To test whether this might be the situation, wave angle estimates were repeated for the above set of cases with the along-scan wavenumber estimate replaced with the ground truth along-scan wavenumber value. The resulting individual case wave angle estimates obtained with 14 scans used and 3 point smoothing of the peak cross correlation function are shown in Fig. 81. The wave angle estimates obtained using the along-scan wavenumber estimates are also repeated (see Fig. 79) for easy comparison.

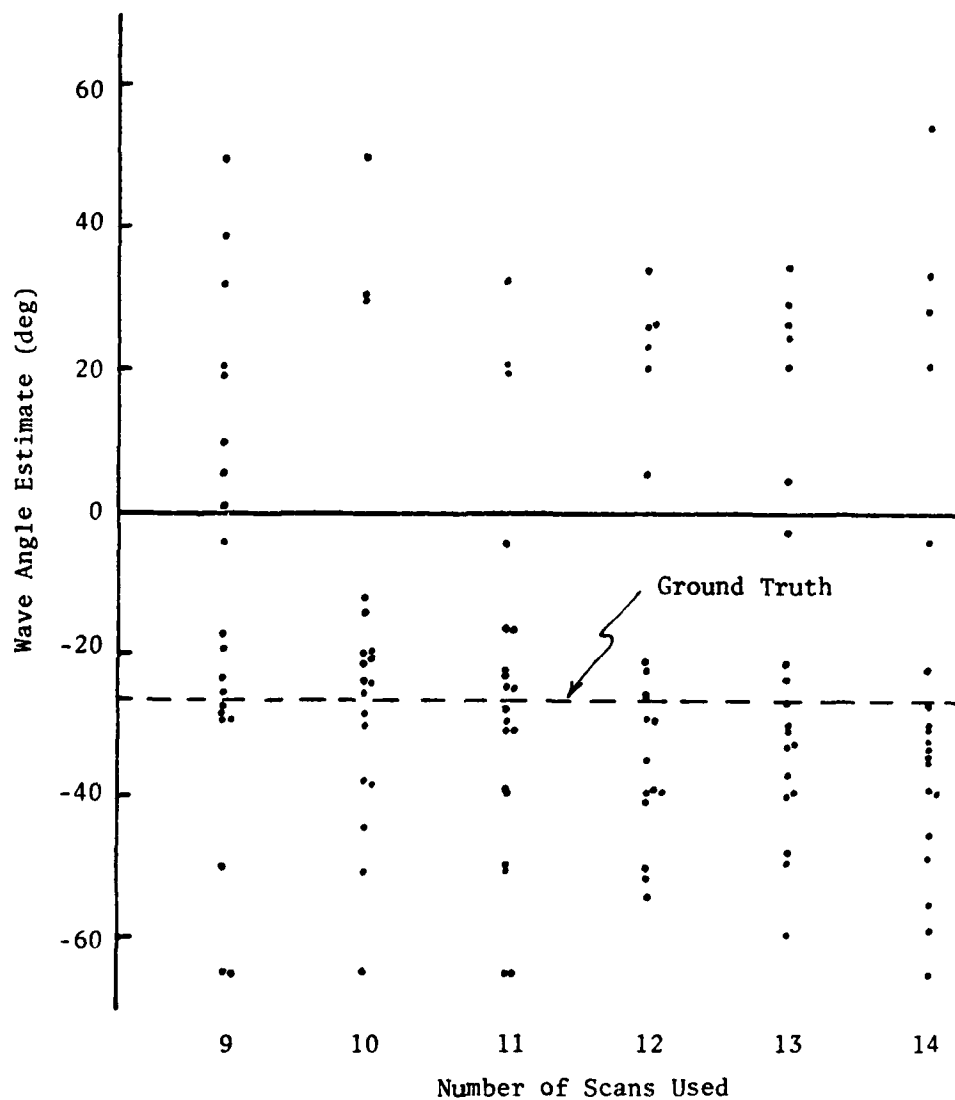


Fig. 78. Individual Case Indicated Propagation Angle Estimates for Third System Concept with No Smoothing as a Function of Number of Scans Used.

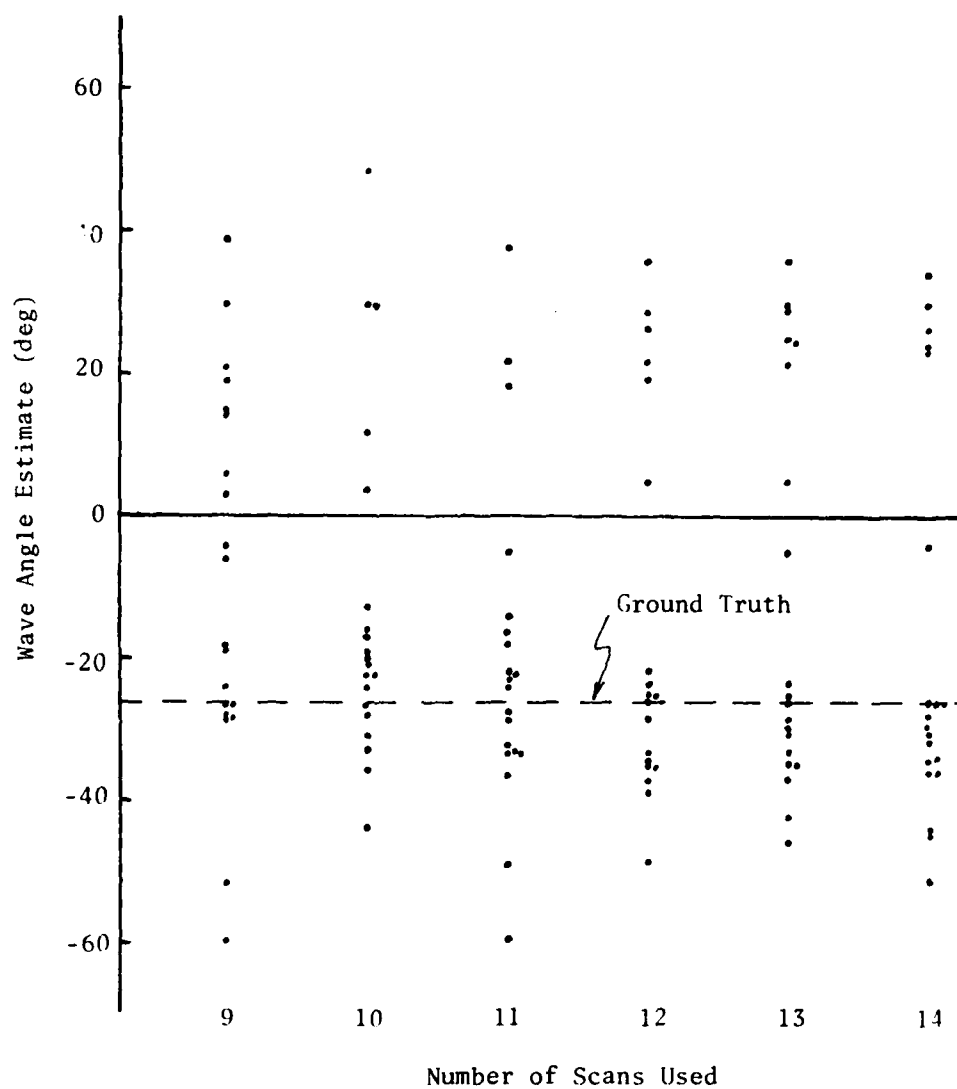


Fig. 79. Individual Case Indicated Propagation Angle Estimates for Third System Concept with 3-Point Smoothing as a Function of Number of Scans Used.

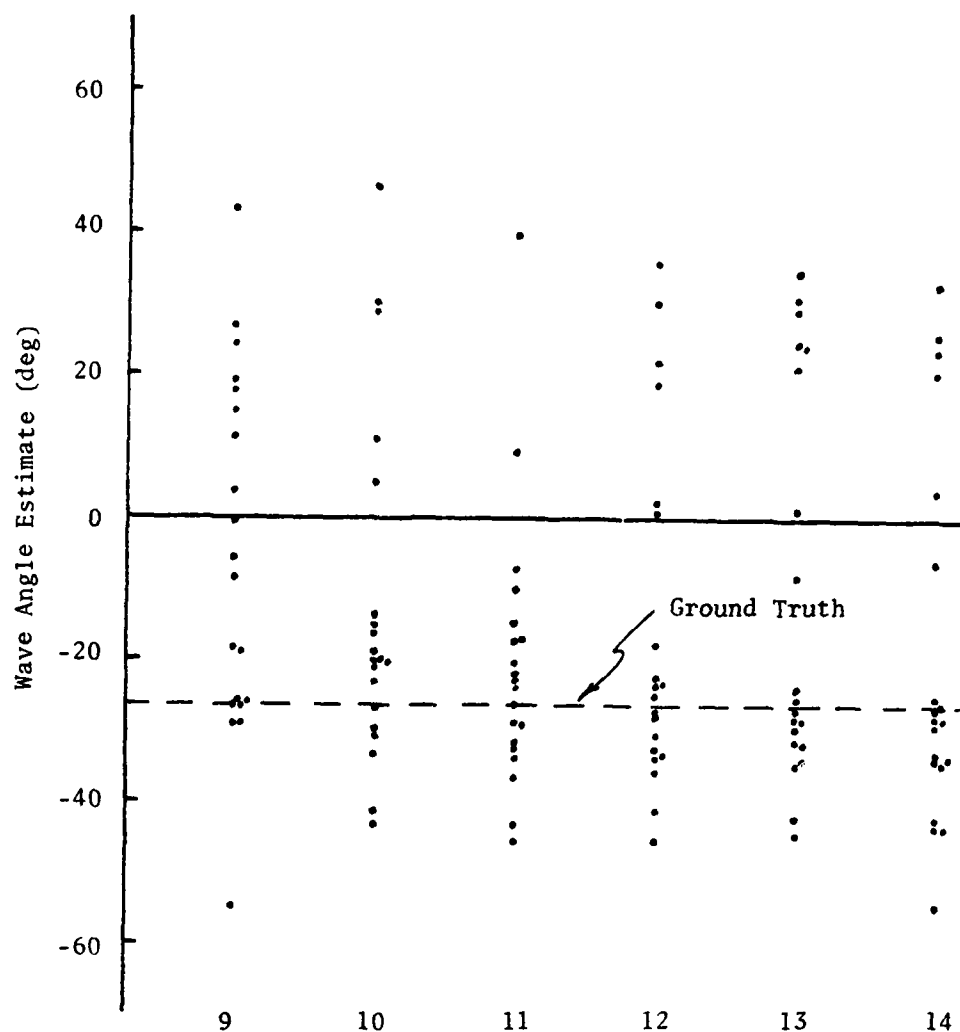


Fig. 80. Individual Case Indicated Propagation Angle Estimates for Third System Concept with 5-Point Smoothing as a Function of Number of Scans Used.

Table XIX. Percent of Indicated Propagation
Angle Estimates Within $\pm 5^\circ$ and $\pm 10^\circ$
for Third System Concept as a Function
of Number of Scans Used.

Number of Scans	Non-Smoothed		3 Pt. Smoothed		5 Pt. Smoothed	
	$\pm 5^\circ$	$\pm 10^\circ$	$\pm 5^\circ$	$\pm 10^\circ$	$\pm 5^\circ$	$\pm 10^\circ$
9	30%	40%	30%	40%	30%	40%
10	35%	45%	30%	60%	20%	50%
11	40%	40%	30%	60%	30%	60%
12	30%	35%	30%	50%	35%	60%
13	20%	35%	30%	45%	35%	50%
14	20%	40%	30%	50%	30%	50%

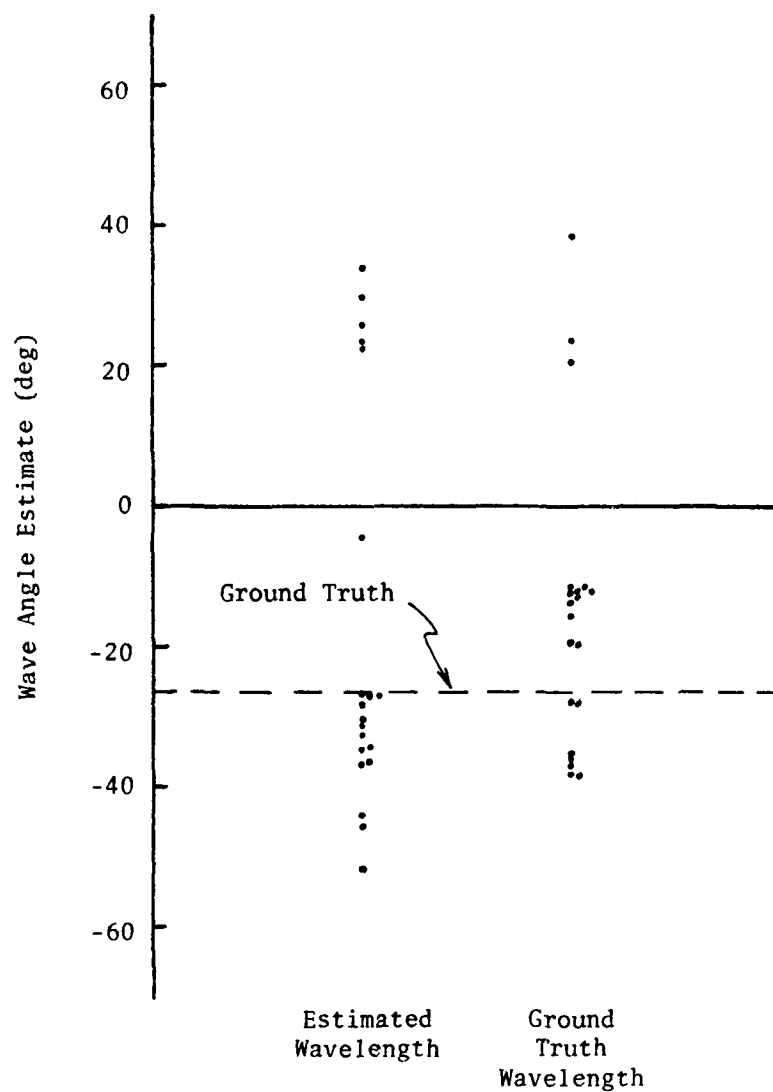


Fig. 81. Individual Case Indicated Propagation Angle Estimates Comparing Use of Estimated and Ground-Truth Wavelengths.

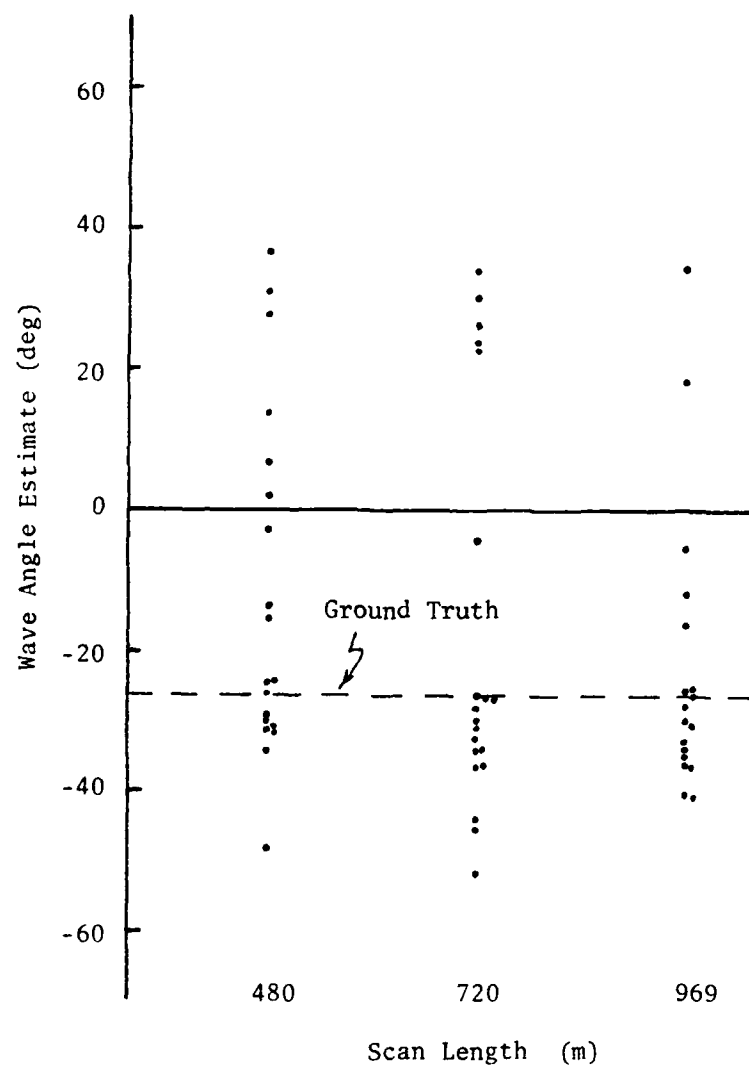


Fig. 82. Individual Case Indicated Propagation Angle Estimates Comparing Use of Different Scan Lengths.

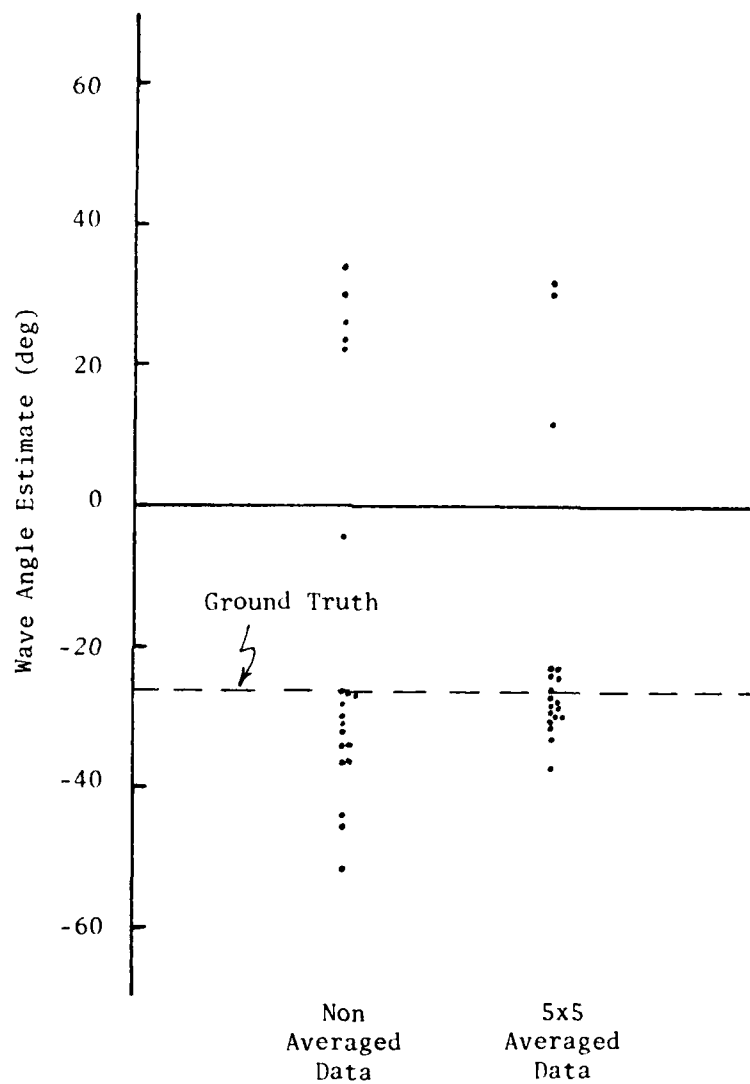


Fig. 83. Individual Case Indicated Propagation Angle Estimates Comparing Use of Non-Smoothed and Smoothed Radar Data.

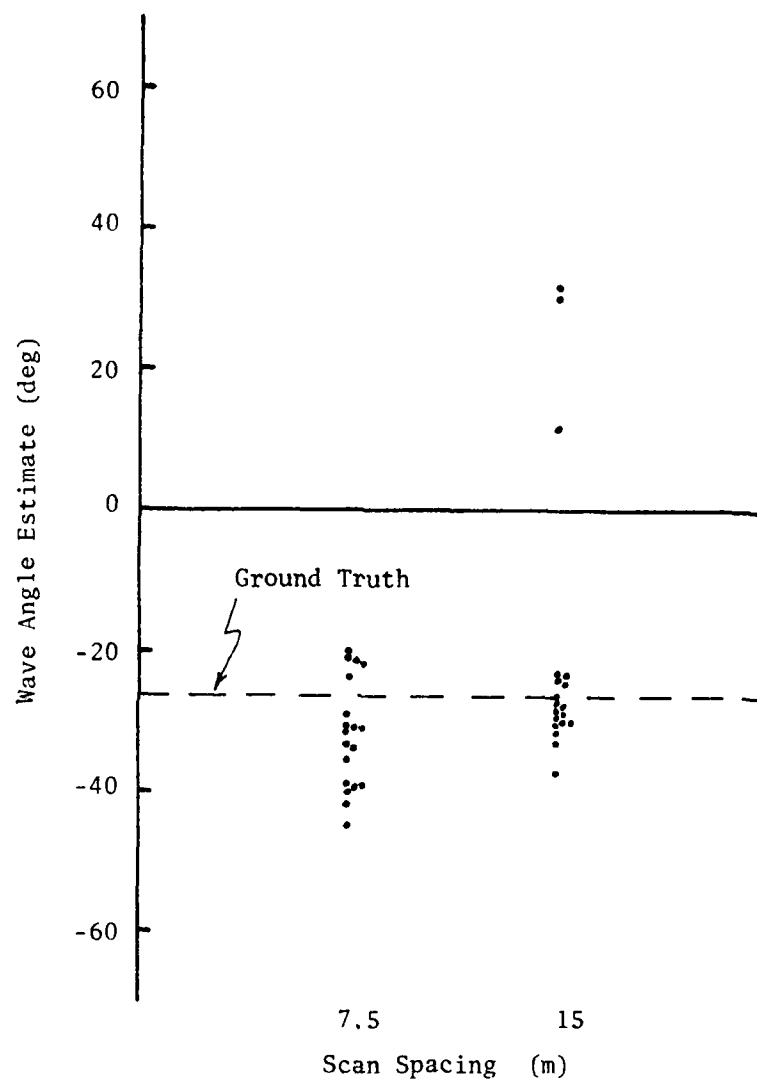


Fig. 84. Individual Case Indicated Propagation Angle Estimates Comparing Use of Different Scan Spacings.

better wave angle estimates and the scan spacing was left at 15m for further analysis (note that this is the same value selected for along-scan wavenumber estimation).

Rotated scans across analysis area A-3 were used to investigate the performance of the third system concept in estimating indicated propagation angles of other than -26.54° . Figure 85 shows the individual case wave angle estimates for the same scans taken at rotation angles $\theta_r = 0^\circ$, 23° , and 35° across 5x5 averaged radar data for analysis area A-3. The scan lengths used are 720m, 975m, and 1071m (8.18, 8.52, and 6.48 ground truth wavelengths) for the rotation angles of 0° , 23° , and 35° respectively. The other system parameters used are $\Delta s = 15m$, $N_s = 14$ scans, and 3 pt. smoothing. The scan length used for $\theta_r = 35^\circ$ was less than 8 ground truth wavelengths since the image edge precluded using scans any longer than 1071m at this rotation angle.

The wave angle estimate performance appears to be quite similar for the various indicated propagation angles considered. The percent of individual case estimates within $\pm 10^\circ$ of the ground truth indicated propagation angle are 75%, 80%, and 75% for $\theta_r = 0^\circ$, 23° , and 35° respectively. The percent of individual estimates within $\pm 5^\circ$ are 70%, 30%, and 60% for $\theta_r = 0^\circ$, 23° , and 35° respectively.

In general, it can be said that the third system concept does provide wave angle estimates which are clustered about the true indicated propagation angle over a range of propagation angles when smoothed radar data (5x5 averaging) from analysis area A-3 is used. However, some estimates are far from the correct value and only approximately 75% are within $\pm 10^\circ$ of the true indicated propagation angle value. Consequently, while the third system concept provides better estimates than either the initial system concept or the second system concept, it still does not provide consistently satisfactory estimation of the indicated propagation angle from a few scans of radar data.

To further investigate these conclusions, scans across analysis area A-4 were also considered both with no rotation and with a rotation angle of 23° . Recall that this analysis area gave poorer along-scan wavenumber estimates than were achieved with analysis area A-3. Figure 86 shows the individual case wave angle estimates for scans taken at rotation angles of $\theta_r = 0^\circ$ and 23° across 5x5 averaged radar data from analysis area A-4. The scan lengths used are 705m and 975m (8.01 and 8.04 ground truth wavelengths) for the rotation angles of 0° and 23° respectively. The other system parameters used are $\Delta s = 15m$, $N_s = 14$ scans, and 3 pt. smoothing.

The wave angle estimates obtained with analysis area A-4 are not clustered nearly as well about the true indicated propagation angles as those obtained with analysis area A-3. Thus, the percent of individual case estimates within $\pm 10^\circ$ of the ground truth indicated propagation angle are reduced to 50% and 30% for $\theta_r = 0^\circ$ and 23° respectively. The percent of individual estimates within $\pm 5^\circ$ are reduced to 5% for both $\theta_r = 0^\circ$ and 23° . As expected, the wave angle estimation

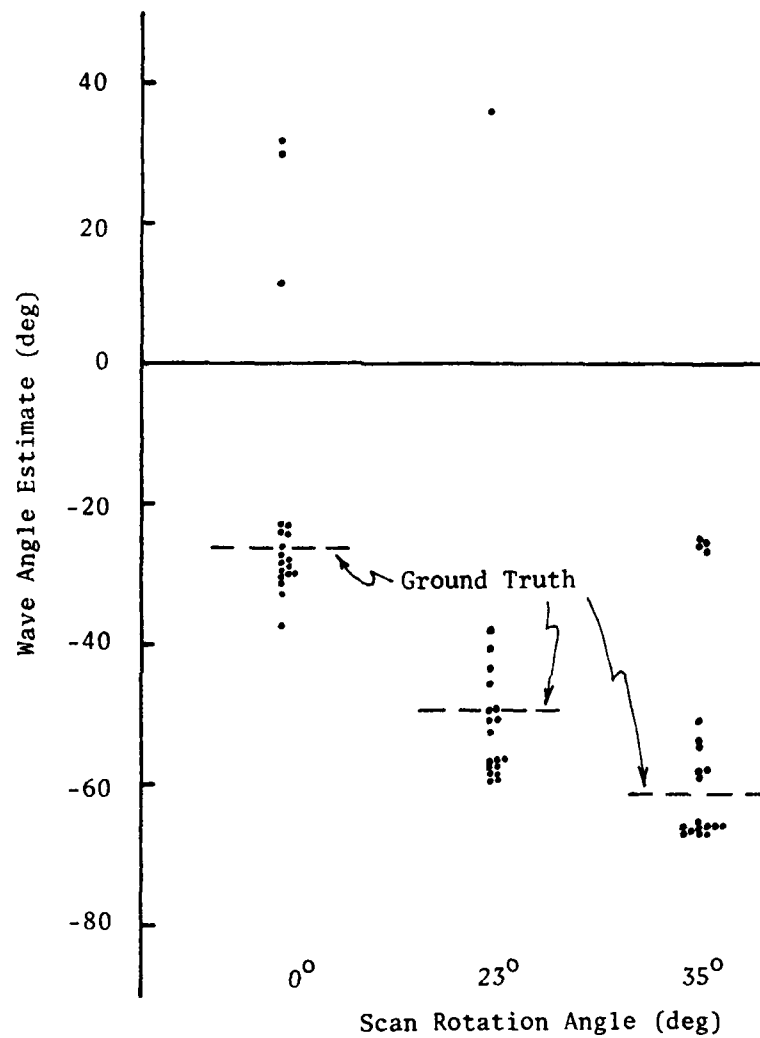


Fig. 85. Individual Case Indicated Propagation Angle Estimates for Three Different Wave Angles for Analysis Area A-3.

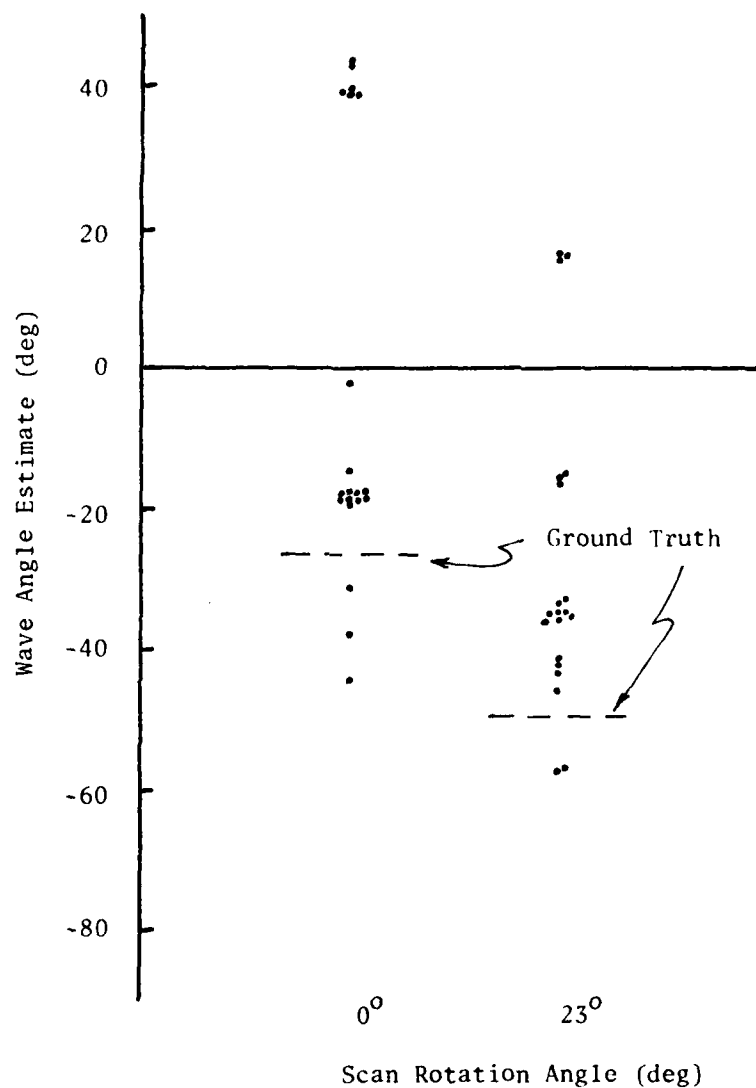


Fig. 86. Individual Case Indicated Propagation Angle Estimates for Two Different Wave Angles for Analysis Area A-4.

performance is not as good for analysis area A-4 as for analysis area A-3 and again points up that consistently satisfactory estimation of the indicated propagation angle is not obtained from a few scans of radar data.

VI. SUMMARY AND CONCLUSIONS

The feasibility of obtaining estimates of the wavenumber and propagation direction of the dominant wave component in a wave field from a few digitized, focused synthetic aperture radar scans has been investigated. An initial system concept was defined which used the peak location of an average periodogram obtained from several scans to estimate the along-scan wavenumber. The initial system concept estimated the indicated propagation angle from the peak location of an average cross correlation function obtained for several pairs of scans. The methods required to compute the estimates of wavenumber and propagation angle from the estimates of along-scan wavenumber and indicated propagation angle were shown.

System analysis was performed using scans of synthetic aperture radar data obtained and processed by the Environmental Research Institute of Michigan (ERIM). The data was obtained on aircraft flights off the coast of Florida near Marineland. Data obtained by the SEASAT-A satellite was also received but was not used since acceptable performance could not be shown using the better aircraft generated data.

The portion of the initial system used to estimate the along-scan wavenumber was analyzed by statistical means and found to give unacceptable estimation performance on the average. This portion of the initial system was modified to eliminate some individual periodograms which were inconsistent with the rest before averaging. Also, cases for which the along-scan wavenumber estimate did not converge as additional periodograms were averaged were declared as cases for which the system could not find an estimate. Some additional variations of this modified system were also identified. A set of system parameters required for along-scan wavenumber estimation were defined from trade-off performance. They are: (1) a $3/4$ width Parzen window for periodogram smoothing, (2) 14 scans, (3) scan length greater than 5.5 along-scan wavelengths, and (4) scan spacing equal to 15m.

Performance of the modified system for along-scan wavenumber estimation was analyzed using data for several different analysis areas on a number of different images. In general, the performance was inconsistent. For those scan lengths which were large enough to give estimate convergence, the number of non-estimable cases ranged from a low of 0% to a high of 35.0%, the relative average bias ranged from 1.8% to 46.5%, and the relative average standard deviation ranged from 13.9% to 60.3% for most of the analysis areas. Performance was best for analysis area A-3 which had a well defined wave structure in the area. In this analysis area, the number of non-estimable cases ranged from 0% to 17.5%, the relative average bias ranged from 1.8% to 6.0%, and the relative average standard deviation ranged from 13.9% to 26.7%. Thus, it appears that the primary deterrent to good along-scan wavenumber estimation with a few scans of radar data is the poor signal-to-noise ratio that is available. If this signal-to-noise ratio could be improved, then it is conceivable that the system would provide

reasonable estimates of along-scan wavenumber with a few radar scans.

The portion of the initial system concept used to estimate the indicated propagation angle was analyzed by considering several individual cases. No cases were found which gave reasonable estimates of the indicated propagation angle from the peak location of average cross correlation functions. Consequently, system redefinitions were considered.

The second system concept defined for estimating the indicated propagation angle used a straight line fit in a least squares error sense to wave crest offset location as a function of distance perpendicular to the scans. The angle made by the straight line estimate of the wave crest location with the radar scan direction was used as the indicated propagation angle estimate. The second system concept did give some good estimates. However, in general the estimation performance was very inconsistent. It was determined that a primary problem was the low signal-to-noise ratio which gives non-unique wave crest signatures. Thus, estimates of the wave displacement from one scan to another were sometimes generated by matches of adjacent wave crests rather than the same wave crest. No solution to this problem was found.

The third system concept defined for estimating the indicated propagation angle attempted to circumvent the non-unique wave crest signature problem by performing a partial two dimensional cross correlation using the few radar scans and a two dimensional square wave with along-scan wavelength determined by the along-scan wavenumber estimated by the system. A number of parameter variations were considered. The only one having much effect on system performance over the images considered was the type of radar scan data used. It was found that it was imperative that the radar scan data be smoothed by averaging data from several adjacent radar scans and for several adjacent points along a radar scan. With smoothed radar data it was found that estimates could be obtained which, for the most part, clustered in the neighborhood of the correct indicated propagation angle when scan data from the analysis area which gave the best wavenumber estimates was used. However, at best only 75% of the cases evaluated in this analysis area gave indicated propagation angle estimates which are within $\pm 10^\circ$ of the correct angle. Poorer results were obtained with a second analysis area. Thus, while the third system concept for indicated propagation angle estimation provides better estimates than either of the other two system concepts, it still does not provide consistently satisfactory estimation of the indicated propagation angle from a few scans of radar data.

The computation of estimates of wavenumber and propagation angle from estimates of along-scan wavenumber and indicated propagation angle was not considered. The fact that unsatisfactory along-scan wavenumber and indicated propagation angle estimates were obtained made it impractical to consider the accuracy of the wavenumber and propagation angle estimates computed from them.

As a final conclusion, it should be reiterated that the primary

cause of the poor estimates achieved with a few radar scans is the poor signal-to-noise characteristics of the radar scan data. Part of this is due to the backscatter characteristics of ocean waves and better understanding of this backscatter mechanism would perhaps aid in interpretation of the data and design of systems to enhance the signal-to-noise characteristics of ocean wave returns.

REFERENCES

1. Manual of Remote Sensing. Falls Church, Virginia: American Society of Photogrammetry, 1975.
2. Derr, V. E., Remote Sensing of the Troposphere, Washington, D.C.: U.S. Dept. of Commerce, National Oceanic and Atmospheric Administration, 1972.
3. Harger, R. O., Synthetic Aperture Radar Systems, New York, N.Y.: Academic Press, 1970.
4. Shuchman, R. A., Jackson, P. L., and Feldkamp, G. B., "Problems of Imaging Ocean Waves with Synthetic Aperture Radar", Tech. Rpt. 124300-1-T, Environmental Research Institute of Michigan, Aug. 1977.
5. Papoulis, A. E., Probability, Random Variables, and Stochastic Processes, New York, N.Y.: McGraw-Hill Inc., 1965.
6. Jenkins, G. M. and Watts, D. G., Spectral Analysis and its Applications, San Francisco, Calif.: Holden Day Inc., 1968.
7. Teleki, P. G., Schuchman, R. A., and others, "Ocean Wave Detection and Direction Measurements with Microwave Radars", pp 639-648, Proceedings from Oceans '78, Washington, D.C., The Marine Technology Society and IEEE, Sept. 1978.

APPENDIX A
PHOTOGRAPHS FOR ADDITIONAL ANALYSIS AREAS

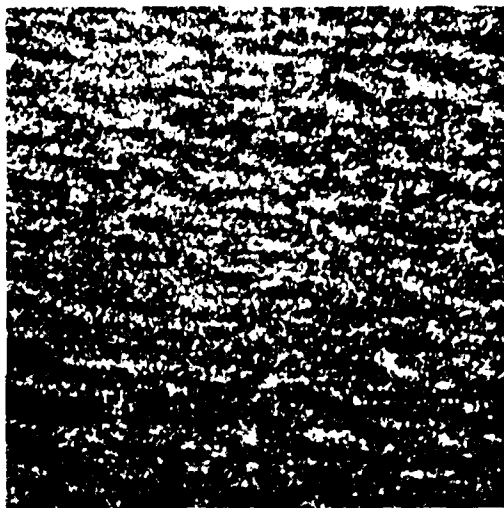


Fig. A1. Digitized Version of Analysis
Area A-4 in Slant-Range Format.

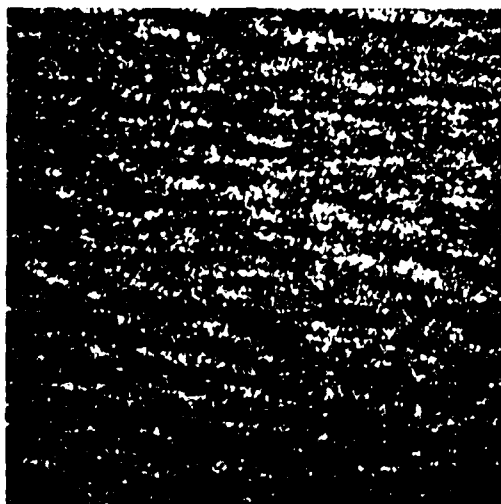


Fig. A2. Digitized Version of Analysis
Area A-5 in Slant-Range Format.



Fig. A3. Digitized Version of Analysis
Area B-1 in Slant-Range Format.

APPENDIX B

SMOOTHED PERIODOGRAMS FOR BARTLETT
AND TUKEY WINDOWS

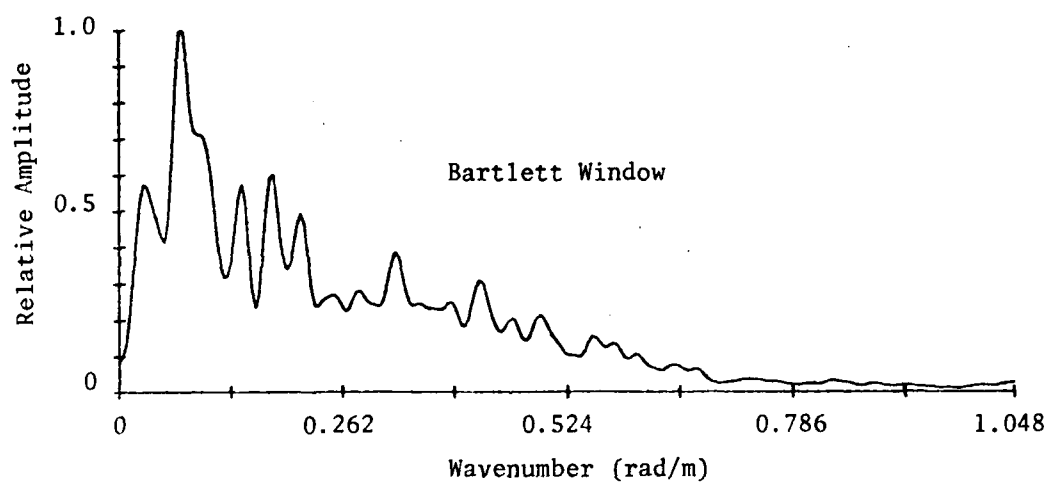
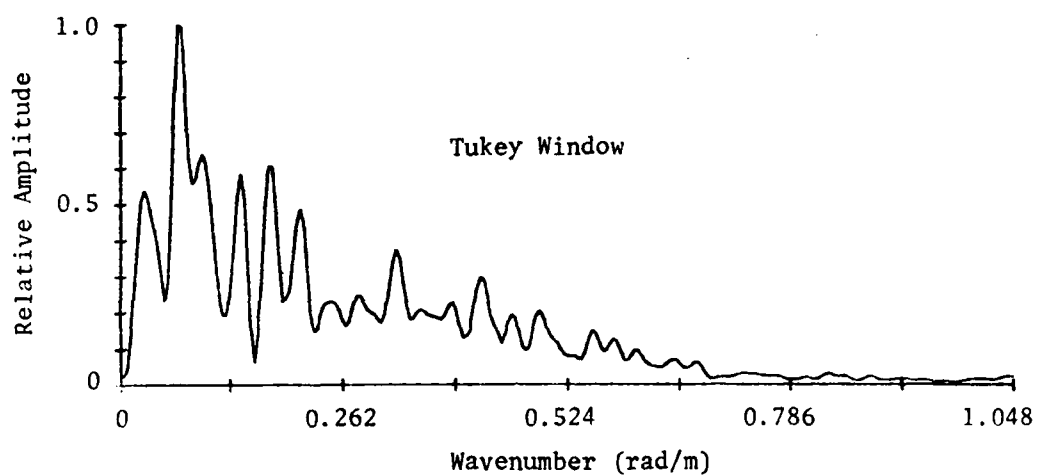


Fig. B1. Periodogram Smoothing Effect for Tukey and Bartlett Windows with $M = N$.

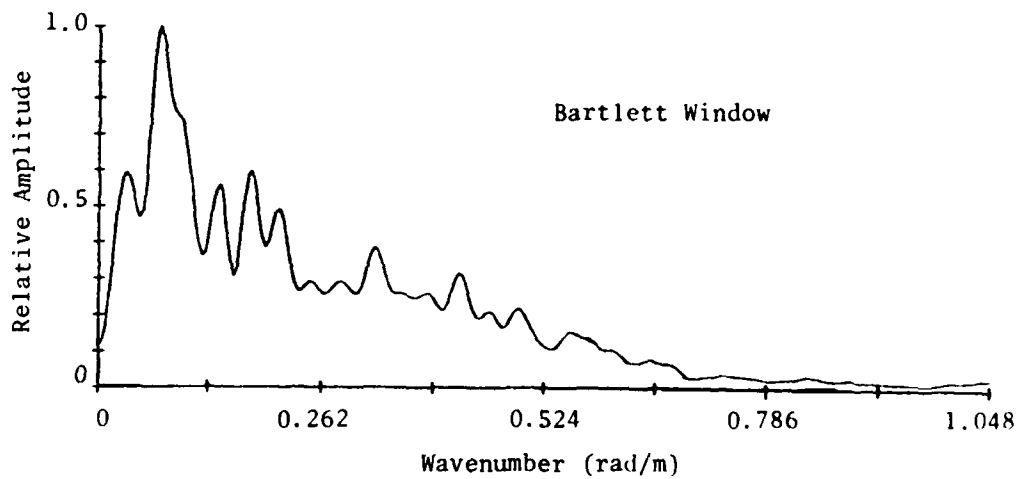
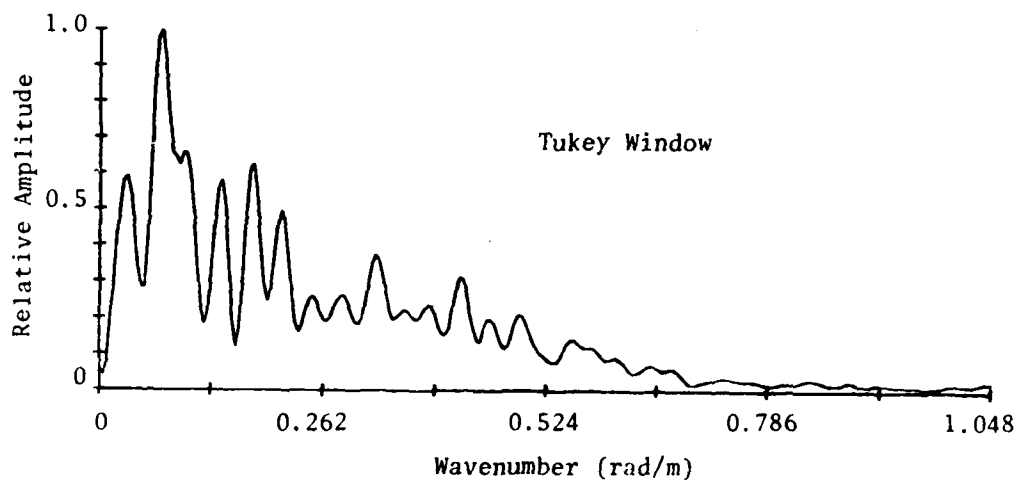


Fig. B2. Periodogram Smoothing Effect for Tukey and Bartlett Windows with $M = 3N/4$.

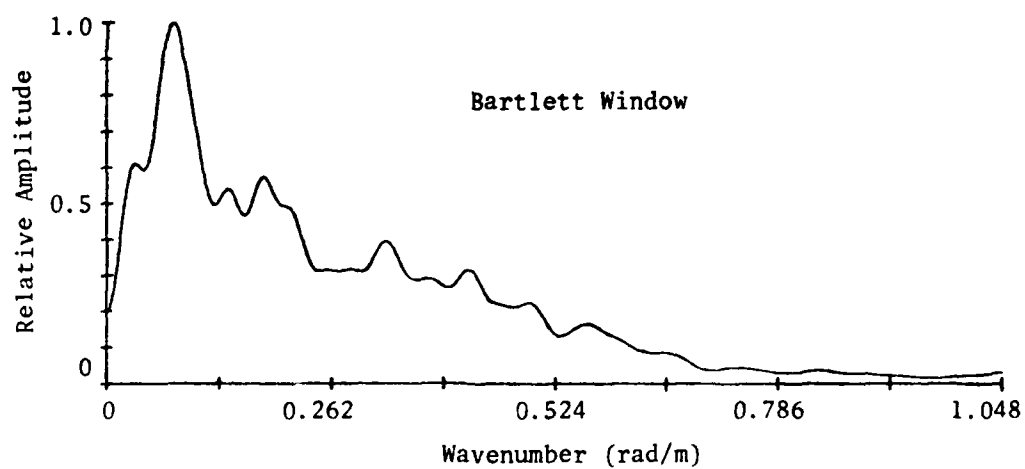
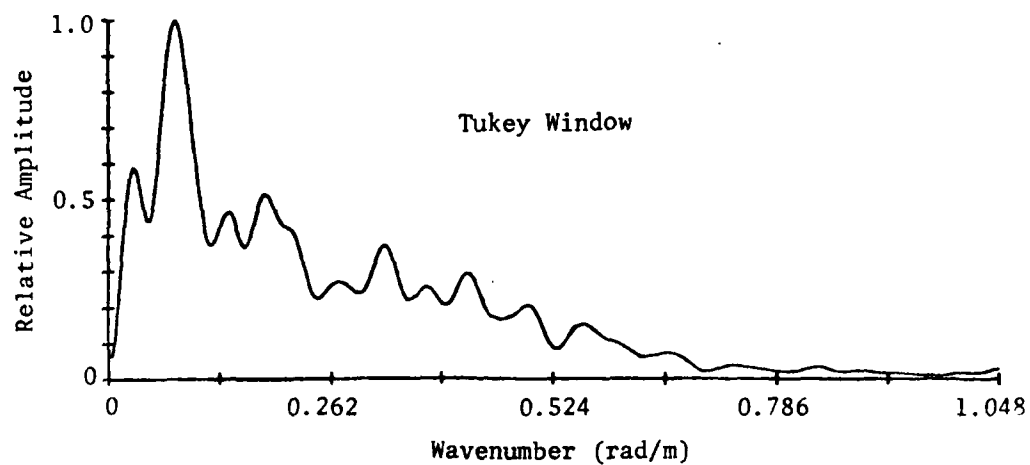


Fig. B3. Periodogram Smoothing Effect for Tukey and Bartlett Windows with $M = N/2$.

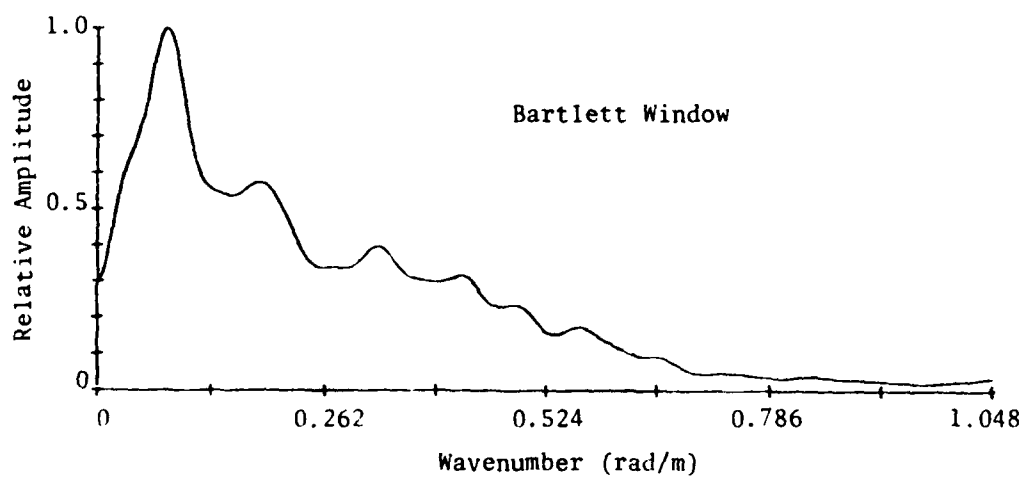
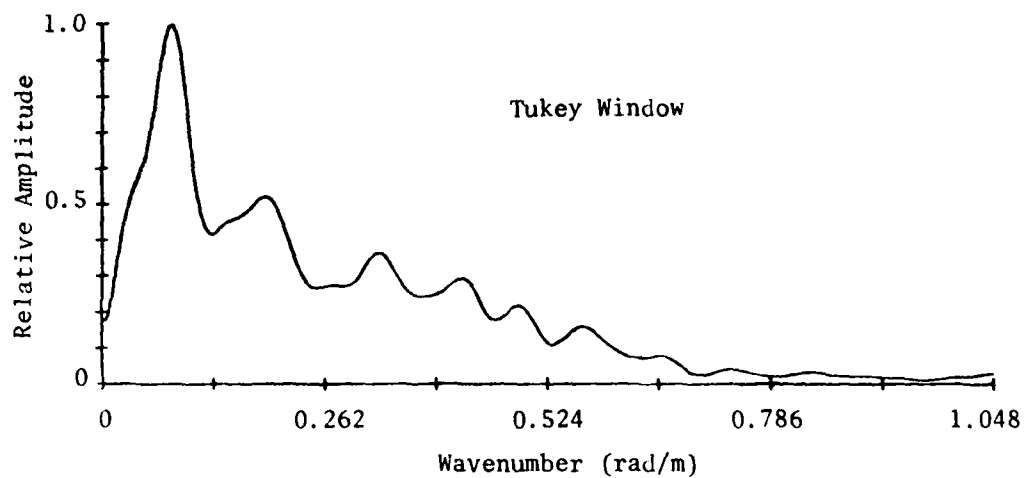


Fig. B4. Periodogram Smoothing Effect for Tukey and Bartlett Windows with $M = 3N/8$.

APPENDIX C
INDIVIDUAL CASE WAVENUMBER ESTIMATES

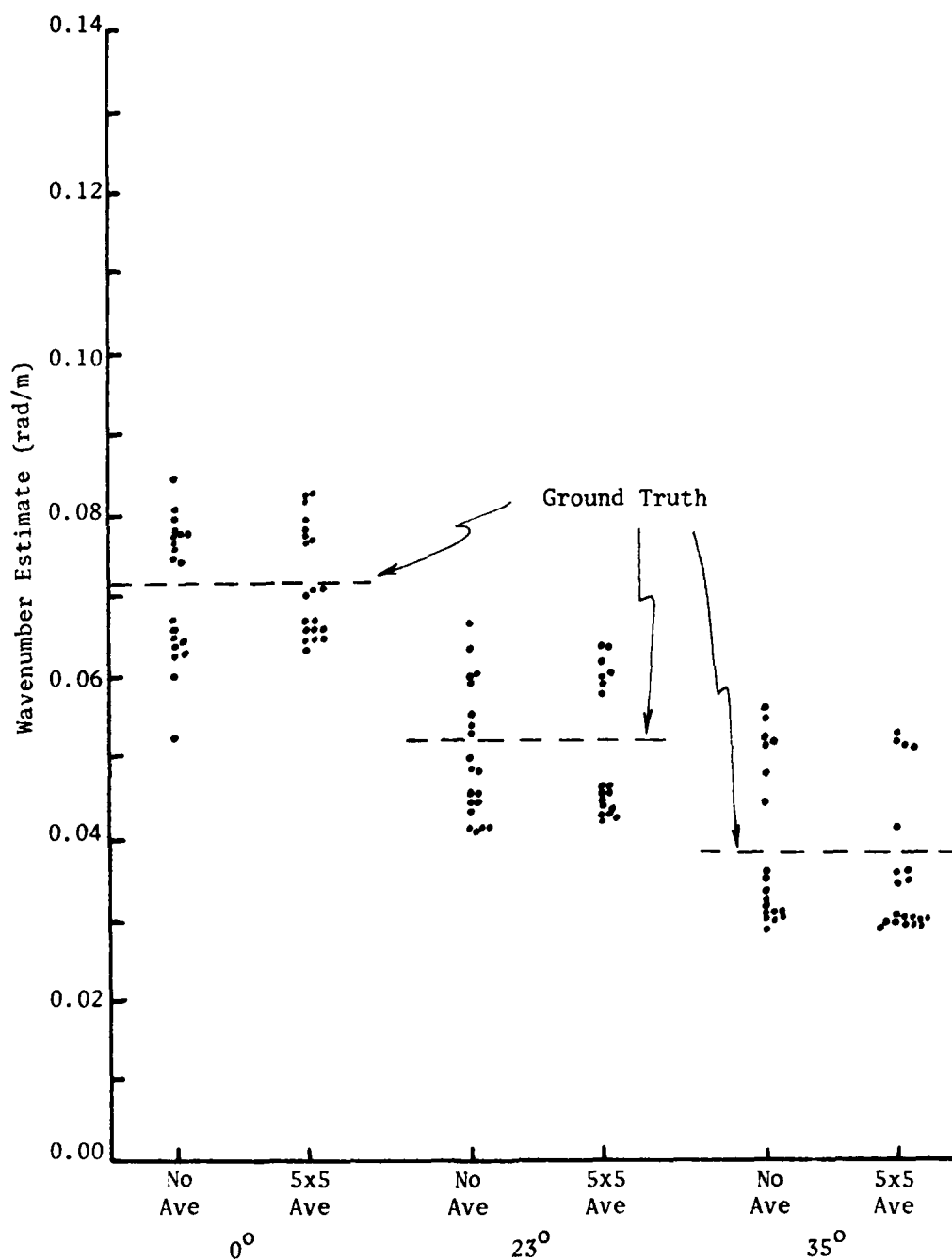


Fig. C1. Individual Case Wavenumber Estimates for Three Scan Rotation Angles and a Scan Length of Approximately 6.5 Wavelengths (Analysis Area A-3).

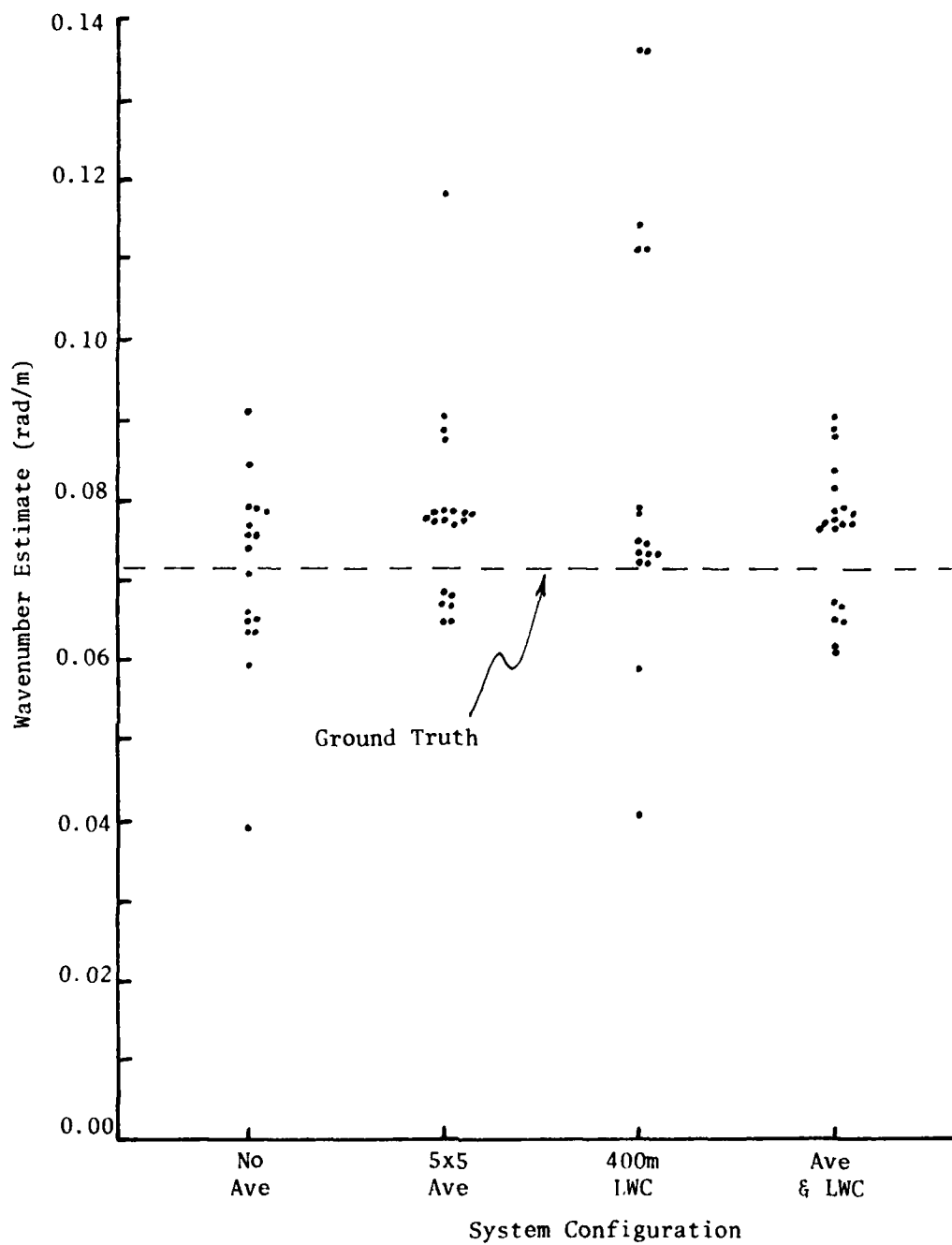


Fig. C2. Individual Case Wavenumber Estimates for Scans Rotated 0° from Data Scan Lines and a Scan Length of Approximately 11 Wavelengths (Analysis Area A-4).

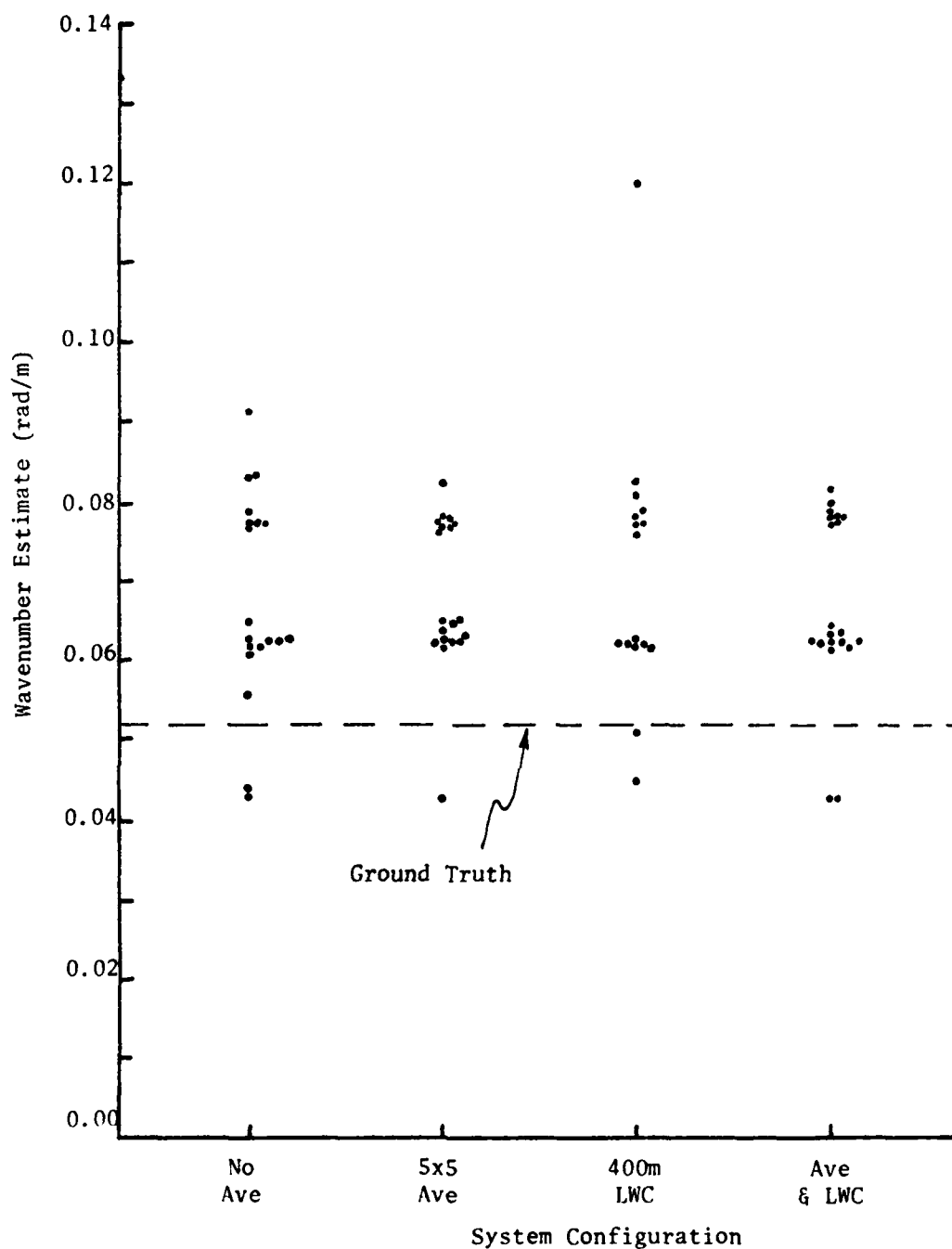


Fig. C3. Individual Case Wavenumber Estimates for Scans Rotated 23° from Data Scan Lines and a Scan Length of Approximately 11 Wavelengths (Analysis Area A-4).

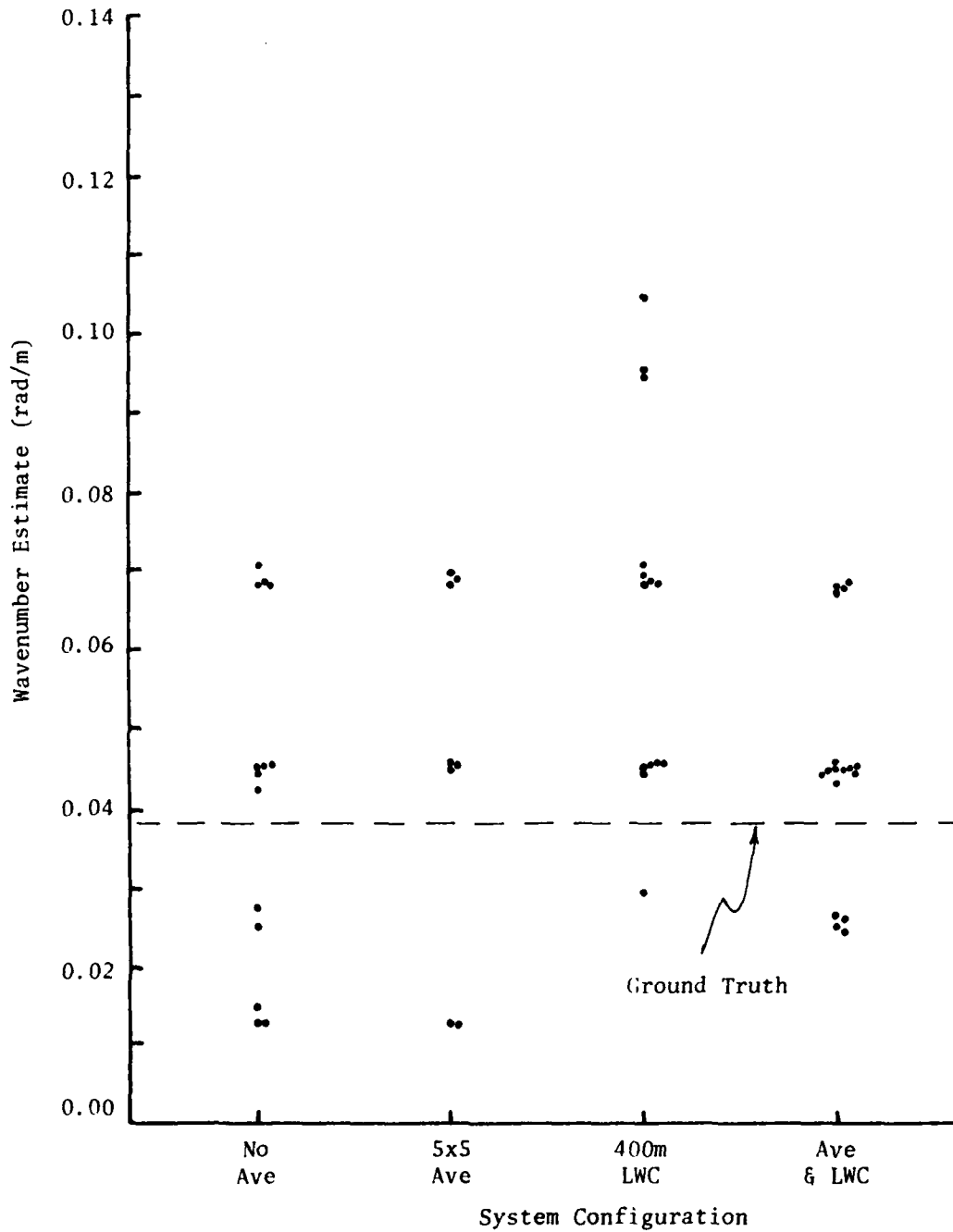


Fig. C4. Individual Case Wavenumber Estimates for Scans Rotated 35° from Data Scan Lines and a Scan Length of Approximately 11 Wavelengths (Analysis Area A-4).

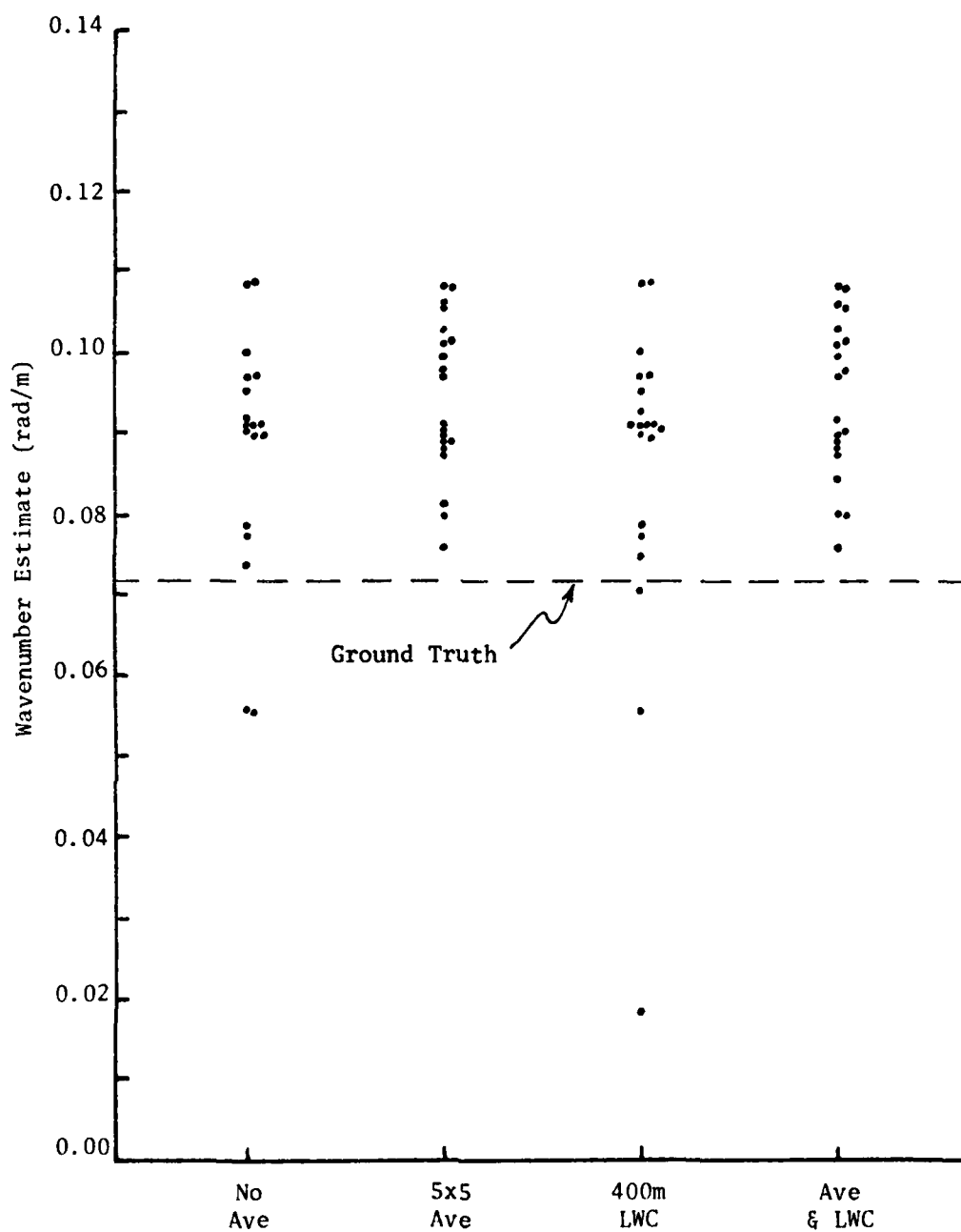


Fig. C5. Individual Case Wavenumber Estimates for Scans Rotated 0° from Data Scan Lines and a Scan Length of Approximately 6.5 Wavelengths (Analysis Area A-5).

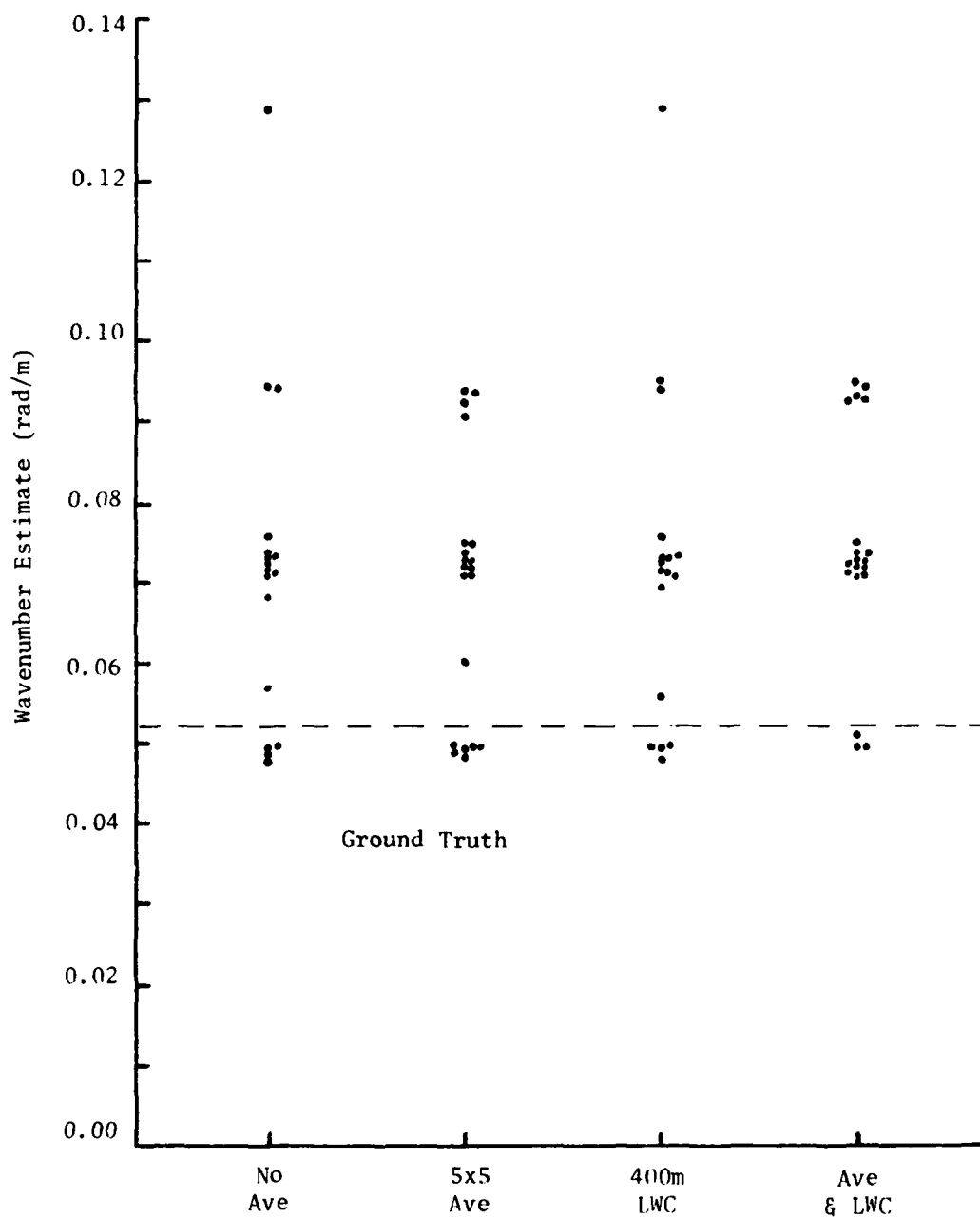


Fig. C6. Individual Case Wavenumber Estimates for Scans Rotated 23° from Data Scan Lines and a Scan Length of Approximately 6.5 Wavelengths (Analysis Area A-5).

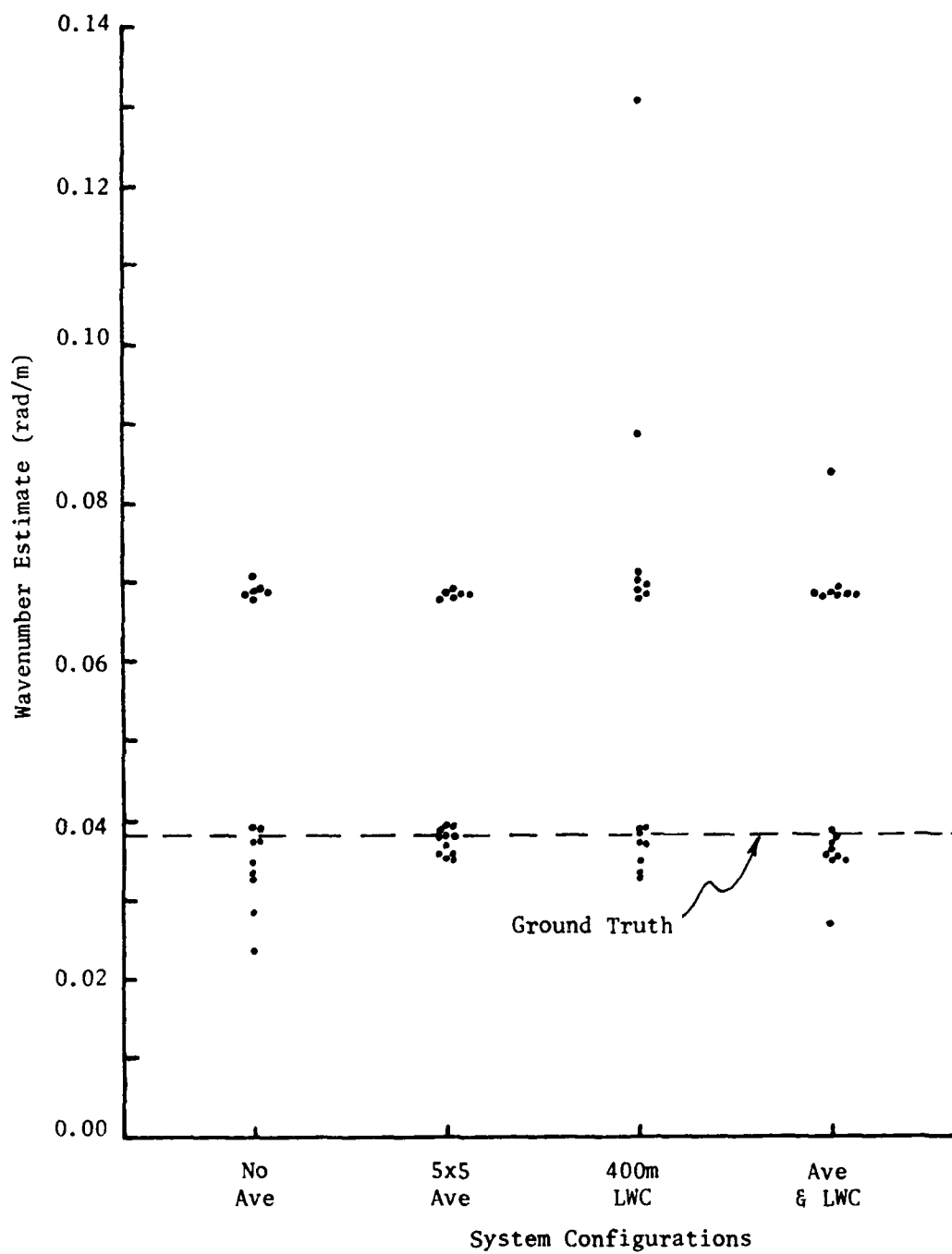


Fig. C7. Area #3 Individual Case Wavenumber Estimates for Scans Rotated 35° from Data Scan Lines and a Scan Length of Approximately 6.5 Wavelengths (Analysis Area A-5).

DISTRIBUTION

Office of Naval Research (12)
Coastal Sciences Program
Code 462
Arlington, VA 22217

Defense Documentation Center (12)
Cameron Station
Alexandria, VA 22314

Director, Naval Research Laboratory (6)
ATTN: Technical Information Officer
Washington, D.C. 20375

Director
Office of Naval Research Branch Office
1030 East Green Street
Pasadena, California 91101

Commanding Officer
Office of Naval Research Eastern/Central
Regional Office
Building 114, Section D
666 Summer Street
Boston, Massachusetts 02210

Office of Naval Research
Code 480
National Space Technology Laboratories
Bay St. Louis, Mississippi 39529

Director, Naval Research Laboratory
ATTN: Library, Code 2628
Washington, D.C. 20375

Commander
Naval Oceanographic Office
ATTN: Library, Code 1600
NSTL Station, MS 39529

Mr. Robert A. Schuchman
Environmental Research
Institute of Michigan
Box 8618
Ann Arbor, Michigan 48107

Dr. Omar Shemdin
Jet Propulsion Laboratory
183-501
4800 Oak Grove Drive
Pasadena, California 91103

Dr. Oscar Huh
Coastal Studies Institute
Louisiana State University
Baton Rouge, Louisiana 70803

END